TM 5-858-2

TECHNICAL MANUAL

DESIGNING FACILITIES TO RESIST NUCLEAR WEAPON EFFECTS

WEAPON EFFECTS

HEADQUARTERS, DEPARTMENT OF THE ARMY

JULY 1984

REPRODUCTION AUTHORIZATION/RESTRICTIONS

TECHNICAL MANUAL

NO. 5-858-2

HEADQUARTERS
DEPARTMENT OF THE ARMY
WASHINGTON, DC *6 JULY 1984*

DESIGNING FACILITIES TO RESIST NUCLEAR WEAPON EFFECTS

WEAPON EFFECTS

REPORTING OF ERRORS

You can help improve this manual. If you find any mistakes or if you know of a way to improve this manual, please let us know. Mail your letter, DA Form 2028 (Recommended Changes to Publications and Blank Forms), or DA Form 2028-2 located in the back of this manual directly to Commander, US Army Corps of Engineers, ATTN: DAEN-ECE-T, Washington, DC, 20314.

A reply will be furnished direct to you.

		Paragraph	*Page*
CHAPTER 1.	INTRODUCTION		
	General	1-1	1-1
	TM 5-858-2: Weapon Effects	1-2	1-1
2.	NUCLEAR-WEAPON EFFECTS		
	High Explosive and Nuclear-Weapon Effects	2-1	2-1
	Nuclear Weapons	2-2	2-1
	Burst Elevations	2-3	2-1
	Weapon Effect, A Random Variable	2-4	2-2
3.	INITIAL NUCLEAR RADIATION		
	Gross Phenomenology	3-1	3-1
	Neutron Radiation	3-2	3-1
	Gamma Radiation	3-3	3-1
4.	ELECTROMAGNETIC PULSE (EMP)		
	Gross Phenomenology	4-1	4-1
	Surface Burst	4-2	4-1
	High-Altitude Burst	4-3	4-13
5.	FIREBALL		
	Gross Phenomenology	5-1	5-1
	Engulfment Radius	5-2	5-1
	Temperature and Density	5-3	5-1
6.	THERMAL RADIATION		
	Gross Phenomenology	6-1	6-1
	Radiant Exposure	6-2	6-1
	Radiation History	6-3	6-12
7.	AIRBLAST		
	Gross Phenomenology	7-1	7-1
	Free-Field Peak Overpressure	7-2	7-2
	Free-Field Peak Dynamic Pressure	7-3	7-15
	Overpressure Positive Phase Duration	7-4	7-21
	Dynamic Pressure Positive Phase Duration	7-5	7-21
	Pressure Waveforms	7-6	7-30
	Overpressure Impulse	7-7	7-33

*This manual together with TM 5-858-1, 31 October 1983 and TM 5-858-3 through TM 5-858-8 supersedes TM 5-856-1, 1 July 1959; TM 5-856-2, 15 March 1957; TM 5-856-3, 15 March 1957; TM 5-856-4, 15 March 1957; TM 5-856-5, 15 January 1958; TM 5-856-6, 15 January 1960; TM 5-856-7, 15 January 1958; TM 5-856-8, 15 January 1960; and TM 5-856-9, 15 January 1960.

		Paragraph	Page
CHAPTER 8.	AIRBLAST-INDUCED GROUND SHOCK		
	Gross Phenomenology	8-1	8-1
	Ground Response	8-2	8-1
	Superseismic Peak Soil Response	8-3	8-1
	Superseismic Peak Rock Response	8-4	8-3
	Superseismic Soil and Rock Waveforms	8-5	8-4
	Outrunning Peak Ground Response	8-6	8-11
	Outrunning Waveforms	8-7	8-15
	Height of Burst Effects	8-8	8-15
9.	CRATER-INDUCED GROUND SHOCK		
	Gross Phenomenology	9-1	9-1
	Ground-Shock Intensity	9-2	9-2
	Pulse Shapes	9-3	9-17
10.	CRATER		
	Gross Phenomenology	10-1	10-1
	Single Burst	10-2	10-1
	Multiple, Pattern Bursts	10-3	10-7
	Repeated Attack (Nail Driving)	10-4	10-10
	Crater Volume	10-5	10-10
11.	EJECTA/DEBRIS IMPACT		
	Gross Phenomenology	11-1	11-1
	Ejected Mass and Particle Size	11-2	11-1
	Number of Impact Particles	11-3	11-2
	Particle Impact Velocities and Angles	11-4	11-2
	Impact Damage Potential	11-5	11-2
12.	EJECTA/DEBRIS DEPTH		
	Gross Phenomenology	12-1	12-1
	Debris Depth	12-2	12-1
	Crater Volumes	12-3	12-1
13.	DUST		
	Gross Phenomenology	13-1	13-1
	Base-Surge Dust Cloud	13-2	13-1
	Ejecta Dust Cloud	13-3	13-5
14.	FIRESTORM		
	Gross Phenomenology	14-1	14-1
	Weather Conditions	14-2	14-1
	Fuel Density	14-3	14-1
15.	RESIDUAL NUCLEAR RADIATION		
	Gross Phenomenology	15-1	15-1
	Early Fallout	15-2	15-1
	Late Fallout	15-3	15-14
	Precipitation Effects	15-4	15-14
	Uncertainty	15-5	15-14
APPENDIX A	GLOSSARY		A-1
B	BIBLIOGRAPHY (References)		B-1

LIST OF TABLES

Table		Page
3-1	Soil Types by Composition	3-25
3-2	Multiplying Factors	3-25
6-1	Daytime Visibility for Generic Cloudlessness	6-8
6-2	Reflectance $\overline{F}_{cb}$ for Layer of Clouds or Haze Below the Burst	6-10

Table *Page*

7-1 Thermally Near-Ideal and Thermally Nonideal Surfaces 7-2
7-2 Parameters for Peak Overpressure 7-3
7-3 Parameters for Positive Phase Duration 7-26
7-4 Parameters for Dynamic Pressure Positive Phase Duration 7-30
7-5 Values of Constants for Overpressure Impulse Functions 7-40

8-1 Mean Parameters for Calculation of Velocity and Displacement Due to Airblast on Rock 8-4
8-2 Values of Parameters for Calculating Outrunning Ground Shock Velocity and Associated Uncertainties 8-12
8-3 Uncertainties of the Initial Peak Velocity 8-15
8-4 Impulse Ratio $I_{(HOB)}/I_{(O)}$ for Displacement Computation 8-17

9-1 Mean Values of Parameters for Calculations of Direct-Induced Ground Motion 9-3
9-2 Factors in Calculating HOB/DOB Effective Yield 9-5
9-3 Factors Γ_m to Account for Geological Properties 9-5

10-1 Mean Value of Parameters 10-8
10-2 Parameters for Increase of True Crater Dimensions Due to Nail Driving 10-12

12-1 Geology Correction Factors 12-4
12-2 Nominal Cratering Efficiencies E_o for Half-Buried HE Charges 12-4

14-1 Physical and Thermal Properties of Wild Land Fuels 14-3
14-2 Comparison of Weapon-Test Data with Predictions Based on Correlation Model 14-4

LIST OF FIGURES

Figure *Page*

3-1 Typical Neutron Fluence Incident on a Receiver Located on or near the Surface of the Earth 3-2
3-2 Neutron Dose F_N as a Function of Slant Range from a 1-kt Surface Burst, Weapon Types I through IV, Short Ranges 3-3
3-3 Neutron Dose F_N as a Function of Slant Range from a 1-kt Surface Burst, Weapon Types I through IV, Long Ranges 3-4
3-4 Neutron Dose F_N as a Function of Slant Range from a 1-kt Surface Burst, Weapon Types V through VIII, Short Ranges 3-5
3-5 Neutron Dose F_N as a Function of Slant Range from a 1-kt Surface Burst, Weapon Types V through VIII, Long Ranges 3-6
3-6 Burst Height Adjustment Factors H_1 for Neutrons and Secondary Gamma Rays 3-7
3-7 Secondary Gamma Ray Dose $F_{\gamma s}$ as a Function of Slant Range from a 1-kt Surface Burst, Weapon Types I through IV, Short Ranges 3-8
3-8 Secondary Gamma Ray Dose $F_{\gamma s}$ as a Function of Slant Range from a 1-kt Surface Burst, Weapon Types I through IV, Long Ranges 3-9
3-9 Secondary Gamma Ray Dose $F_{\gamma s}$ as a Function of Slant Range from a 1-kt Surface Burst, Weapon Types V through VIII, Short Ranges 3-10
3-10 Secondary Gamma Ray Dose $F_{\gamma s}$ as a Function of Slant Range from a 1-kt Surface Burst, Weapon Types V through VIII, Long Ranges 3-11
3-11 Fission Product Gamma Ray Dose $F_{\gamma f}$ as a Function of Slant Range from a 1-kt (Fission Yield) Surface Burst, Short Ranges 3-13
3-12 Fission Product Gamma Ray Dose $F_{\gamma f}$ as a Function of Slant Range from a 1-kt (Fission Yield) Surface Burst, Intermediate Ranges 3-14
3-13 Fission Product Gamma Ray Dose $F_{\gamma f}$ as a Function of Slant Range from a 1-kt (Fission Yield) Surface Burst, Long Ranges 3-15
3-14 Range-Dependent Burst Height Adjustment Factors H_R for Fission Product Gamma Rays 3-16
3-15 Yield-Dependent Burst Height Adjustment Factors H_W for Fission Product Gamma Rays 3-17
3-16 Fission-Product Gamma Ray Hydrodynamic Enhancement Factors E as a Function of Slant Range for Relative Air Density of 1.1 3-18
3-17 Fission-Product Gamma Ray Hydrodynamic Enhancement Factors E as a Function of Slant Range for Relative Air Density of 1.0 3-19
3-18 Fission-Product Gamma Ray Hydrodynamic Enhancement Factors E as a Function of Slant Range for Relative Air Density of 0.9 3-20
3-19 Fission-Product Gamma Ray Hydrodynamic Enhancement Factors E as a Function of Slant Range for Relative Air Density of 0.8 3-21
3-20 Fission-Product Gamma Ray Hydrodynamic Enhancement Factors E as a Function of Slant Range for Relative Air Density of 0.7 3-22
3-21 Neutron-Induced Gamma Dose Rate $D_{\gamma I}$ as a Function of Slant Range at a Reference Time of 1 Hour After Burst 3-23
3-22 Decay Factors for Neutron-Induced Gamma Activity $D_{\gamma I}$ 3-24

Figure		*Page*
3-23	Total Radiation Dose Received (rad/kt) in an Area Contaminated by Neutron-Induced Gamma Activity, Soil Type I	3-26
3-24	Total Radiation Dose Received (rad/kt) in an Area Contaminated by Neutron-Induced Gamma Activity, Soil Type II	3-27
3-25	Total Radiation Dose Received (rad/kt) in an Area Contaminated by Neutron-Induced Gamma Activity, Soil Type III	3-28
3-26	Total Radiation Dose Received (rad/kt) in an Area Contaminated by Neutron-Induced Gamma Activity, Soil Type IV	3-29
4-1	Surface-Burst EMP	4-1
4-2	Peak Magnetic Field B_Φ Vs. Overpressure at the Air/Ground Interface for Varying Ground Conductivities and Yields	4-2
4-3	Peak Radial Electric Field E_R Vs. Overpressure at the Air/Ground Interface for Varying Ground Conductivities and Yields	4-3
4-4	Peak Transverse Electric Field E_θ Vs. Overpressure at the Air/Ground Interface for Varying Ground Conductivities and Yields	4-4
4-5	B_Φ-Time Waveform at the Air/Ground Interface for Several Overpressure Levels	4-5
4-6	E_R-Time Waveform at the Air/Ground Interface for Several Overpressure Levels	4-6
4-7	E_θ-Time Waveform at the Air/Ground Interface for Several Overpressure Levels	4-7
4-8	Fourier Amplitude of B_Φ Waveform at the Air/Ground Interface for Several Overpressure Levels	4-8
4-9	Fourier Amplitude of E_R Waveform at the Air/Ground Interface for Several Overpressure Levels	4-9
4-10	Fourier Amplitude of E_θ Waveform at the Air/Ground Interface for Several Overpressure Levels	4-10
4-11	Uncertainty Bands ($\sigma = 1$) of the B_Φ Fourier Amplitude at the Air/Ground Interface	4-11
4-12	Uncertainty Bands ($\sigma = 1$) of the E_R Fourier Amplitude at the Air/Ground Interface	4-11
4-13	Uncertainty Bands ($\sigma = 1$) of the E_θ Fourier Amplitude at the Air/Ground Interface	4-12
4-14	E_r-Time Waveform of High-Altitude Radiated Signal	4-13
4-15	Fourier Amplitude of E_r Waveform of High-Altitude Radiated Signal	4-14
5-1	Fireball Temperature Vs. Radius at Early Times in the Fireball History	5-2
5-2	Fireball Density Vs. Radius at Early Times in the Fireball History	5-3
5-3	Late Fireball Temperature Vs. Radius	5-4
5-4	Temperature Vs. Time at High Peak Overpressures	5-5
6-1	Mean Transmittance for a Ground-Surface Target (1 of 5)	6-3
6-1	Mean Transmittance for a Ground-Surface Target (2 of 5)	6-4
6-1	Mean Transmittance for a Ground-Surface Target (3 of 5)	6-5
6-1	Mean Transmittance for a Ground-Surface Target (4 of 5)	6-6
6-1	Mean Transmittance for a Ground-Surface Target (5 of 5)	6-7
6-2	Visibility: Calculation of Mean and Coefficient of Variation	6-9
6-3	Clouds-Below Reflectance: Calculation of Mean and Coefficient of Variation	6-11
6-4	Fractional Radiant Exposure	6-13
6-5	Mean Normalizing Time	6-14
7-1	Composition of Shocks Due to Nuclear Airburst	7-1
7-2	Peak Overpressure at Thermally Near-Ideal Surfaces	7-4
7-3	Peak Overpressure at Thermally Nonideal Surfaces	7-5
7-4	Peak Overpressures at a Near-Ideal Surface, Very High Overpressure Region	7-6
7-5	Peak Overpressures at a Near-Ideal Surface, High Overpressure Region	7-7
7-6	Peak Overpressures at a Near-Ideal Surface, Low Overpressure Region	7-8
7-7	Peak Overpressures at a Near-Ideal or Thermally Nonideal Surface, Very Low Overpressure Region	7-9
7-8	Peak Overpressures at a Thermally Nonideal Surface, High Overpressure Region	7-10
7-9	Peak Overpressures at a Thermally Nonideal Surface, Low Overpressure Region	7-11
7-10	Peak Overpressure at the Surface from a Contact Surface Burst	7-12
7-11	High-Altitude Bursts, Peak Reflected Overpressure at Ground Zero as a Function of Scaled Slant Range	7-13
7-12	Blast Efficiency Factor for High-Altitude Bursts	7-14
7-13	Dynamic Pressure at a Perfect Surface	7-15
7-14	Dynamic Pressure at a Light Dust Surface	7-16
7-15	Dynamic Pressure at a Heavy Dust Surface	7-17
7-16	Peak Dynamic Pressure at an Ideal Surface	7-18
7-17	Peak Dynamic Pressure at a Surface with Light Dust Conditions	7-19
7-18	Peak Dynamic Pressure at a Surface with Heavy Dust Conditions	7-20
7-19	Duration of Positive Overpressure at a Near-Ideal Surface	7-22
7-20	Duration of Positive Overpressure at a Thermally Nonideal Surface	7-23
7-21	Duration of Positive Overpressure at the Surface	7-24
7-22	Duration of Positive Overpressure at the Surface	7-25
7-23	Duration of Positive Dynamic Pressure at the Surface	7-27
7-24	Duration of Positive Dynamic Pressure at a Dust-Free or Light-Dust Surface	7-28

Figure		*Page*
7-25	Duration of Positive Dynamic Pressure at a Heavy-Dust Surface	7-29
7-26	Positive Overpressure Waveforms for an Ideal Shock Wave in a Standard Sea Level Atmosphere	7-31
7-27	Positive Dynamic Pressure Waveforms for an Ideal Shock Wave in a Standard Sea Level Atmosphere	7-32
7-28	Typical Sequence of Overpressure Waveforms over Thermally Nonideal Surfaces	7-34
7-29	Type of Overpressure Waveform Developed over a Thermally Nonideal Surface	7-35
7-30	Typical Sequence of Dynamic Pressure Waveforms over Thermally Nonideal Surfaces	7-36
7-31	Positive Overpressure Impulse at a Near-Ideal Surface	7-37
7-32	Positive Overpressure Impulse at a Thermally Nonideal Surface	7-38
7-33	Positive Overpressure Impulse at a Near-Ideal Surface, Different Burst Heights	7-39
7-34	Positive Overpressure Impulse at a Nonideal Surface, Different Burst Heights	7-40
8-1	Vertical Velocity Waveforms for Soils at all Depths	8-5
8-2	Horizontal Velocity Waveforms for Soils at all Depths	8-6
8-3	Vertical Velocity Waveforms for Rock, Scaled Depth of 4.3 ft/kt$^{1/3}$ (1.31 m/kt$^{1/3}$)	8-7
8-4	Vertical Velocity Waveforms for Rock, Scaled Depths Below 30.8 ft/kt$^{1/3}$ (11.83 m/kt$^{1/3}$)	8-8
8-5	Horizontal Velocity Waveforms for Rock for all Depths	8-9
8-6	Ratios of Initial to Oscillatory Peak Particle Velocities	8-13
8-7	Characteristic Vertical Outrunning Waveforms	8-14
8-8	Normalized Horizontal Velocities for Clay over Shale and Sand over Sandstone Sites	8-16
9-1	Regions of Ground Shock	9-1
9-2	Attenuation of Scaled Acceleration—Dry Alluvium	9-5
9-3	Attenuation of Scaled Acceleration—Dry Tuff	9-6
9-4	Attenuation of Scaled Acceleration—Wet Tuff	9-7
9-5	Attenuation of Scaled Acceleration—Hard Rock	9-8
9-6	Attenuation of Particle Velocity—Dry Alluvium	9-9
9-7	Attenuation of Particle Velocity—Dry Tuff	9-10
9-8	Attenuation of Particle Velocity—Wet Tuff	9-11
9-9	Attenuation of Particle Velocity—Hard Rock	9-12
9-10	Attenuation of Scaled Displacement—Dry Alluvium	9-13
9-11	Attenuation of Scaled Displacement—Dry Tuff	9-14
9-12	Attenuation of Scaled Displacement—Wet Tuff	9-15
9-13	Attenuation of Scaled Displacement—Hard Rock	9-16
9-14	Pulse Shape Parameters	9-18
10-1	Typical Crater from a Near-Surface Explosion	10-2
10-2	Apparent Crater Dimensions for Dry Soil or Soft Rock (≤ 10% Water Content)	10-3
10-3	Apparent Crater Dimensions for Wet Soil or Soft Rock (> 10% Moisture Content)	10-4
10-4	Apparent Crater Dimensions for Dry Hard Rock (≤ 3% Moisture Content)	10-5
10-5	Apparent Crater Dimensions for Wet Hard Rock (> 3% Moisture Content)	10-6
10-6	Enhancement of Single-Charge Apparent Crater Dimensions in a Row Crater as a Function of Charge Spacing at Optimum DOB in Soil	10-9
10-7	Enhancement in True-Crater Dimensions for Nail-Driving	10-11
11-1	Ejection Angle Distribution for High-Yield Surface Bursts	11-3
12-1	Ejecta Depth Prediction Curves for Nuclear Events, $\leq R/_{V_a}1/3 \leq 12$ (1 of 2)	12-2
12-1	Ejecta Prediction Curves for Nuclear Events, $0 \leq R/_{V_a}1/3 \leq 40$ (2 of 2)	12-3
12-2	High-Yield Nuclear Surface-Burst Cratering Efficiencies in Layered Geologies, Soil Over Soft Rock With Water Table	12-7
12-3	High-Yield Nuclear Surface-Burst Cratering Efficiencies in Layered Geologies, Soil Over Hard Rock With Water Table	12-8
12-4	High-Yield Nuclear Surface-Burst Cratering Efficiencies in Layered Geologies, Alluvial Soil Over Hard Rock Basement With Water Table	12-9
12-5	Scaled Ejecta Depth vs. Cratering Efficiency at 600- and 1000-PSI Levels	12-10
12-6	Scaled Median Ejecta Depth vs. Cratering Efficiency at Varying Levels	12-11
13-1	Mean Vertical Settlement Speed of Dust Particles	13-3
13-2	Mean Settle-Out Time of Dust Particles—Base Surge	13-4
15-1	Idealized Early Fallout Dose-Rate Contour (DNA, 1972)	15-1
15-2	Downwind Distance and Fallout Radiation at t = 1 hr After Burst as a Function of Yield, 10-Knot Effective Wind	15-2
15-3	Downwind Distance and Fallout Radiation at t = 1 hr After Burst as a Function of Yield, 20-Knot Effective Wind	15-3
15-4	Downwind Distance and Fallout Radiation at t = 1 hr After Burst as a Function of Yield, 40-Knot Effective Wind	15-4

Figure		*Page*
15-5	Maximum Width and Fallout Radiation at t = 1 hr After Burst as a Function of Yield, 10-Knot Effective Wind	15-5
15-6	Maximum Width and Fallout Radiation at t = 1 hr After Burst as a Function of Yield, 20-Knot Effective Wind	15-6
15-7	Maximum Width and Fallout Radiation at t = 1 hr After Burst as a Function of Yield, 40-Knot Effective Wind	15-7
15-8	Distance to Maximum Width and Fallout Radiation at t = 1 hr After Burst as a Function of Yield, 10-Knot Effective Wind	15-8
15-9	Distance to Maximum Width and Fallout Radiation at t = 1 hr After Burst as a Function of Yield, 20-Knot Effective Wind	15-9
15-10	Distance to Maximum Width and Fallout Radiation at t = 1 hr After Burst as a Function of Yield, 40-Knot Effective Wind	15-10
15-11	Ground Zero Width and Fallout Radiation at t = 1 hr After Burst as a Function of Yield	15-11
15-12	Height of the Stabilized Cloud Bottom as a Function of Yield	15-12
15-13	Height of the Stabilized Cloud Top as a Function of Yield	15-13
15-14	Typical Hodograph of a Vertical Wind Structure	15-14
15-15	Minimum Height of Burst Below Which Fallout Occurs as a Function of Yield	15-15
15-16	Height of Burst Adjustment Factors for Various Yields	15-16
15-17	Fission Product Decay Factors Normalized to Unity at 1 Hour After Detonation	15-17
15-18	Normalized Dose Accumulated in a Fallout Contaminated Area From H + 1 Hour to H + 1000 Days	15-18

CHAPTER 1
INTRODUCTION

1-1. General.

a. This series of manuals, entitled Designing Facilities to Resist Nuclear Weapon Effects, is organized as follows:

TM 5-858-1	Facilities System Engineering
TM 5-858-2	Weapon Effects
TM 5-858-3	Structures
TM 5-858-4	Shock Isolation Systems
TM 5-858-5	Air Entrainment, Fasteners, Penetration Protection, Hydraulic-Surge Protective Devices, EMP Protective Devices
TM 5-858-6	Hardness Verification
TM 5-858-7	Facility Support Systems
TM 5-858-8	Illustrative Examples

A list of references pertinent to each manual is placed in an appendix. Additional appendixes and bibliographies are used, as required, for documentation of supporting information. Pertinent bibliographic material is identified in the text with the author's name placed in parentheses. Such bibliographic material is not necessary for the use of this manual; the name and source of publications related to the subject of this manual is provided for information purposes.

b. The purpose of this series of manuals is to provide guidance to engineers engaged in designing facilities that are required to resist nuclear weapon effects. It has been written for systems, structural, mechanical, electrical, and test engineers possessing state-of-the-art expertise in their respective disciplines, but having little knowledge of nuclear weapon effects on facilities. While it is applicable as general design guidelines to all Corps of Engineers specialists who participate in designing permanent military facilities, it has been written and organized on the assumption a systems-engineering group will coordinate design of the facilities.

c. Technical Manual 5-858 addresses only the designing of hardened facilities; other techniques to achieve survival capacity against nuclear weapon attacks are deception, duplication, dispersion, nomadization, reconstitution, and active defense. A facility is said to be hardened if it has been designed to directly resist and mitigate the weapon effects. Most of the hardening requirements are allocated to the subsidiary facilities, which house, support, and protect the prime mission materiel/personnel (PMMP). This manual is applicable to permanent facilities, such as those associated with weapon systems, materiel stockpiles, command centers, manufacturing centers, and communications centers.

d. The nuclear weapon threats considered are listed below. Biological, chemical, and conventional weapon attacks are not considered.

- Weapons aimed at the facility itself or at nearby targets
- A range from many, relatively small-yield weapons to a single super-yield weapon
- Weapon yields from tens of kilotons to hundreds of megatons
- Weapon delivery by aerial bombing, air-to-surface missile, surface-to-surface missile, or satellite-launched vehicle
- Detonation (burst) of a weapon in the air, at the ground surface, or beneath the ground surface
- Direct-overhead bursts for a deep-buried facility
- Near-miss bursts for a near-surface facility, producing peak over-pressures from tens to thousands of psi at the facility

e. The designing of facilities resistant to nuclear weapon effects is an evolving specialty that uses a relatively narrow data base that incorporates both random and systematic uncertainties. The range of these uncertainties may vary from significant (order of 1 to 2 magnitudes) to normal (10% to 100% variation from average values). The applicable uncertainty value depends on the specific weapon effect or hardening objective under consideration. Loading uncertainty is generally more significant than resistance uncertainty. Awareness of the appropriate uncertainty factor is essential not only for system engineering trade-offs but in the utilization of available analysis or test procedures. Studies and experiments are being conducted to improve methodology, to better define random uncertainties, and to reduce systematic uncertainties. This manual will be revised as significant improvements occur in either methodology or data base.

1-2. TM 5-858-2: Weapon effects.

This manual presents the 13 weapon effects that act as the facility "loads." Each effect is described by its expected value, its random coefficient of variation, and its systematic coefficient of variation. Uncertainties in the weapon, the weapon delivery, the site, and other factors are considered. The effects data are presented both graphically and analytically.

CHAPTER 2
NUCLEAR-WEAPON EFFECTS

2-1. High explosive and nuclear-weapon effects.

a. A nuclear explosion produces 13 potentially destructive effects, or environments, that must be accounted for during facility design:

- Initial nuclear radiation
- Electromagnetic pulse (EMP)
- Fireball
- Thermal radiation
- Airblast
- Airblast-induced ground shock
- Crater-induced ground shock
- Crater
- Ejecta/debris impact
- Ejecta/debris depth
- Dust
- Firestorm
- Residual nuclear radiation

With the exception of the first and last, the nuclear radiations, these effects are also produced by a high-explosive (HE) explosion. Even an HE explosion can produce the electromagnetic pulse and the mushroom-shaped cloud that are commonly identified with nuclear explosion. The gross non-nuclear effects produced by the two types of explosions are so similar that the explosive energy of a nuclear explosion is also expressed in terms of an equivalent TNT-charge weight.

b. This equivalent TNT-charge weight is referred to as the explosive energy release, or yield, W. A facility designed to withstand the effects produced by an HE explosion would be quite similar to a facility designed to withstand the effects produced by a nuclear explosion of equivalent yield. This statement is true for peak overpressure larger than a few tens of psi, which are the hardness levels addressed in this volume.

c. Since the protective measures required for the non-nuclear effects also provide, in general, sufficient protection against nuclear radiation, the protective measures required for the two facilities would be of the same kind—but would differ drastically in degree when the effects are produced by weapons of war. HE weapons (e.g., conventional bombs) have yields of only several tons or less, whereas state-of-the-art nuclear weapons range in yield from a few kilotons to a few tens of megatons. The potential destructiveness of a weapon at a given distance varies between $W^{1/3}$ and W, depending on the particular weapon effect under consideration. Thus, a small state-of-the-art nuclear weapon is 10 to 1000 times more destructive than the largest HE weapon, and a large nuclear weapon, 1000 to 1,000,000 times more destructive. It is this much larger magnitude of potential destructiveness that creates disparity between hardening against nuclear weapons and hardening against conventional HE weapons.

2-2. Nuclear weapons.

Nuclear weapons include atomic and thermo-nuclear weapons. The explosive energy of an atomic weapon results from the fission of uranium and plutonium; the yields of atomic weapons are tens of kilotons or less. A thermo-nuclear weapon employs both fission and fusion reactions to obtain a very large yield. An ordinary nuclear weapon of either basic type can be modified to produce an "enhanced" weapon, e.g., the output of the weapon can be channeled to produce relatively large amounts of nuclear radiation, or if the weapon is so designed, it may enter the earth prior to detonation resulting in a buried or partially buried detonation.

2-3. Burst elevations.

a. The burst elevation of a nuclear weapon can be classifed as follows:

100,000 ft	<	High-altitude burst	<	
3500 ft/$Mt^{0.4}$	<	Air burst	<	100,000 ft
0	<	Low-altitude burst	<	3500 ft/$Mt^{0.4}$
		Contact burst	≈	0
−1000 ft/$Mt^{0.25}$	<	Shallow-buried burst	<	0
		Deep-buried burst	<	−1000 ft/$Mt^{0.25}$

Note the following characteristics. Air burst: Fireball does not touch the ground. Contact burst: Center of gravity of weapon is slightly above the surface; some penetration required with true surface burst in which c.g. is at ground surface. Deep-buried burst: Completely contained and does not vent to the atmosphere.

b. State-of-the-art weapons cannot penetrate to sufficient depths to result in a deep-buried burst, i.e., a contained burst. High-altitude and air bursts generally are not effective burst elevations for the higher hardness levels considered in this volume. However, there may be threat scenarios that would require the consideration of these burst elevations; their effects are selectively included in this volume. Low-altitude bursts, contact bursts, and shallow-buried bursts pose the greatest threat. They are collectively referred to in this volume as near-surface bursts.

2-4. Weapon effect, a random variable.

a. Parameters. The specification of a weapon effect for use during the designing of a facility requires that the following basic parameters be quantified:

- Weapon design
- Weapon yield
- Burst elevation
- Slant range
- Weather and atmospheric conditions
- Geologic factors

Because of the uncertainty associated with these basic parameters, it is necessary to treat them, and thus the weapon effects, as random variables.

b. Definition of a random variable. A random variable X is a numerical variable, the specific value of which cannot be predicted with certainty. Every specific value of the random variable X, denoted by x, represents a possible outcome of the random phenomenon under consideration.

c. Density function. The probability density function of X, denoted by $f_X(x)$, describes the relative likelihood of the various outcomes of X. It is defined such that

$$\int_{-\infty}^{\infty} f_X(x)\,dx = 1.0 \qquad (2\text{-}1)$$

where $f_X(x)\,dx$ represents the likelihood of X being between x and x + dx. This relative likelihood or relative frequency of occurrence is known as the probability of $x < X < x + dx$, i.e.,

$$P(x < X < x + dx) = f_X(x)\,dx \qquad (2\text{-}2)$$

Also, note the probability that $x_1 < X < x_2$ is

$$P(x_1 < X < x_2) = \int_{x_1}^{x_2} f_X(x)\,dx \qquad (2\text{-}3)$$

d. Mean and variability of a random variable. The mean (the average, or expected) value of the random variable X is

$$\mu_X = \int_{-\infty}^{\infty} x\, f_X(x)\,dx \qquad (2\text{-}4)$$

A useful measure of the randomness, or variability, of the random variable X is its coefficient of variation:

$$\delta_X = \sigma_X/\mu_X \qquad (2\text{-}5)$$

where σ_X is the standard deviation of X and is equal to

$$\sigma_X = \left| \left[\int_{-\infty}^{\infty} (x - \mu_X)^2 f_X(x)\,dx \right]^{1/2} \right| \qquad (2\text{-}6)$$

e. Evaluation of probabilities. In general, obtain the probability of $x_1 < X < x_2$ from equation 2-3. For a number of special density functions, these probabilities are tabulated in reference books. (see, for example, Abramowitz, 1972). As an example, for a Gaussian or normal density function

$$f_X(x) = \frac{1}{\sigma_X\sqrt{2\pi}} \exp\left[-0.5(x - \mu_X)^2/\sigma_X^2 \right] \qquad (2\text{-}7)$$

Letting z denote the number of standard deviations above mean, one obtains

$$P(z) = P(X \leq \mu_X + z\sigma_X) = \int_{-\infty}^{\mu_X + z\sigma_X} \frac{1}{\sigma_X\sqrt{2\pi}} \exp \left[-0.5\,(x - \mu_X)^2/\sigma_X^2\right] dx = \int_{-\infty}^{z} \frac{1}{\sqrt{2\pi}} \exp\left[-\frac{u^2}{2}\right] du \qquad (2\text{-}8)$$

where transformation $u = (x - \mu_X)/\sigma_X$ is used. Values of this integral for a number of values of z are given below.

z	P(z)
0	0.500
0.1	0.540
0.25	0.599
0.50	0.691
0.75	0.773
1.00	0.841
2.50	0.994
5.00	0.999

The above table may be used to evaluate other probabilities for the Gausian distribution; for example:

$$P(-z) = 1 - P(z)$$

$$P(\mu_X + z_1\sigma_X < X < \mu_X + z_2\,\sigma_X) = P(z_2) - P(z_1)$$

f. Accounting for uncertainties: A single variable. The uncertainty associated with a random variable is due to two factors: (1) the natural or inherent randomness of the random variable itself, and (2) errors which result from the inability to accurately estimate the mean, the standard deviation, or the density function of the random variable. The latter may result, for example, from lack of sufficient data. To account for both uncertainties the random variable X is written as

$$X = N_X \hat{X} \tag{2-9}$$

where X is the random variable as represented by the available data and has a mean $\bar{x}$ and a coefficient of variation δ_X which are estimated from the data. N_X is a random correction factor which is included to model the estimation errors. Its mean value $\bar{N}_X$ represents the bias in data, whereas its coefficient of variation Δ_X is a measure of the uncertainty resulting from estimation errors. As a first approximation Δ_X is considered as the error in estimation of the mean value $\bar{x}$. The mean value of the random variable X is evaluated from

$$\mu_x = \bar{N}_X \bar{x} \tag{2-10}$$

However, if an unbiased set of data is used to evaluate $\bar{x}$, then $N_X = 1.0$ and

$$\mu_X = \bar{x} \tag{2-11}$$

i.e., for an unbiased set of data, $\bar{x}$ is the best estimate of the actual mean. The total coefficient of variation of X, designated by Ω_X, is obtained from

$$\Omega_X = \sqrt{\delta_X^2 + \Delta_X^2} \tag{2-12}$$

Here, δ_X models the natural randomness of X, whereas Δ_X represents the uncertainty arising from errors in estimation. As an example, when a set of n unbiased samples are available, it is usually assumed that

$$\Delta_X = (1/\sqrt{n})\, \delta_X. \tag{2-13}$$

g. Accounting for uncertainties: Multiple variables. If X itself is a function of several random variables,

$$X = f(Y_1, Y_2, Y_3, \ldots, Y_n, \ldots, Y_N) \tag{2-14}$$

then using first-order linear approximations (Ang-Cornell, 1974)

$$\bar{x} = f(\bar{y}_1, \bar{y}_2, \bar{y}_3, \ldots, \bar{y}_n, \ldots, \bar{y}_N) \tag{2-15}$$

and

$$\Omega_X^2 = \Omega_f^2 + \sum_{n=1}^{N} \frac{\bar{y}_n^2}{\bar{x}^2} \left(\frac{\partial f}{\partial Y_n} \right)_o^2 \Omega_{Y_n}^2 - \sum_{n \neq m}^{N} \sum^{N} \frac{\bar{y}_n \bar{y}_m}{\bar{x}^2} \left(\frac{\partial f}{\partial Y_n} \frac{\partial f}{\partial Y_m} \right)_o \varrho_{nm} \Omega_{Y_n} \Omega_{Y_m} \tag{2-16}$$

where

Ω_f = Total coefficient of variation associated with the functional form of X

$$= \sqrt{d_f^2 = \Delta_f^2}$$

Ω_{Y_n} = Total coefficient of variation associated with Y_n

$$= \sqrt{\delta_{Y_n}^2 + \Delta_{Y_n}^2}$$

ϱ_{nm} = Correlation coefficient of Y_n and Y_m, $-1 \leq \varrho_{nm} \leq 1$

The subscript "o" in equation 2-16 denotes that $\partial f / \partial Y_n$ is to be evaluated at the mean values of the variables. Implicit in equations 2-15 and 2-16 are the assumptions that $\Omega_{Y_n}^2 << 1$ and the nonlinearity in f near the mean values is not large. In this manual, both symbols Ω or Ω^2 are called "uncertainty" to avoid the repetitive use of the term "uncertainty squared."

h. Distributions. If a particular distribution is defined, the uncertainty can be calculated in terms of the upper and lower bounds assigned to the data. For example, suppose that data are presented within bounds that are said to include 95% of the data. If the data are assumed to have a Gaussian distribution, the bounds correspond to the $\pm$ two-standard deviation limits (see *e* above). Procedures for a number of specific distributions are described in the following paragraphs.

(1) *Normal*: The coefficient of variation of a normal distribution is

$$\delta_x = \frac{1}{n} \left(\frac{R - 1}{R + 1} \right) \tag{2-17}$$

where $R = L_2/L_1$, and L_1 and L_2 are the lower and upper bounds corresponding to n standard deviations on either side of the mean.

(2) *Log-normal*: The coefficient of variation of a log-normal distribution is

$$\delta_x = \left[\exp \left[\frac{(ln R)^2}{4n^2} \right] - 1 \right]^{1/2} \tag{2-18}$$

where $R = k^2$, $k = \bar{x}/L_1$ or $k = L_2/\bar{x}$, and L_1 and L_2 are the lower and upper bounds of the distribution. The quantity n is that number of standard deviations of the bounds from that log mean.

(3) *Uniform*: The coefficient of variation of a uniform distribution is

$$\delta_x = \frac{1}{\sqrt{3}} \sqrt{\frac{L_2 - L_1}{L_2 + L_1}} \tag{2-19}$$

where L_1 and L_2 are the lower and upper bounds of the data.

(4) *Log-Uniform*: The coefficient of variation of a log-uniform distribution is

$$\delta_x = \left\{ \left(\frac{1}{2} \ln \frac{L_2}{L_1} \right) \left(\frac{L_2 + L_1}{L_2 - L_1} \right) - 1 \right\}^{1/2} \qquad (2\text{-}20)$$

where L_1 and L_2 are the lower and upper bounds of the data.

i. Uncertainty in nuclear weapon effects. Uncertainties in nuclear weapon effects arise from yield, delivery accuracy, weapon capability (air bursts, penetrating bursts), as well as from imperfect knowledge of specific effects for known yield, range, etc. In the following chapters an attempt is made to identify the level of uncertainty of our knowledge of weapon effects. The uncertainties relative to weapon yield, range, and burst conditions are defined, but since they are considered a part of threat definition they are not quantified; however, provision is made for incorporating uncertainties in these parameters from threat definition applicable to specific problems.

CHAPTER 3
INITIAL NUCLEAR RADIATION

3-1. Gross phenomenology.

a. A nuclear explosion is accompanied by the emission of nuclear radiations consisting of gamma rays, neutrons, beta particles, and alpha particles. The range of beta and alpha particles is so short that they can be neglected in the estimate of the initial radiation. The initial nuclear radiation is considered to be composed of neutron and gamma ray radiation from both initial effects ($t < 1$ minute) and secondary interactions. Because induced radioactivity (a threat to personnel for many hours) begins during $t < 1$ min, it is included in this chapter.

b. The basic variables affecting the destructiveness of initial nuclear radiation are:

- Weapon design
- Weapon yield
- Burst elevation
- Slant range
- Atmospheric conditions

The destructiveness of the initial nuclear radiation will be enhanced by any of the following: Larger weapon yield, higher burst, smaller slant range.

c. The primary direct effect of nuclear radiation is an antipersonnel effect. Direct nuclear radiation effects on equipment and materials are less significant, but certain detector materials and electronic components can be damaged. The designer must either design for these effects (by shielding, for example) or he must preclude them (by burial, for example). The two significant aspects of initial nuclear radiation, neutron radiation and gamma ray radiation, are considered separately.

3-2. Neutron radiation.

a. Initial. The weapon type will have an influence on the energy spectrum of the source radiation. The location of the weapon source (and the target) will also affect the spectrum. (Specific situations relating these parameters are too numerous and specialized for presentation here; however, such information can be found in the report prepared by SAI, 1971). Only initial neutron radiation effects (occurring within 1 minute after detonation) are considered in this chapter; residual neutron effects (after 1 minute) are discussed in chapter 15.

b. Equipment. The vulnerabilities of electronic equipment are expressed in terms of fluence spectra (i.e., incident neutrons/in.^{2} or neutrons/cm^2 at various energy levels expressed in MeV). Typically, fluence spectra are presented in charts of the kind shown in figure 3-1, which are based on the weapon (source) spectrum and the attenuation characterization of the standard atmosphere.

c. Personnel. Personnel injury resulting from radiation exposure is complex and numerous (Glasstone, 1977). If the type of weapon treat is known and if the slant range is less than 5000 yd (4572 m), it is possible to quickly estimate the neutron does to personnel regardless of the spectral content of the pulse. For low-altitude atmosphere bursts, where personnel are located on or near the earth's surface, the neutron dose absorbed by human tissue is (DNA, 1972).

$$D_N = \frac{WF_N H_1}{R^2} \text{ rad (J/kg)} \qquad (3\text{-}1)$$

where

W = Weapon yield, kt
R = Slant range, yd (m)
F_N = Normalized neutron dose, yd^2 rad/kt[m^2 (J/kg)/kt]
H_1 = Burst height correction factor

(1) The mean value of equation 3-1 is calculated by referring to figures 3-2 through 3-5 (which show the relationship between F_N and R), and to figure 3-6 (which shows the relationship between H_1 and the height of burst) for the standard division (DNA, 1972) of weapon types, I through VIII.

(2) The uncertainty associated with equation 3-1 is

$$\Omega^2_{D_N} = \Omega^2_f + \Omega^2_W + \Omega^2_{F_N} + \Omega^2_{H_1} + 4\,\Omega^2_R \qquad (3\text{-}2)$$

where Ω_f is the uncertainty of the functional form of equation 3-1, Ω_W is the uncertainty of the yield, etc. Consider that $\Omega_f \approx 0.2$, $\Omega_{F_N} = 0.30$; using equation 2-19 and the assumption that figures 3-2 through 3-5 represent mean values of data uniformly distributed with upper and lower bounds within $\pm 25\%$ of the mean (from DNA, 1972) and $\Omega_{H_1} \approx 0.3$. Thus, equation 3-2 reduces to

$$\Omega^2_{D_N} = 0.22 + \Omega^2_W + 4\,\Omega^2_R \qquad (3\text{-}3)$$

3-3. Gamma radiation.

a. Prompt and delayed. Gamma radiation can be divided into two components: Prompt (within 1 or 2 shakes, a shake being equal to 10^{-8} sec), and delayed (up to 1 min). Electronic equipment is sensitive to the energy spectrum of the radiation—only prompt dosage is calculated; personnel are influenced primarily by

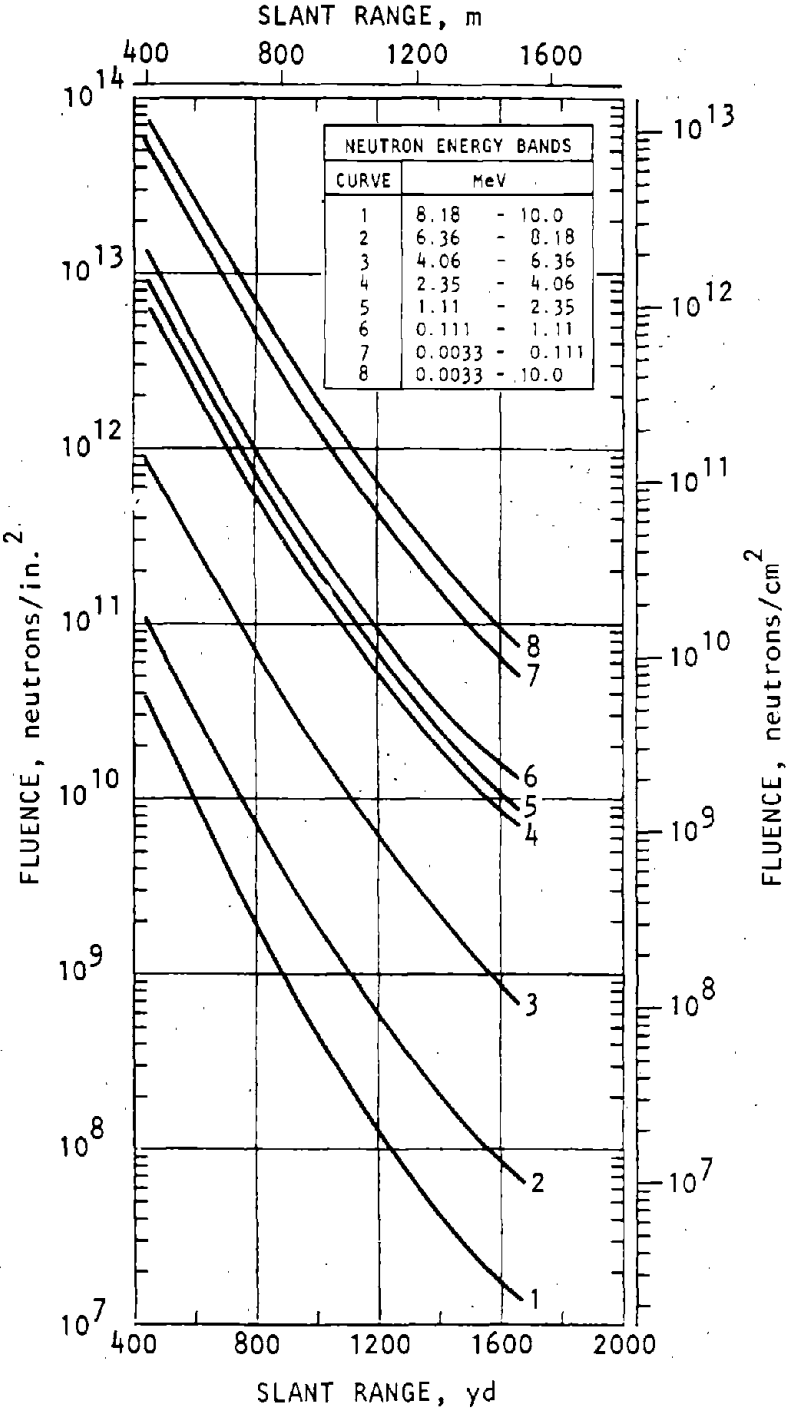

Figure 3–1. Typical Neutron Fluence Incident on a Receiver Located on or near the Surface of the Earth (DNA, 1972)

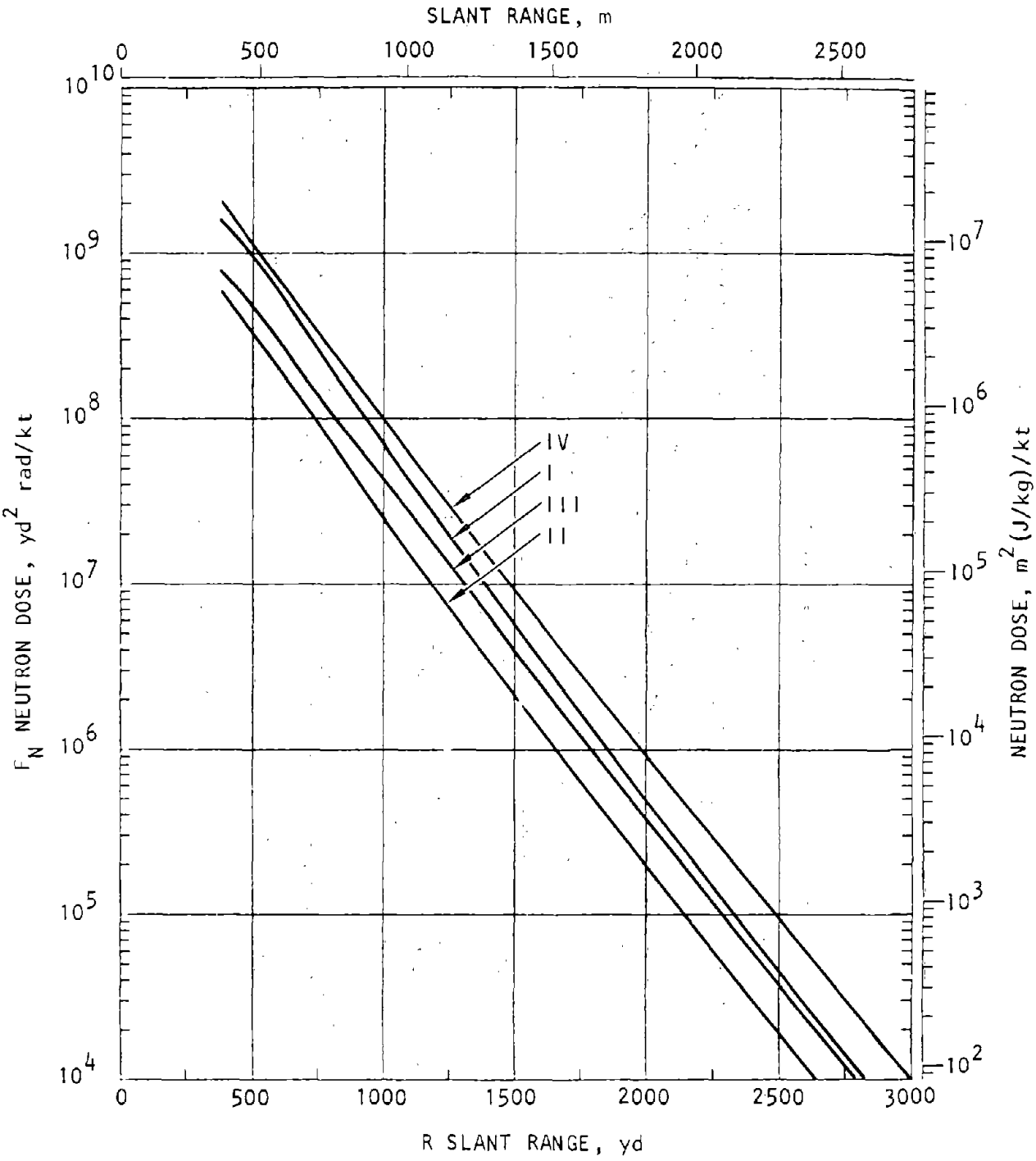

Figure 3–2. Neutron Dose F_N as a Function of Slant Range from a 1-kt Surface Burst, Weapon Types I through IV, Short Ranges (DNA, 1972)

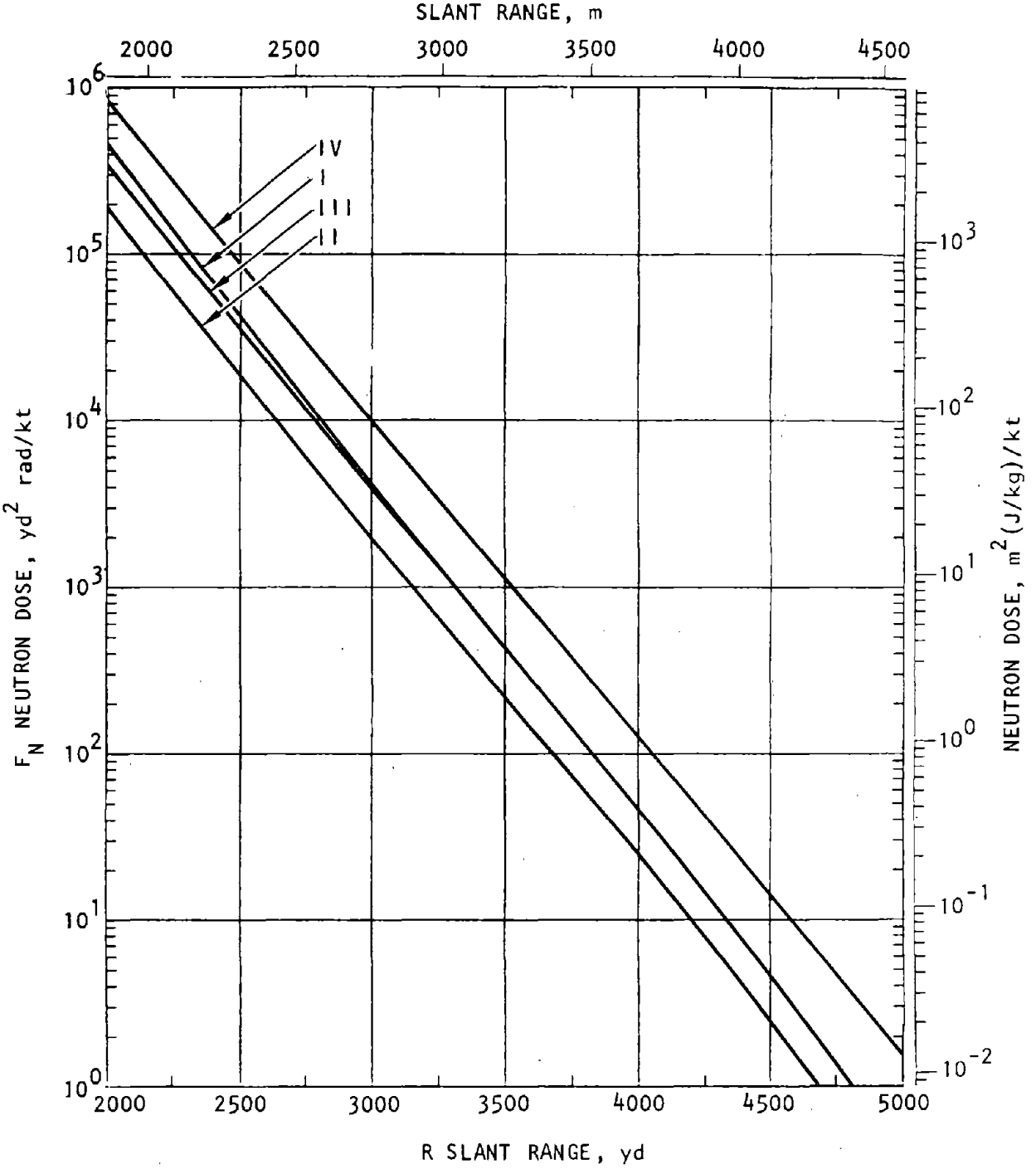

Figure 3–3. Neutron Dose F_N as a Function of Slant Range from a 1-kt Surface Burst, Weapon Types I through IV, Long Ranges (DNA, 1972)

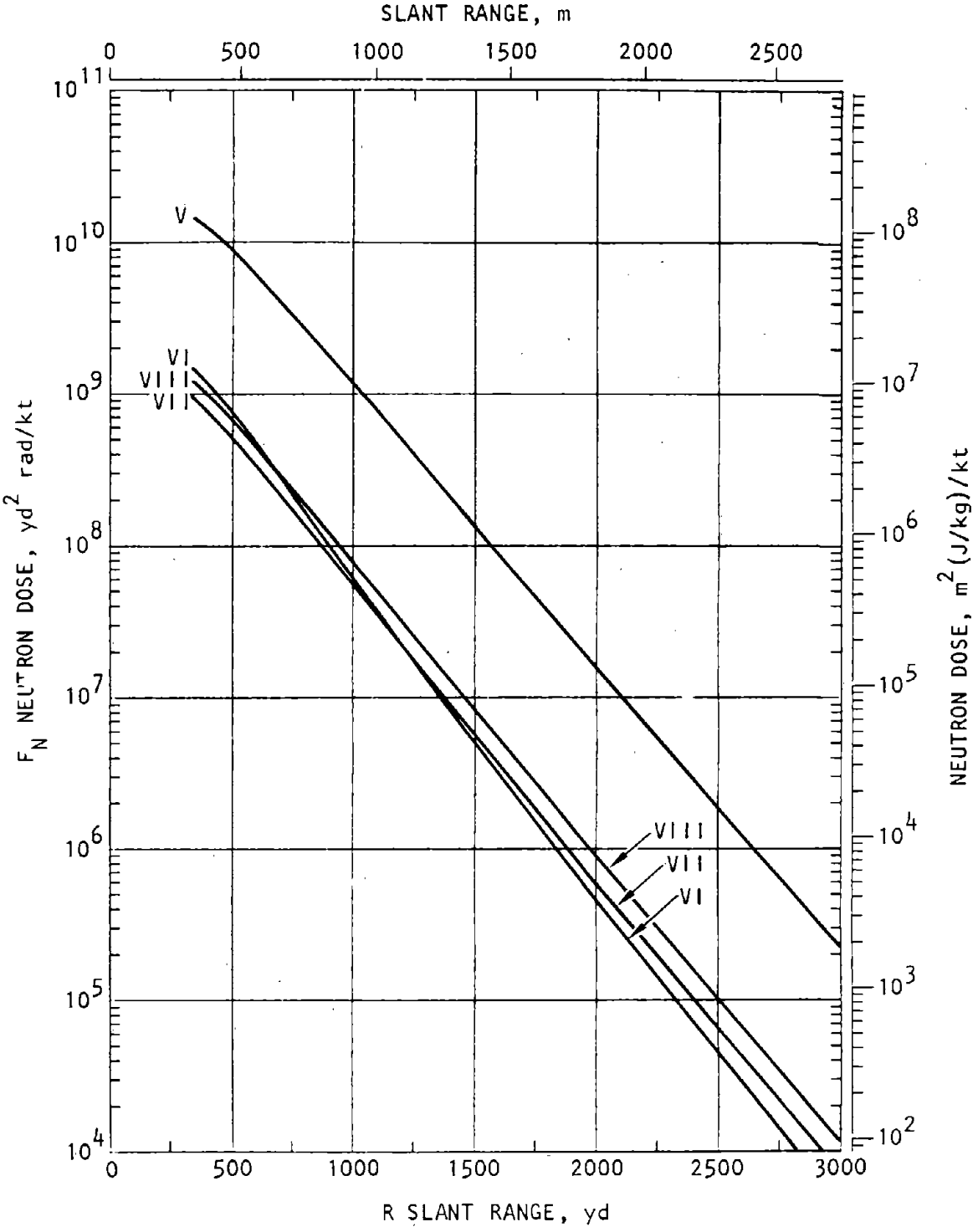

Figure 3–4. Neutron Dose F_N as a Function of Slant Range from a 1-kt Surface Burst, Weapon Types V through VIII, Short Ranges (DNA, 1972)

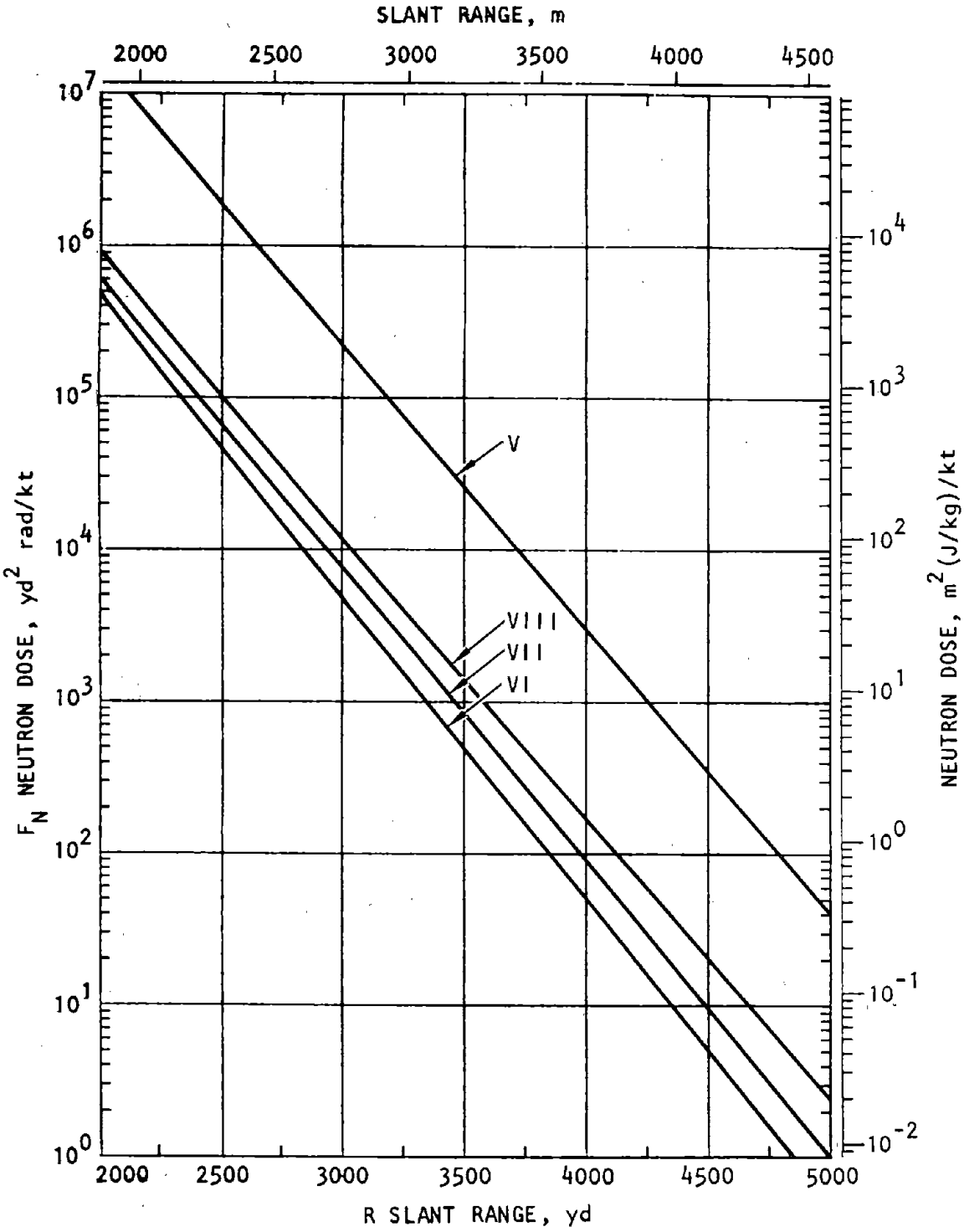

Figure 3–5. Neutron Dose F_N as a Function of Slant Range from a 1-kt Surface Burst, Weapon Types V through VIII, Long Ranges (DNA, 1972)

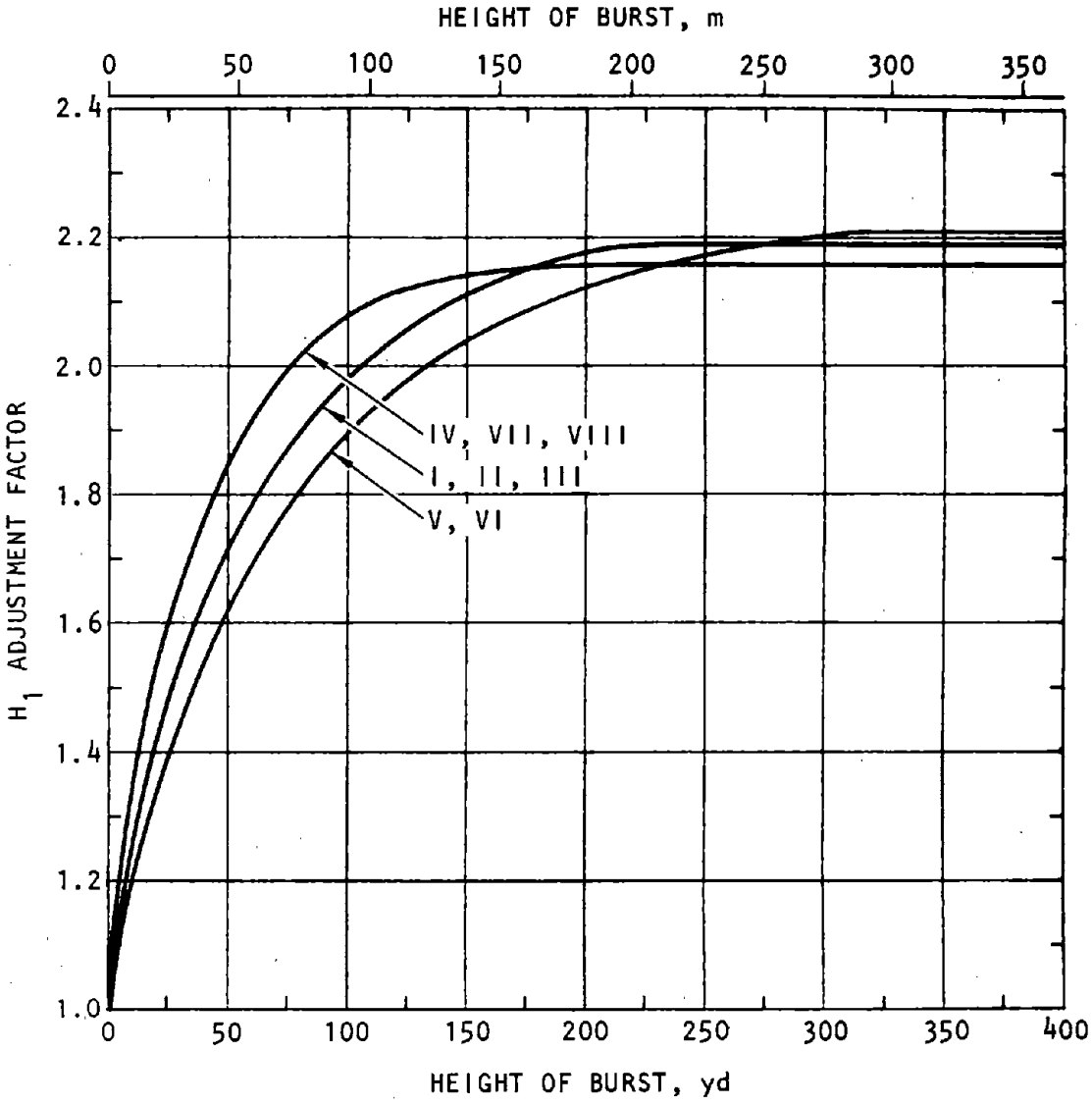

Figure 3-6. Burst Height Adjustment Factors H_1 for Neutrons and Secondary Gamma Rays (DNA, 1972)

the total dose absorbed—both prompt and delayed effects are important because the effect is cumulative.

b. Prompt gamma ray dose on equipment. Prompt gamma radiation that effects electronic equipment can be expressed by an equation of the form

$$D_{\gamma p} = \frac{K_1 W}{R^2} \exp(K_2 \varrho R) \text{ rad (J/kg)} \qquad (3\text{-}4)$$

where

K_1, K_2 = Constants
W = Yield in kt
R = Slant range in cm
ϱ = Air density in gm/cm^3

Other sources of gamma rays include inelastic scattering of neutrons and the decay of fission products. These sources depend primarily on weapon design (SAI, 1971). Equation 3-4 will generally apply to materials with atomic number 20 or less.

(1) The magnitude of the constants in equation 3-4 should be determined from the upper bound estimates of the prompt gamma ray flux equation ($\Phi_{\gamma p}$). Moreover, the source energy density MeV/cm^2 should be converted to absorbed energy expressed in rays (by the conversion factor presented in the reference), and the result multiplied by 2 shakes to obtain the prompt gamma ray dose.

(2) The uncertainty associated with equation 3-4 is expressed by

$$\Omega^2_{D_{\gamma p}} = \Omega^2_f + \Omega^2_{K_1} + \Omega^2_W + K_2^2 \varrho^2 R^2 \Omega^2_\varrho + (RK_2\varrho - 2)^2 \Omega^2_R \qquad (3\text{-}5)$$

where Ω_f is the uncertainty in the form of equation 3-4, Ω_W is the uncertainty in the yield, etc. Assume that $\Omega_f \approx 0.2$, $\Omega_\varrho \approx 0.05$, and that $\Omega_{K_1} = 0.3$ (using equation 2-19 and the assumption (DNA, 1972) that the bounds are within $\pm$ 33% of the mean).

c. Secondary gamma ray dose on personnel. In addition to the neutron dose described in paragraph 3-2 *c*, secondary gamma rays and fission-product gamma rays will be significant to personnel. If the type of weapon is known and if the slant range is less than 5000 yd (4572 m), it is possible to estimate the secondary gamma ray dose. For a low-altitude burst in a standard atmosphere where the personnel are located on or near the earth's surface, the secondary gamma ray dose is

$$D_{\gamma s} = \frac{WF_{\gamma s}H_1}{R^2} \text{ rad (J/kg)} \qquad (3\text{-}6)$$

where

W = Weapon yield, kt
$F_{\gamma s}$ = Normalized secondary gamma ray dose, yd^2 rad/kt ($[m^2(J/kg)/kt]$)
H_1 = Detonation height correction factor
R = Slant range, yd (m)

(1) The mean values of equation 3-6 are calculated by referring to figures 3-6 through 3-10 for the standard division of weapon types (DNA, 1972), I through VIII.

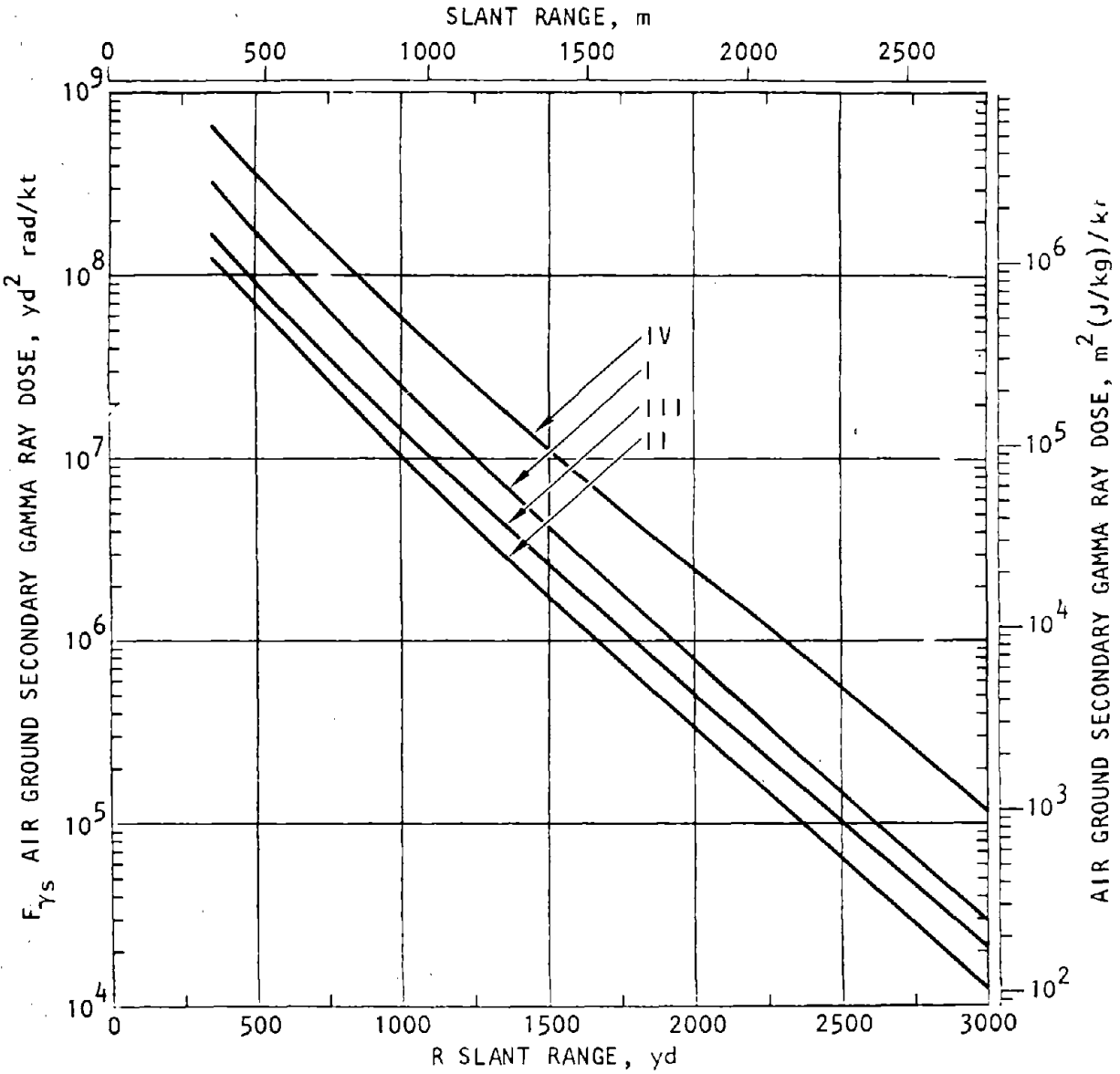

Figure 3-7. Secondary Gamma Ray Dose $F_{\gamma s}$ as a Function of Slant Range from a 1-kt Surface Burst, Weapon Types I through IV, Short Ranges (DNA, 1972)

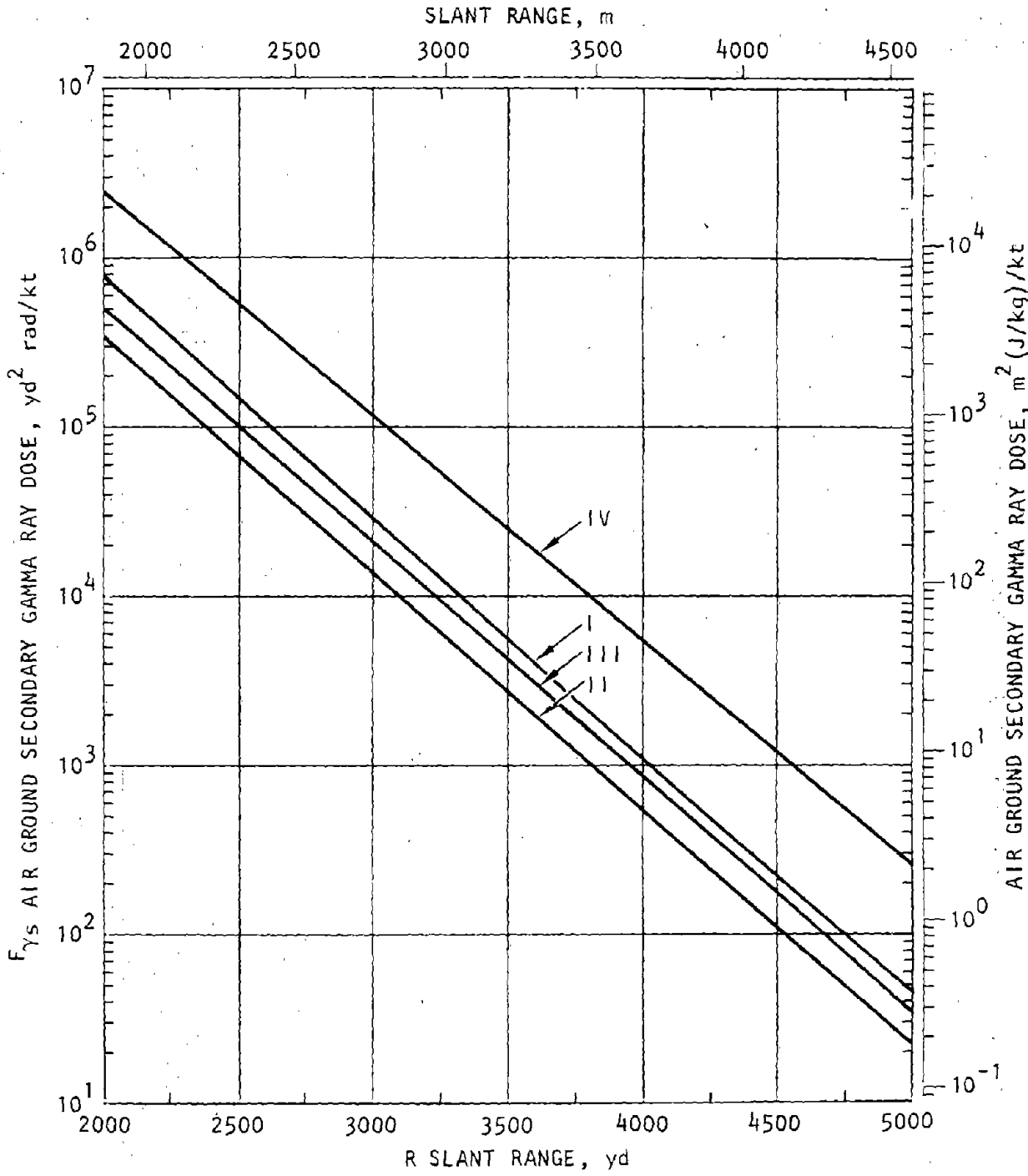

Figure 3-8. Secondary Gamma Ray Dose $F_{\gamma s}$ as a Function of Slant Range from a 1-kt Surface Burst, Weapon Types I through IV, Ranges (DNA, 1972)

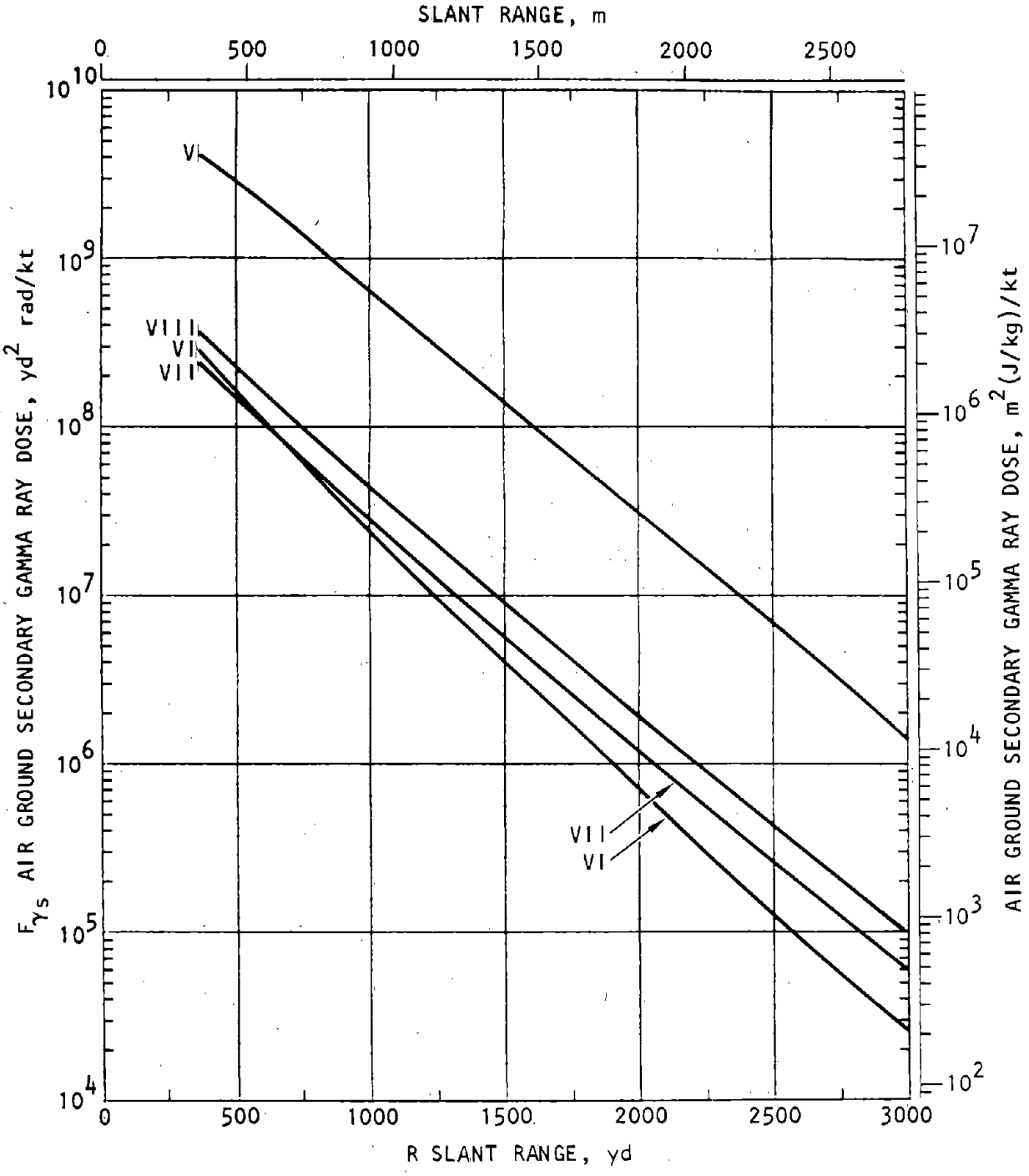

Figure 3-9. Secondary Gamma Ray Dose $F_{\gamma s}$ as a Function of Slant Range from a 1-kt Surface Burst, Weapon Types V through VIII, Short Ranges (DNA, 1972)

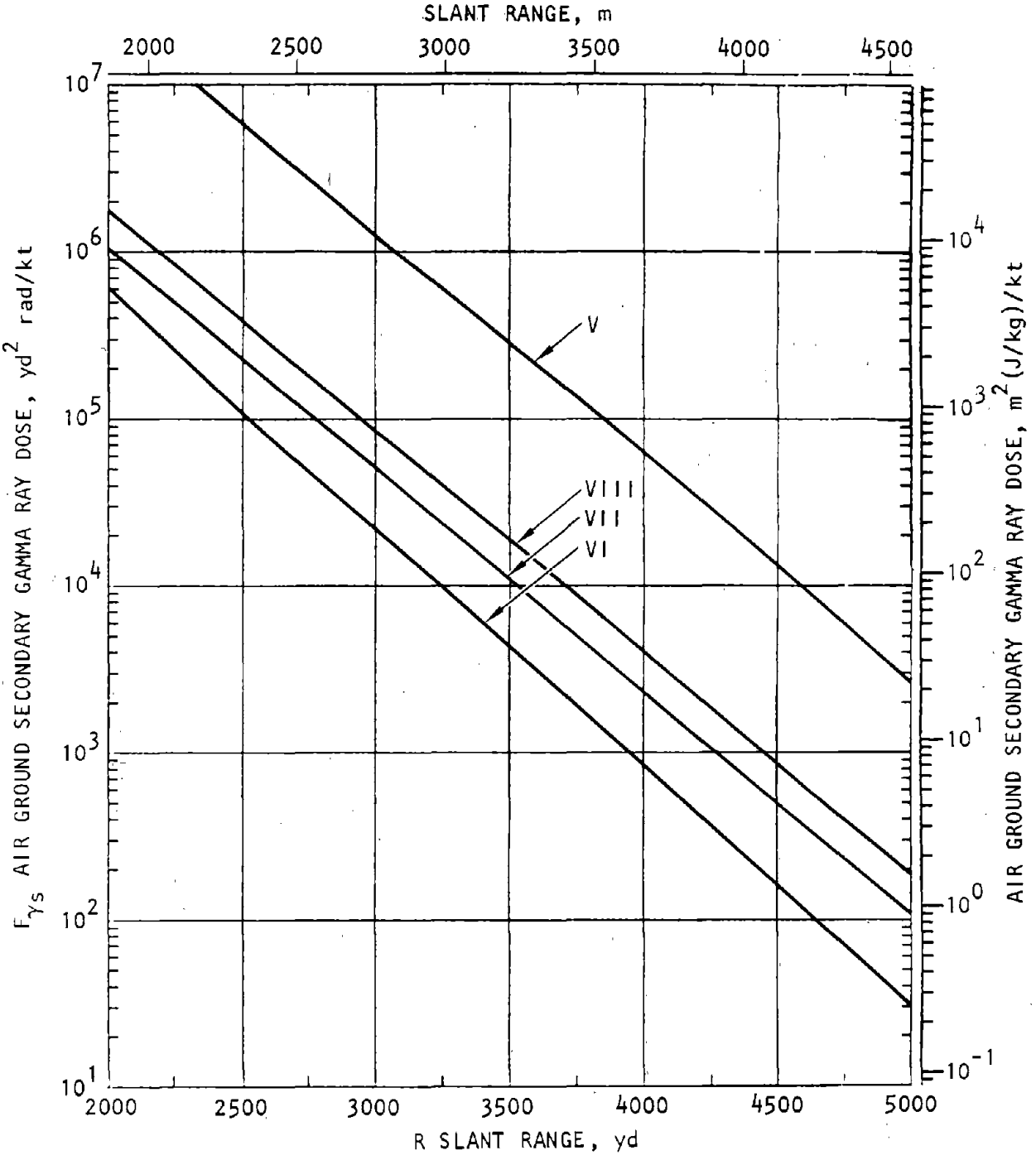

Figure 3–10. Secondary Gamma Ray Dose $F_{\gamma s}$ as a Function of Slant Range from a 1-kt Surface Burst, Weapon Types V through VIII, Long Ranges (DNA, 1972)

(2) The uncertainty associated with equation 3-6 is

$$\Omega^2_{D_{\gamma s}} = \Omega^2_f + \Omega^2_W + \Omega^2_{F_{\gamma s}} + \Omega^2_{H_1} + 4\Omega^2_R \quad (3\text{-}7)$$

where Ω_f is the uncertainty in the form of the equation, Ω_W is the uncertainty of the yield, etc. Consider that $\Omega_f \approx 0.2$, $\Omega_{F_{\gamma s}} = 0.3$ and using equation 2-19 with the assumption that figures 3-7 through 3-10 represent mean values of data uniformly distributed with bounds of ±25% (DNA, 1972), and $\Omega_{H_1} \approx 0.3$. Thus, equation 3-7 reduces to

$$\Omega^2_{D_{\gamma s}} = 0.22 + \Omega^2_W + 4\Omega^2_R \quad (3\text{-}8)$$

d. Fission-product gamma ray dose on personnel. If the weapon yield, height of burst, slant range, and air density are known, the fission-product gamma ray dose absorbed by human tissue can be estimated. The fission-product gamma ray dose $D_{\gamma f}$ is

$$D_{\gamma f} = W_f F_{\gamma f} H_R H_W E \text{ rad (J/kg)}, \quad (3\text{-}9)$$

where

W_f = Fission yield (kt)
$F_{\gamma f}$ = Normalized fission-product gamma ray dose, rad/kt [(J/kg/kt)]
H_R = Slant-range-dependent adjustment factor
H_W = Yield-dependent adjustment factor
E = Hydrodynamic enhancement factor

(1) The mean value of equation 3-9 can be calculated by referring to figures 3-11 through 3-20. In these figures, $\bar{\varrho} = \varrho/\varrho_0$, where ϱ and ϱ_0 (= 1.2250×10^{-3} gm/cm^3) are, respectively, the mean actual and ambient standard air densities (15.5 °C and 14.7 psia).

(2) The uncertainty of equation 3-9 is

$$\Omega^2_{D_{\gamma f}} = \Omega^2_f + \Omega^2_{W_f} + \Omega^2_{F_{\gamma f}} + \Omega^2_{H_R} + \Omega^2_{H_W} + \Omega^2_E \quad (3\text{-}10)$$

where Ω_f is the uncertainty of equation 3-9, Ω_{W_f} is the uncertainty of the yield, etc. Using equation 2-19 and the assumption that figures 3-11 through 3-13 represent mean values of data that are uniformly distributed and whose bounds are within ±25% of the mean values (DNA, 1972); and assuming other values of uncertainty,

$$\Omega_f \approx 0.2,\ \Omega_{F_{\gamma f}} = 0.3, \text{ and } \Omega_{H_R} = \Omega_{H_W} = \Omega_E \approx 0.3;$$

then equation 3-10 reduces to

$$\Omega^2_{D_{\gamma f}} = 0.4 + \Omega^2_{W_f} \quad (3\text{-}11)$$

e. Total personnel dose. The total dose to personnel is the sum of the neutron dose, the secondary gamma ray dose, and the fission-product gamma ray dose.

(1) The total mean dose to personnel is the sum of equations 3-1, 3-6, and 3-9.

(2) The uncertainty Ω^2_T of the total dose to personnel is the uncertainty of the sum of equations 3-1, 3-6, and 3-9. Thusly,

$$\Omega^2_T = 0.09 + \Omega^2_W + \frac{H_1^2 W^2}{D_T^2 R^4}\left[0.09\, F_N^2 + (0.09 + 4\Omega^2_R)(F_N + F_{\gamma s})^2\right] + \frac{0.36\, W_f^2 F_{\gamma f}^2 H_R^2 H_W^2 E^2}{D_T^2} \quad (3\text{-}12a)$$

except for megaton weapons where R < 1000 yd (914 m), then

$$\Omega^2_T = 0.17 + \Omega^2_W + \frac{H_1^2 W^2}{D^2 R^4}\left[0.09\, F_N^2 + (0.09 + 4\Omega^2_R)(F_N + F_{\gamma s})^2\right] + \frac{0.36\, W_f^2 F_{\gamma f}^2 H_R^2 H_W^2 E^2}{D^2} \quad (3\text{-}12b)$$

f. Neutron-induced gamma activity in soils, residual effect on personnel. Neutron-induced soil activity must be considered for a scaled burst height below 75 ft/kt$^{0.35}$ (23 m/kt$^{0.35}$) but above the ground. Soils that contain sodium, manganese, and aluminum will contribute most to the induced radioactivity. For times after burst of less than one-half hour, aluminum is most important; between one-half hour and five hours, manganese is most important; at later times, sodium becomes increasingly more important.

(1) Figure 3-21 presents upper and lower bounds on the neutron-induced gamma dose rate at a reference time one hour after burst. At any given slant range, assume that the mean is the logarithmic average of the upper and lower bounds. For a time other than one hour after burst, this mean must be multiplied by the factors shown in figure 3-22 for the four types of soil presented in table 3-1. Additionally, all data must be multiplied by the factors shown in table 3-2 to obtain a final estimate of the mean dose rate.

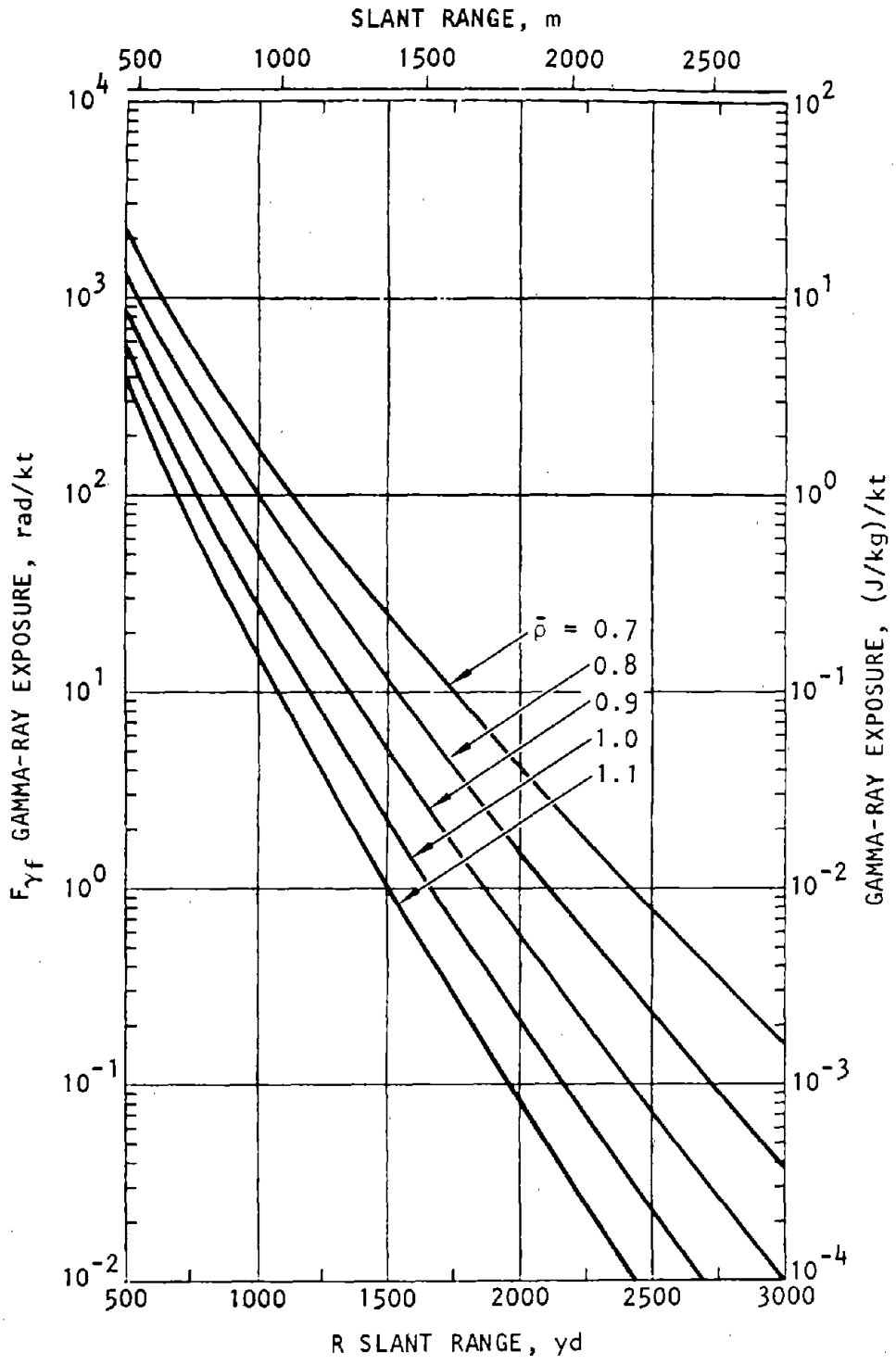

Figure 3–11. Fission Product Gamma Ray Dose $F_{\gamma f}$ as a Function of Slant Range from a 1-kt (Fission Yield) Surface Burst, Short Ranges (DNA, 1972)

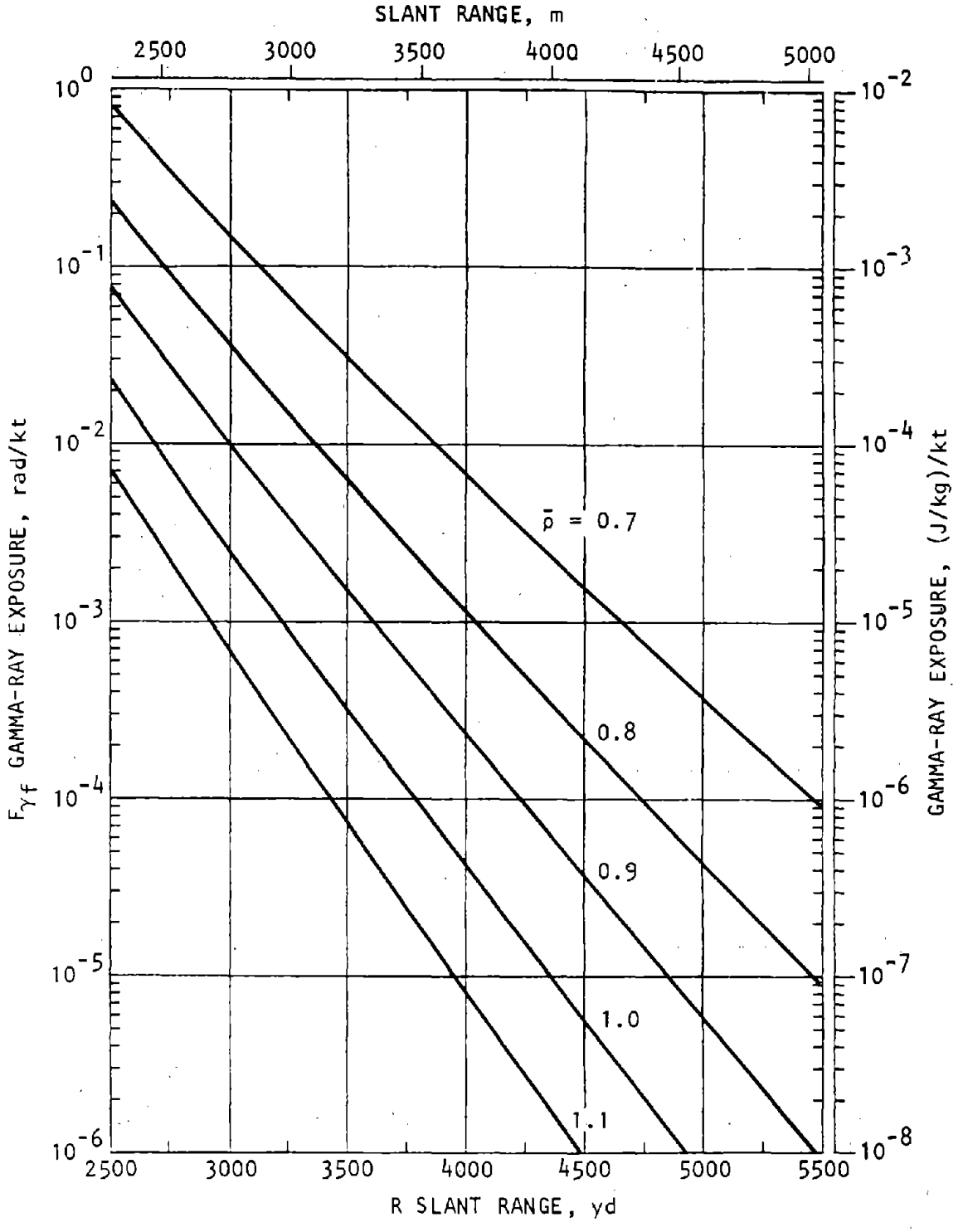

Figure 3-12. Fission Product Gamma Ray Dose $F_{\gamma f}$ as a Function of Slant Range from a 1-kt (Fission Yield) Surface Burst, Intermediate Ranges (DNA, 1972)

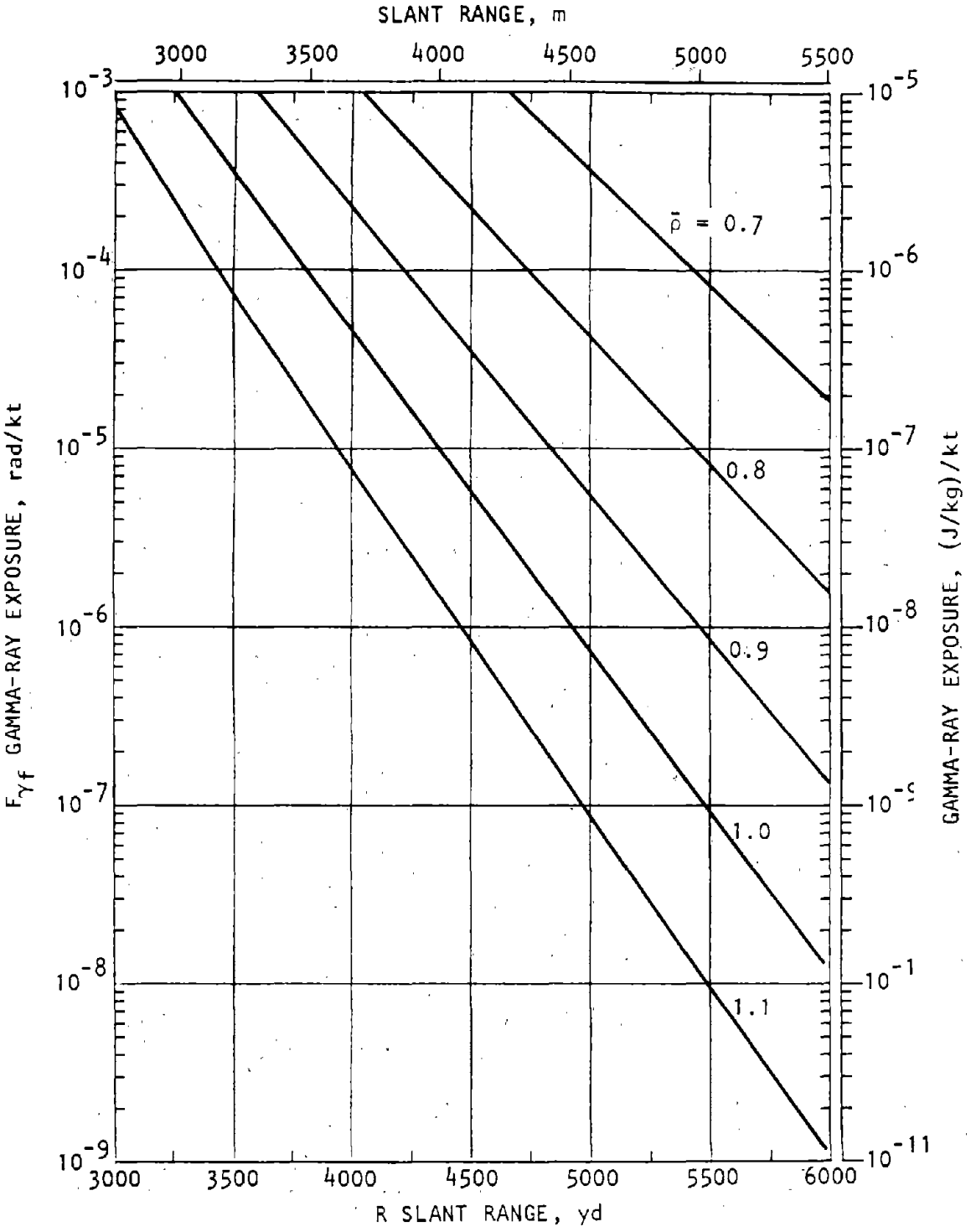

Figure 3-13. Fission Product Gamma Ray Dose $F_{\gamma f}$ as a Function of Slant Range from a 1-kt (Fission Yield) Surface Burst, Long Ranges (DNA, 1972)

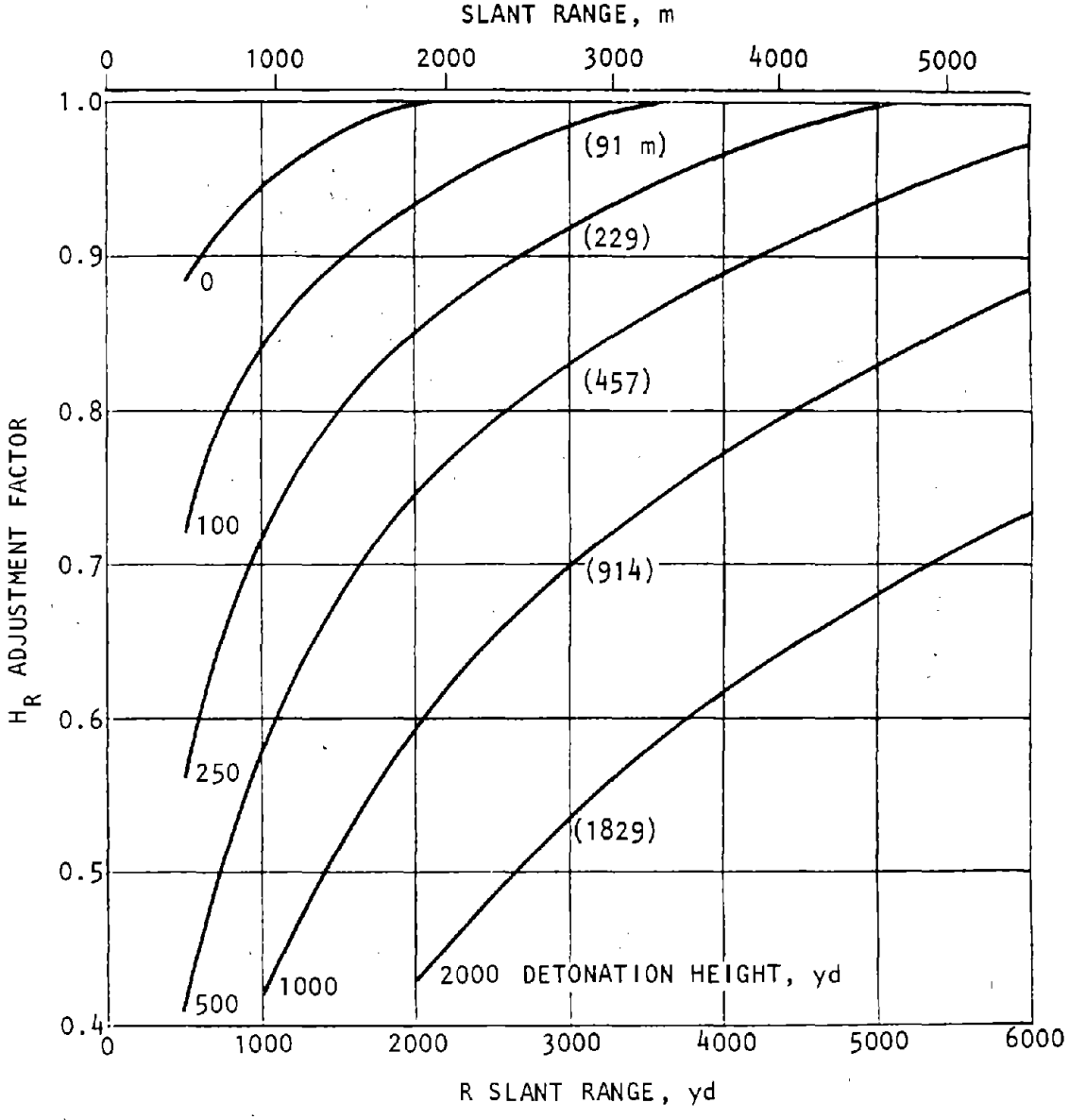

Figure 3-14. Range-Dependent Burst Height Adjustment Factors H_R for Fission Product Gamma Rays (DNA, 1972)

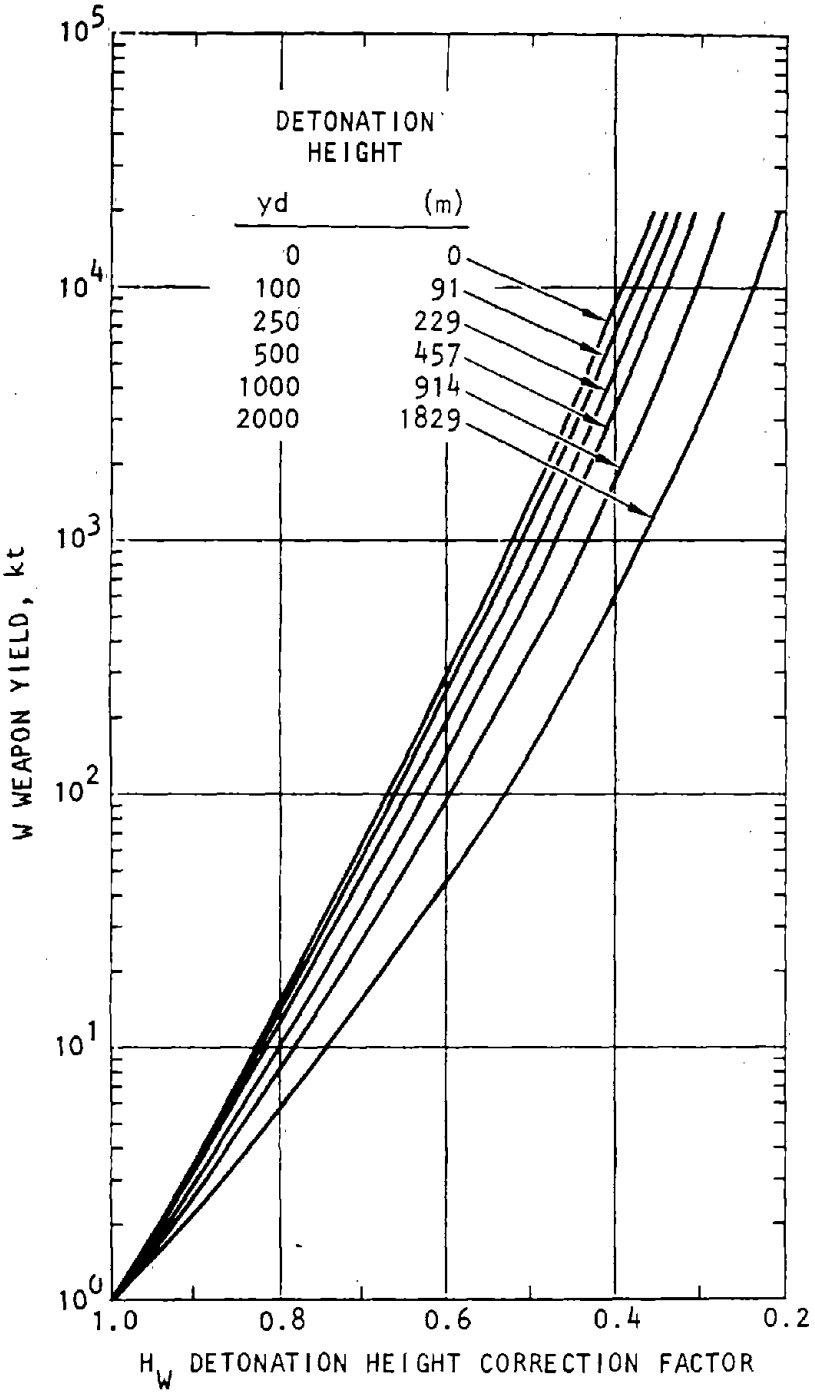

Figure 3–15. Yield-Dependent Burst Height Adjustment Factors H_W for Fission Product Gamma Rays (DNA, 1972)

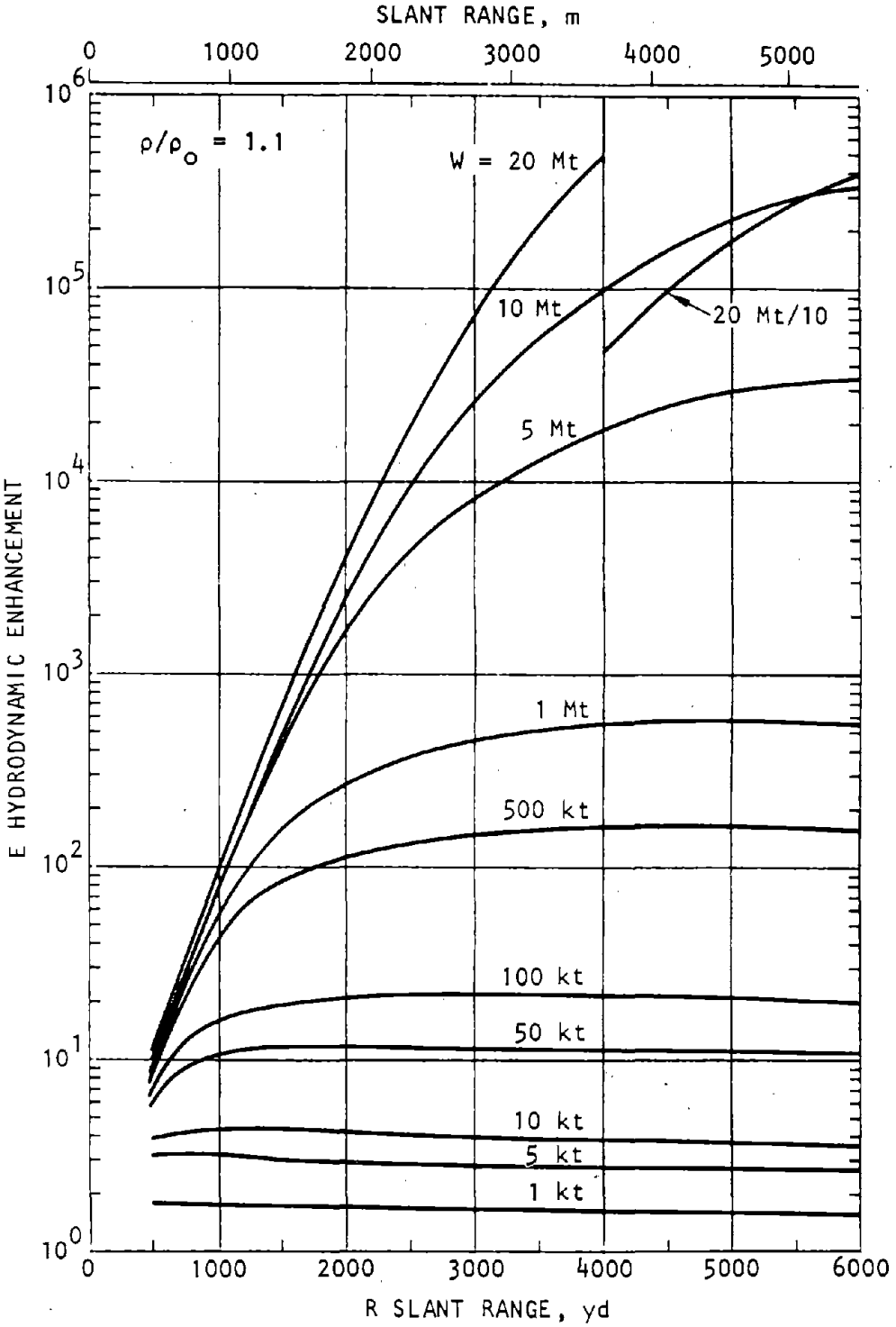

Figure 3–16. Fission-Product Gamma Ray Hydrodynamic Enhancement Factors E as a Function of Slant Range for Relative Air Density of 1.1 (DNA, 1972)

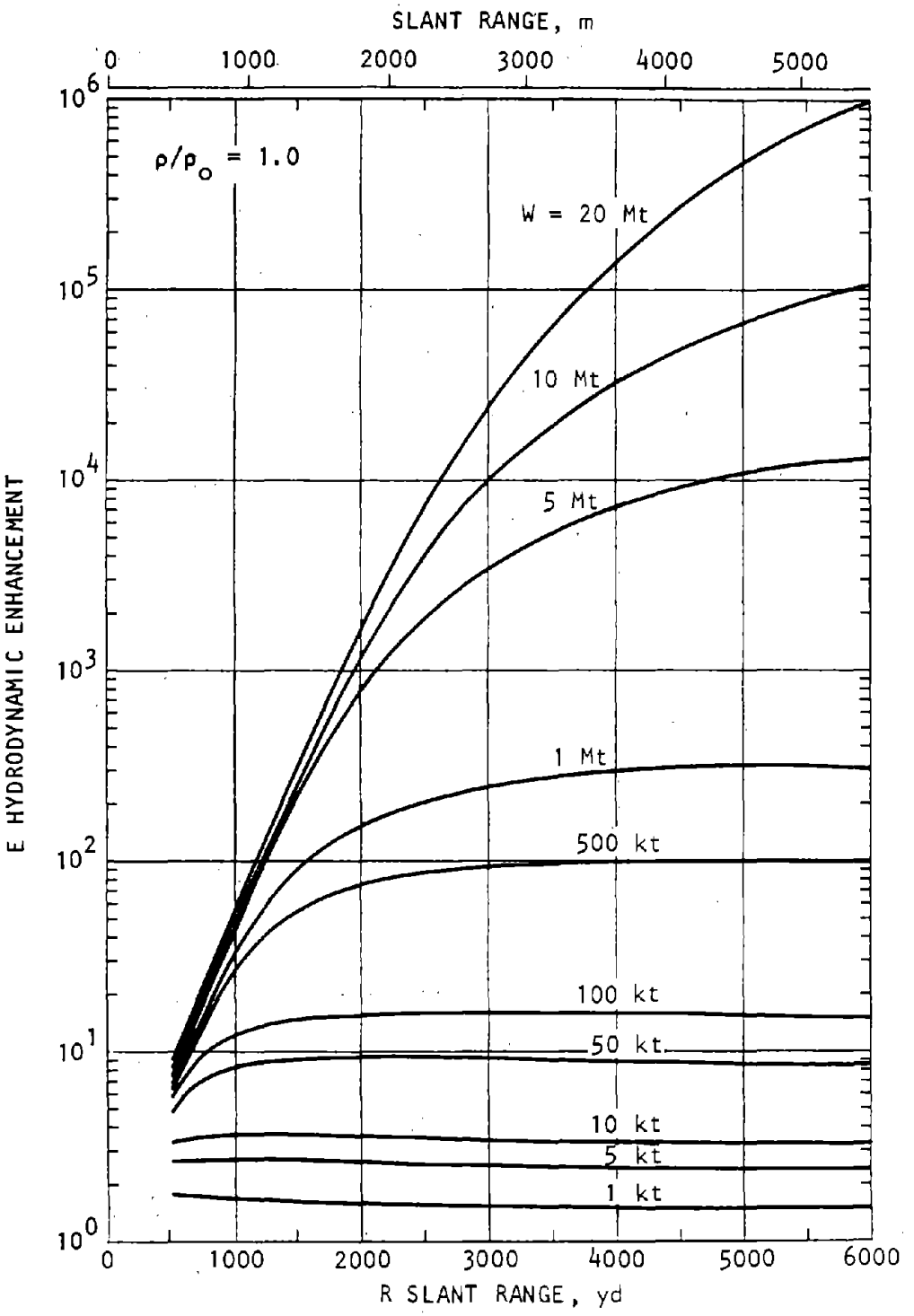

Figure 3-17. Fission-Product Gamma Ray Hydrodynamic Enhancement Factors E as a Function of Slant Range for Relative Air Density of 1.0 (DNA, 1972)

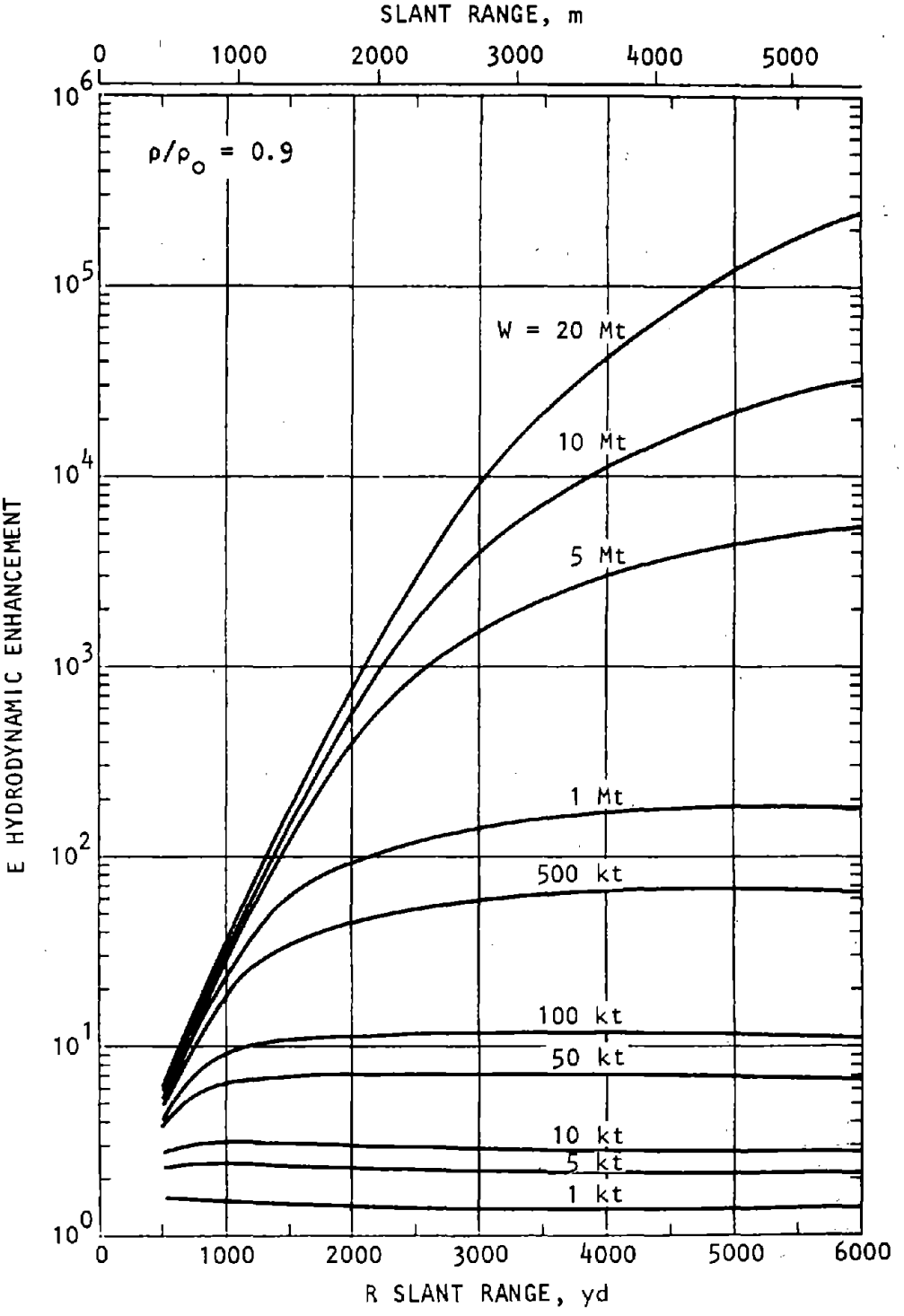

Figure 3–18. Fission-Product Gamma Ray Hydrodynamic Enhancement Factors E as a Function of Slant Range for Relative Air Density of 0.9 (DNA, 1972)

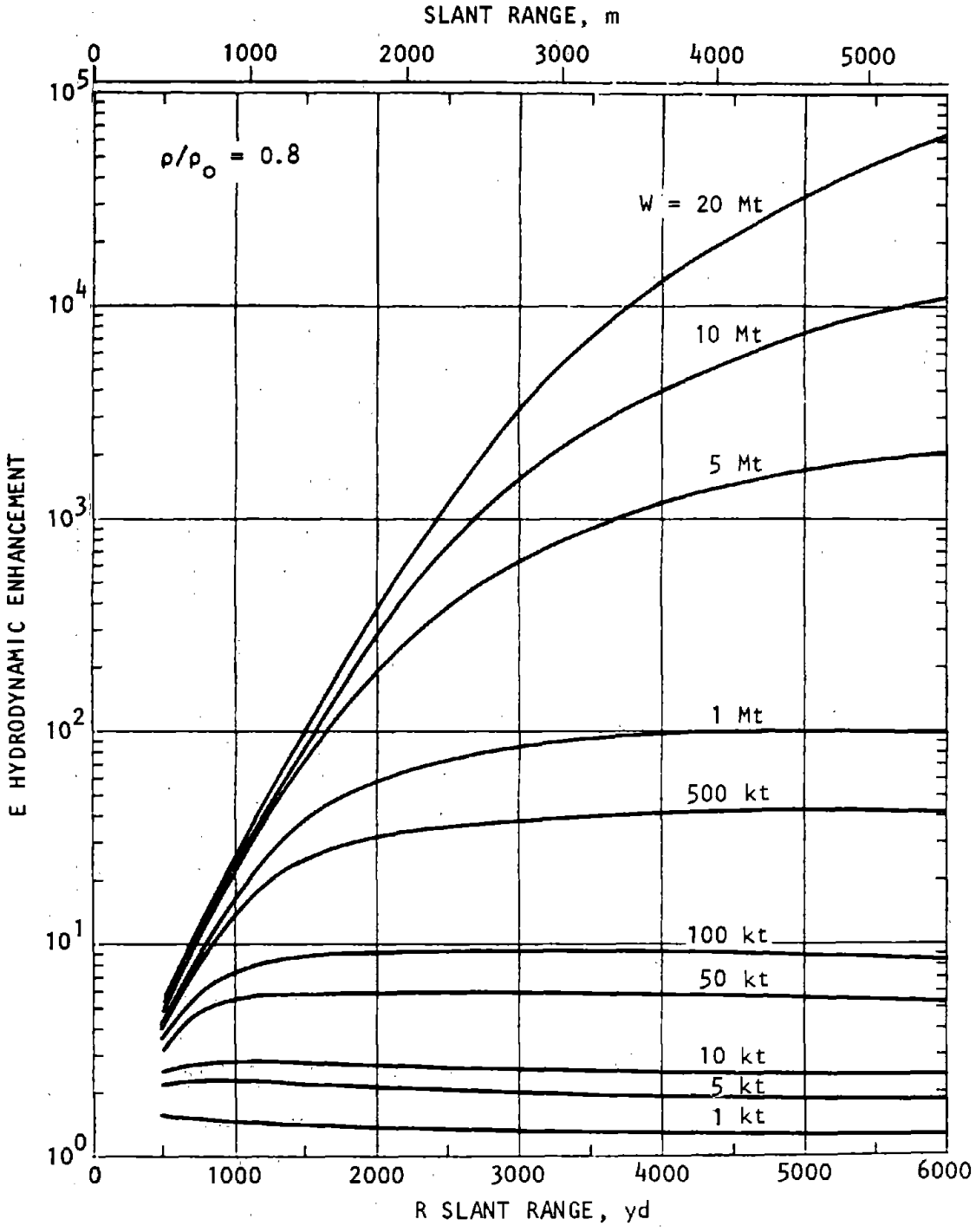

Figure 3-19. Fission-Product Gamma Ray Hydrodynamic Enhancement Factors E as a Function of Slant Range for Relative Air Density of 0.8 (DNA, 1972)

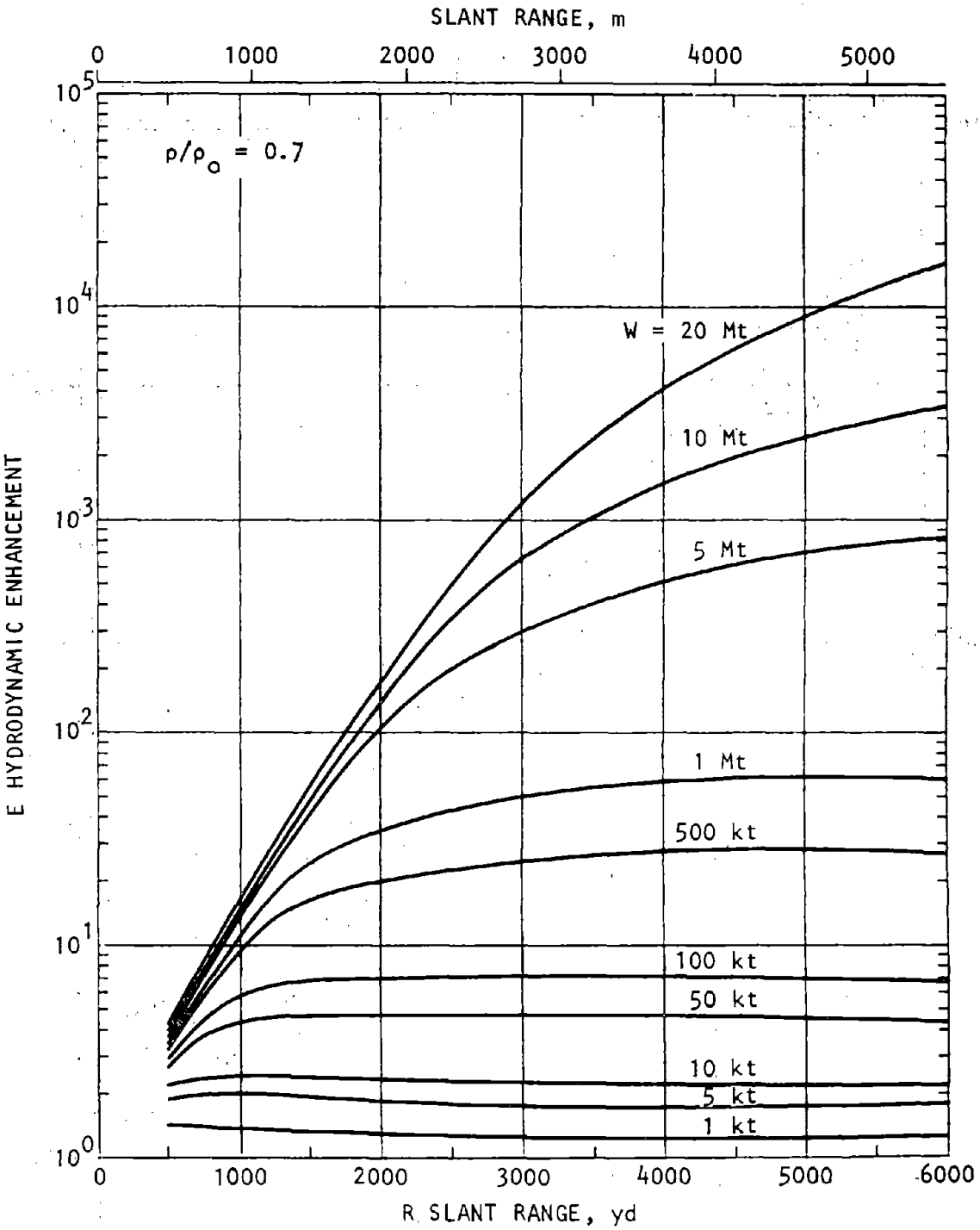

Figure 3–20. Fission-Product Gamma Ray Hydrodynamic Enhancement Factors E as a Function of Slant Range for Relative Air Density of 0.7 (DNA, 1972)

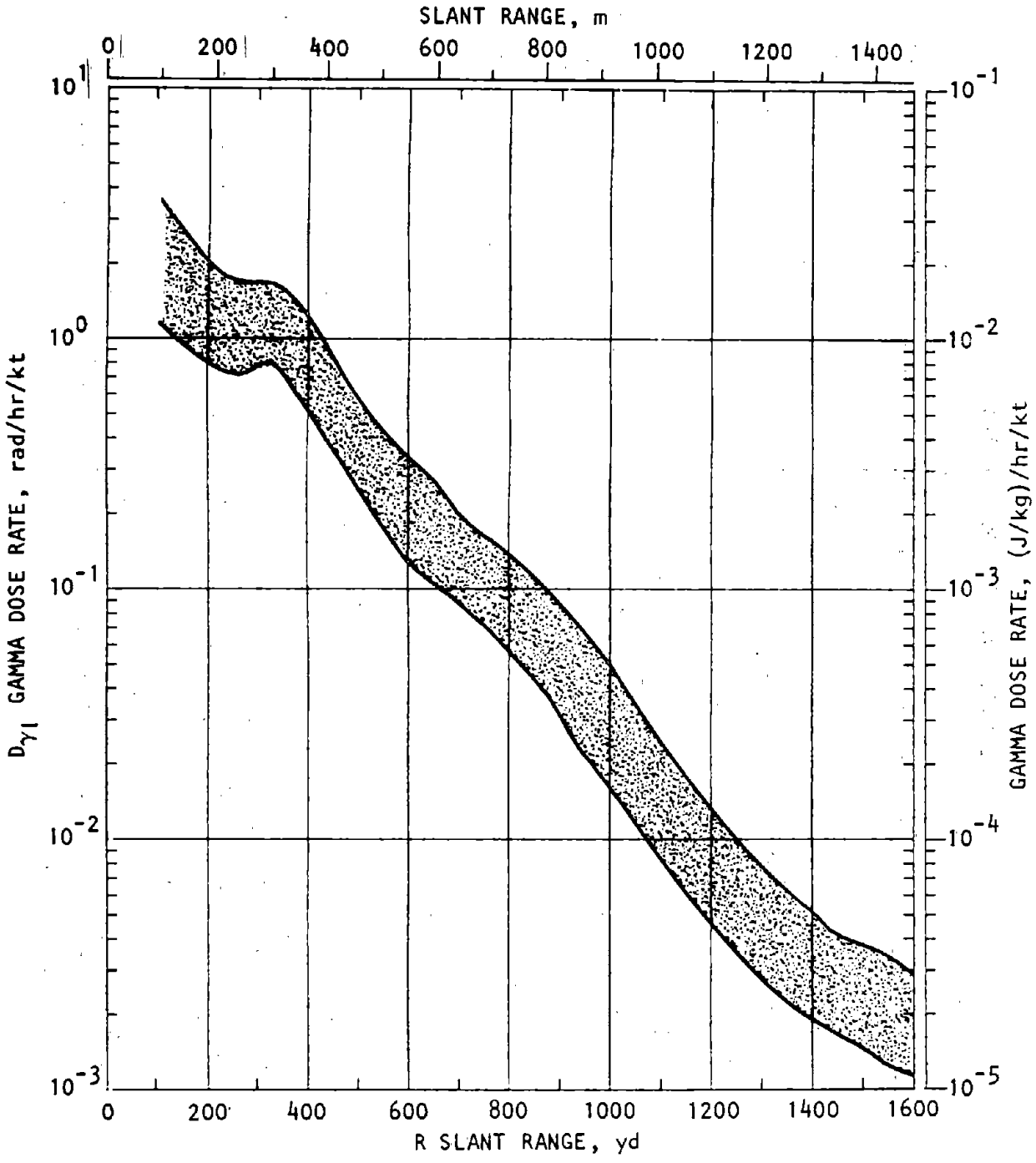

Figure 3-21. Neutron-Induced Gamma Dose Rate $D_{\gamma I}$ as a Function of Slant Range at a Reference Time of 1 Hour After Burst (DNA, 1972)

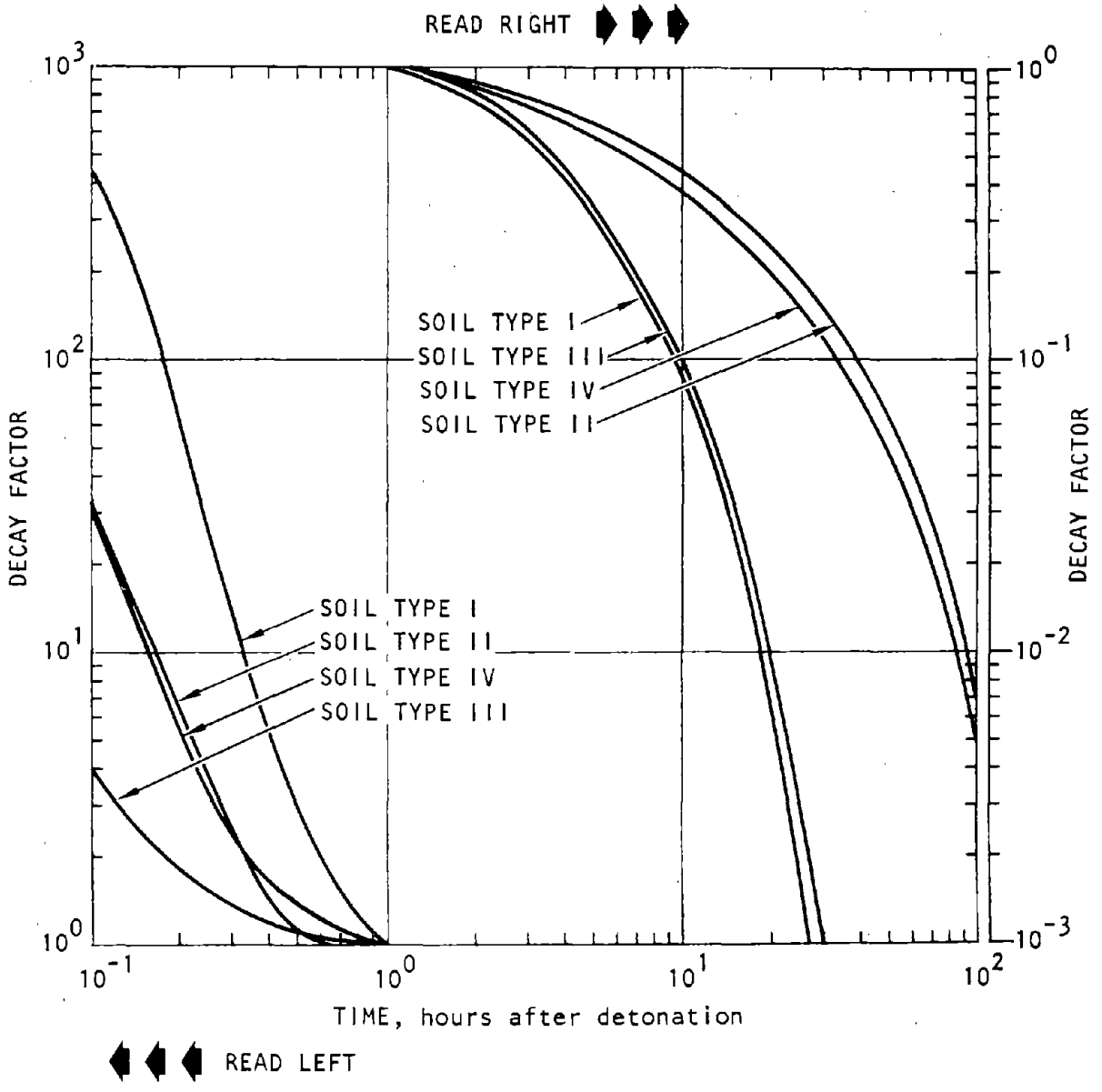

Figure 3–22. Decay Factors for Neutron-Induced Gamma Activity, $D_{\gamma I}$ (DNA, 1972)

Table 3-1. Soil Types by Composition (DNA, 1972)

Element	Percentage of Soil Type (by weight)			
	Type I (Liberia, Africa)	Type II (Nevada desert)	Type III (lava, clay, Hawaii)	Type IV (beach sand, Pensacola, Florida)
Sodium	-	1.30	0.16	0.001
Manganese	0.008	0.04	2.94	-
Aluminum	7.89	6.90	18.79	0.006
Iron	3.75	2.20	10.64	0.005
Silicon	33.10	32.00	10.23	46.65
Titanium	0.39	0.27	1.26	0.004
Calcium	0.08	2.40	0.45	-
Potassium	-	2.70	0.88	-
Hydrogen	0.39	0.70	0.94	0.001
Boron	-	-	-	0.001
Nitrogen	0.065	-	0.26	-
Sulfur	0.07	0.03	0.26	-
Magnesium	0.05	0.60	0.34	-
Chromium	-	-	0.04	-
Phosphorous	0.008	0.04	0.13	-
Carbon	3.87	-	9.36	-
Oxygen	50.33	50.82	43.32	53.332

Table 3-2. Multiplying Factors (DNA, 1972)

Soil Type	Multiplying Factor
I	1.0
II	9.1
III	109.0
IV	0.024

(2) In a particular situation, it may be necessary to construct a representative decay factor curve based on the chemical composition of the soil as compared to the data presented in table 3-1. For example, assume that a particular site has properties in which the percentage of aluminum most nearly matches that of Soil I but that manganese and sodium are most accurately represented by Soils II and III, respectively. Construct a decay factor curve from figure 3-22 which approximates Soil I for times up to one-half hour, Soil II from one-half hour to five hours, and sodium after four hours.

(3) Obtain the total gamma ray dose experienced by personnel from figures 3-23 through 3-26, which are applied to the one-hour dose rate presented in figure 3-21. The factor obtained from the appropriate soil type in figures 3-23 through 3-26 depends on the time of entry into a contaminated area and the amount of time spent in that area. These factors are multiplied by the appropriate dose rate in figure 3-21.

(4) As an example, for the particular soil type discussed in (2) above, assume that the area is to be entered after two hours and to be occupied for seven hours. Enter figure 3-24 (for Soil II) for an entry time of two hours and an occupancy time of three hours (period during which manganese contribution is most important). Read the multiplying factor. Then enter figure 3-25 (for Soil III) for an entry time of five hours and occupancy time of two hours (period during which sodium is most important) and read the multiplying factor. Add the factors and multiply this number by the mean value of data in figure 3-21.

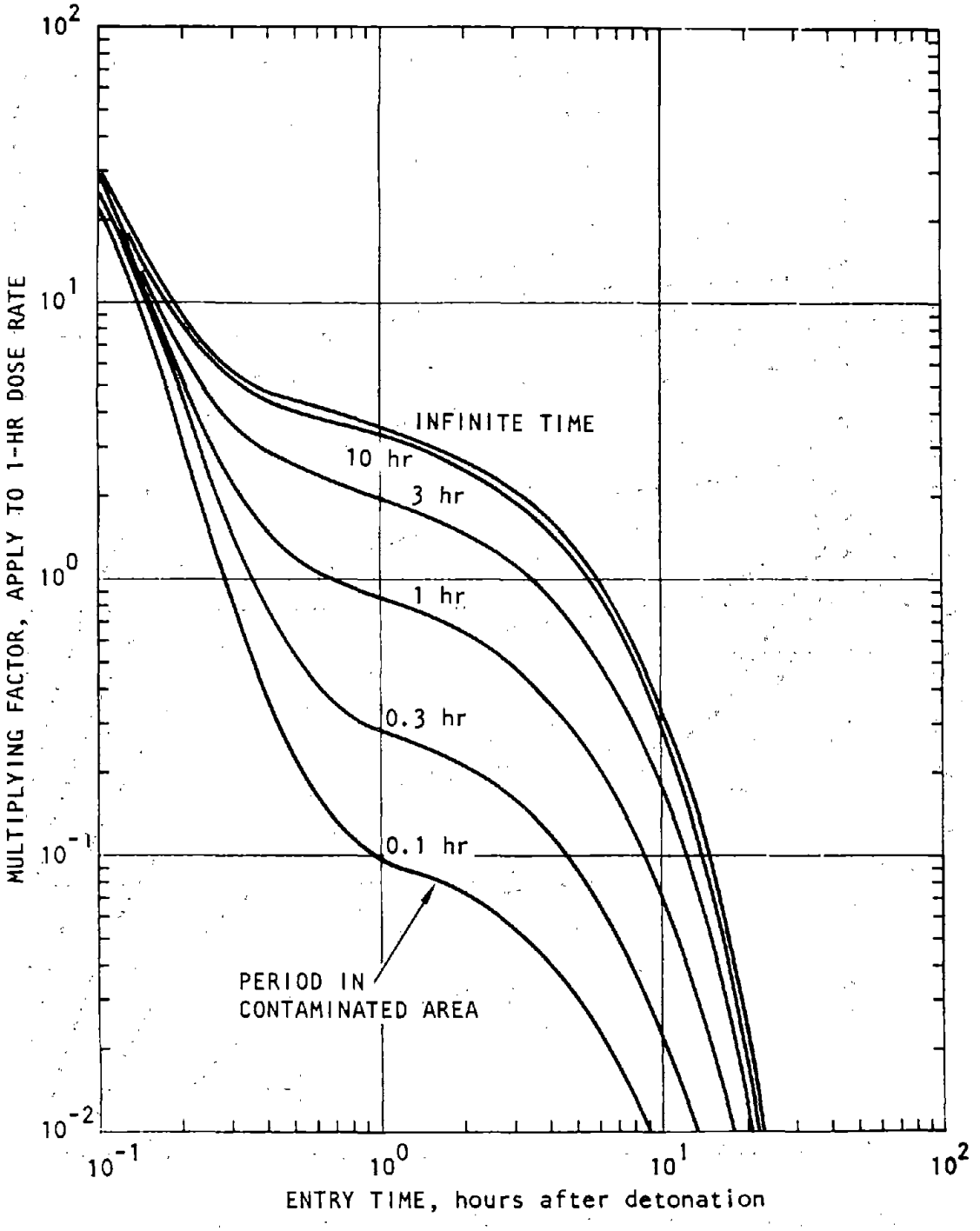

Figure 3-23. Total Radiation Dose Received (rad/kt) in an area contaminated by Neutron-Induced Gamma Activity, Soil Type I (DNA, 1972)

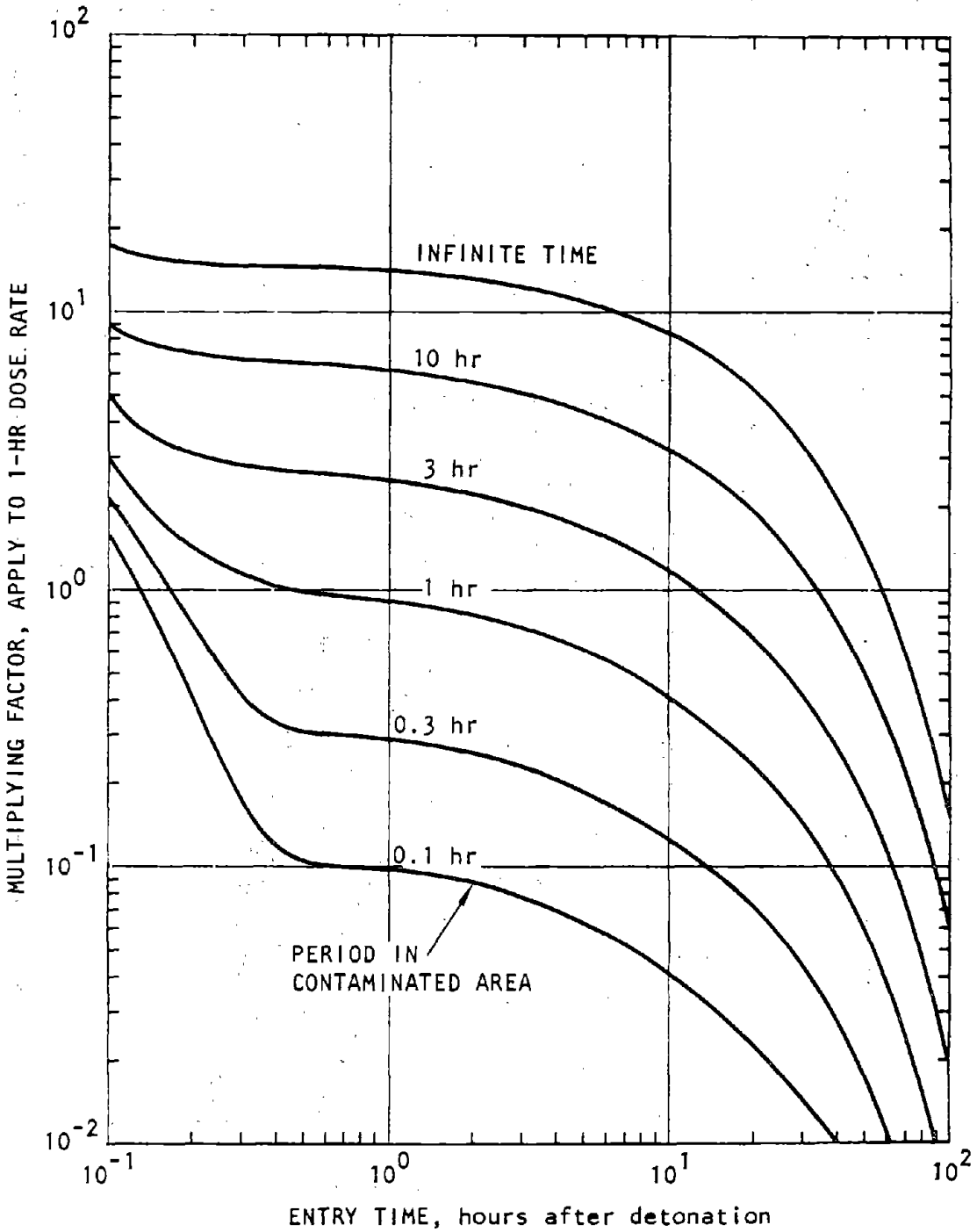

Figure 3-24. Total Radiation Dose Received (rad/kt) in an area contaminated by Neutron-Induced Gamma Activity, Soil Type II (DNA, 1972)

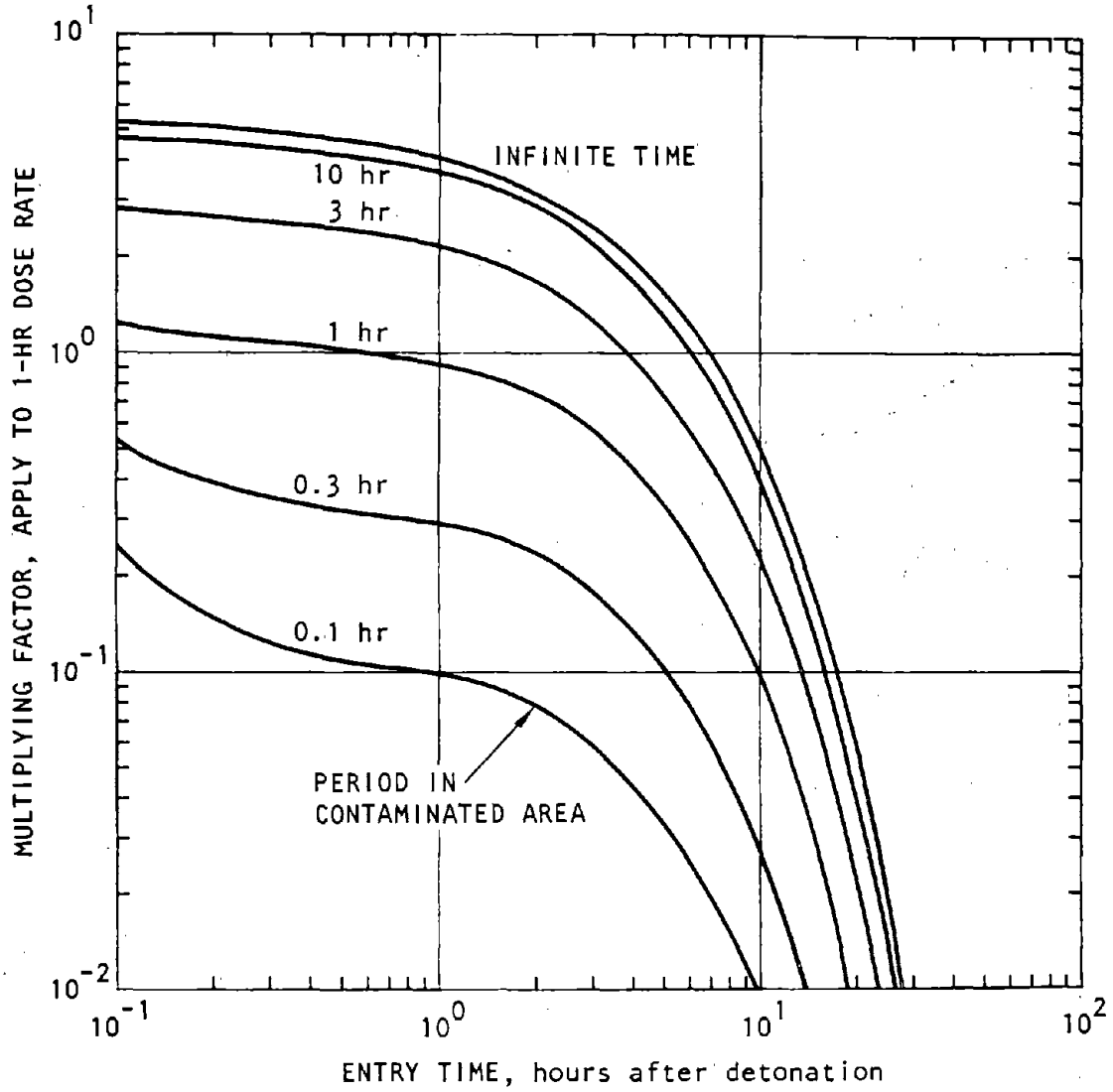

Figure 3–25. Total Radiation Dose Received (rad/kt) in an area contaminated by Neutron-Induced Gamma Activity, Soil Type III (DNA, 1972)

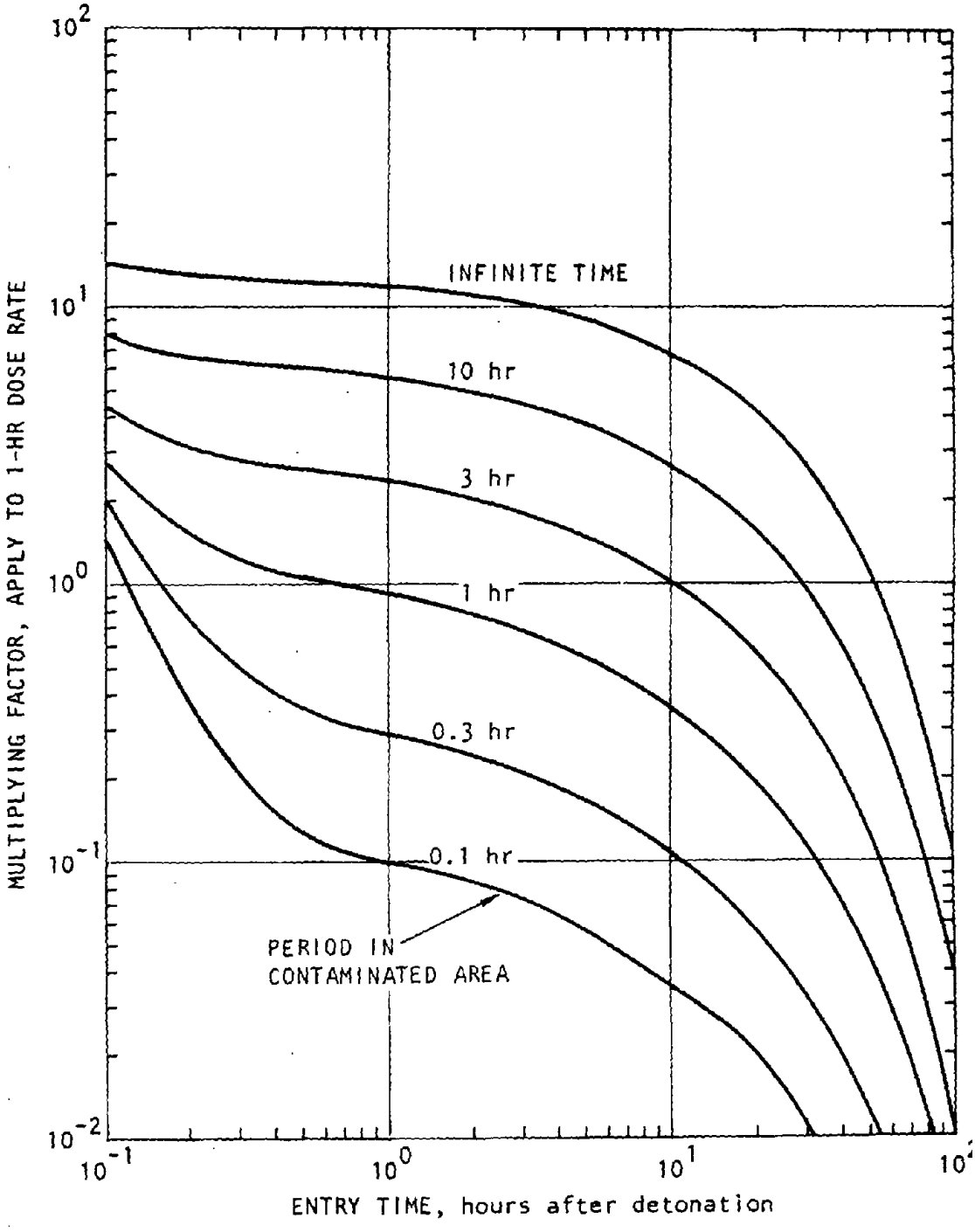

Figure 3–26. Total Radiation Dose Received (rad/kt) in an area contaminated by Neutron-Induced Gamma Activity, Soil Type IV (

(5) As an estimate of uncertainty of the neutron-induced gamma activity in soils $\Omega_{D_{\gamma I}}$, use the equation

$$\Omega^2_{D_{\gamma I}} = \Omega^2_f + 0.00003\ R^2\ \Omega^2_R \qquad (3\text{–}13)$$

where Ω_f is the uncertainty of total dose and Ω_R is the uncertainty in slant range (yd). Assuming that the dose rate is log-uniformly distributed in figure 3–21, calculate Ω_f from equation 2–19 where L_1 and L_2 are the lower and upper bounds at any slant range in figure 3–21.

CHAPTER 4
ELECTROMAGNETIC PULSE (EMP)

4-1. Gross phenomenology.

a. Time-varying electric and magnetic fields are produced by nuclear detonations. Their frequency spectrum varies from direct current to about 10 GHz. The gamma radiation produced by the nuclear detonation impinges on air molecules and induces a Compton current via ionization of the air. As the Compton current expands away from the source, separation of the ions occurs and produces a radial electric field in the entire deposition region. Because of the atmospheric density gradient, the earth's magnetic field, and the weapon configuration itself, a magnetic field is also created, resulting in the radiation of an electromagnetic wave for a medium-altitude (where the deposition region does not touch the earth) or a high-altitude burst. In a surface burst, the relatively large conductivity of the earth induces electric and magnetic fields (as shown in figure 4-1) whose intensities are much larger than for an air burst.

b. The basic variables contributing to the EMP for exposed, flush, and shallow-buried facilities are

- Weapon design
- Weapon yield
- Burst elevation
- Atmospheric conductivity
- Ground conductivity

c. Hardened ground-based or shallow-buried systems are subject to EMP caused by high-altitude bursts or by contact (or penetrating) bursts. Each system must be investigated to determine which burst condition predominates. Hardened ground-based or very shallow-buried systems will be susceptible to EMP caused by contact (or penetrating) bursts only if within the deposition region. The deposition region is that region in space where EMP fields are generated.

4-2. Surface burst.

a. In a surface burst, the conducting ground provides an effective return path for electrons traveling outward in the air from the burst point. These current loops produce very large azimuthal magnetic fields in the deposition region, especially near the ground. Large electric fields are also produced. The EMP for a surface burst will be one to two orders of magnitude greater than for air bursts.

b. The magnitude and shape of the electric and magnetic fields in the deposition region cannot be described by simple functional relationships because of the complex nature of the underlying variables. For maximum accuracy, the currents induced in a system should be calculated with the recognition that the system, itself, influences the characteristics of the

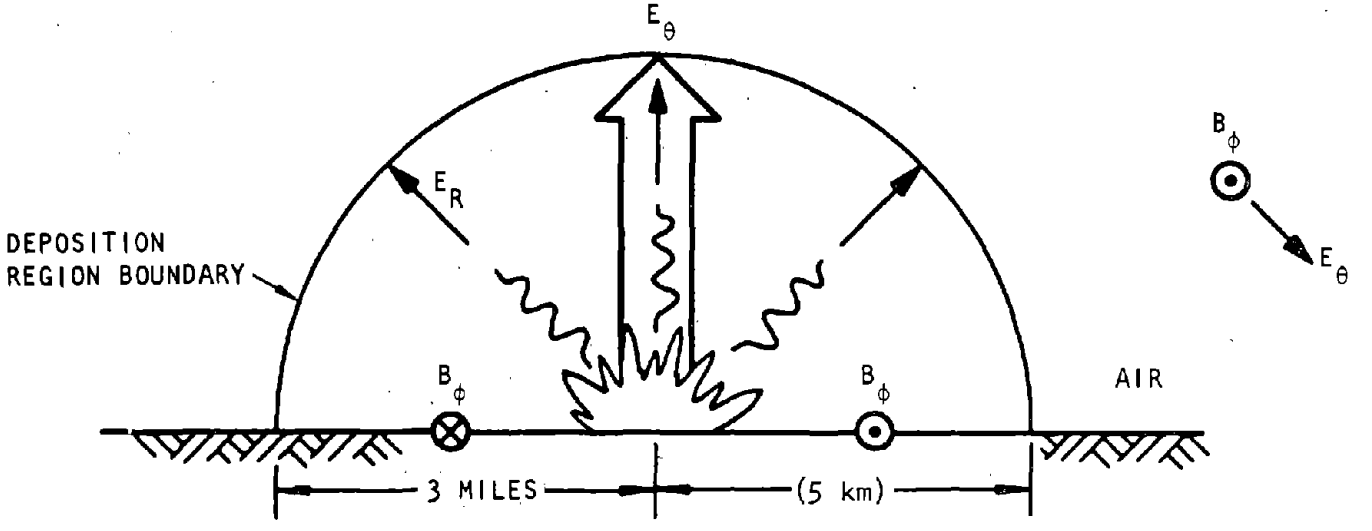

B_ϕ = MAGNETIC FIELD

E_R = RADIAL ELECTRIC FIELD

E_θ = TRANSVERSE ELECTRIC FIELD

Figure 4-1. Surface-Burst EMP

EMP environment. Exact solutions for individual cases can be solved by using the computer programs described in the *DNA EMP Handbook* (GE-TEMPO, 1971) and in the NWE Computer Code Directory (GE-TEMPO, 1974). For approximations, the relative changes in peak values of both the radial and polar electric fields and the azimuthal magnetic fields created in the deposition region are presented in figures 4-2 through 4-4 for two weapon yields and two ground conductivities. The time histories for these same fields are presented in figures 4-5 through 4-7. Their corresponding frequency spectra are presented in figures 4-8 through 4-10. These data should be used for guidance only. Situations involving other weapon yields or conductivities will require the execution of the appropriate computer program.

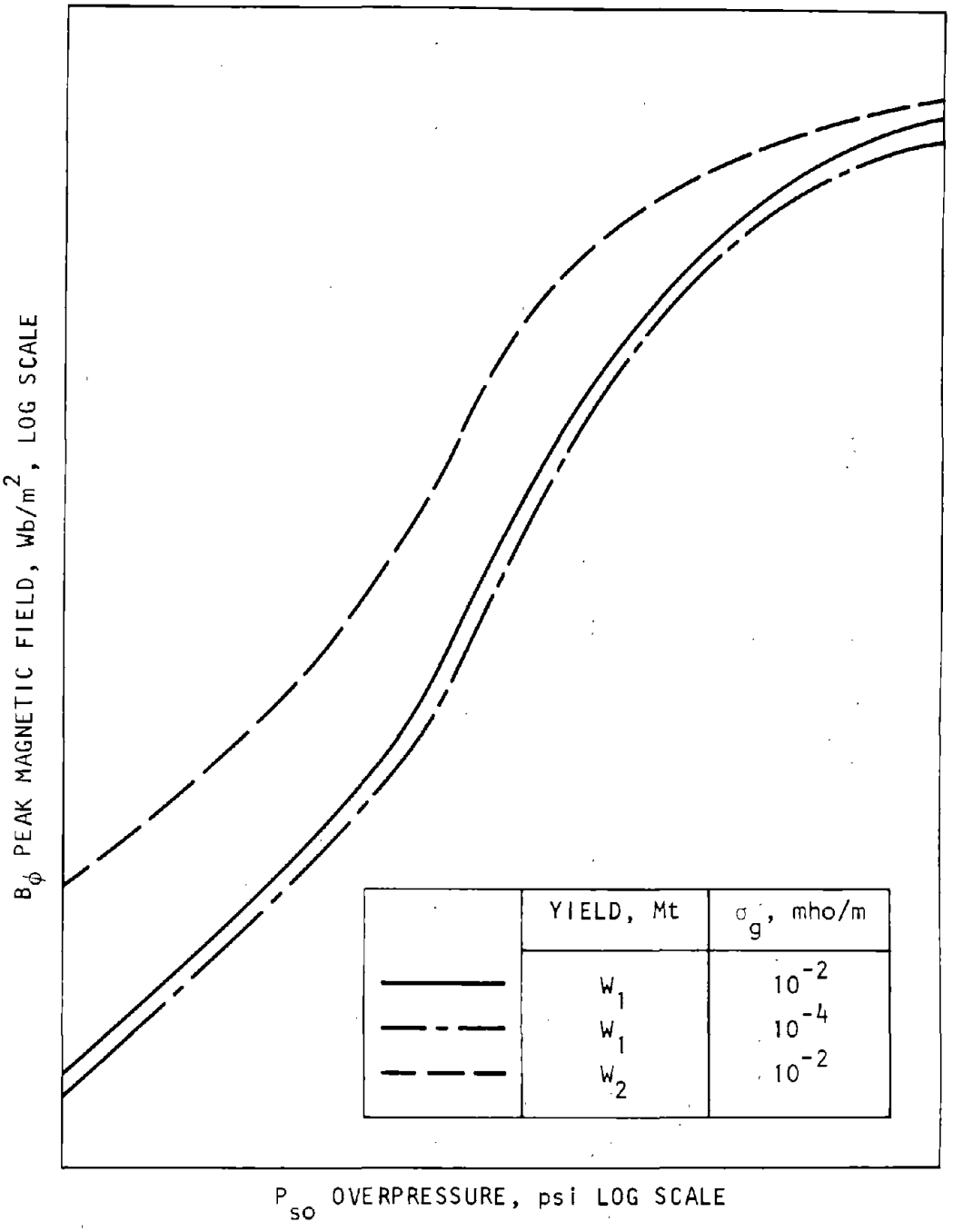

Figure 4-2. Peak Magnetic Field B_ϕ Vs. Overpressure at the Air/Ground Interface for Varying Ground Conductivities and Yields (DNA, 1972)

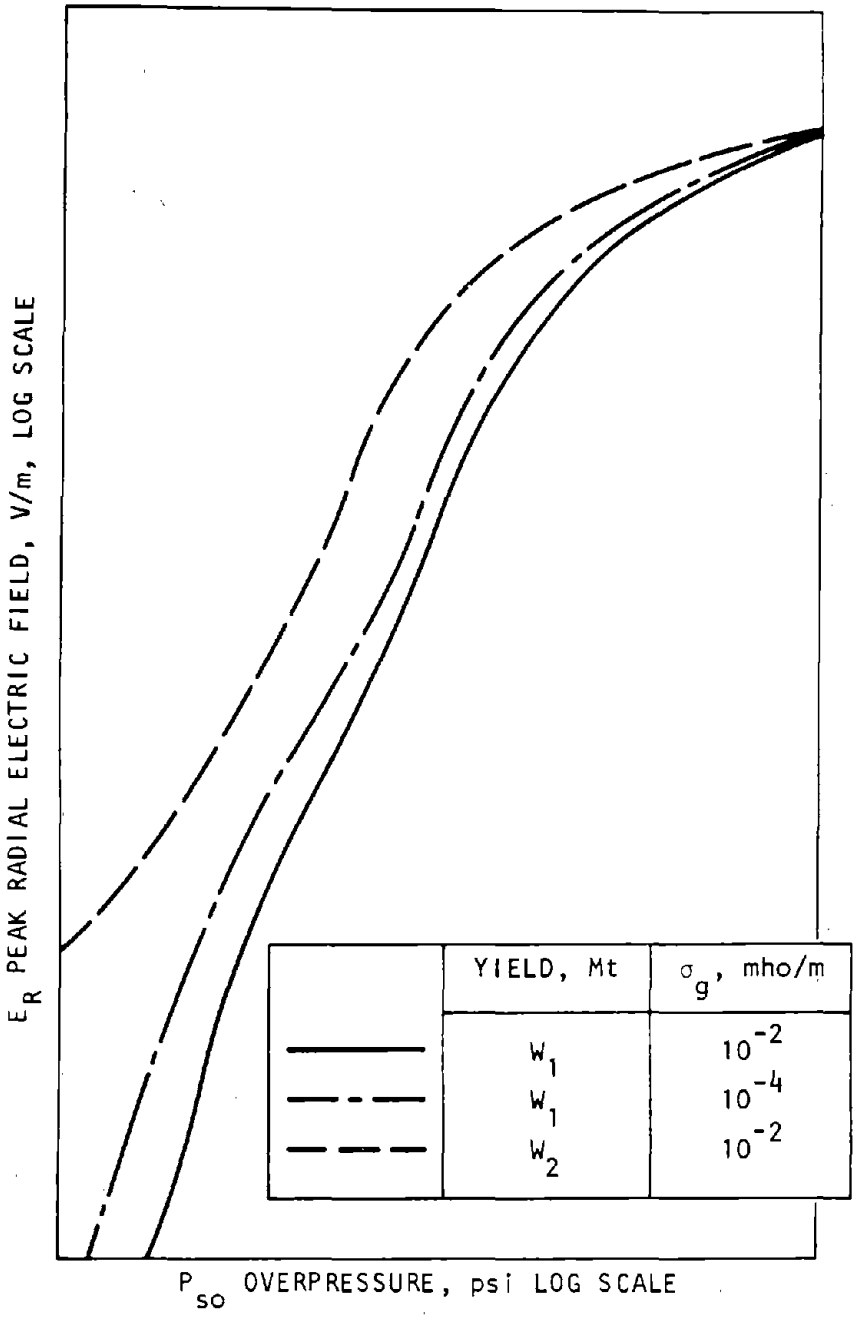

Figure 4–3. Peak Radial Electric Field E_R Vs. Overpressure at the Air/Ground Interface for Varying Ground Conductivities and Yields (DNA, 1972)

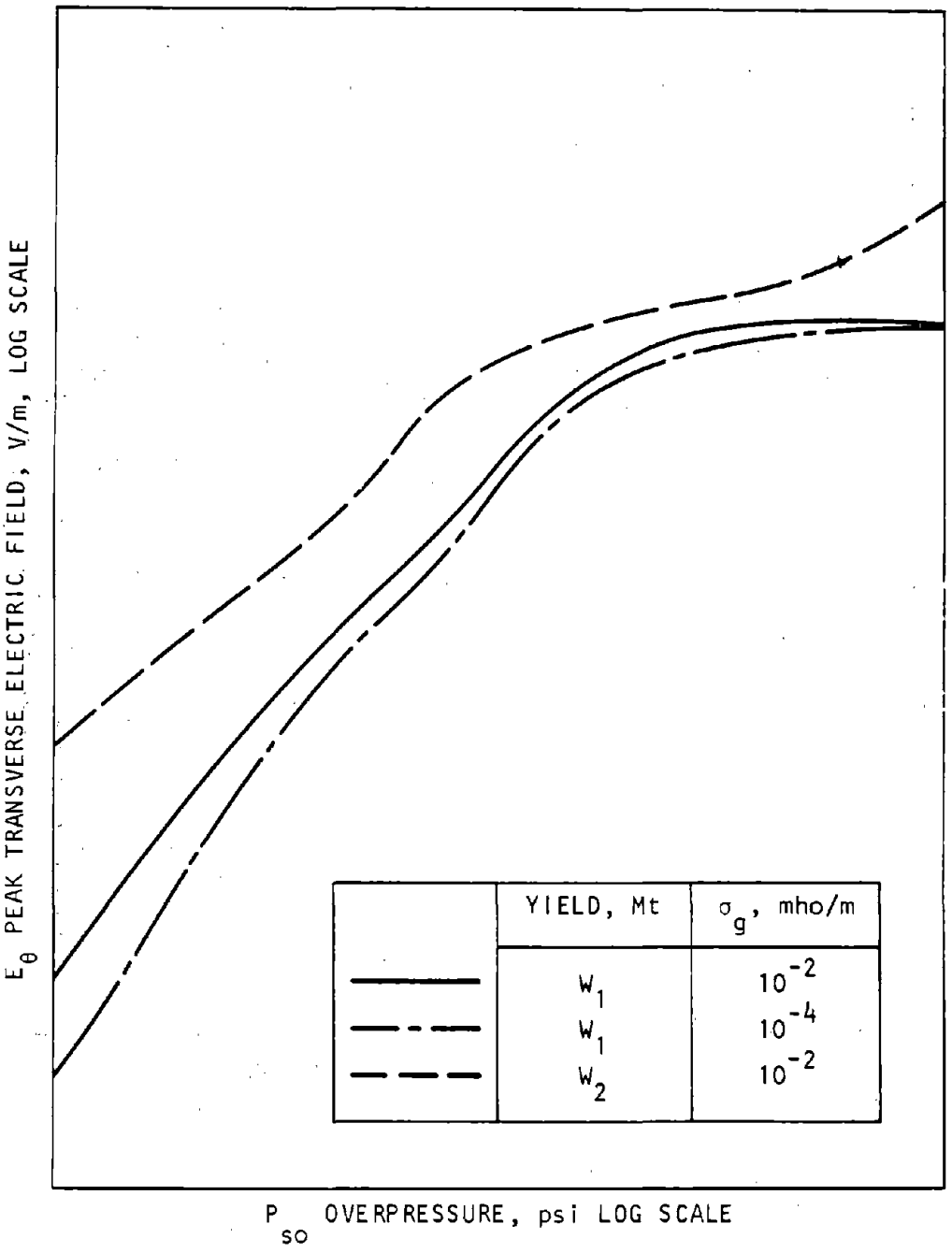

Figure 4–4. Peak Transverse Electric Field E_θ Vs. Overpressure at the Air/Ground Interface for Varying Ground Conductivities and Yields (DNA, 1972)

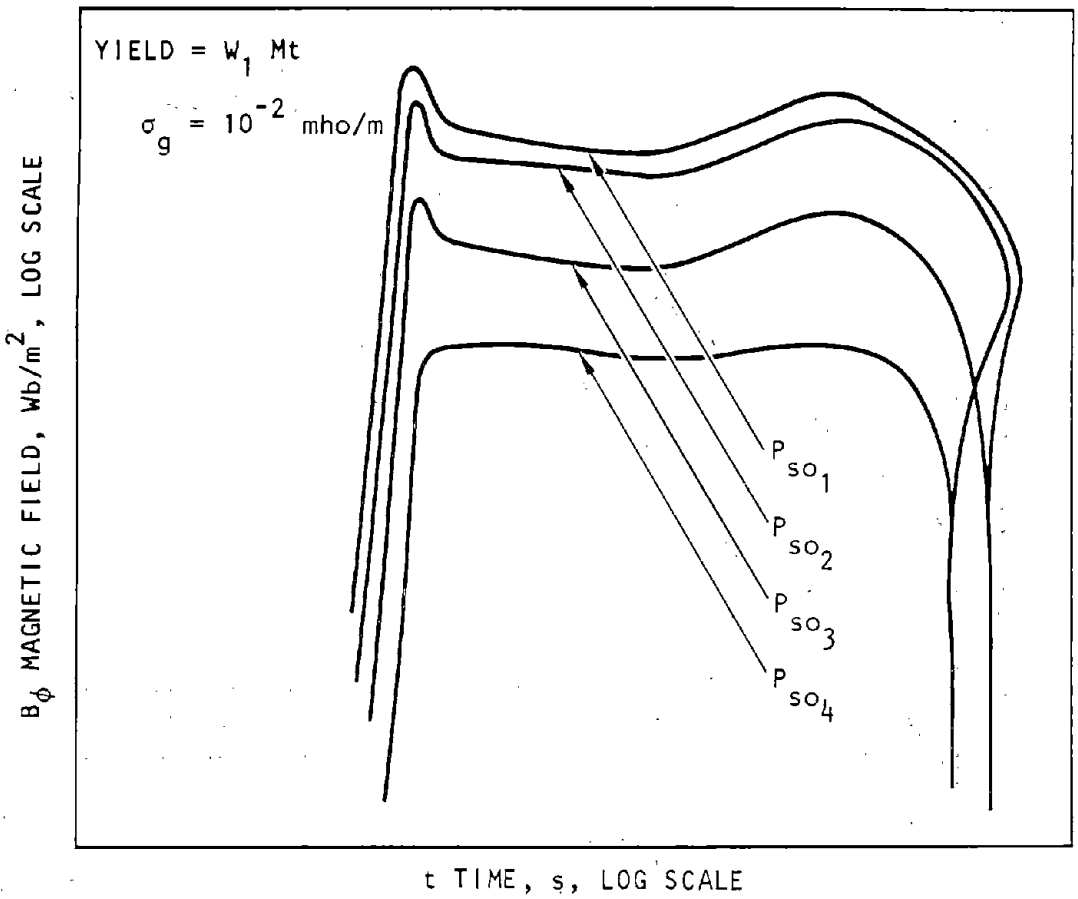

Figure 4–5. B_ϕ-Time Waveform at the Air/Ground Interface for Several Overpressure Levels (SAI, 1971)

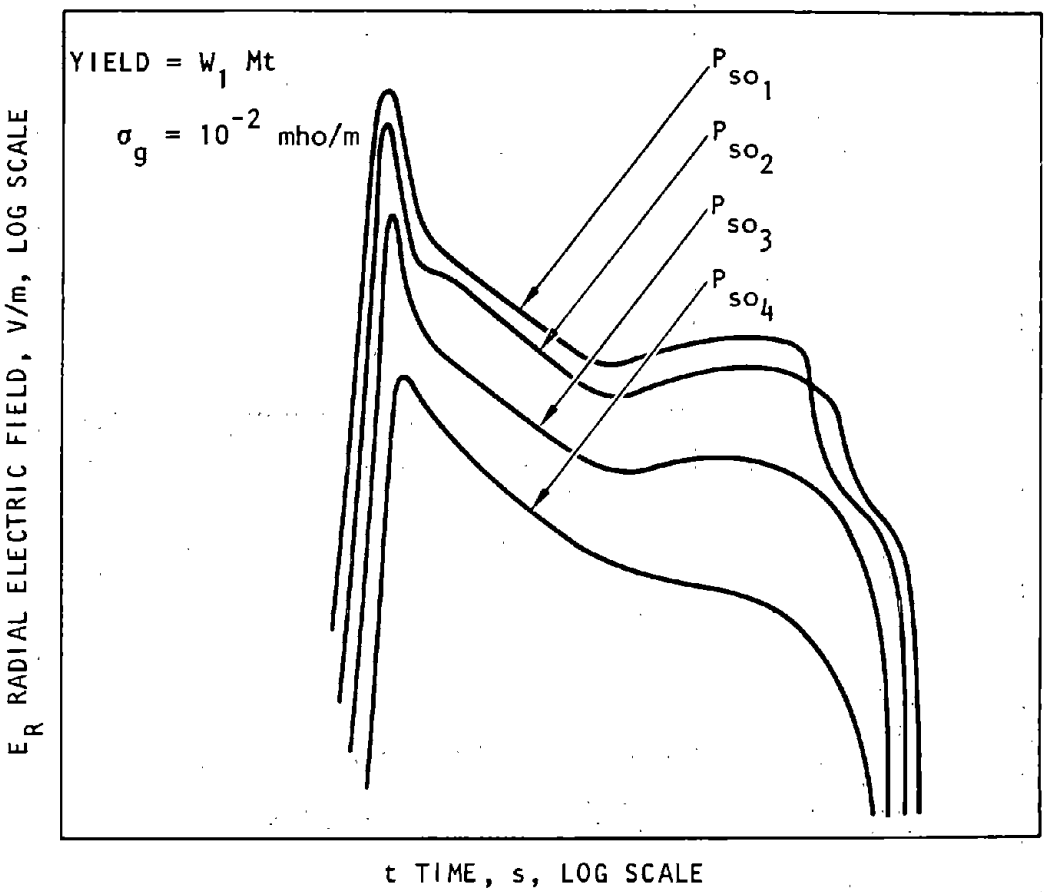

Figure 4-6. E_R-Time Waveform at the Air/Ground Interface for Several Overpressure Levels (SAI, 1971)

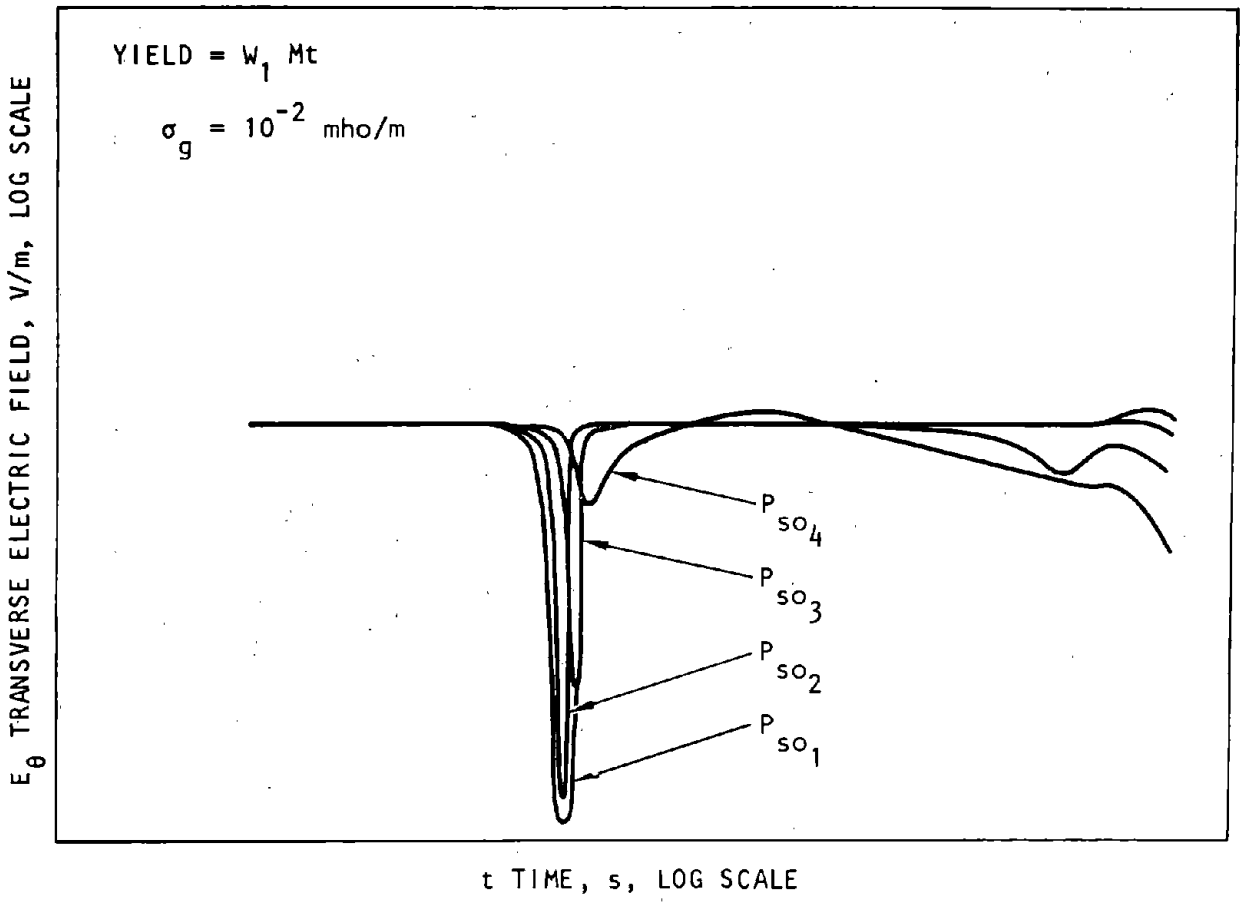

Figure 4-7. E_g-Time Waveform at the Air/Ground Interface for Several Overpressure Levels (SAI, 1971)

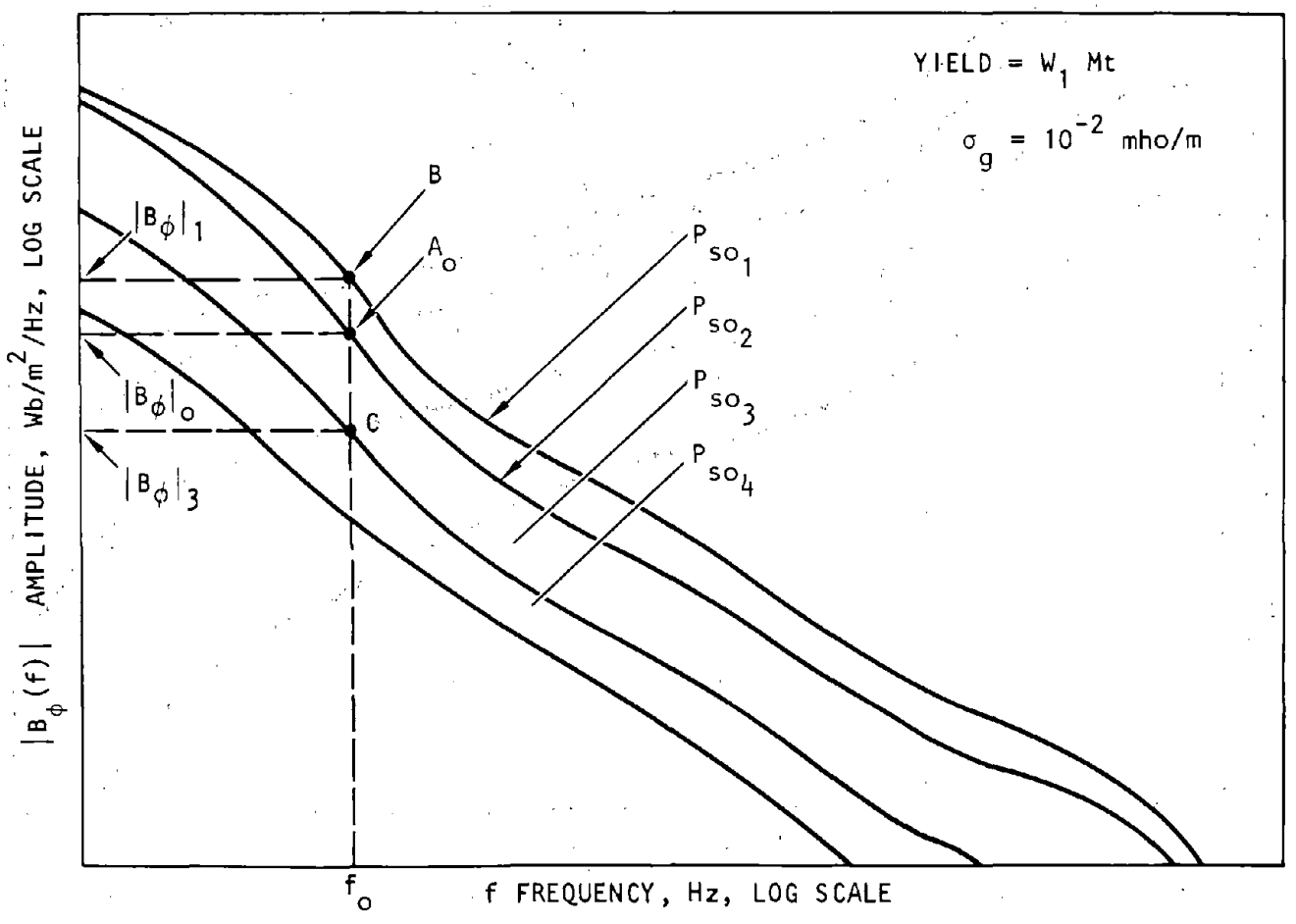

Figure 4–8. Fourier Amplitude of B_ϕ Waveform at the Air/Ground Interface for Several Overpressure Levels (DNA, 1972)

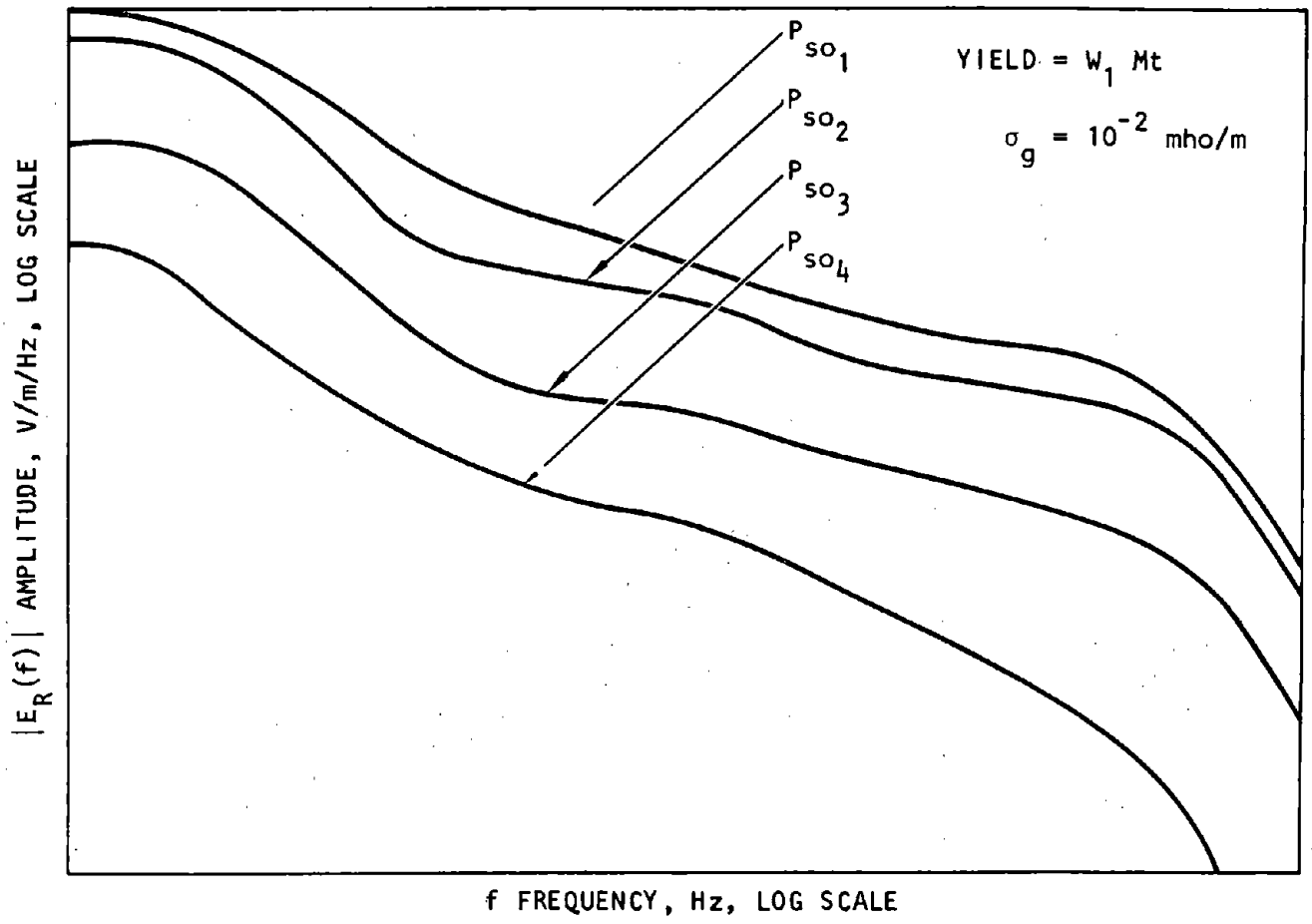

Figure 4-9. Fourier Amplitude of E_R Waveform at the Air/Ground Interface for Several Overpressure Levels (DNA, 1972)

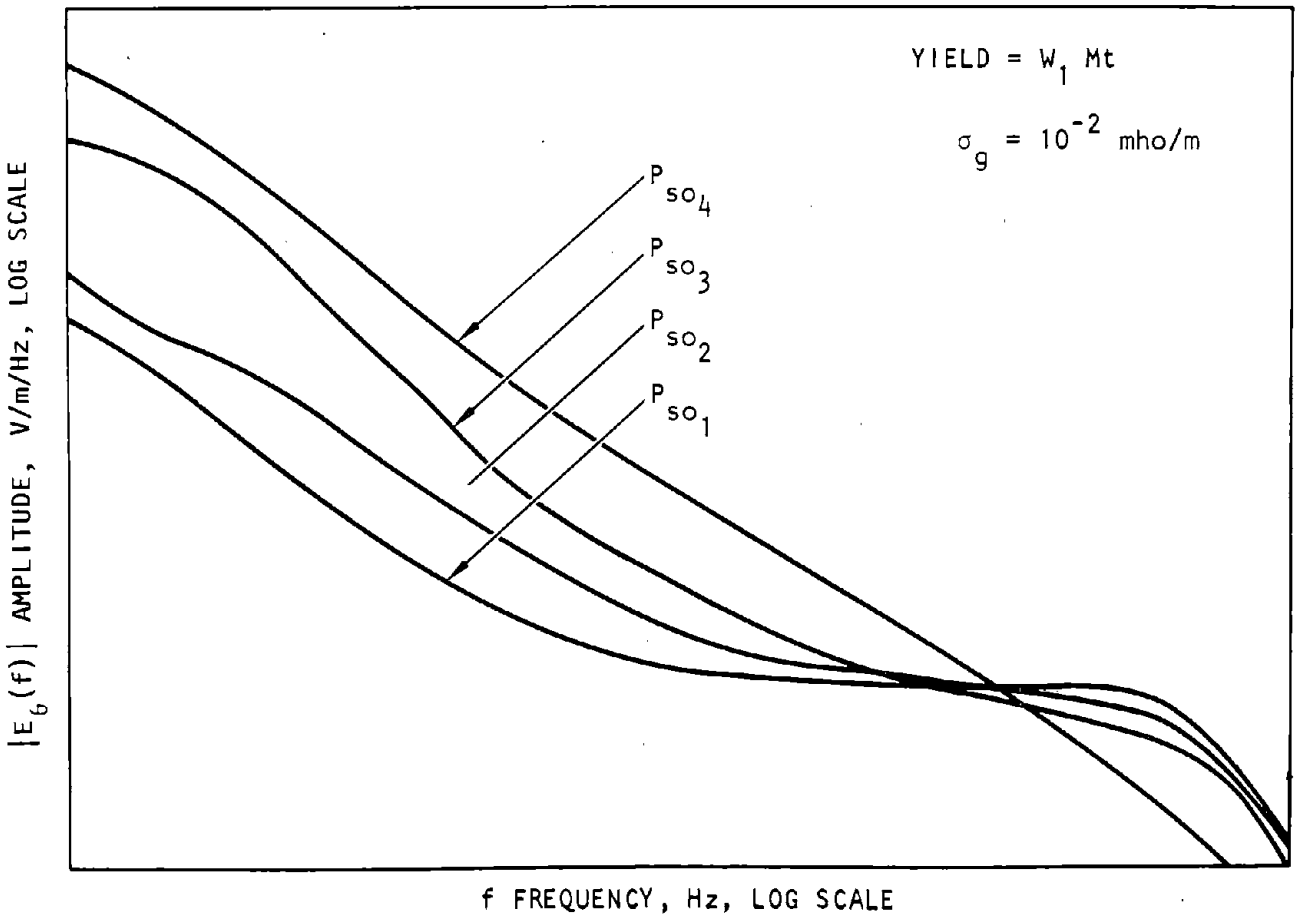

Figure 4–10. Fourier Amplitude of E_θ Waveform at the Air/Ground Interface for Several Overpressure Levels (DNA, 1972)

c. Facilities buried in the earth will experience a decrease in the amplitude of the EMP fields that occur at the air/earth interface. Facilities elevated several meters above the surface will experience a general (but not universal) attenuation of the EMP fields. Figures 4–2 through 4–10 illustrate characteristic curves. The uncertainty is derived as described in *d* below.

d. The uncertainties in predictions for surface-burst EMP depend on many variables; but for the threats of interest in this volume, the prime factors are overpressure and weapon yield, frequency, and calculational procedures. These uncertainties are sometimes referred to as tactical and calculational errors (AFWL EMP Handbook, 1972), which correspond to the terms "random" and "ignorance" uncertainties as used in this manual. Typical uncertainty bands for certain conditions are presented in figures 4–8 through 4–10. Typical examples are presented in figures 4–11 through 4–13 for the uncertainty bands on the Fourier amplitudes of the B_ϕ, E_R, and E_θ fields at the P_{so_2} range at a yield of W_1 and conductivity of 10^{-2} mho/m. (Similar curves are available in the *AFWL EMP Handbook* for other overpressure regimes and yields.) These data may be used directly to assess the uncertainties of EMP environments.

e. The method used for determining uncertainty throughout this volume is embodied in equation 2–16. Because of the lack of useable information, it is customary to neglect the second term (relating correlation between uncertainties). Thus,

$$\Omega_X^2 = \Omega_g^2 + \sum_{n=1}^{N} \frac{\bar{y}_n^2}{\bar{x}^2}\left(\frac{\partial g}{\partial Y_n}\right)_o^2 \Omega_{Y_n}^2 + \sum_{n\neq m}^{N}\sum^{N} \frac{\bar{y}_n \bar{y}_m}{\bar{x}^2}\left(\frac{\partial g}{\partial Y_n}\frac{\partial g}{\partial Y_m}\right)_o \varrho_{nm}\Omega_{Y_n}\Omega_{Y_m} \quad (2\text{–}16)$$

where $\bar{x} = g(\bar{y}_1, \bar{y}_2, \ldots \bar{y}_n)$ has the same meaning as in equation 2–15. Wherever possible in this manual, the function g is defined in closed form so that the derivatives $\frac{\partial g}{\partial Y_n}$ can be directly evaluated for each independent variable (such as P_{so}, W_1, Hz, σ_g). However, for EMP the form of the equations representing the data presented in figures 4–2 through 4–10 is too complicated for functional description. Accordingly, an alternate method is required, as described in *f* below.

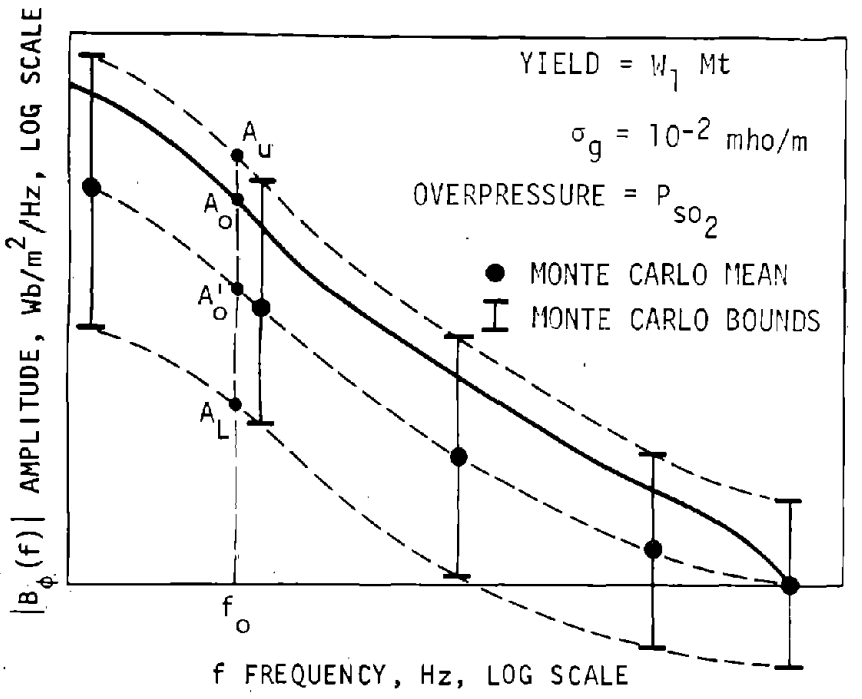

Figure 4–11. Uncertainty Bands ($\sigma = 1$) of the B_ϕ Fourier Amplitude at the Air/Ground Interface (AFWL, 1972)

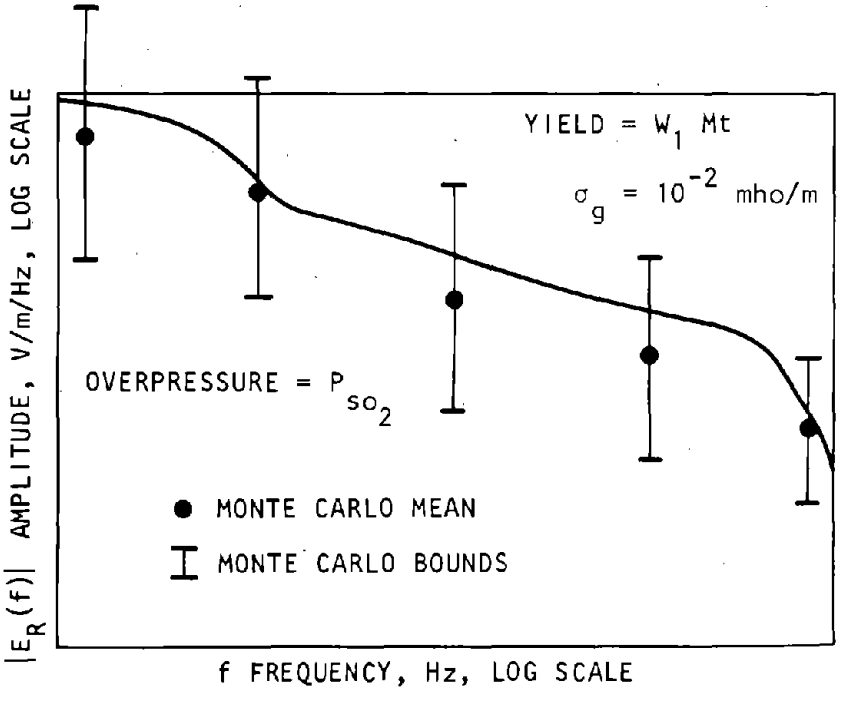

Figure 4–12. Uncertainty Bands ($\sigma = 1$) of the E_R Fourier Amplitude at the Air/Ground Interface (AFWL, 1972)

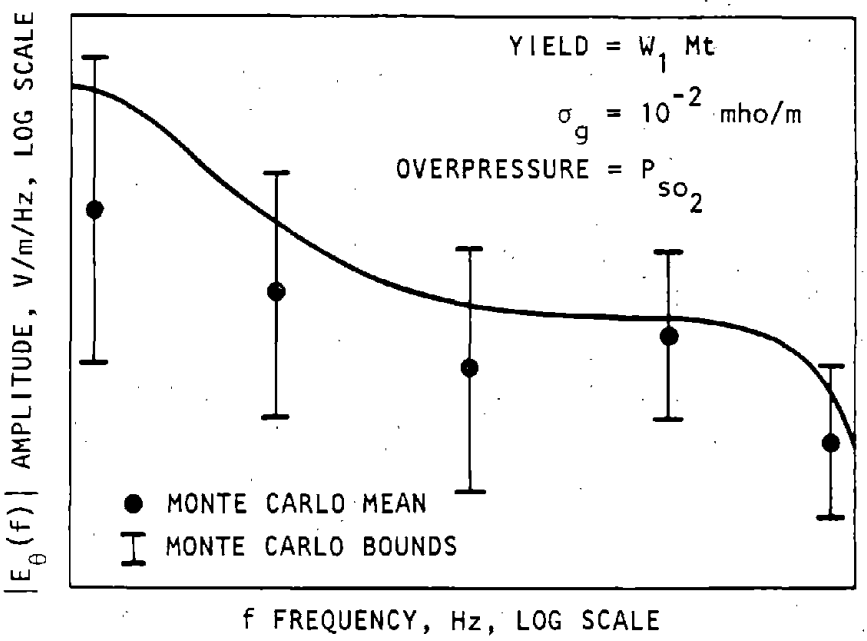

Figure 4-13. Uncertainty Bands (σ = 1) of the E_θ Fourier Amplitude at the Air/Ground Interface (AFWL, 1972)

f. Select a mean overpressure, mean weapon yield, mean ground conductivity, and mean frequency (DNA, 1972; AFWL, 1972). For example, in figure 4-8 select $\bar{y}_1 = \bar{P}_{so} = P_{so_2}$, $\bar{y}_2 = \bar{W} = W_1$, $\bar{y}_3 = \bar{\sigma}_g = 10^{-2}$ mho/m, and $\bar{y}_4 = \bar{f} = f_o$. This defines point A_o on figure 4-8 in which $\bar{x} = |\bar{B}_\phi(f)| = |B_\phi|_o$. Vary $\bar{y}_1$ within the limits, say of P_{so_1} and P_{so_3}, which produces a corresponding change in $\bar{x}$ (represented by the points B and C in figure 4-8). Thus, in equation 2-16, for the first independent variable y_1 and for n = 1,

$$\bar{y}_1^2 = (P_{so_2})^2$$

$$\bar{x}^2 = (|B_\phi|_o)^2$$

$$(\partial g)^2 \approx (\Delta g)^2 = (|B_{\phi_1}| - |B_{\phi_3}|)^2$$

$$(\partial y_1)^2 \approx (\Delta y_1)^2 = (P_{so_1} - P_{so_3})^2 \qquad (4\text{-}1)$$

The user must select Ω_{Y_1} as the uncertainty he wishes to assign to the overpressure variable. Therefore, for the first component of uncertainty, equation 2-16 becomes

$$\Omega^2_{B_\phi} = \Omega^2_g + \frac{(P_{so_2})^2}{(|B_\phi|_o)^2}\left[\frac{|B_{\phi_1}| - |B_{\phi_3}|}{P_{so_1} - P_{so_3}}\right]^2$$

$$\Omega^2_{P_{so}} + \sum_{n=2}^{4} \frac{\bar{y}_n^2}{\bar{x}^2}\left(\frac{\partial g}{\partial Y_n}\right)^2_0 \Omega^2_{Y_n} \qquad (4\text{-}2)$$

Equation 4-2 is completed by performing the same operation for the variables W, σ_g, and f (if desired) and the summation in equation 4-2 is replaced as three individual terms corresponding to the uncertainties in these three variables.

g. The uncertainty Ω_g in equation 4-2 is determined from the data presented in figures 4-11 through 4-14 (AFWL, 1972). Here, Ω_g refers to the data scatter obtained from Monte Carlo simulations performed by the AFWL.

h. Note that the Monte Carlo mean values (denoted by the symbol •) differ from the nominal mean values (denoted by the solid lines). Using the nominal curves as a guide, construct new curves through the Monte Carlo means and bounds as exemplified in figure 4-11 for $|B_\phi(f)|$ by the dashed lines. These curves may then be used to estimate the uncertainties of the Fourier spectra at any frequency.

i. From figure 4-11, for example, which corresponds to figure 4-8, the uncertainty Ω_g is determined from equation 2-18 where

$$R = \frac{1}{4}(A'_o/A_L + A_u/A'_o)^2$$

n = 1

Here, R is simply the squared averaged ratios of the bounds above and below the Monte Carlo mean. Note also that the mean value of $|B_\phi|$ (denoted by A_o in figure 4-11) was obtained from figure 4-8 and subsequently used in equation 4-2, whereas Ω_g was obtained from the mean and scatter bands in the Monte Carlo simulation.

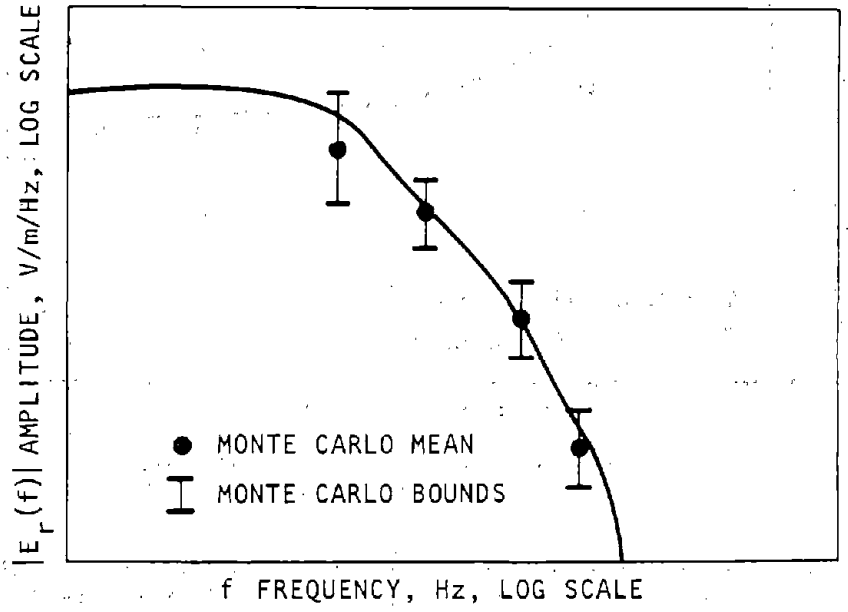

Figure 4–14. Fourier Amplitude of E_r Waveform of High-Altitude Radiated Signal (AFWL, 1972)

j. As noted in *b* above, the currents induced in a system should be calculated by including the system within the EMP environment, i.e., by considering the system and free field environment to be coupled. When making EMP calculations using computer programs, the uncertainties in the field calculations depend on the uncertainties in the mathematical model and the value of its parameters. With these calculations it is recommended that sufficient data be computed to allow evaluation of equation 2–15. This means that a few auxiliary computations should be made to allow for determination of the derivatives in that equation as outlined in the previous paragraphs. The user will be required to ascertain for himself the nonrandom and random errors involved in such calculations.

4–3. High-altitude burst.

a. Any burst occurring at altitudes above 100,000 ft (30,480 m) is a high-altitude burst and may produce EMP fields that cover geographical areas as large as the continental United States.

b. The electric field of the EMP is defined by

$$E_r = E_o \left[1 - e^{-t/\tau_1}\right] e^{-t/\tau_2} \quad V/m \qquad (4\text{–}3)$$

where τ_1 and τ_2 control the rise and decay times of the pulse and E_o is the peak amplitude of the pulse (*DNA EMP Handbook*, GE-TEMP, 1971). It is noted that the amplitude of the EMP depends on (1) the prompt gamma ray yield, which is a function of nuclear weapon yield, and (2) the location of the system relative to the detonation point. A typical pulse is shown in figure 4–15. The corresponding Fourier spectrum is presented in figure 4–14. The radiated magnetic field B_r is proportional to E_r (eq. 4–3) according to the relation

$$B_r = \frac{E_r}{C_o} \quad Wb/m^2 \qquad (4\text{–}4)$$

where C_o is the speed of light in a vacuum (3.0×10^8 m/s).

c. The data referenced in GE-TEMPO (1971) should be considered mean values of the free-field environment.

d. Accounting for the uncertainties of high-altitude-burst EMP predictions parallels the procedures discussed in paragraphs 4–2 *d* through *i* for determining surface-burst EMP environments, and should be calculated accordingly.

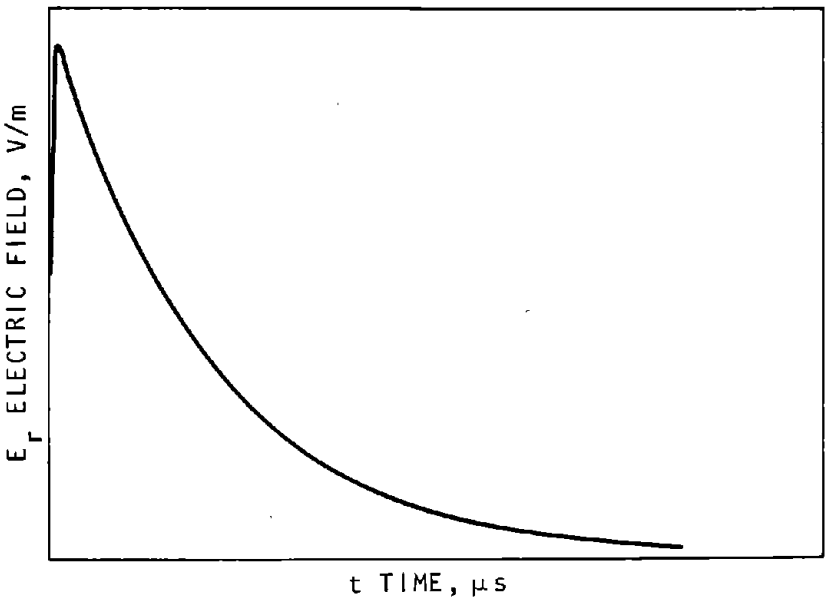

Figure 4–15. E_r-Time Waveform of High-Altitude Radiated Signal (DNA, 1972)

CHAPTER 5
FIREBALL

5-1. Gross phenomenology.

a. In the explosion of nuclear weapons, a large amount of energy (kilotons to megatons TNT equivalent) is released in a time much less than a millionth of a second and in a small volume extending slightly beyond the weapon. The resulting high-energy density produces a high-temperature (millions of degrees Kelvin, °K), high-pressure, thermally radiating plasma core. This core (the fireball) expands hydrodynamically because of the high internal pressure and radiates because of the high temperature. The radiation, primarily in the x-ray region of the electro-magnetic spectrum, is absorbed and reradiated by the surrounding air. Temperatures in the neighborhood of 1,000,000°K persist for a few hundred microseconds. As the fireball expands and its temperature drops, radiation diffusion becomes less important. Hydrodynamic expansion, which produces compression heating of the air behind the radiation front, overtakes the radiation front, developing a strong shock that continues to heat air to temperatures in excess of 10,000°K for tens of milliseconds.

b. The variables affecting the potential destructiveness of the fireball at a ground surface location are the weapon yield and slant range. The larger the weapon yield, the greater the temperature and the engulfment duration will be at a given range. If the burst elevation is greater than the fireball radius, then engulfment will not occur and the effects of thermal radiation will control the design. How to determine the effects from thermal radiation is presented in chapter 6.

c. Immersion of the facility or its components in the fireball, or ingestion of fireball gases by the facility can lead to debilitating thermal loads. Knowledge of the fireball size and its time/temperature/density characteristics are required to determine the design strategy—avoidance or resistance—and the degree of protection required.

5-2. Engulfment radius.

a. The maximum fireball radius is represented by an equation of the form

$$R_{max} = C_1 W^{n_1} e^{n_2 Z} ft \qquad (5\text{–}1)$$

where W is weapon yield in kilotons (kt); z is HOB in ft; and C_1, n_1, and n_2 are constants. Within this radius, facilities will be engulfed by the fireball. The temperatures within the fireball are presented below in paragraph 5-3.

b. The mean radius is calculated from equation 5-1 using $C_1 = 250$ for a contact burst or 220 for a surface intersecting fireball, $n_1 = 0.35$, and $n_2 = 8.8 \times 10^{-6}$.

c. The uncertainty associated with equation 5-1 is

$$\Omega^2_{R_{max}} = \Omega^2_f + \Omega^2_{C_1} + n_1^2\Omega^2_W + Z^2\Omega^2_z \qquad (5\text{–}2)$$

where Ω_f is the uncertainty in the form of equation 5-1, Ω_{C_1} is the uncertainty of the coefficient C_1, etc. Assume that $\Omega_f \approx 0.2$ and $\Omega_{C_1} = 0.15$ (from equation 2.16 in which n = 2 and R = 1.86).

5-3. Temperature and density.

a. The temperature and density within the fireball are shown in figures 5-1 and 5-2 as a function of range for a family of early times. Fireball temperature is shown in figure 5-3 as a function of range for a series of later times, and in figure 5-4 as a function of time for a family of ranges.

b. The peak fireball temperature vs. range can be represented by an equation of the form

$$\log T_o = A + B \log (R/W^{1/3}) + C \log^2(R/W^{1/3}) + D \log^3(R/W^{1/3}) \qquad (5\text{–}3)$$

where

T_o = Peak temperature in K
R = Range from GZ in ft
W = Yield in kt
A,B,C,D are constants

c. The mean peak fireball temperature in equation 5-3 is given by the following coefficients for mean peak fireball temperature:

A	B	C	D
-479.2	566.4	-235.4	32.36

d. The uncertainty associated with equation 5-3 is

$$\Omega^2_T = \Omega^2_f + 5.3\left[A^2 + B^2 \log^2 (R/W^{1/3}) + C^2 \log^4 (R/W^{1/3}) + D^2 \log^6 (R/W^{1/3})\right]\Omega^2_{C_o} + \left[B + 2C \log (R/W^{1/3}) + 3D \log^2 (R/W^{1/3})\right]^2 (\Omega^2_R + \Omega^2_W/9) \qquad (5\text{–}4)$$

where Ω_f is the uncertainty of the functional form of equation 5-3, Ω_{C_o} is the uncertainty of the coefficients, Ω_R is the uncertainty of the range. Although

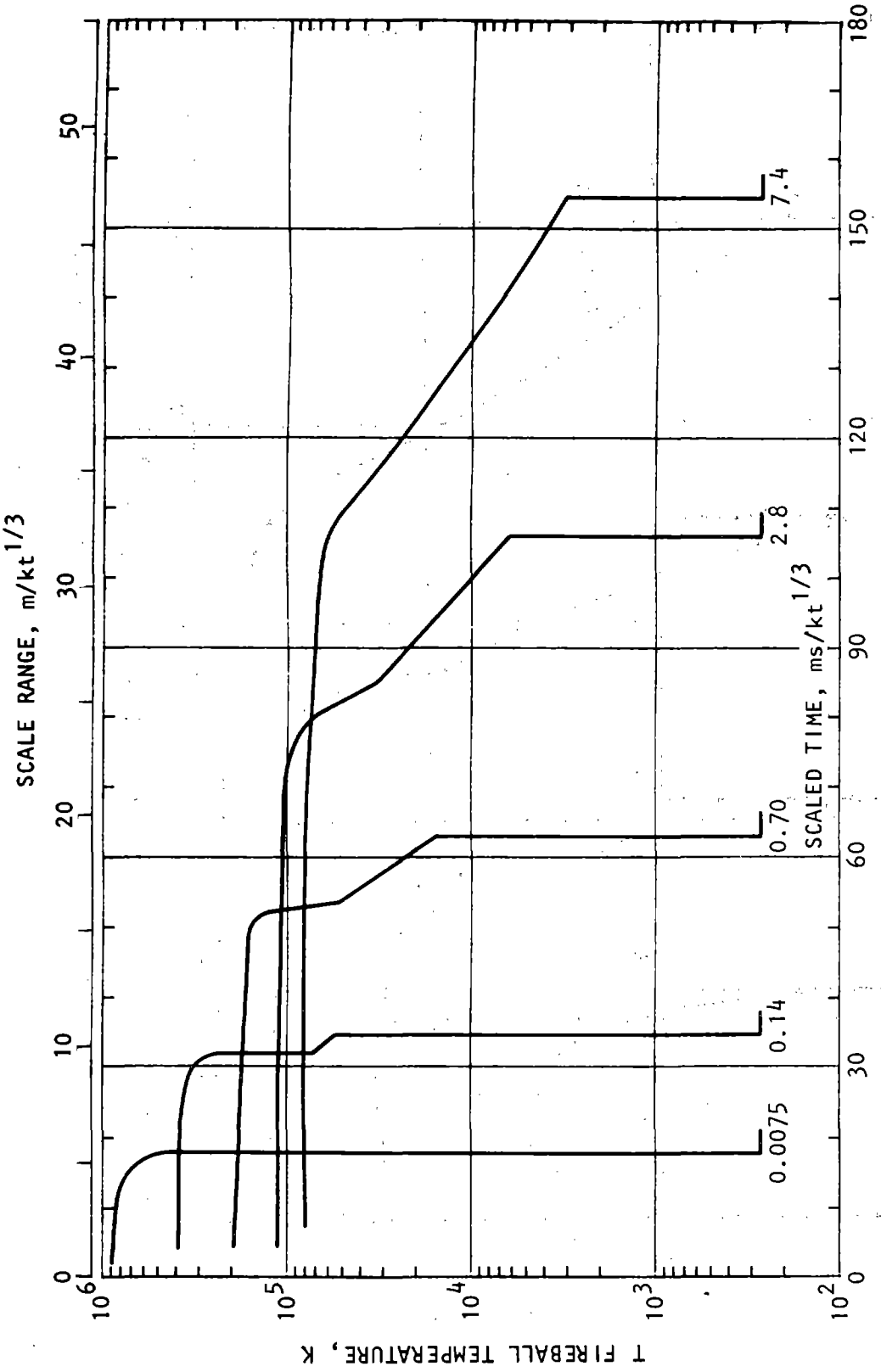

Figure 5-1. Fireball Temperature Vs. Radius at Early Times in the Fireball History (adapted from Brode, 1964)

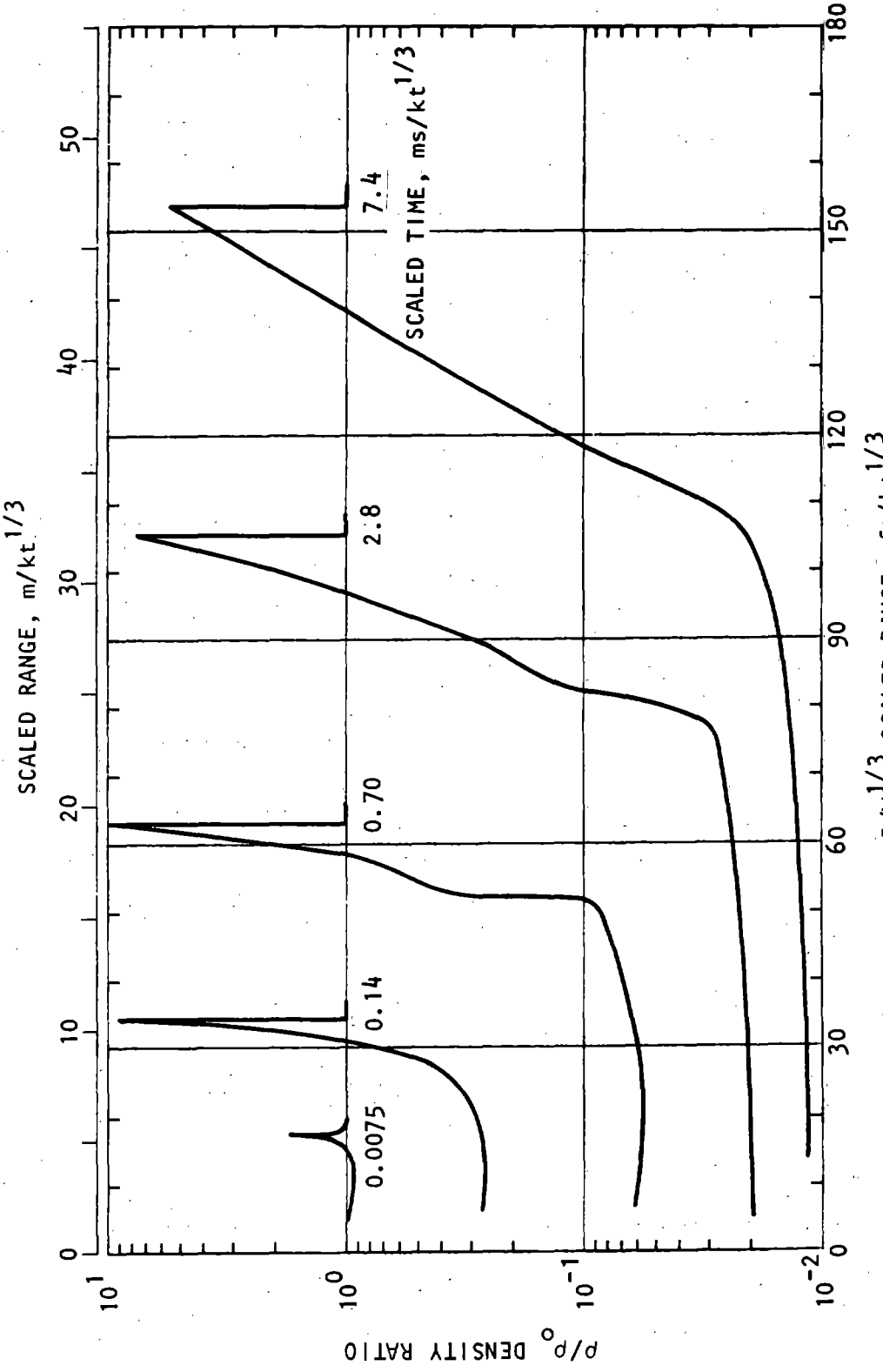

Figure 5-2. Fireball Density Vs. Radius at Early Times in the Fireball History (adapted from Brode, 1964)

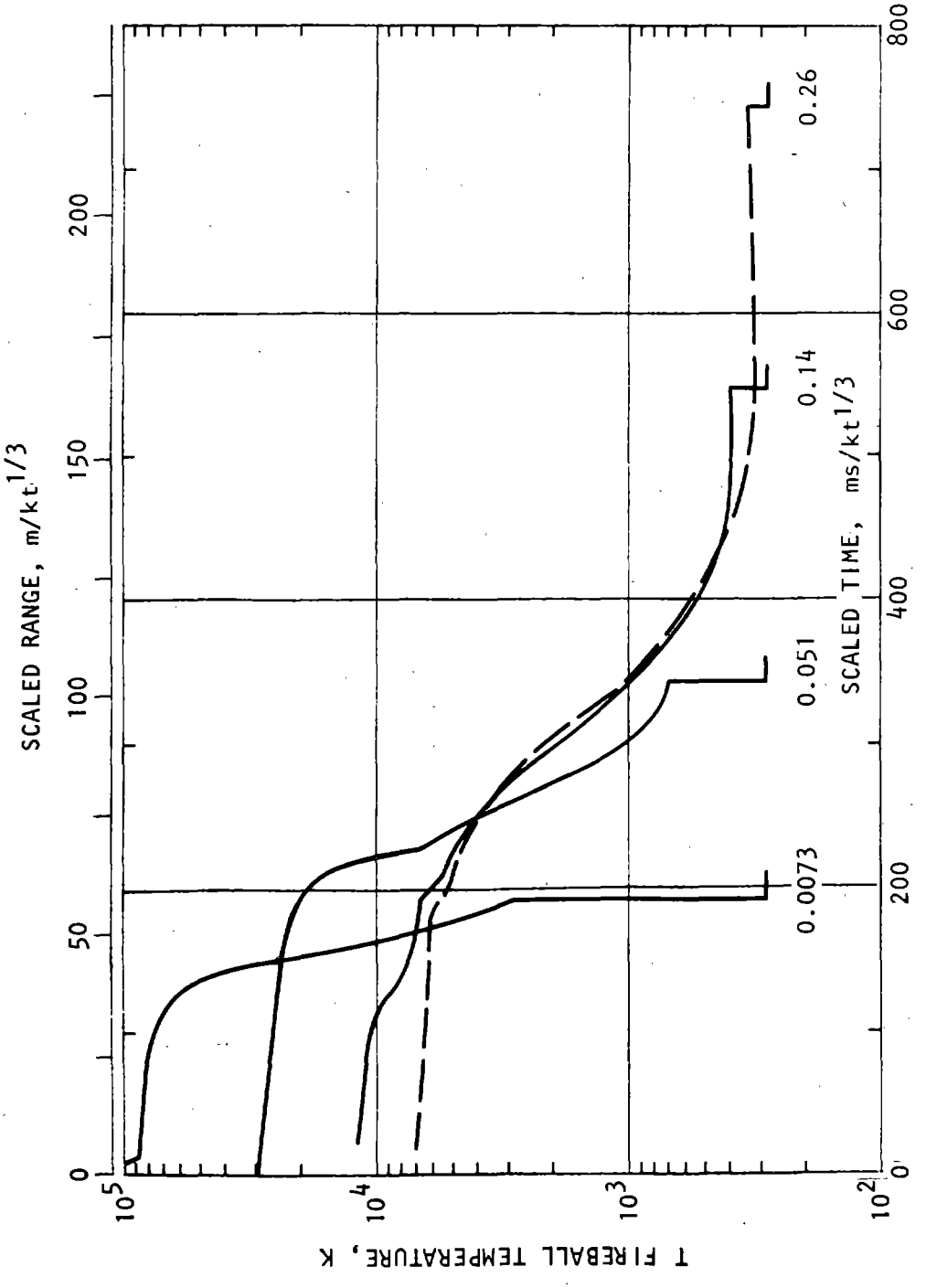

Figure 5–3. Late Fireball Temperature Vs. Radius (adapted from Brode, 1964)

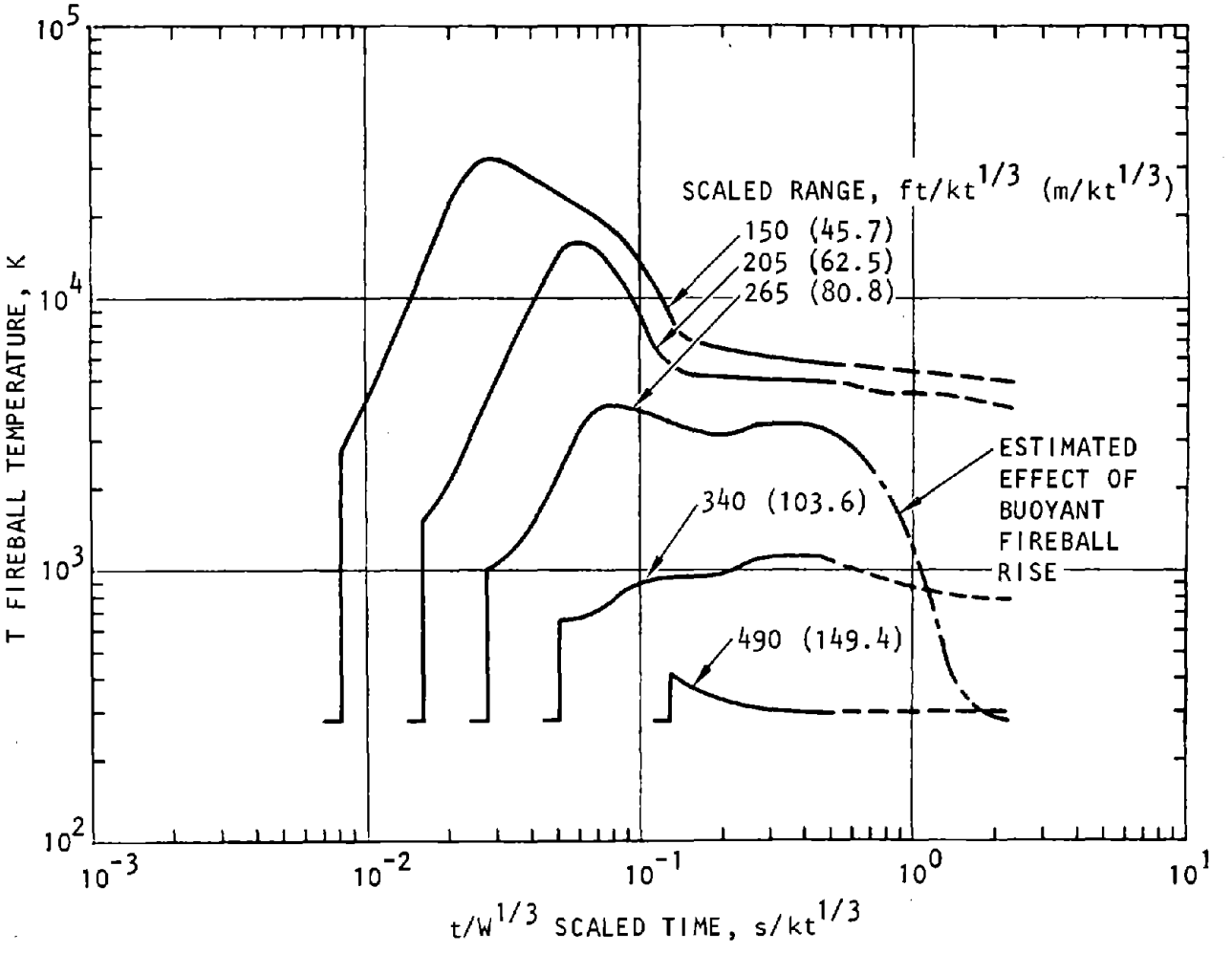

Figure 5–4. Temperature Vs. Time at High Peak Overpressures (adapted from Brode, 1964)

insufficient data exist to accurately assess the uncertainty of equation 5–3 at this time, it is recommended that $\Omega_f \approx 0.2$ and $\Omega_{C_0} \approx 0.3$.

e. Duration of temperature is of interest. Since the fireball is like a bubble in the atmosphere, it begins to rise, and pulls away from the earth's surface in only a few tenths of a second/kt$^{1/3}$. Using a very approximate model for the effect of buoyant fireball rise on the temperature history at a scaled ground range of 265 ft/kt$^{1/3}$ (80.8 m/kt$^{1/3}$), it appears that the late-time temperature environment will be reduced in approximately the manner indicated by the decreasing tail in figure 5–4. Thus a sharp temperature decrease begins after 0.4 or 0.5 s/kt$^{1/3}$ of exposure, and in 1.5 to 2.0 s/kt$^{1/3}$ the air temperature has returned to normal ambient. Temperatures at other ranges would be similarly reduced at late times by the same effect. At the scaled ranges of 205 and 150 ft/kt$^{1/3}$ (62.5 and 45.7 m/kt $^{1/3}$), temperatures increase even more but subsequently show a more rapid drop (at times less than 0.1 scaled second) because of thermal radiation loss, which becomes significant even before the fireball has begun to rise.

CHAPTER 6
THERMAL RADIATION

6-1. Gross phenomenology.

a. A thermal-radiation pulse is emitted by the expanding fireball. The thermal radiation received at a ground surface of design interest to this volume comprises energy in the ultraviolet, the visible, and the infrared spectral bands. The radiated thermal power reaches a peak in about 1 s/$Mt^{0.5}$. The pulse lasts, for all practical design purposes, about 10 s/$Mt^{0.5}$.

b. The basic variables affecting affecting the potential destructiveness of the free-field thermal-radiation pulse are the:

- Weapon design
- Weapon yield
- Burst elevation
- Slant range
- Transmittance by the intervening atmosphere
- Reflectance of clouds and of ground surface

The larger the weapon yield, the greater the height of burst, the smaller the slant range, the greater the transmittance, or the greater the reflectance, the greater will be the potential destructiveness from thermal radiation.

c. The thermal-radiation pulse can cause fires and the degradation of the mechanical properties (possibly melting) of an exposed facility or facility component. The facility designers must either account for these effects in their design or preclude them by burying (or otherwise protecting) the facility or facility component. Knowledge of two characteristics of the free-field thermal-radiation pulse is required to implement design measures: Radiant exposure and radiation history.

6-2. Radiant exposure.

a. The total amount of radiant energy impinging on a unit area of a surface that is facing the fireball is called the radiant exposure of the surface. The radiant exposure is

$$Q = AWfTF/R^2 \text{ cal/cm}^2 \qquad (6\text{–}1)$$

where W = Weapon yield, Mt
f = Thermal efficiency of the weapon (*b* below)
T = Transmittance of the intervening atmosphere (*c* below)
F = Reflectance of clouds and the ground surface (*e* below)
R = Slant range, kft
A = Constant

Equation 6–1 is applicable for slant ranges greater than about $1100kT^{0.4}$ for an airburst or $145kT^{0.4}$ for a contact surface burst. The radius of the fireball at which the airblast shock breaks away and races ahead. The radiant exposure at closer points is negligible compared to the subsequent heat load in the enveloping fireball gases, which is treated in chapter 5.

(1) The mean radiant exposure is obtained from equation 6–1 where A = 86,000.

(2) The uncertainty associated with the radiant exposure is

$$\Omega_Q^2 = \Omega_g^2 + \Omega_A^2 + \Omega_W^2 + \Omega_f^2 + \Omega_T^2 + \Omega_F^2 + 4\Omega_R^2 \qquad (6\text{–}2)$$

where Ω_g is the uncertainty parameter associated with the functional form of Q, Ω_W is the uncertainty parameter associated with the weapon yield W, and so forth. Assume that $\Omega_g^2 + \Omega_A^2 \approx 0.1$. The uncertainties of the transmittance, thermal efficiency, and reflectance are developed in the paragraphs below.

b. The thermal efficiency f of a weapon is the ratio of the thermal energy radiated by the fireball to the total yield of the weapon. The thermal efficiency of an ordinary nuclear weapon that is detonated in a low-altitude burst is

$$f = C + Bh/W^{1/3} \quad 0 < h < 2.5 \text{ kft/Mt}^{1/3} \qquad (6\text{–}3)$$

where
h = Height of burst, kft
W = Weapon yield, kt
B and C are constants

(1) The mean thermal efficiency of an ordinary nuclear weapon that is detonated as a low-altitude burst is obtained from equation 6–3 where B = 0.078 and C = 0.21. Assume that the mean thermal efficiency of an air burst is 0.4, and of a contact burst is 0.2. The thermal efficiency of a shallow-buried burst is small compared to that for a contact burst. A so-called enhanced weapon (enhanced nuclear radiation) exhibits lower thermal efficiencies than those cited above.

(2) The uncertainty associated with the thermal efficiency of an ordinary nuclear weapon that is detonated as a low-altitude burst is

$$\Omega_f^2 = \Omega_g^2 + \frac{h^2B^2}{f^2W^{2/3}}\left(\Omega_h^2 + \Omega_W^2/9\right) \qquad (6\text{–}4)$$

Assume, $\Omega_g \approx 0.24$ for an air burst and ≈ 0.3 for a contact burst.

c. The transmittance T is the ratio of the radiant energy reaching a surface facing the fireball to the radiant exposure that the surface would receive if the

intervening atmosphere were perfectly transparent and there were no reflecting surfaces. The transmittance for ground-surface targets is

$$T = (1 + aR/V) \exp (bR/V) , \; h < 1.5 \text{ kft} \qquad (6\text{–}5a)$$

$$T = \exp\left[(\alpha + \beta h + \gamma h^2)\, \Gamma R/V\right], \qquad (6\text{–}5b)$$
$$1.5 \text{ kft} < h < 10 \text{ kft}$$

where

R = Slant range, kft
V = Daytime visibility, kft
a, b, Γ, α, β, and γ are constants

Equation 6–5 is based on the assumption that the atmosphere is cloudless, but not necessarily clear of haze, fog, smoke, or dust.

(1) The mean transmittance is obtained from equation 6–5 where a = 1.9, b = –2.9, Γ = –84.5, α = 3.0, β = –0.286, γ = 0.01. Equation 6–5 is plotted in figure 6–1. The discontinuity in the transmittance shown in the figure is not physical, but is a consequence of the uncertainty in the two transmittance models for the two ranges of burst height in equation 6–5.

(2) The uncertainty associated with the transmittance for the two ranges of burst heights are

$$\Omega_T^2 = \Omega_f^2 + \frac{R^2 \exp(2bR/V)}{V^2 T^2}\left[b(1 + aR/V) + a\right]^2 (\Omega_R^2 + \Omega_V^2) , \quad h < 1.5 \text{ kft} \qquad (6\text{–}6a)$$

$$\Omega_T^2 = \Omega_f^2 + \frac{R^2\Gamma^2}{V^2}\left[(\alpha + \beta h + \gamma h^2)^2 (\Omega_R^2 + \Omega_V^2) + h^2(\beta + 2\gamma h)^2\, \Omega_h^2\right], \quad 1.5 < h \leq 10 \text{ kft} \qquad (6\text{–}6b)$$

where Ω_f is the uncertainty parameter for the functional form of equation 6–5, Ω_R is the uncertainty parameter for the slant range, etc. Assume $\Omega_f \approx 0.1$. The uncertainty of the visibility is calculated subsequently.

d. The U.S. Weather Bureau defines day-time visibility as the distance at which a prominent dark object, located near the ground and silhouetted against the sky, is visible and recognizable. Night-time visibility is defined as the distance an unfocused, moderately intense light source is visible. The day-time visibility for generic cloudless atmospheric conditions is given in table 6–1. Assume that the day-time and night-time visibilities are identical for identical atmospheric conditions.

(1) Establish the facility-site, relative-frequency visibility function using visibility statistics obtained from a local weather station or from personnel at the site vicinity. For the seven classes of visibility delineated in table 6–1 the facility-site, relative-frequency function ϕ is constructed as shown in figure 6–2 such that the sum of $\phi_{0.8} + \phi_{1.5} + \ldots \phi_{32} = 1.0$. The subscripts refer to the seven classes of visibility. A typical relative-frequency factor is depicted in figure 6–2. Convert the weather station's night-time visibilities to equivalent day-time visibilities using

$$V = 20\, V_{\text{night}}^{5/4} \text{ kft} \qquad (6\text{–}7)$$

Calculate the mean visibility $\overline{V}$ as shown in figure 6–2. Use a base period of one year for calculating visibility.

(2) The uncertainty associated with the visibility is

$$\Omega_V^2 = \Delta_V^2 + \delta_V^2 \qquad (6\text{–}8)$$

where

Δ_V = Coefficient of variation of the mean of V relative to its true value
δ_V = Coefficient of variation of V, as illustrated in figure 6–2.

Assume that $\Delta_V \approx 0.17$.

(3) The effect of prior bursts can be important. Bursts below about 2900 ft/Mt$^{0.4}$ create a dust cloud that will shroud the facility for many hours. Consider the effect of the dust cloud when calculating the visibility for each burst of a multiple-burst attack, except the first burst (chap. 13).

e. The reflectance F is the ratio of the radiant energy reaching a surface facing the fireball when there are clouds and/or a reflecting ground surface, to the radiant exposure that the surface would receive in the absence of clouds and a reflecting ground surface. The reflectance is

$$F = F_{ca}\, F_{cb}\, F_g \qquad (6\text{–}9)$$

where

F_{ca} = Reflectance of a layer of clouds above the burst
F_{cb} = Reflectance of a layer of clouds below the burst
F_g = Reflectance of the ground surface

(1) The mean reflectance is obtained from equation 6–9 where the mean values of F_{ca}, F_{cb}, and F_g are obtained from *f, g, h* below

(2) The uncertainty associated with the reflectance is

$$\Omega_F^2 = \Omega_{F_{ca}}^2 + \Omega_{F_{cb}}^2 + \Omega_{F_g}^2 \qquad (6\text{–}10)$$

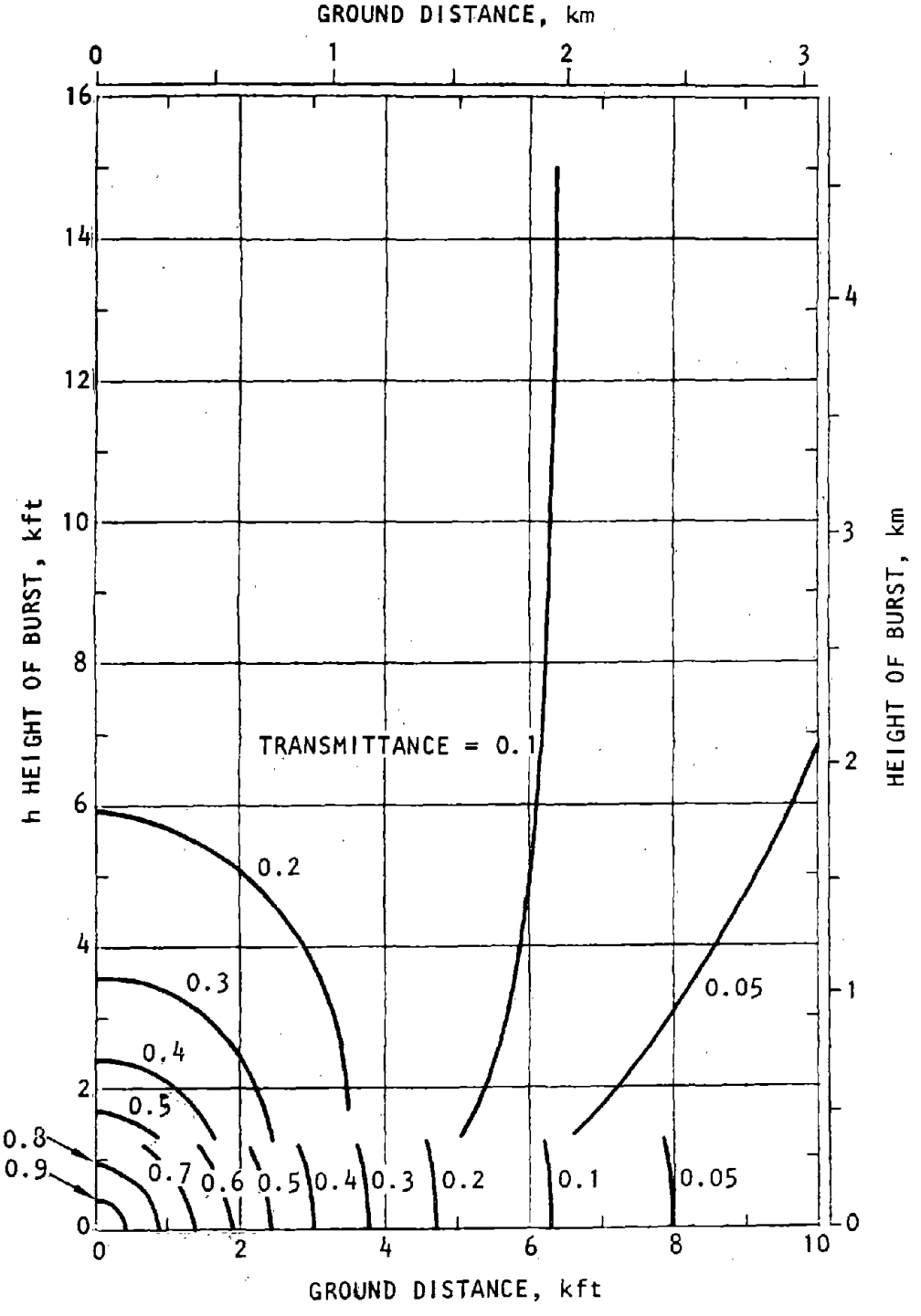

(a) Visibility = 1 mi

Figure 6-1. Mean Transmittance for a Ground-Surface Target (SAI, 1971) (1 of 5)

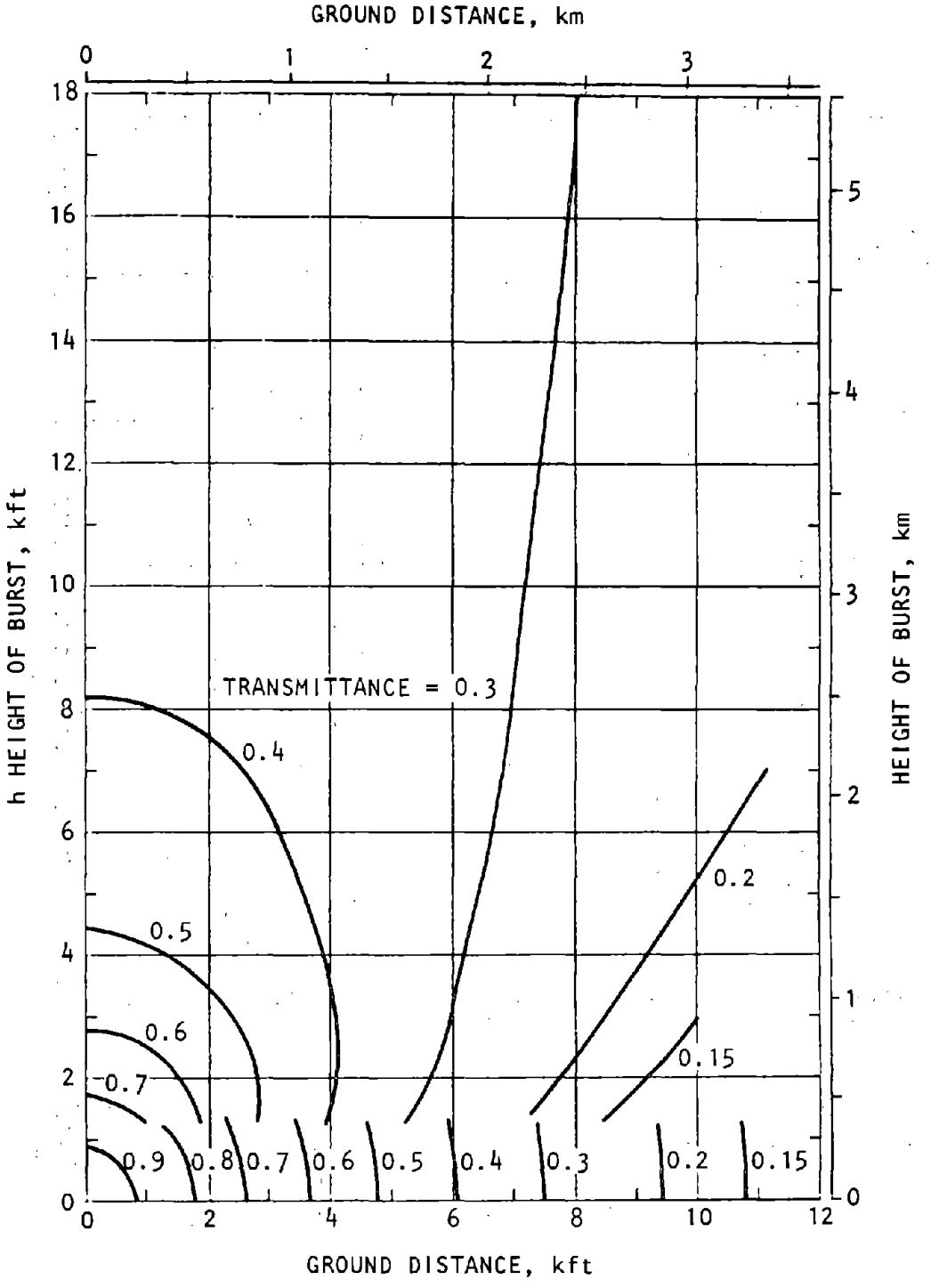

(b) Visibility = 2 mi

Figure 6–1. Mean Transmittance for a Ground-Surface Target (SAI, 1971) (2 of 5)

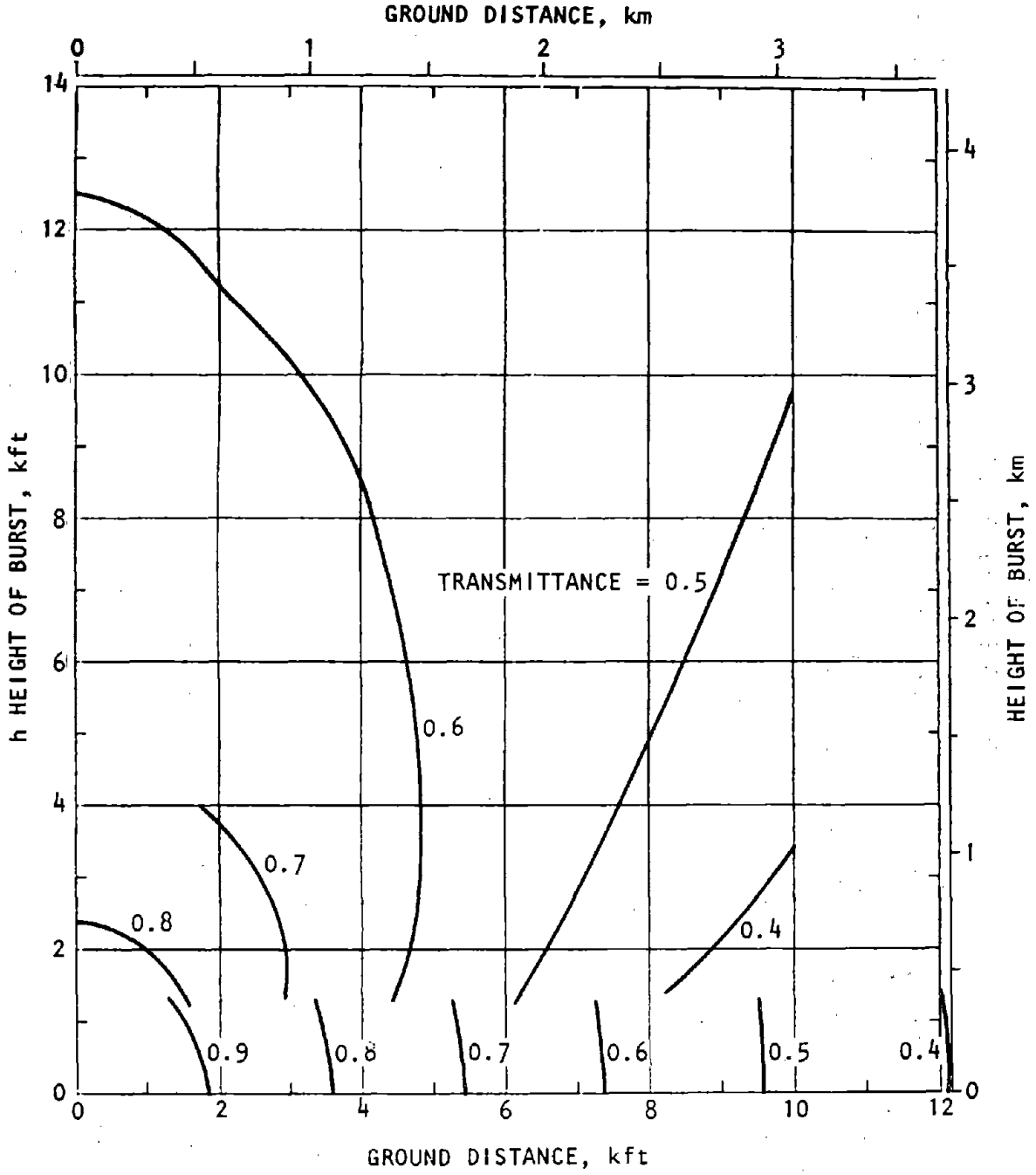

(c) Visibility = 4 mi

Figure 6-1. Mean Transmittance for a Ground-Surface Target (SAI, 1971) (3 of 5)

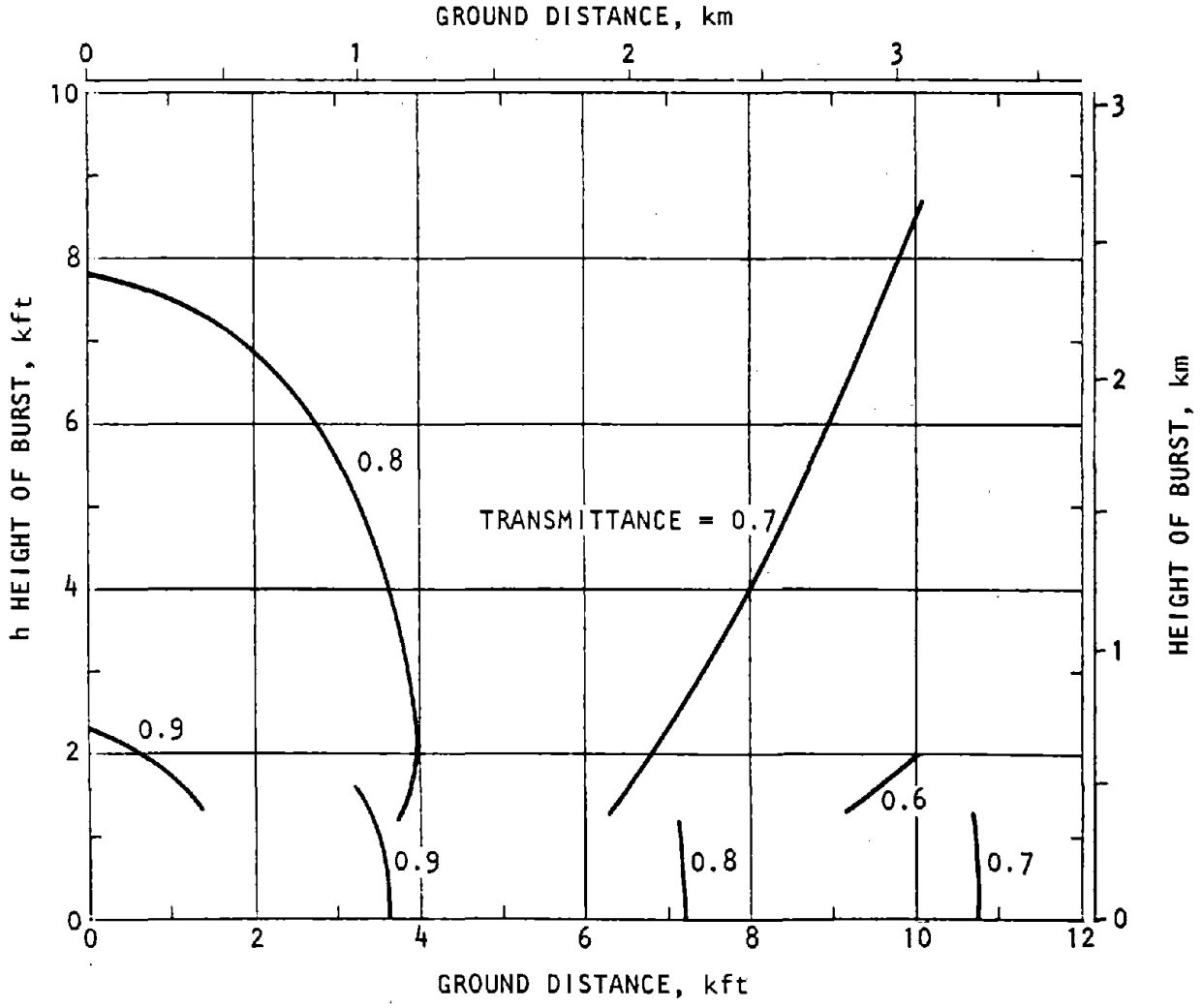

(d) Visibility = 8 mi

Figure 6–1. Mean Transmittance for a Ground-Surface Target (SAI, 1971) (4 of 5)

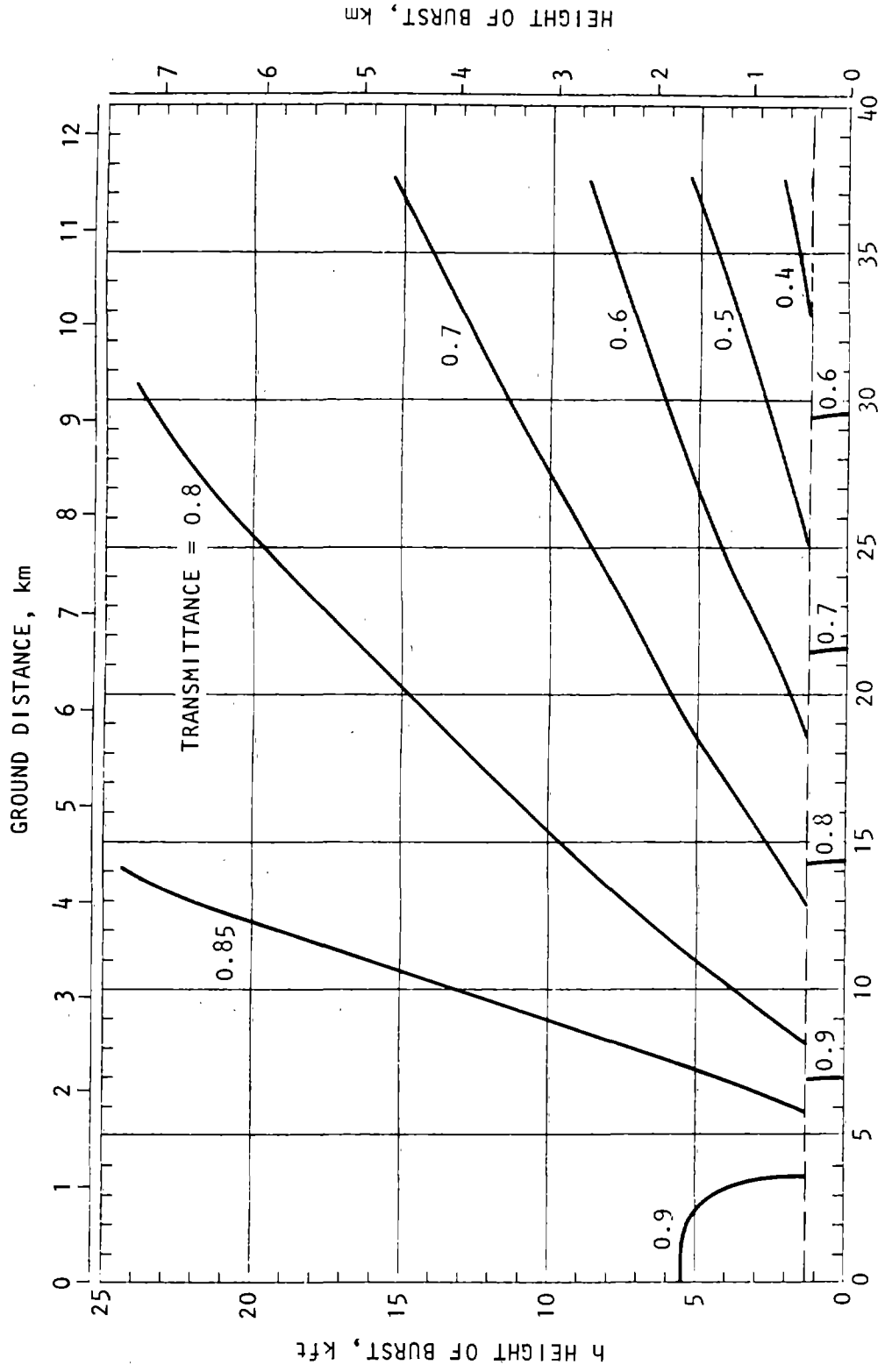

(e) Visibility = 16 mi

Figure 6-1. Mean Transmittance for a Ground-Surface Target (SAI, 1971) (5 of 5)

Table 6-1. Day-time Visibility for Generic Cloudlessness (DNA, 1972)

Type	Description	Visibility	
		mi	(km)
Very clear	This condition rare except at high-altitude locations.	32.0	51.5
Clear	Sky deep blue. Shadows distinct, dark.	16.0	25.7
Light haze	Sky white; dazzling near sun. Shadows visible, gray.	8.0	12.9
Medium haze	Sky bright grayish-white. View sun without serious discomfort. Shadows visible but faint.	4.0	6.4
Heavy haze	Sky dull gray-white. Sun's disc just visible. Shadows barely discernible.	3.0	4.8
Thin fog	Sky light gray with maximum luminance around sun. Sun's disc not visible, no shadows.	1.5	2.4
Light fog	Sky dull gray with maximum luminance at zenith.	0.8	1.3

$$\phi_{0.8} + \phi_{1.5} + \phi_{3.0} + \ldots + \phi_{32} = 1.0$$

$$\bar{V} = 0.8\,\phi_{0.8} + 1.5\,\phi_{1.5} + 3.0\,\phi_{3.0} + \ldots + 32\,\phi_{32}$$

$$\delta_V^2 = (1 - 0.8/\bar{V})^2\,\phi_{0.8} + (1 - 1.5/\bar{V})^2\,\phi_{1.5} + \ldots + (1 - 32/\bar{V})^2\,\phi_{32}$$

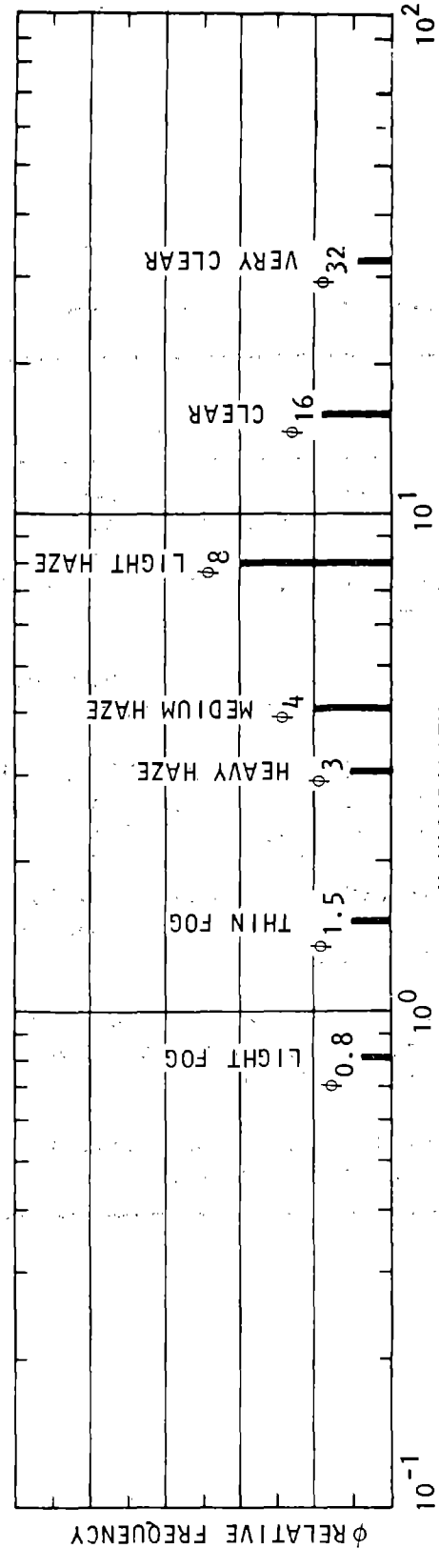

Figure 6-2. Visibility: Calculation of Mean and Coefficient of Variation (Adjust ordinate so that $\Sigma\phi_n = 1.0$)

f. When the burst occurs below a cloud layer, the reflectance is

$$F_{ca} = A + B\phi_{ca} \qquad (6\text{-}11)$$

where A and B are constants and ϕ_{ca} is the fraction of a year that clouds appear in the site vicinity at a height above burst elevations of interest.

(1) The mean clouds-above reflectance is obtained from equation 6-11 where A = 1.0 and B = 0.5.

(2) The uncertainty associated with the clouds-above reflectance is

$$\Omega^2_{F_{ca}} = \Delta^2_{F_{ca}} + \frac{0.25\,\phi_{ca}\left(1 - \phi_{ca}\right)}{\left(1 + 0.5\,\phi_{ca}\right)^2} \qquad (6\text{-}12)$$

where $\Delta^2_{F_{ca}}$ is the coefficient of variation of F_{ca} relative to its true value. Assume that $\Delta_{F_{ca}} \approx 0.1$.

g. When a layer of haze or clouds is below the burst, but high enough not to affect visibility, the reflectance F_{cb} is as shown in table 6-2. For this condition, use V = 16 mi in the calculation of transmittance.

(1) Calculate the mean value of the clouds-below reflectance as illustrated in figure 6-3. Use a base period of one year for calculating the mean value of F_{cb}. The method of calculating the mean reflectance parallels the procedure described in *d* above.

Table 6-2. Reflectance F_{cb} for Layer of Clouds or Haze Below the Burst (DNA, 1972)

Type	Description	Reflectance
Very clear	This condition rare except at high-altitude locations.	1.0
Clear	Sky deep blue. Shadows distinct, dark.	0.95
Light haze	Sky white; dazzling near sun. Shadows visible, gray.	0.75
Medium haze	Sky bright grayish-white. View sun without serious discomfort. Shadows visible but faint.	0.5
Heavy haze	Sky dull gray-white. Sun's disc just visible. Shadows barely discernible.	0.4
Light cloud	Sky light gray with maximum luminance around sun. Sun's disc not visible, no shadows.	0.3
Medium cloud	Sky dull gray with maximum luminance at zenith.	0.2
Heavy cloud	Sky dark gray; brightness pattern gives no indication of sun's position.	0.13
Dense cloud	The low luminance level suggests the approach of nightfall. Murky.	0.06

$$\phi_{0.06} + \phi_{0.13} + \phi_{0.2} + \cdots + \phi_{1.0} = 1.0$$

$$\bar{F}_{cb} = 0.06\ \phi_{0.06} + 0.13\ \phi_{0.13} + 0.2\ \phi_{0.2} + \cdots + 1.0\ \phi_{1.0}$$

$$\delta^2_{F_{cb}} = \left(1 - 0.06/\bar{F}_{cb}\right)^2 \phi_{0.06} + \left(1 - 0.13/\bar{F}_{cb}\right)^2 \phi_{0.13} + \cdots + \left(1 - 1.0/\bar{F}_{cb}\right)^2 \phi_{1.0}$$

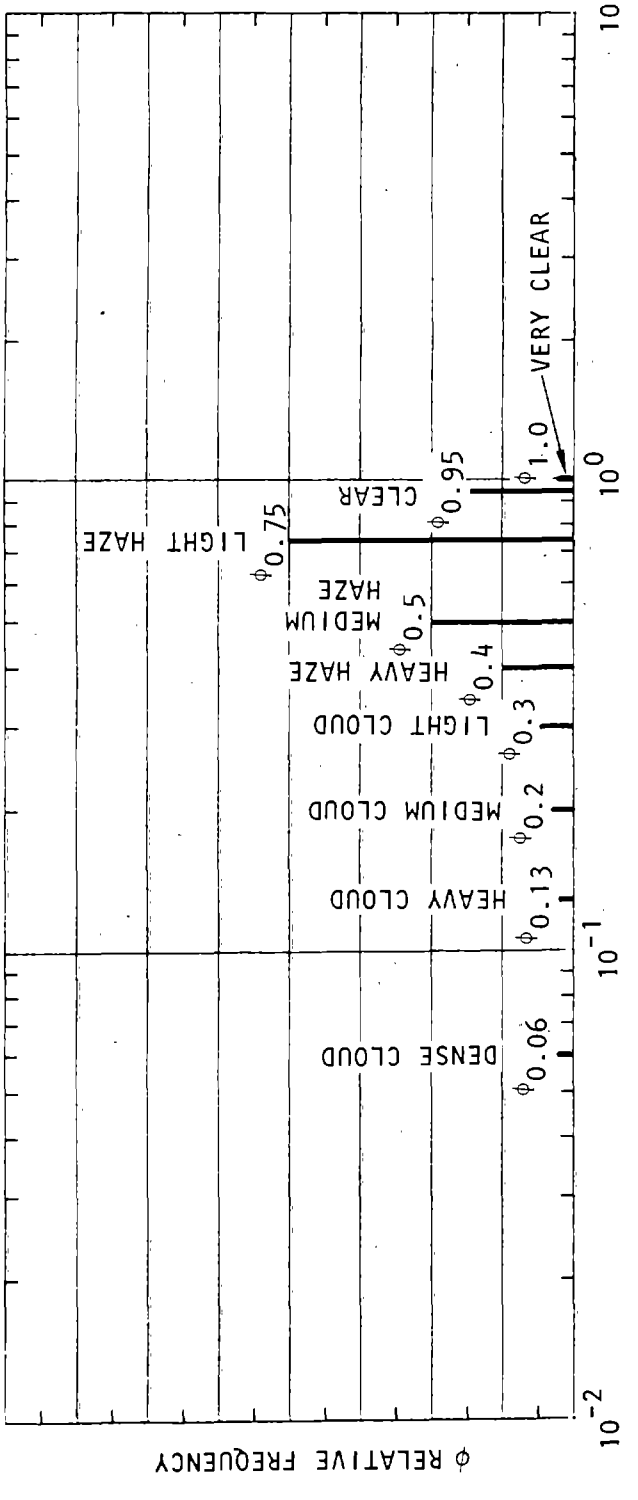

Figure 6–3. Clouds-Below Reflectance: Calculation of Mean and Coefficient of Variation

(2) The uncertainty associated with the clouds-below reflectance is

$$\Omega^2_{F_{cb}} = \Delta^2_{F_{cb}} + \delta^2_{F_{cb}} \quad (6\text{-}13)$$

where

$\Delta_{F_{cb}}$ = Coefficient of variation of the mean value of F_{cb} relative to its true value
$\delta_{F_{cb}}$ = Coefficient of variation of F_{cb}, as calculated in figure 6–3

Assume that $\Delta_{F_{cb}} \approx 0.40 - 0.35\ F_{cb}$.

h. The ground surface reflectance in the facility-site vicinity is given by

$$F_g = K_1 + K_2\phi_g \quad (6\text{-}14)$$

where ϕ_g is the fraction of the year that the ground surface appears bright. Snow and light-colored soil qualify as bright surfaces.

(1) The mean ground-surface reflectance is obtained from equation 6–14 where $K_1 = 1$ and $K_2 = 0.5$.

(2) The uncertainty associated with ground-surface reflectance is

$$\Omega^2_{F_g} = \Delta^2_{F_g} + \frac{0.25\ \phi_g(1 - \phi_g)}{(1 + 0.5\ \phi_g)^2} \quad (6\text{-}1)$$

where Δ_{F_g} is the coefficient of variation of F_g relative to its true value. Assume that $\Delta_{F_g} \approx 0.1$.

(3) Dust created by prior bursts will settle out and decrease the reflectance of a bright surface. Consider this effect when calculating the reflectance for each burst of a multiple-burst attack, except the first burst (chap. 13).

6–3. Radiation history.

a. The history of the radiation energy is relatively complex, exhibiting several peaks and valleys. The details of the history are strongly influenced by the weapon yield, and the burst elevation. For purposes of design, the simple fractional radiant-exposure history shown in figure 6–4 can be used in place of the radiation history. The functional form of a curve fitted to the fractional radiant-exposure history of figure 6–4 is

$$Q_t = Q\left[1 - \exp\left[\alpha t/t_o + \beta\,(t/t_o)^2\right]\right] \text{ cal/cm}^2,\ 1 < t/t_o < 10 \quad (6\text{-}15)$$

where

Q = Total radiant exposure, cal/cm^2
t = Time, seconds
t_o = Normalizing time, seconds (*b* below)
α, β are constants

(1) The mean fractional radiant-exposure is obtained from equation 6–16 where $\alpha = -0.5$ and $\beta = 0.33$.

(2) The uncertainty associated with the fractional radiant-exposure is

$$\Omega^2_{Q_t} = \Omega^2_g + \Omega^2_Q + \left(1 - \frac{Q}{Q_t}\right)^2\left[\alpha t/t_o + 2\beta(t/t)^2\right]^2\ \Omega^2_{t_o} \quad (6\text{-}16)$$

Assume $\Omega_g = 0.1$.

b. The normalizing time t_o is

$$t_o = AW^{\varepsilon}\left[1 + Bh + Ch^2\right]^{\sigma} \text{ sec} \quad (6\text{-}17)$$

where

W = Weapon yield in Mt
h = Height of burst, kft
A, B, C, ε, σ are constants

(1) The mean normalizing time is obtained from equation 6–18 where $A = 0.84$, $\varepsilon = 0.431$, $B = -0.0162$ $C = 7.2 \times 10^5$ and $\sigma = 0.764$. The mean normalizing time can also be obtained from figure 6–5.

(2) The uncertainty associated with the normalizing time is

$$\Omega^2_{t_o} = \Omega^2_g + \varepsilon^2\ \Omega^2_W + \sigma^2 h^2\left[\frac{B + 2Ch}{1 + Bh + Ch^2}\right]^2 \Omega^2_h \quad (6\text{-}19)$$

where Ω_W is the uncertainty parameter for the yield and Ω_h is the uncertainty parameter for the HOB. Assume $\Omega_g \approx 0.17$.

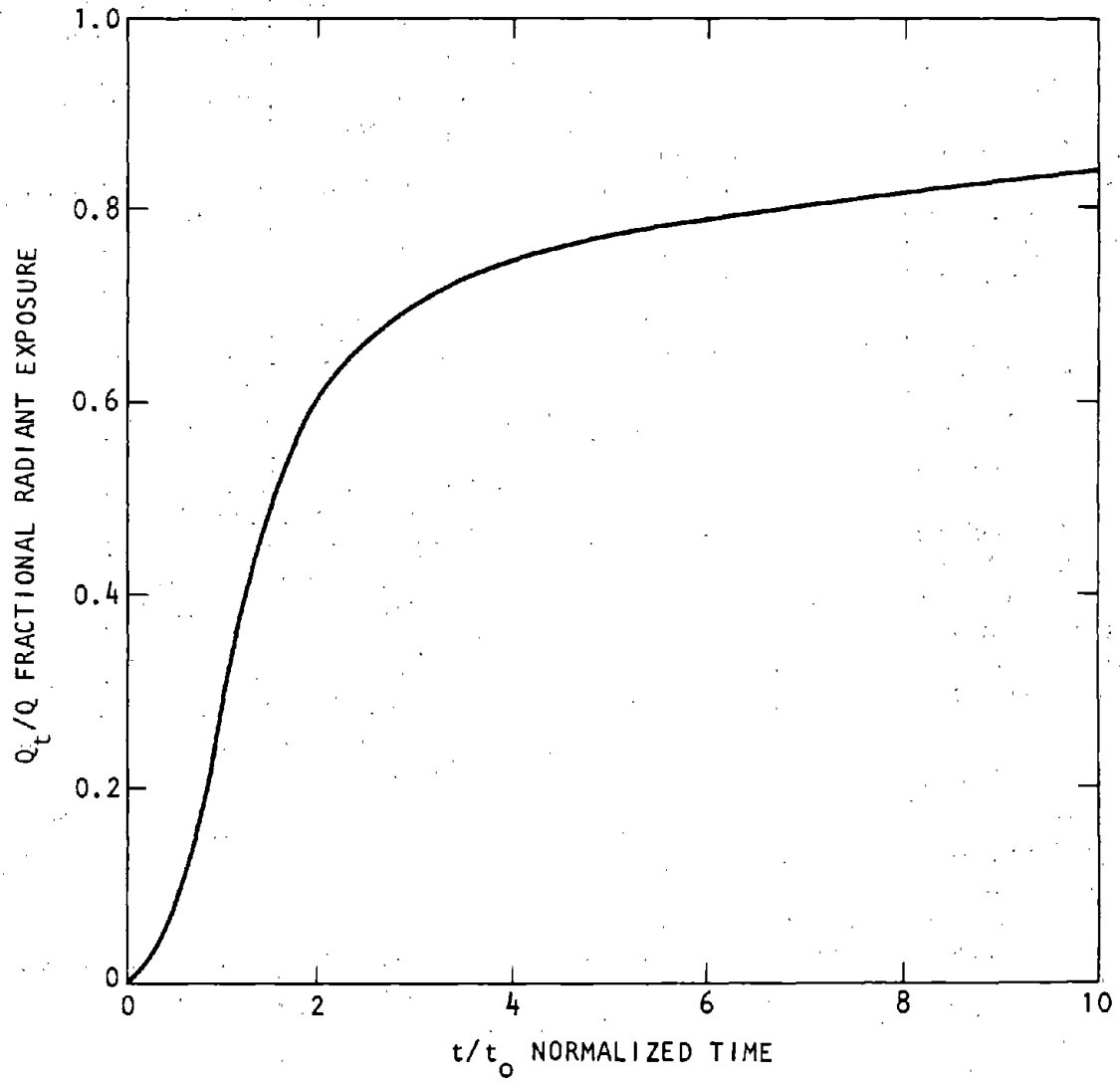

Figure 6–4. Fractional Radiant Exposure

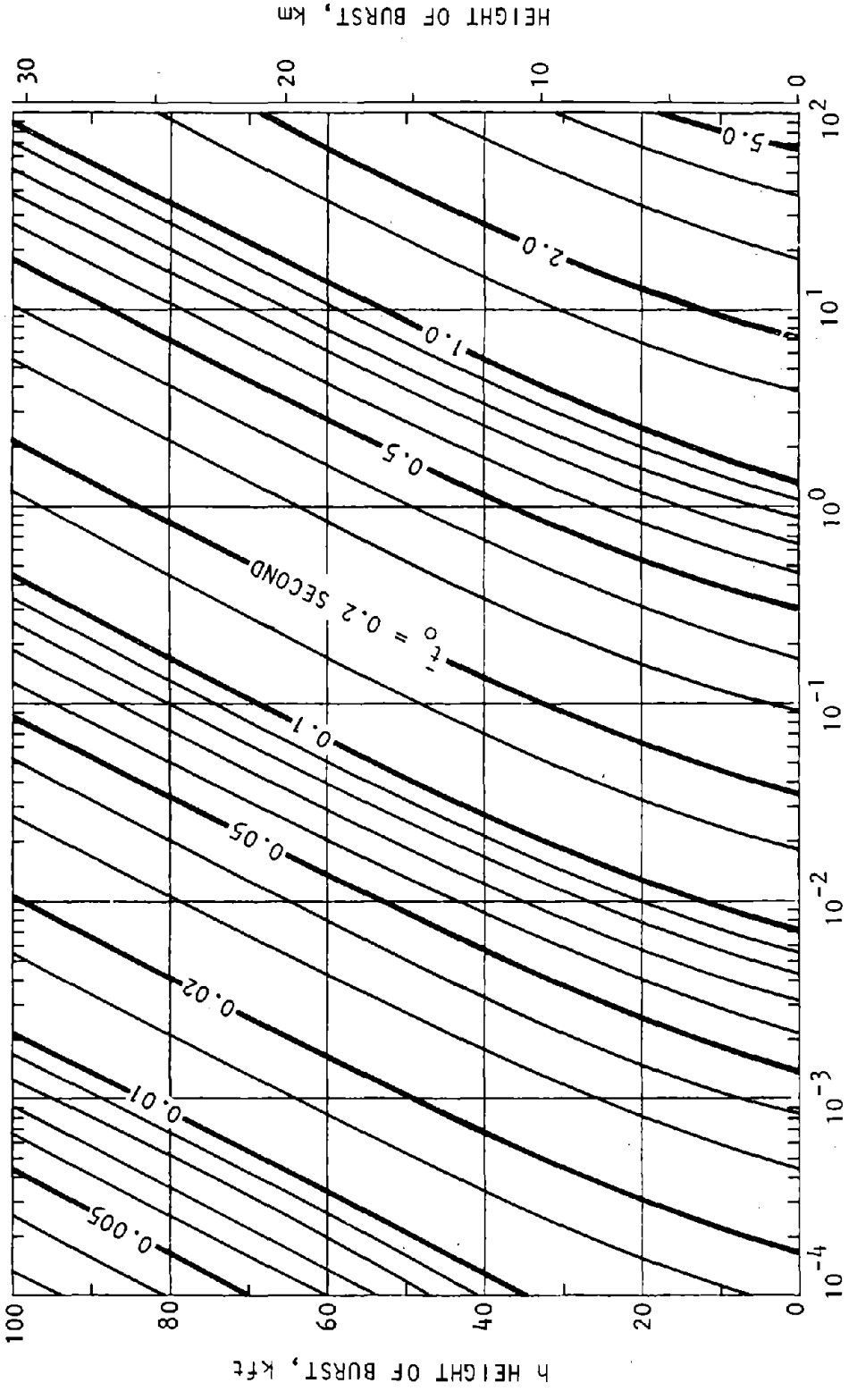

Figure 6-5. Mean Normalizing Time (DNA, 1972)

CHAPTER 7
AIRBLAST

7-1. Gross phenomenology.

a. Hydrodynamic expansion of bomb debris and fireball produces an expanding shock wave in the surrounding air. Interaction with the ground surface affects the detailed structure and geometry of the expanding shock wave.

b. A contact burst at a scaled elevation no greater than 5 ft/kt$^{1/3}$ (1.5 m/kt$^{1/3}$) produces a hemispherical shock front expanding supersonically. At scaled heights of burst between 5 and 160 ft/kt$^{1/3}$ (48.8 m/kt$^{1/3}$), the incident spherical shock reflects from the ground (fig. 7–1); the reflected signal, traveling at a higher speed in air heated by the incident shock, eventually overtakes the incident shock, forming a Mach stem that connects the ground with the triple point (which is the intersection of incident, reflected, and Mach stem shocks). The dynamic movement of the air behind the Mach stem causes a second shock to form, producing double shock phenomena (Brode-Lewis, 1975). Thermal-radiant heating of the ground ahead of the Mach stem causes the formation of a precursor shock, which trails back and merges with the Mach stem. The aspects of airblast important to the designer are the overpressure and dynamic pressure pulses. These are often described by the principal parameters: peak pressure, positive phase duration, and positive phase impulse (the time integral of the pressure history). Overpressure and dynamic pressure histories are also required; they are summarized in paragraphs 7–2 and 7–3.

c. The basic variables governing airblast are:

- Weapon design
- Weapon yield
- Range from detonation
- Burst elevation
- Surface conditions
- Surface contour
- Structural configuration

The larger the weapon yield, the greater the height of burst up to the limit of the Mach stem, or the

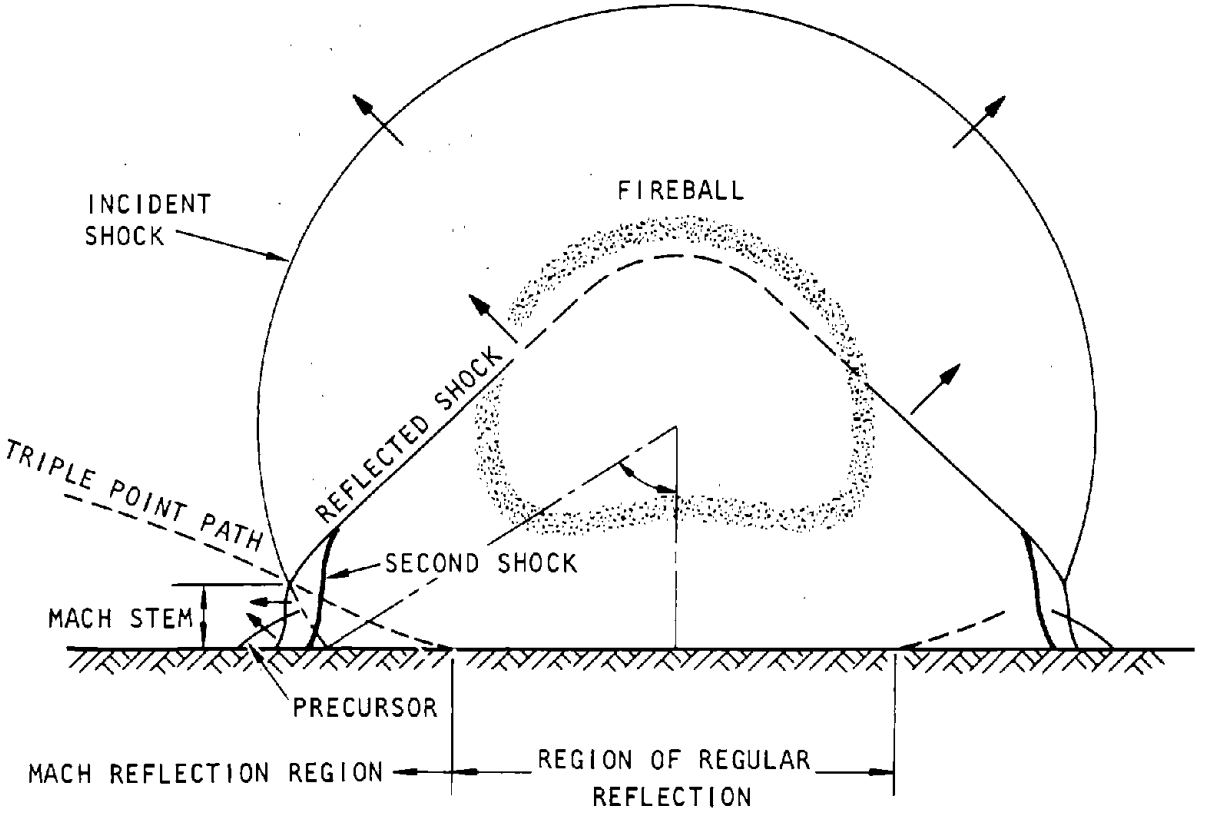

Figure 7–1. Composition of Shocks Due to Nuclear Airburst (Brode, 1964)

shorter the range, the greater will be the potential destructiveness of the airblast. The influence of the other variables is more complex; changes in weapon design and terrain conditions may amplify or attenuate the local airblast environment.

d. At the ground surface or in exposed configurations, structures can be dealt a crippling or fatal blow by the airblast. The facility designer must either account for the effects in the design or prevent the structures' direct exposure to airblast. To determine the degree of resistance necessary and to support selection of the design approach, knowledge of the airblast waveform, peak pressure, positive phase duration, and positive phase impulse are required.

7-2. Free-field peak overpressure.

a. Surface to moderately high airburst. The peak overpressure P_{so} depends on scaled HOB (height of burst), scaled range from GZ (ground zero), and terrain characteristics. In general, the peak overpressure P_{so} may be defined as a piecewise function of scaled range for a given scaled HOB, as indicated in the following equation:

$$P_{so} = C_p \left(\frac{R}{W^{1/3}}\right)^{n_p} \text{psi}, \; R_{p-1} < R < R_p$$

$$p = 1, 2, \ldots, N \qquad (7\text{-}1)$$

where R is the range from GZ in ft and W is yield in kt. The coefficients C_p and exponents n_p depend on scaled range, scaled HOB and the terrain characteristics.

(1) Ground surfaces are characterized as thermally "near-ideal" (in which a precursor shock is not likely to form) or thermally "nonideal" (in which a precursor shock is likely to form). Table 7-1 presents a compilation of ideal and nonideal surfaces. These categories are used to define the parameters of equation 7-1.

(2) The mean values to be used in equation 7-1 are presented in table 7-2 for ideal and nonideal surfaces. The corresponding data from which the table was prepared are presented in figures 7-2 and 7-3. These data are also presented in figures 7-4 through 7-10, which should be used directly for selecting mean values.

Table 7-1. Thermally Near-Ideal and Thermally Nonideal Surfaces (DNA, 1972)

Thermally Near-Ideal (precursor unlikely)	Thermally Nonideal (precursor may occur)
Water	Desert sand
Ground covered by white smoke layer	Coral
Heat-reflecting concrete	Asphalt
Frozen tundra	Surfaces with low, thick vegetatio
Ice	Surfaces covered by a dark smoke layer
Packed snow	Dark colored rock
Soil with sparse vegetation	Most agricultural areas; residential areas in cities
Commercial and industrial areas	Dry soil with sparse vegetation

Table 7-2. Parameters for Peak Overpressure

Scaled HOB		Scaled Range			
$ft/kt^{1/3}$	$(m/kt^{1/3})$	$ft/kt^{1/3}$	$(m/kt^{1/3})$	C_p	n_p
Near-Ideal Surface					
0	(0)	170 to 330	(52 to 101)	1.80×10^9	-2.93
		330 to 1000	(101 to 305)	1.84×10^7	-2.09
		1000 to 3800	(305 to 1158)	1.55×10^6	-1.73
200	(61)	270 to 330	(82 to 101)	4.76×10^9	-3.04
		330 to 1220	(101 to 372)	6.85×10^6	-1.92
		1220 to 4400	(372 to 1341)	2.60×10^4	-1.67
400	(122)	290 to 500	(88 to 152)	1.63×10^9	-2.92
		500 to 1350	(152 to 411)	3.19×10^7	-1.78
		1350 to 4900	(411 to 1494)	1.04×10^6	-1.63
600	(183)	200 to 520	(61 to 158)	7.86×10^2	-0.52
		520 to 1520	(158 to 463)	*	*
		1520 to 5600	(463 to 1707)	1.06×10^6	-1.61
800	(244)	450 to 1500	(137 to 457)	6.92×10^3	-0.58
		1500 to 6000	(457 to 1829)	1.50×10^6	-1.63
1000	(305)	300 to 800	(91 to 244)	1.65×10^2	-0.42
		800 to 2000	(244 to 610)	*	*
		2000 to 6500	(610 to 1981)	5.79×10^5	-1.51
2000	(610)	600 to 2500	(183 to 762)	8.09×10^1	-0.47
		2500 to 5300	(762 to 1615)	3.17×10^3	-0.94
Nonideal Surface					
0	(0)	150 to 340	(46 to 104)	1.18×10^9	-2.79
		340 to 1000	(104 to 305)	1.95×10^7	-2.09
		1000 to 3700	(305 to 1128)	1.91×10^6	-1.76
200	(61)	240 to 750	(73 to 229)	4.89×10^8	-2.68
		750 to 1200	(229 to 366)	2.40×10^2	-0.48
		1200 to 4400	(366 to 1341)	6.75×10^5	-1.60
400	(122)	210 to 480	(64 to 146)	2.46×10^5	-1.46
		480 to 1650	(146 to 503)	*	*
		1650 to 5000	(503 to 1524)	7.83×10^5	-1.59
600	(183)	140 to 360	(43 to 110)	7.21×10^2	-0.54
		360 to 880	(110 to 268)	2.79×10^3	-0.77
		880 to 5600	(268 to 1707)	9.93×10^5	-1.60
800	(244)	300 to 600	(91 to 183)	2.19×10^2	-0.42
		600 to 1500	(183 to 457)	1.14×10^3	-0.68
		1500 to 6000	(457 to 1829)	4.02×10^5	-1.48
1000	(305)	300 to 800	(91 to 244)	1.55×10^2	-0.41
		800 to 1920	(244 to 585)	4.16×10^2	-0.56
		1920 to 6400	(585 to 1951)	4.68×10^5	-1.49
2000	(610)	550 to 2500	(168 to 762)	7.29×10^1	-0.46
		2500 to 5300	(762 to 1615)	1.96×10^3	-0.88

*Note: Compute values from Figures 7-2 or 7-3.

U.S. Army Corps of Engineers

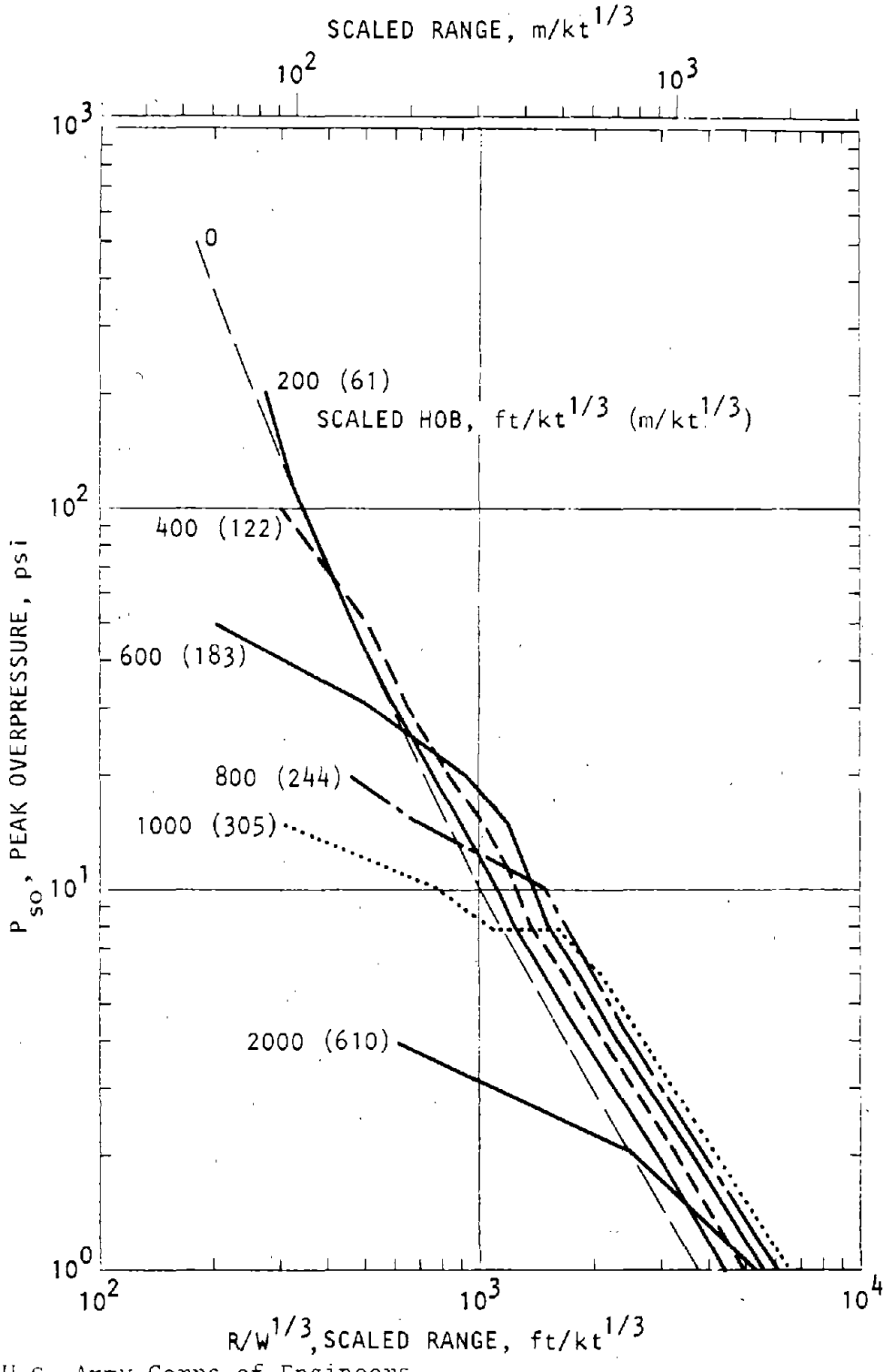

Figure 7-2. Peak Overpressure at Thermally Near-Ideal Surfaces

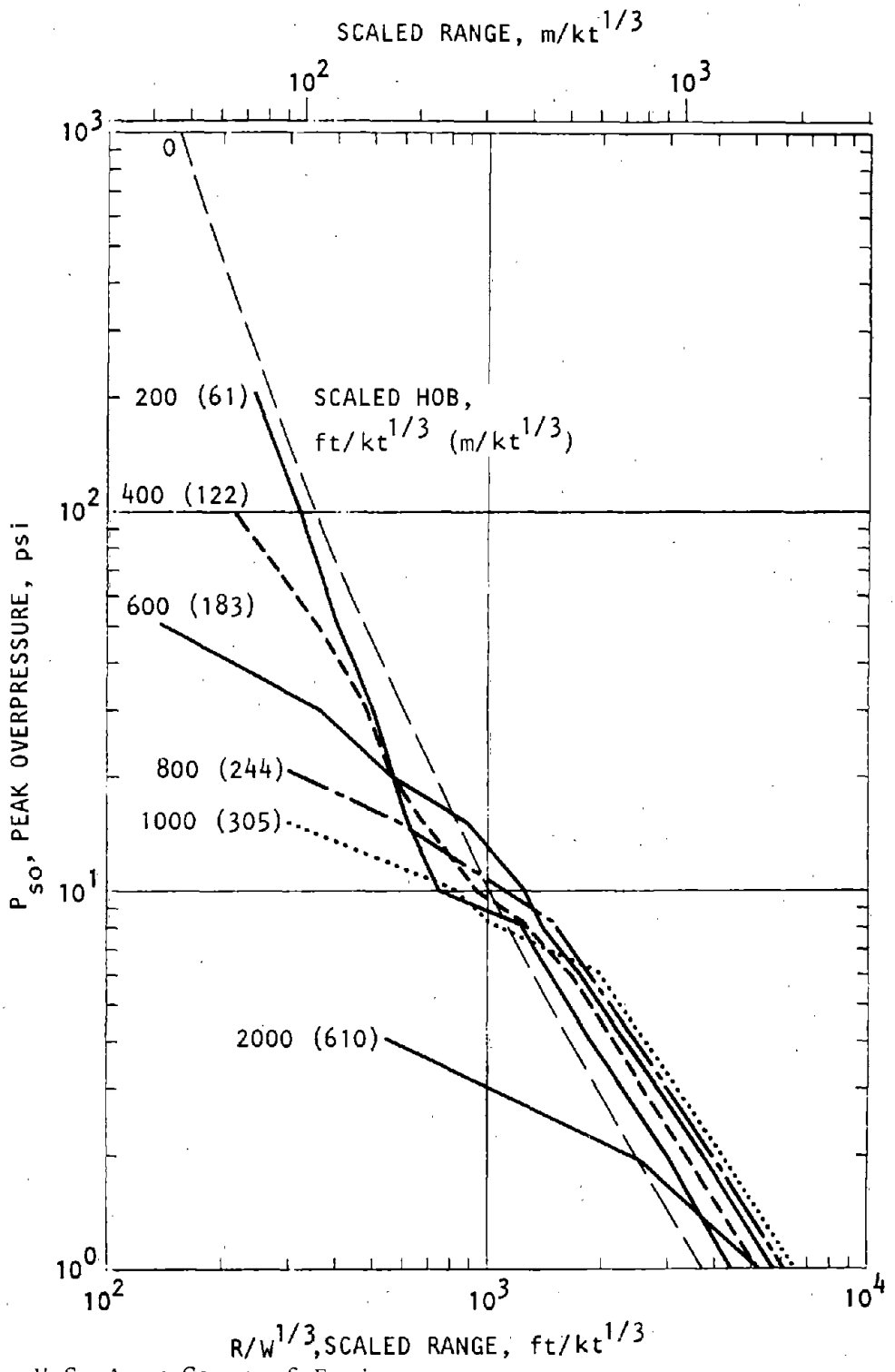

Figure 7–3. Peak Overpressure at Thermally Nonideal Surfaces

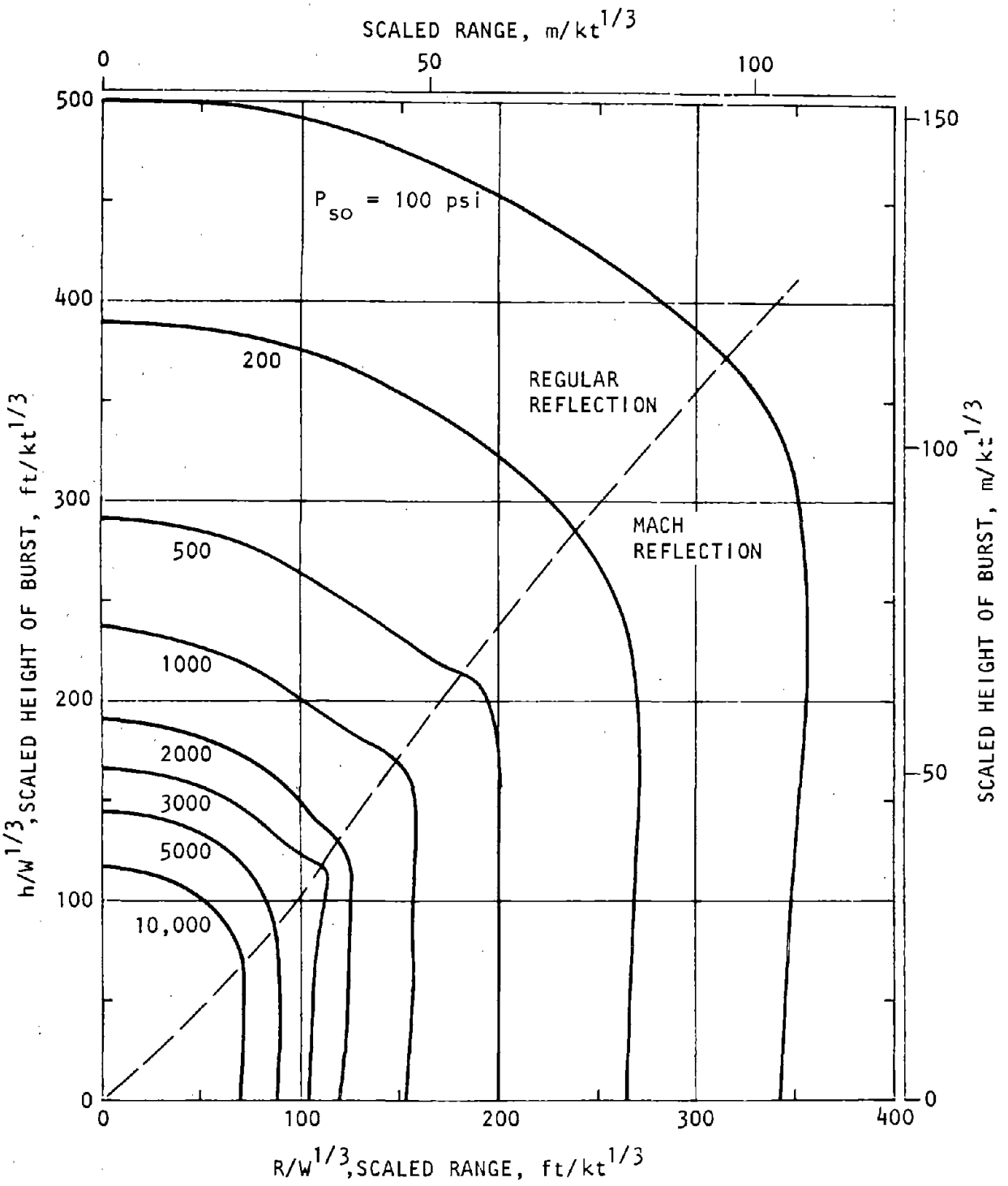

Figure 7–4. Peak Overpressures at a Near-Ideal Surface, Very High Overpressure Region (DNA, 1972; Brode-Lewis, 1975)

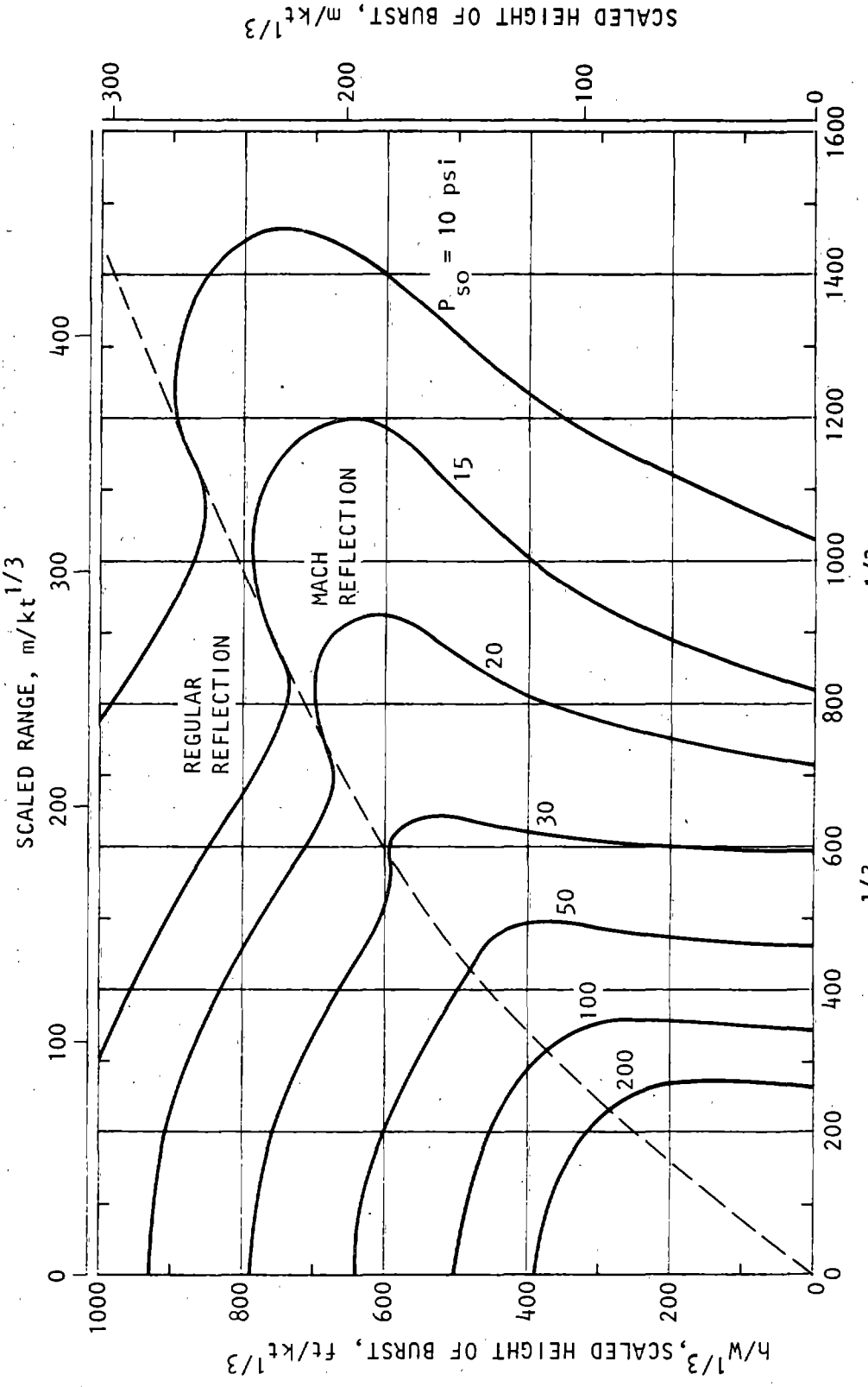

Figure 7-5. Peak Overpressures at a Near-Ideal Surface, High Overpressure Region (DNA, 1972)

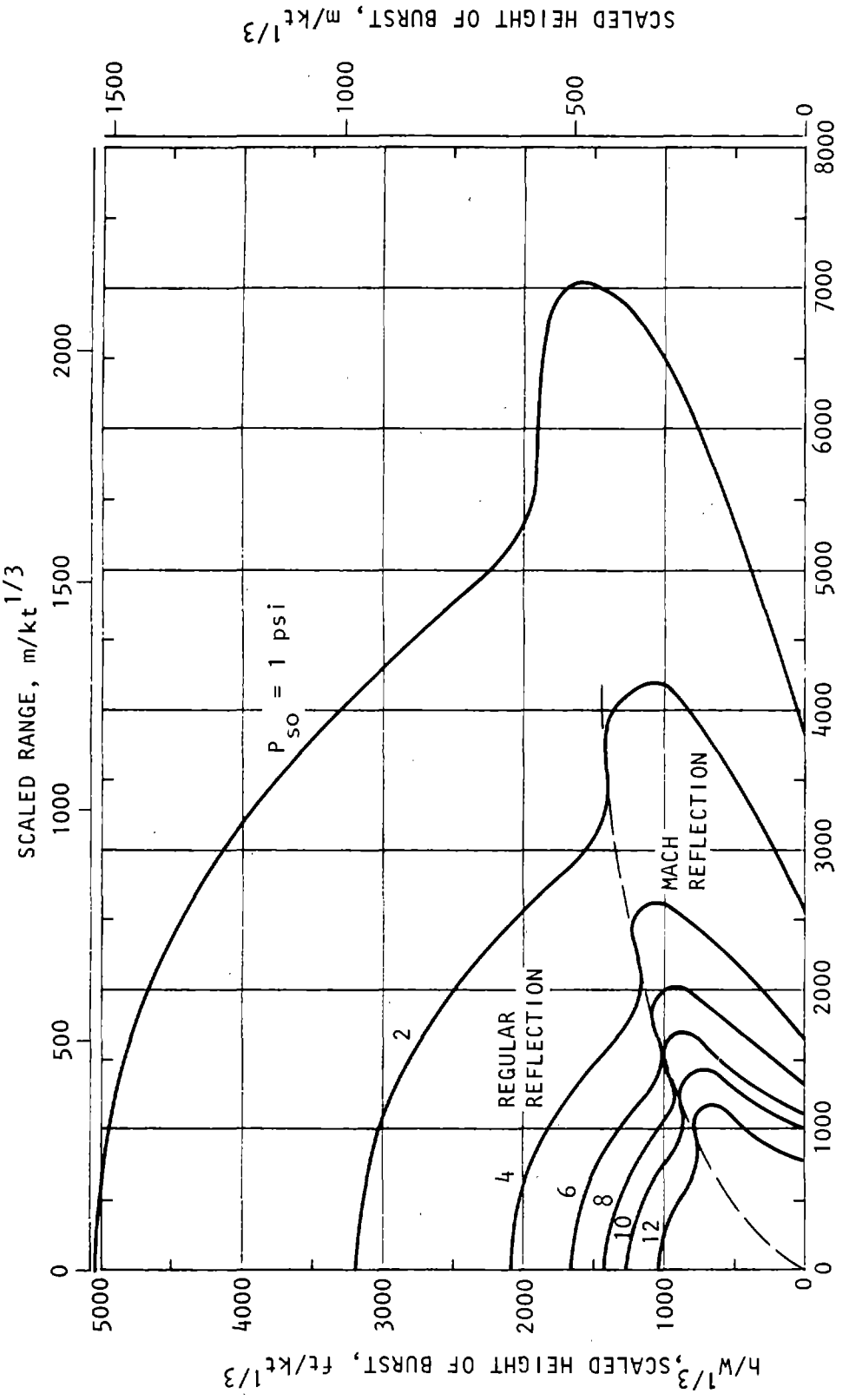

Figure 7–6. Peak Overpressures at a Near-Ideal Surface, Low Overpressure Region (DNA, 1972)

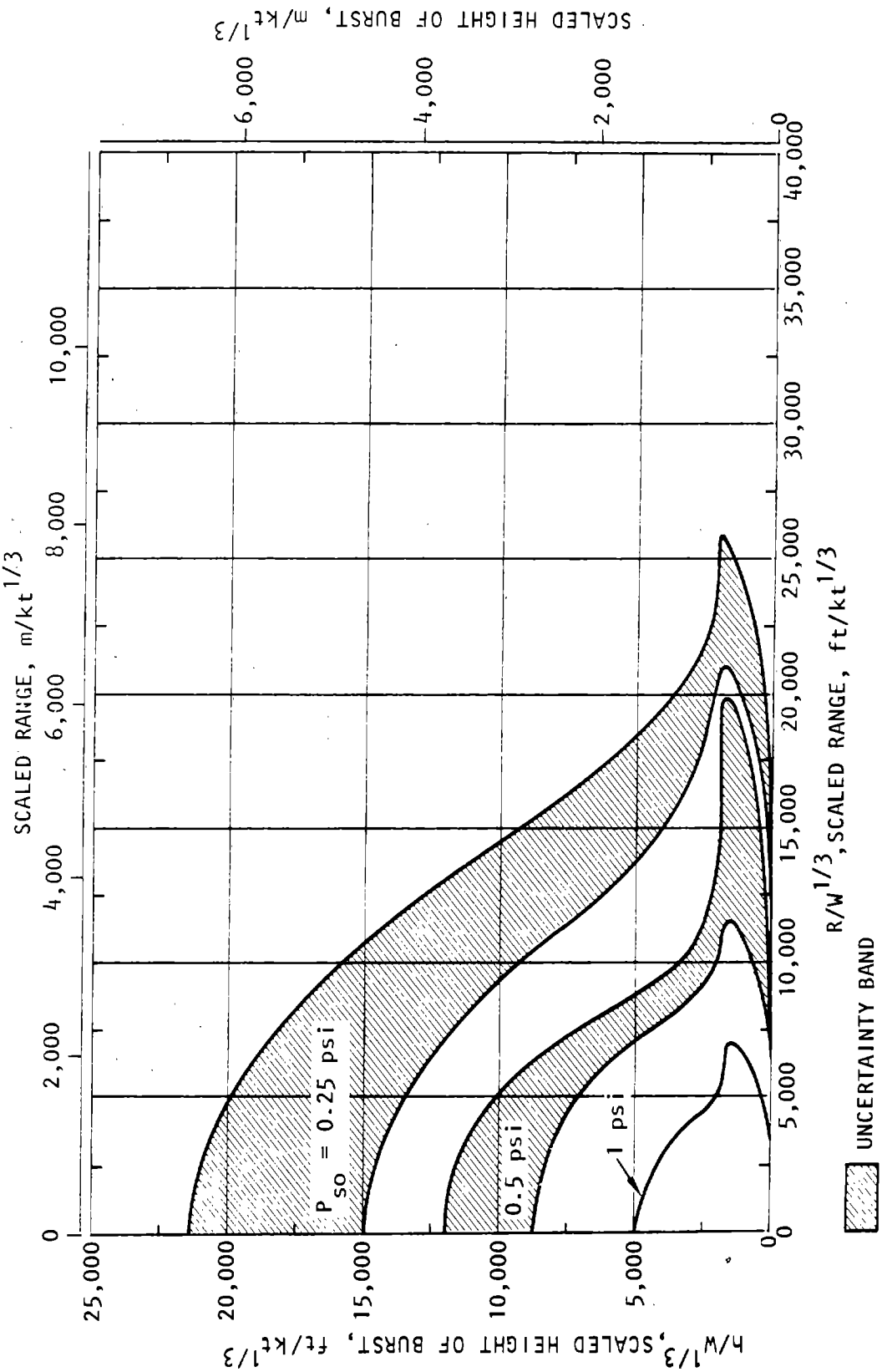

Figure 7-7. Peak Overpressures at a Near-Ideal or Thermally Nonideal Surface, Very Low Overpressure Region (DNA, 1972)

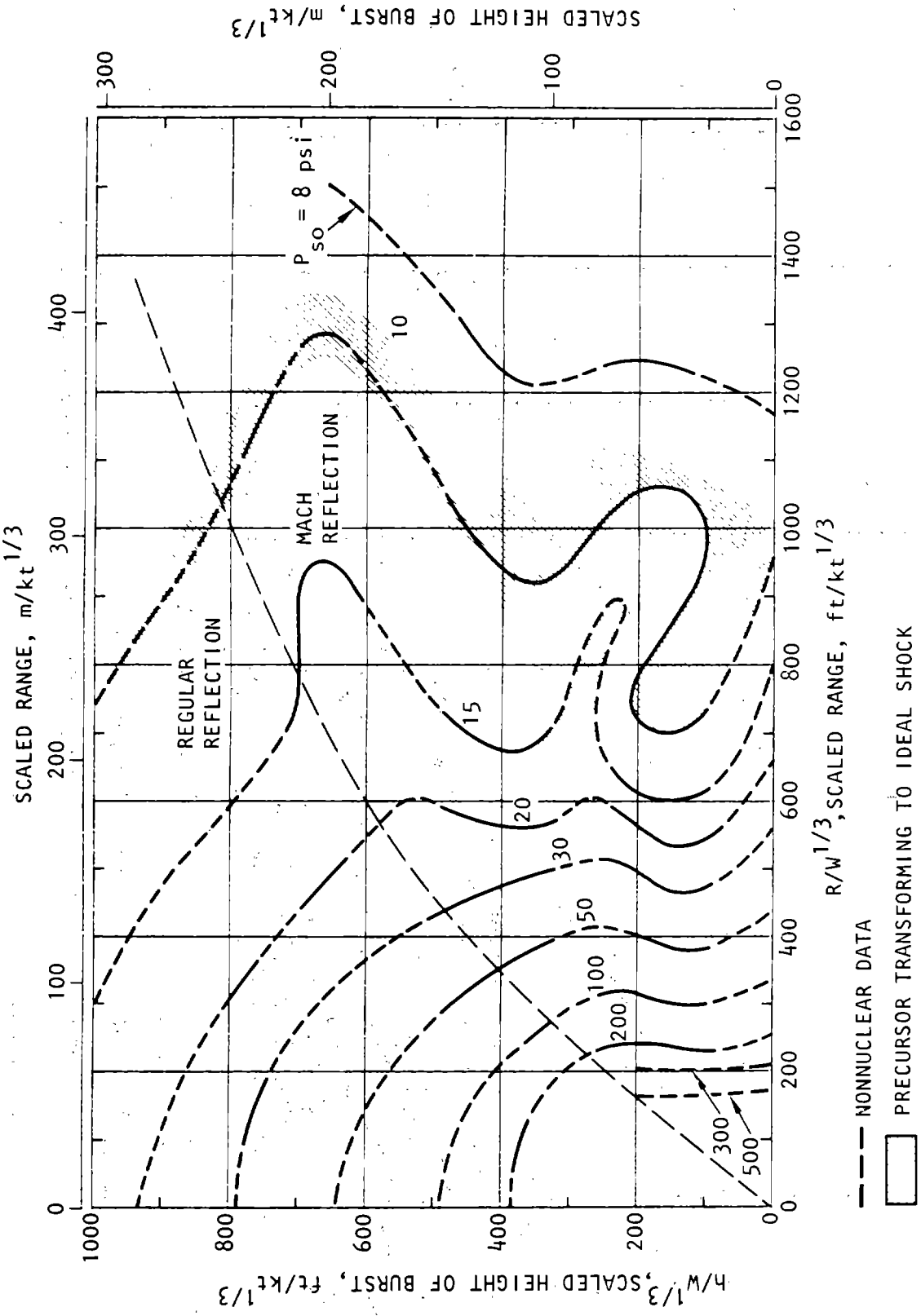

Figure 7-8. Peak Overpressures at a Thermally Nonideal Surface, High Overpressure Region (DNA, 1972)

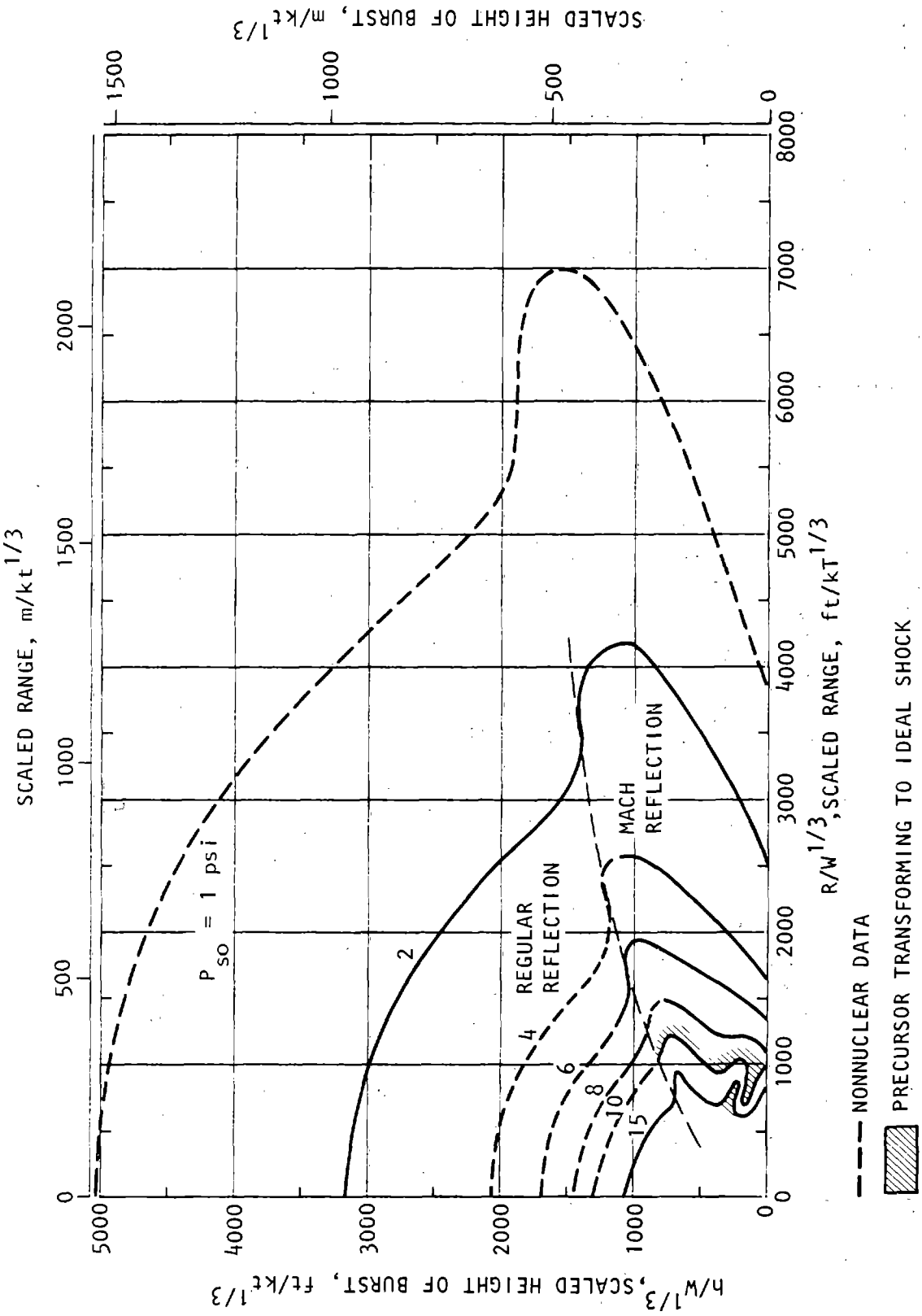

Figure 7-9. Peak Overpressures at a Thermally Nonideal Surface, Low Overpressure Region (DNA, 1972)

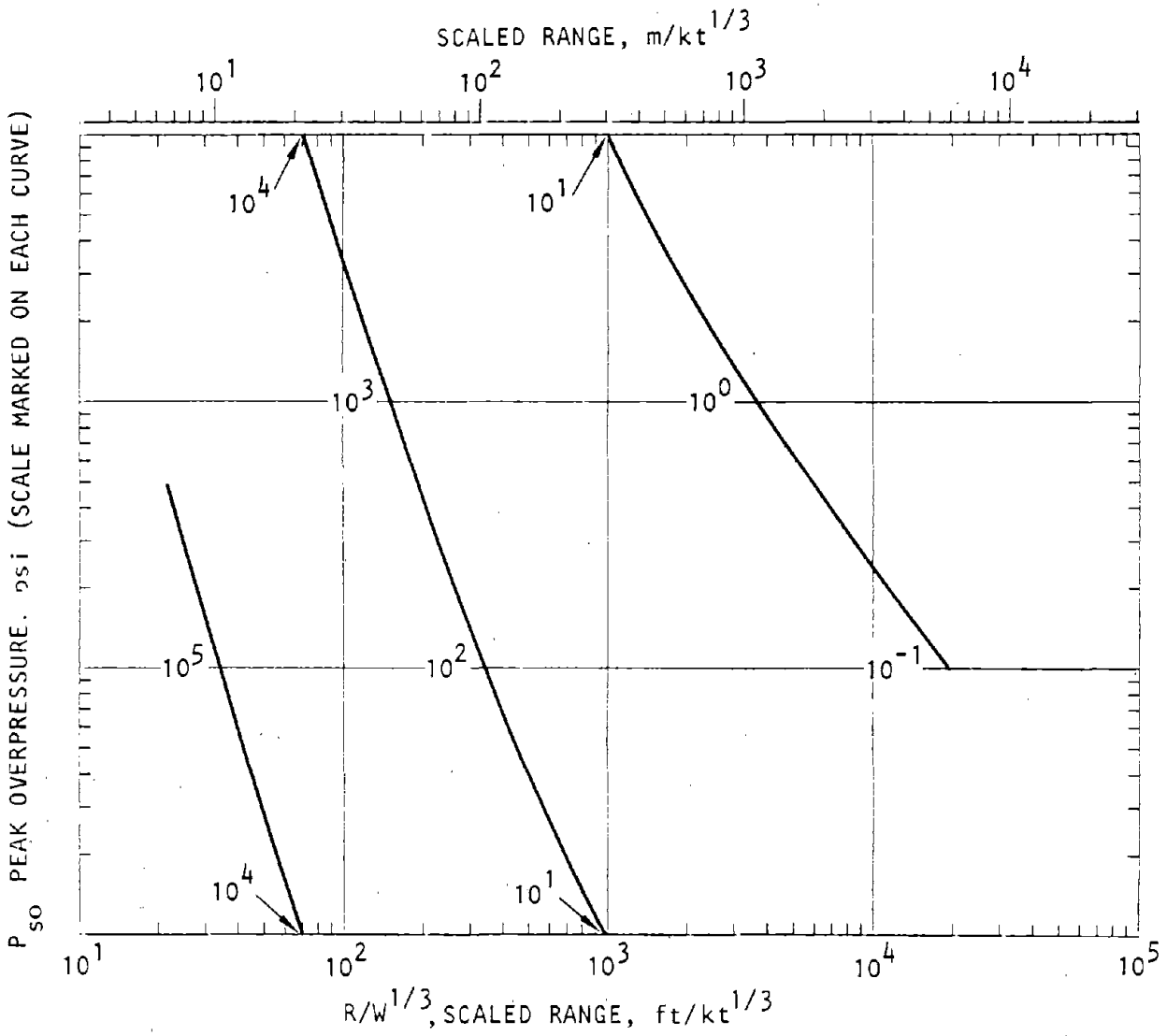

Figure 7-10. Peak Overpressure at the Surface from a Contact Surface Burst (DNA, 1972)

(3) The uncertainty associated with the peak overpressure is:

$$\Omega^2_{P_{so}} = \Omega^2_f + \Omega^2_{C_p} + n_p^2\Omega^2_R + \frac{n_p^2}{9}\Omega^2_W \qquad (7\text{-}2)$$

where Ω_f is the uncertainty associated with the functional form of p_{so}, Ω_{C_p} is the uncertainty of the coefficient, and so forth. For practical use, the major uncertainty in equation 7-1 as a representation of experimental and theoretical data is in the coefficient C_p. It is recommended that $\Omega_f \approx 0.05$ be used and that $\Omega_{C_p} = 0.2$ (which assumes that the data are log-normally distributed and that the bounds of ± 2 standard deviations are located between 3/2 and 2/3 times the mean value).

b. High-altitude bursts. Peak overpressures from high-altitude bursts (large HOB) are obtained from figure 7-11, which shows peak pressure as a function of scaled slant range. These data may be used at points other than at surface zero if the target remains in the region of regular reflection, that is, if the burst point is no more than 30 deg (0.52 rad) off the vertical.

(1) The equation of the data presented in figure 7-11 (construed to be the mean value) can be represented by:

$$P_{so} = 10^{A + B\log(R_s/W_e^{1/3}) + C\log^2(R_s/W_e^{1/3}) + D\log^3(R_s/W_e^{1/3})} \qquad (7\text{-}3)$$

where P_{so} is the peak overpressure in psi, R_s is slant range in ft, W_e is the effective yield in kt, and A, B, C, and D are constants. The effective yield is given by the Blast Efficiency Factor;

$$\frac{W_e}{W} = \alpha + \beta h + \gamma h^2 \qquad (7\text{-}4)$$

where W is the actual yield in kt, h is the HOB in kft, and α, β, and γ are constants. Equation 7-4 is

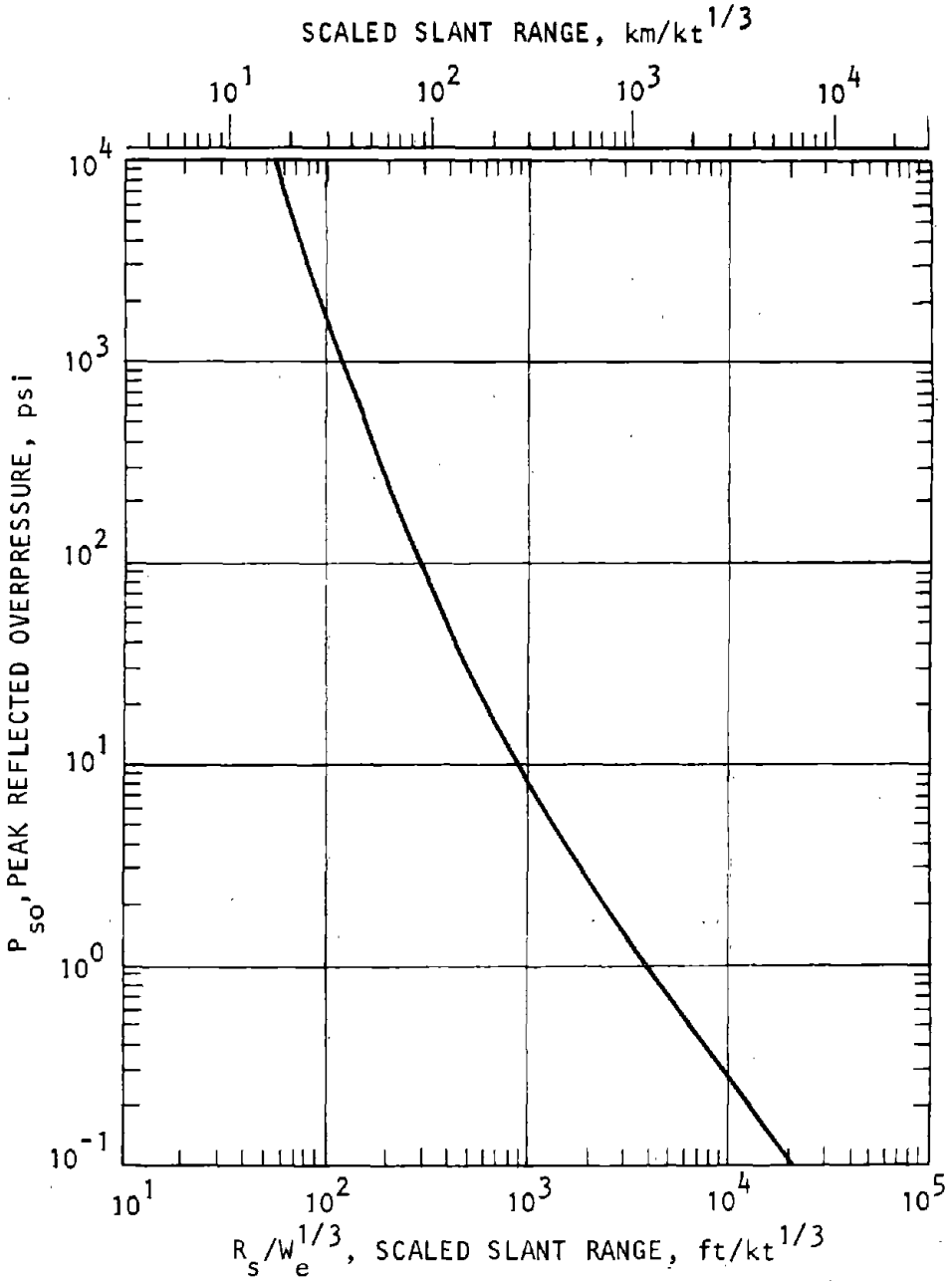

Figure 7–11. High-Altitude Bursts, Peak Reflected Overpressure at Ground Zero as a Function of Scaled Slant Range (DNA, 1972)

plotted in figure 7–12. It is preferable to use data directly from figure 7–11 and 7–12 rather than from equations 7–3 and 7–4 to calculate the mean overpressure and the mean effective yield.

(2) The uncertainty of the overpressure at the ground surface due to a high-altitude burst as represented by equation 7–3 is:

$$\Omega^2_{P_{so}} = \Omega^2_f + 5.3\Big[A^2 + B^2\log^2(R_s/W_e^{1/3}) + C^2\log^4(R_s/W_e^{1/3}) + D^2\log^6(R_s/W_e^{1/3})\Big]\Omega^2_{C_o} + \Big[B + 2C\log(R_2/W_e^{1/3}) + 3D\log^2(R_s/W_e^{1/3})\Big]^2\left(\Omega^2_{R_s} + \frac{\Omega^2_{W_e}}{9}\right) \qquad (7\text{–}5)$$

where Ω_f is the uncertainty in the form of equation 7–3, Ω_{R_s} is the uncertainty of the slant range, etc. Assume that $\Omega_f \approx 0.1$ to account for inaccuracies in fitting the function in equation 7–3 to the curve in figure 7–11. Also let

$$\Omega^2_{W_e} = \Omega^2_W + \frac{1}{\Big[\alpha + \beta h + \gamma h^2\Big]^2}\left\{\Big[\alpha^2 + \beta^2h^2 + \gamma^2h^4\Big]\Omega^2_{COF} + h^2\Big[\beta + 2\gamma h\Big]^2\,\Omega^2_h\right\} \qquad (7\text{–}6)$$

The values of the constants in equations 7–3 through 7–6 are A = 12.0, B = –6.08, C = 0.976, and D = –0.0608; for h ≤ 40 kft, α = 1.0, β = 0.0015, and

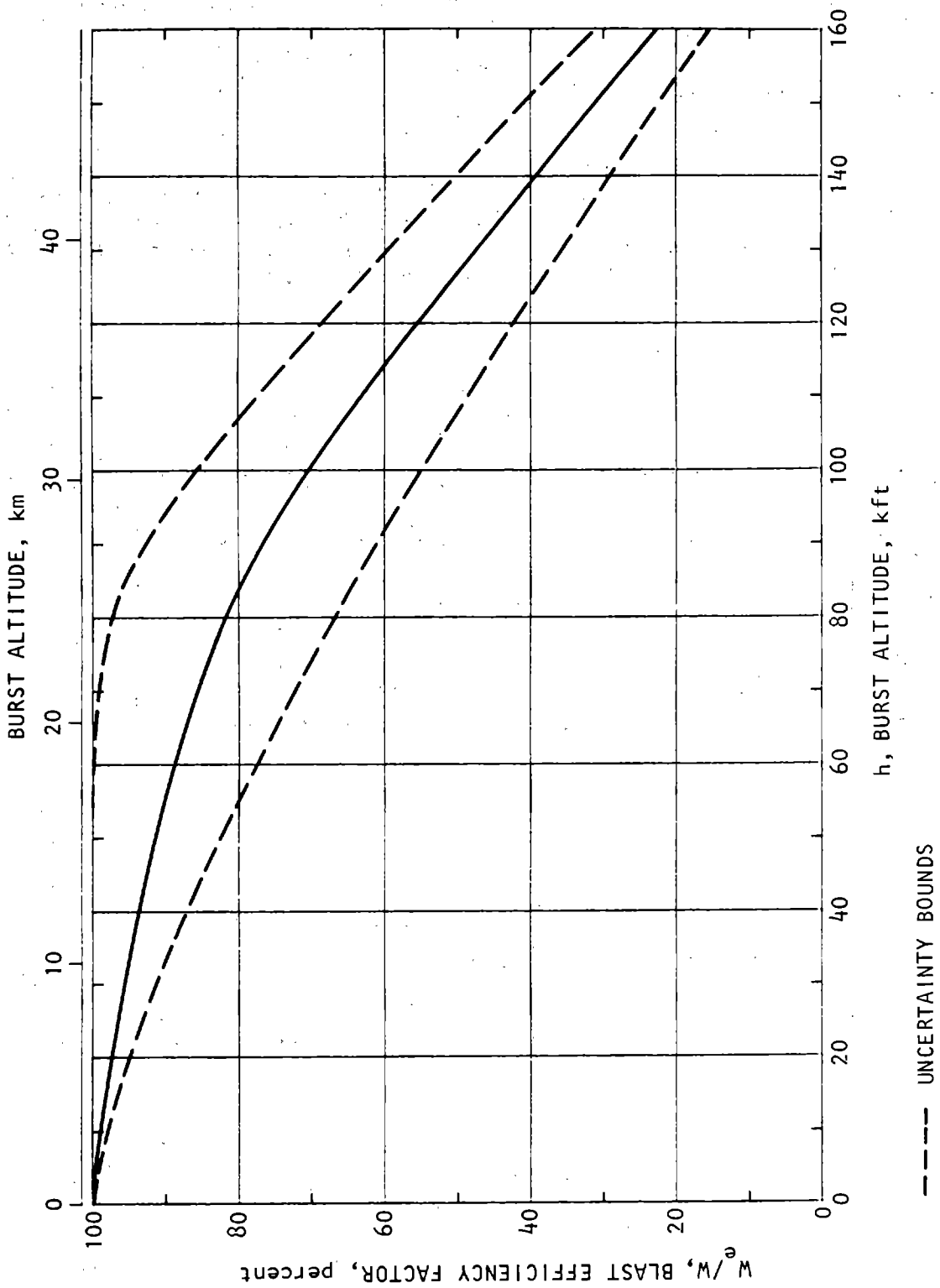

Figure 7-12. Blast Efficiency Factor for High-Altitude Bursts (DNA, 1972)

$\gamma = 0$; for $h > 40$ kft, $\alpha = 0.956$, $\beta = 0.00101$, and $\gamma = -3.55 \times 10^{-5}$. The uncertainty of Ω_{COF} is obtained by applying equation 2-19 to the data in figure 7-12 where L_2 and L_1 are the upper and lower bounds of the Blast Efficiency Factor at any particular HOB. Consider that $\Omega_{C_0} = 0.13$ to account for the uncertainty in the data comprising figure 7-11 (derived from equation 2-18 in which $\sqrt{R} = n = 2$).

7-3. Free-field peak dynamic pressure.

a. At GZ the ground-surface dynamic pressure is zero for all HOB. Outward from GZ, the peak dynamic pressure rises and then falls with increasing range. Unlike overpressure, the dynamic pressure is relatively insensitive to the surface properties and depends more on the dust loading. Peak dynamic pressure, a complicated function of HOB and range, is not easily represented by simple linear relationships, regardless of the manner in which the data are presented. Figures 7-13 through 7-15 present dynamic pressure curves in their simplest forms. In general, these curves may be represented by

$$\log Q = A_i\left(\frac{R}{W^{1/3}}\right)^2 + B_i\left(\frac{R}{W^{1/3}}\right) + C_i,$$

$$R_{i-1} \leq R < R_i \quad i = 1, 2, \ldots, N \qquad (7\text{-}7)$$

where Q is the dynamic pressure in psi, R is the range from GZ in ft, W is yield in kt, and A, B, and C are coefficients to be defined in *c* below for various HOBs within certain scaled ranges.

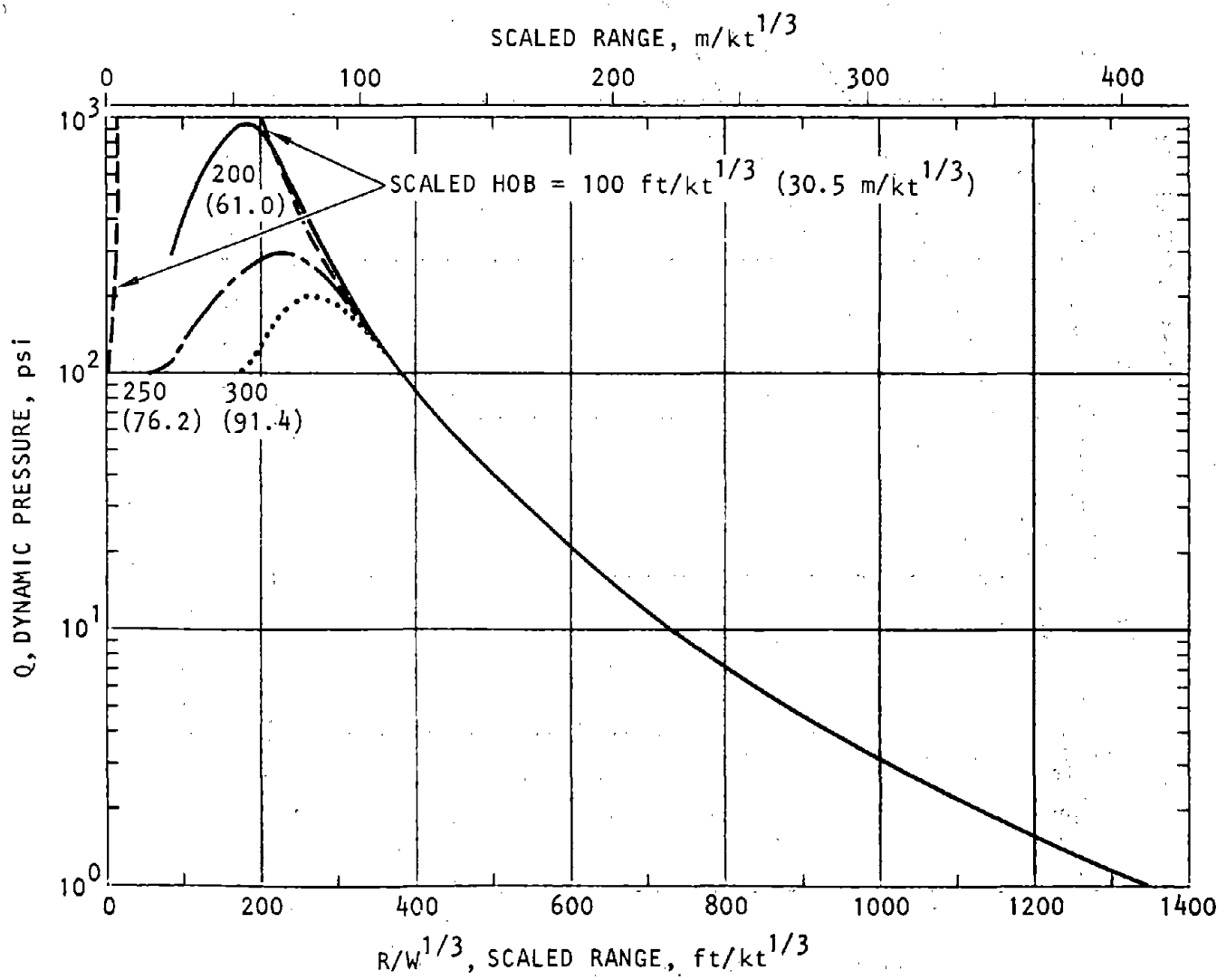

Figure 7-13. Dynamic Pressure at a Perfect Surface (DNA, 1972)

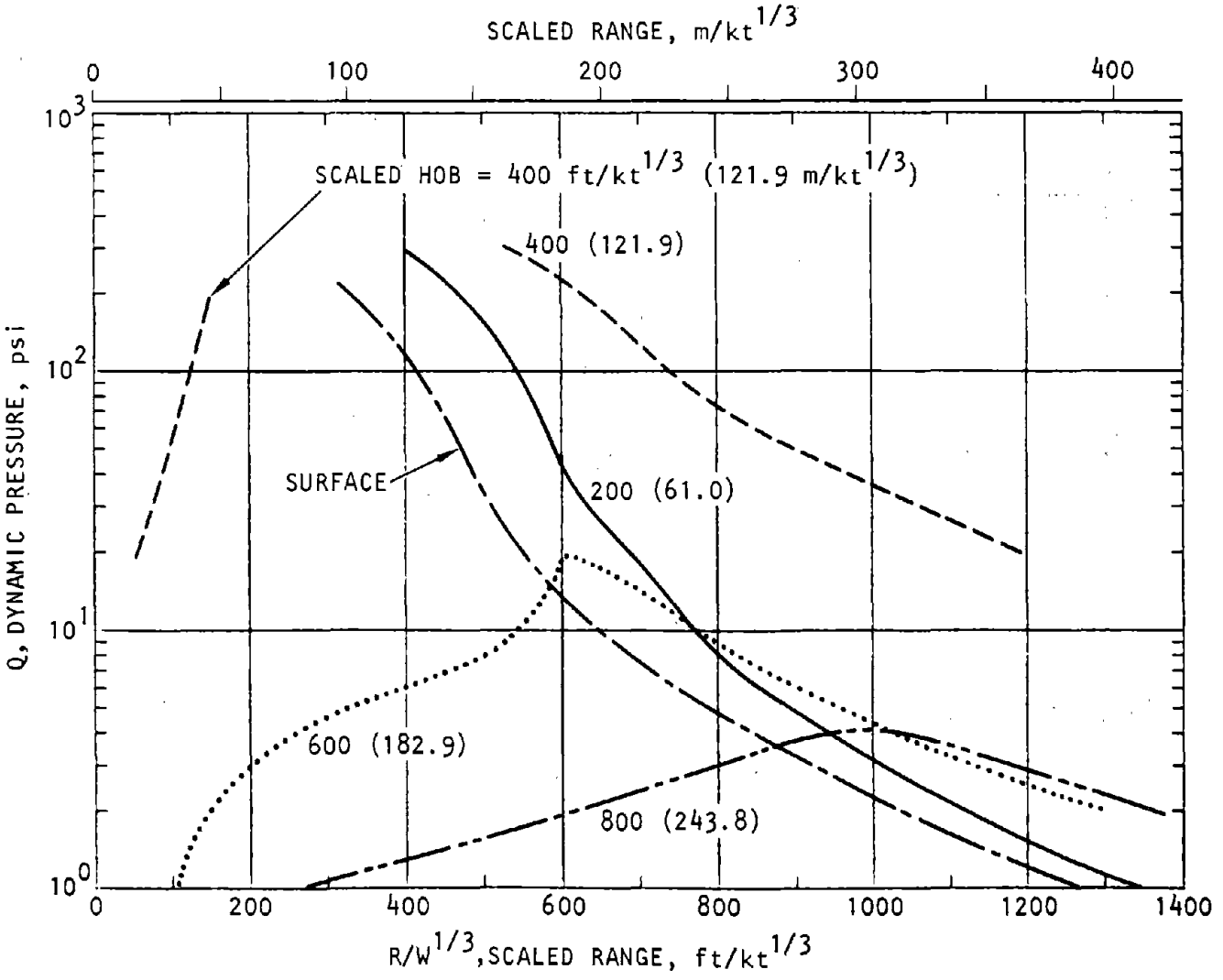

Figure 7-14. Dynamic Pressure at a Light Dust Surface (DNA, 1972)

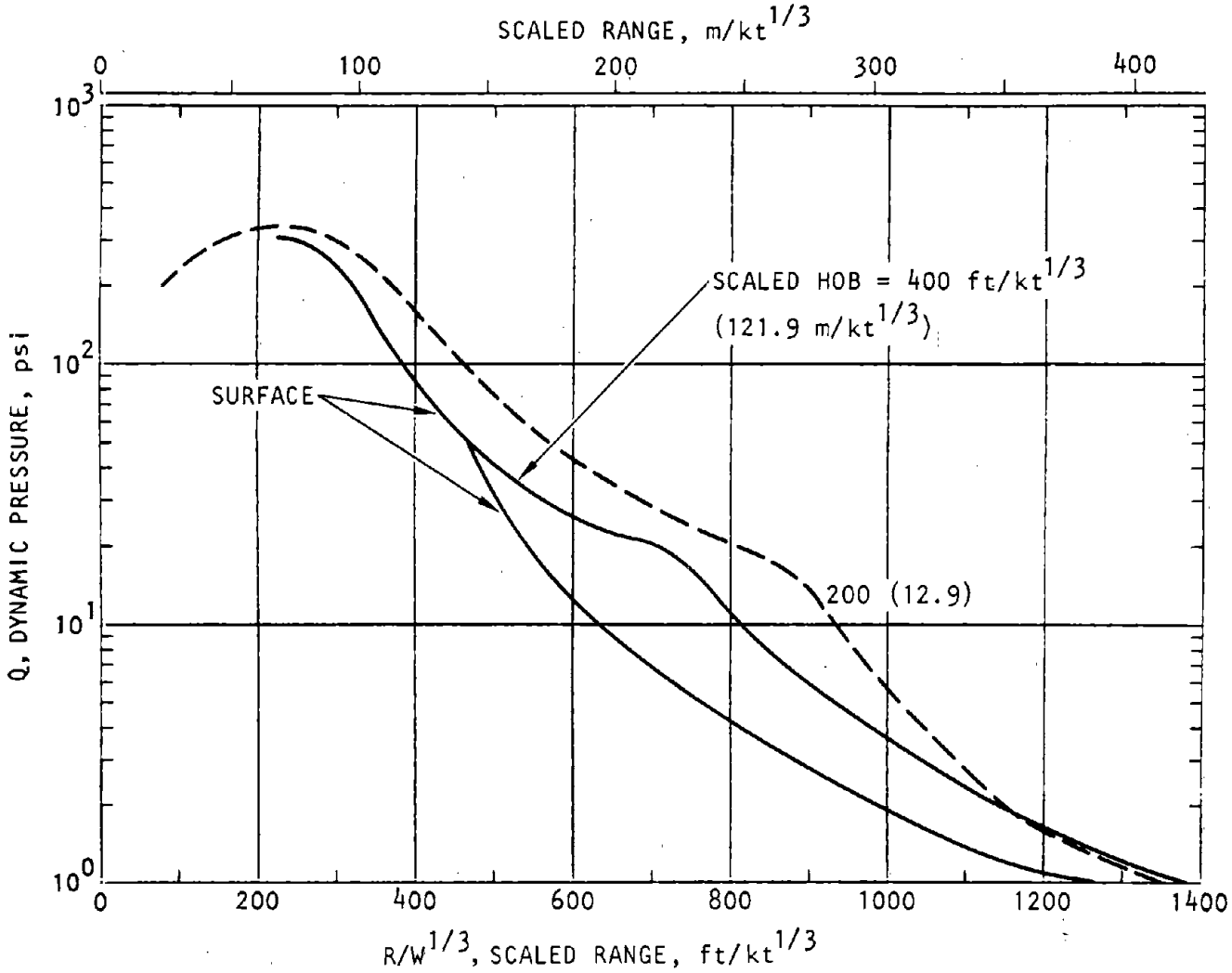

Figure 7–15. Dynamic Pressure at a Heavy Dust Surface (DNA, 1972)

b. It is recommended that the mean values for dynamic pressure be taken directly from figures 7–13 through 7–15 or from the source data presented in figures 7–16 through 7–18.

c. The uncertainty associated with equation 7–7 is

$$\Omega_Q^2 = \Omega_f^2 + 5.3\left\{\left[A^2(R/W^{1/3})^4 + B^2(R/W^{1/3})^2 + C^2\right]\Omega_{C_o}^2 + (R/W^{1/3})^2\left[2A(R/W^{1/3}) + B\right]^2\left[\Omega_R^2 + \frac{\Omega_W^2}{9}\right]\right\} \quad (7\text{–}8)$$

where Ω_f is the uncertainty in the form of equation 7–7, Ω_{C_o} is the uncertainty of the data in figures 7–13 through 7–15, Ω_W is the uncertainty of the yield. Due to the complexity of the curves in figures 7–13 through 7–15, the coefficients A, B, and C have not been calculated in advance. They can be determined for any range of the data by fitting equation 7–7 to the data within the range of interest. For example, if the curve corresponding to the scaled HOB of 400 ft/kt$^{1/3}$ in figure 7–14 is fitted by equation 7–7 in the scaled range $570 \leq R/W^{1/3} \leq 1200$ ft/kt$^{1/3}$, the approximate regression equation will be specified when $A = 1.021 \times 10^{-6}$, $B = -3.485 \times 10^{-3}$, and $C = 4.013$. Credible estimates of the values of Ω_{C_o} are not currently available from the library of data. However, for design purposes assume $\Omega_f = 0.1$ and $\Omega_{C_o} \approx 0.3$.

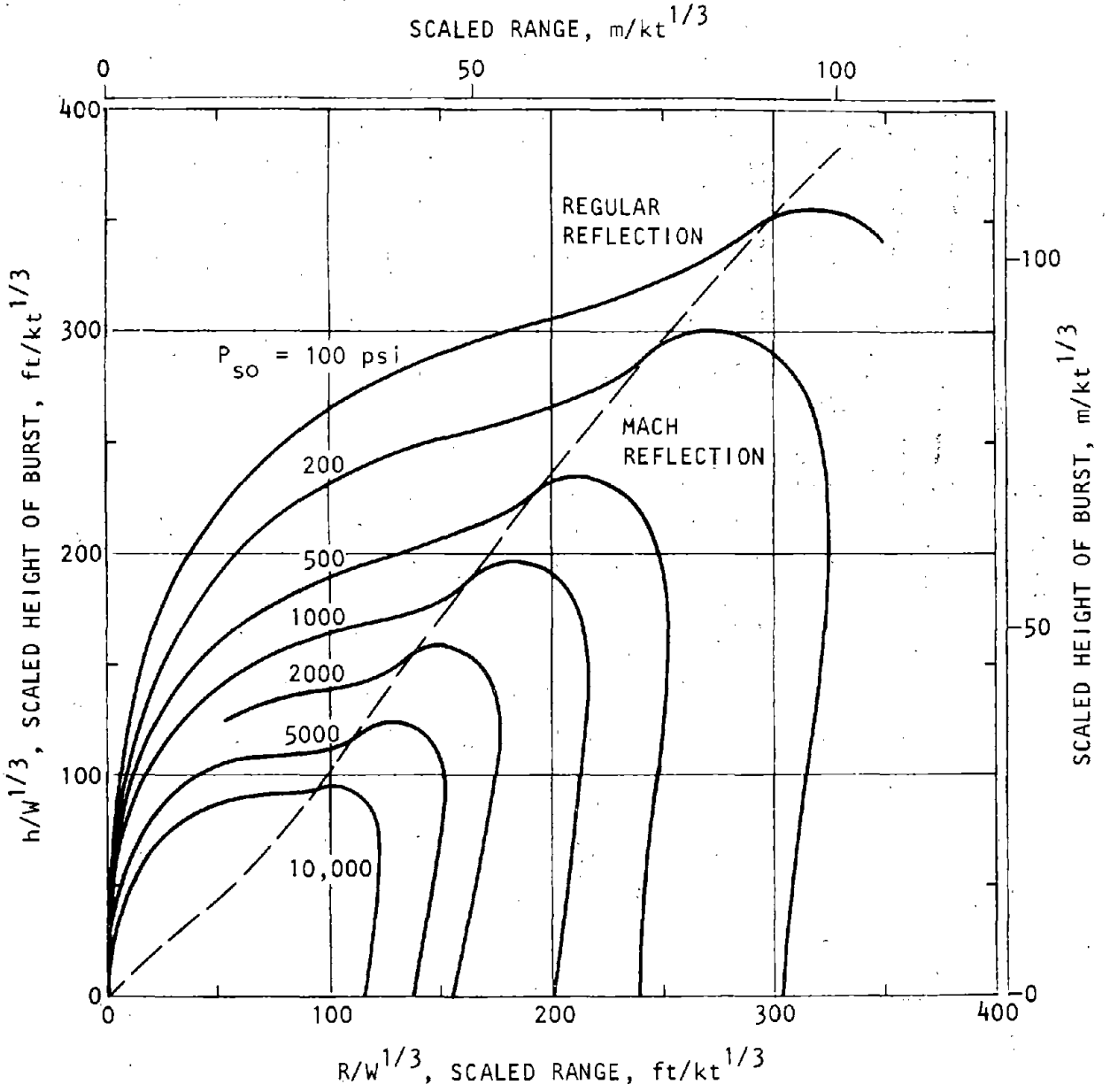

Figure 7-16. Peak Dynamic Pressure at an Ideal Surface (DNA, 1972)

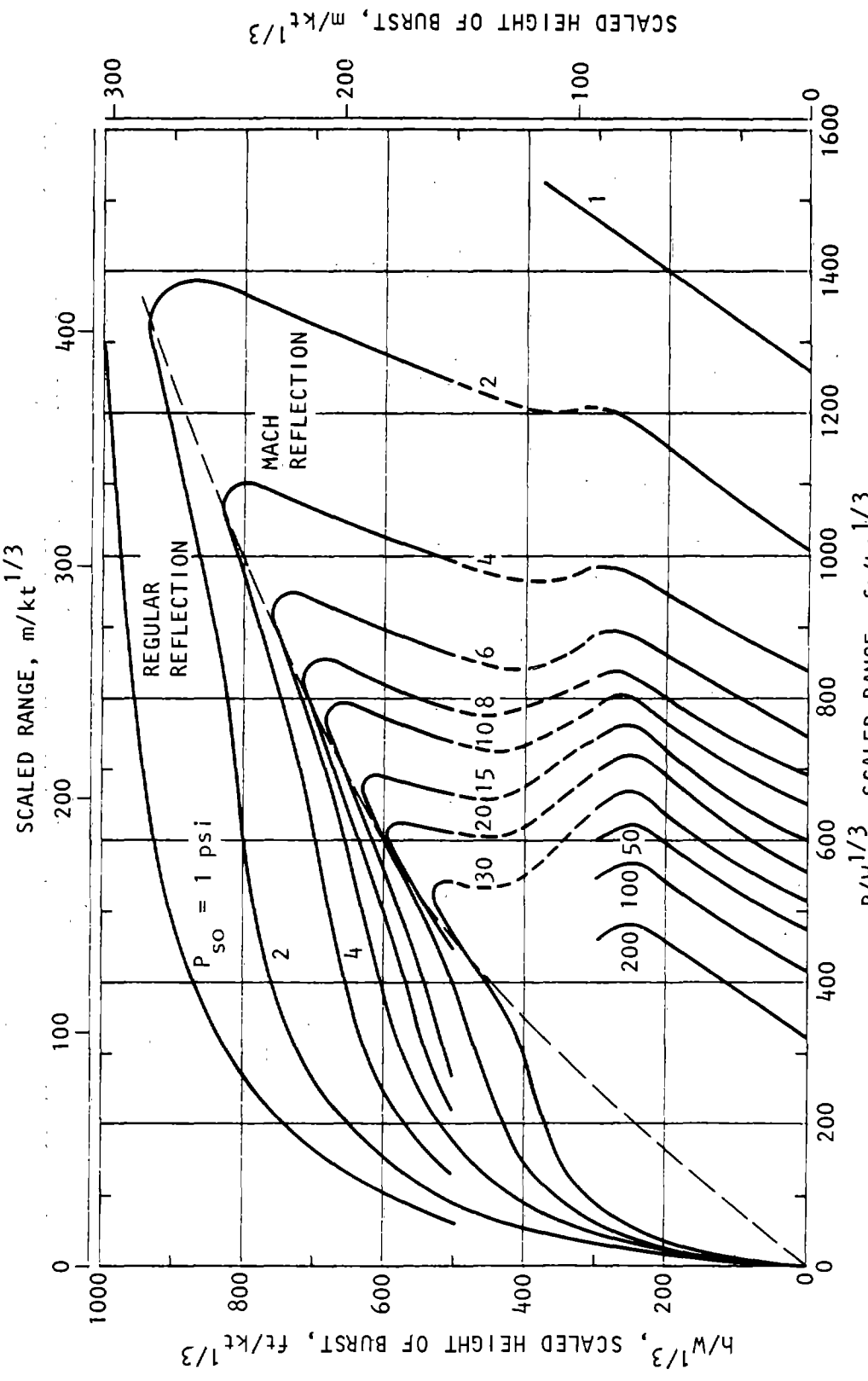

Figure 7-17. Peak Dynamic Pressure at a Surface with Light Dust Conditions (DNA, 1972)

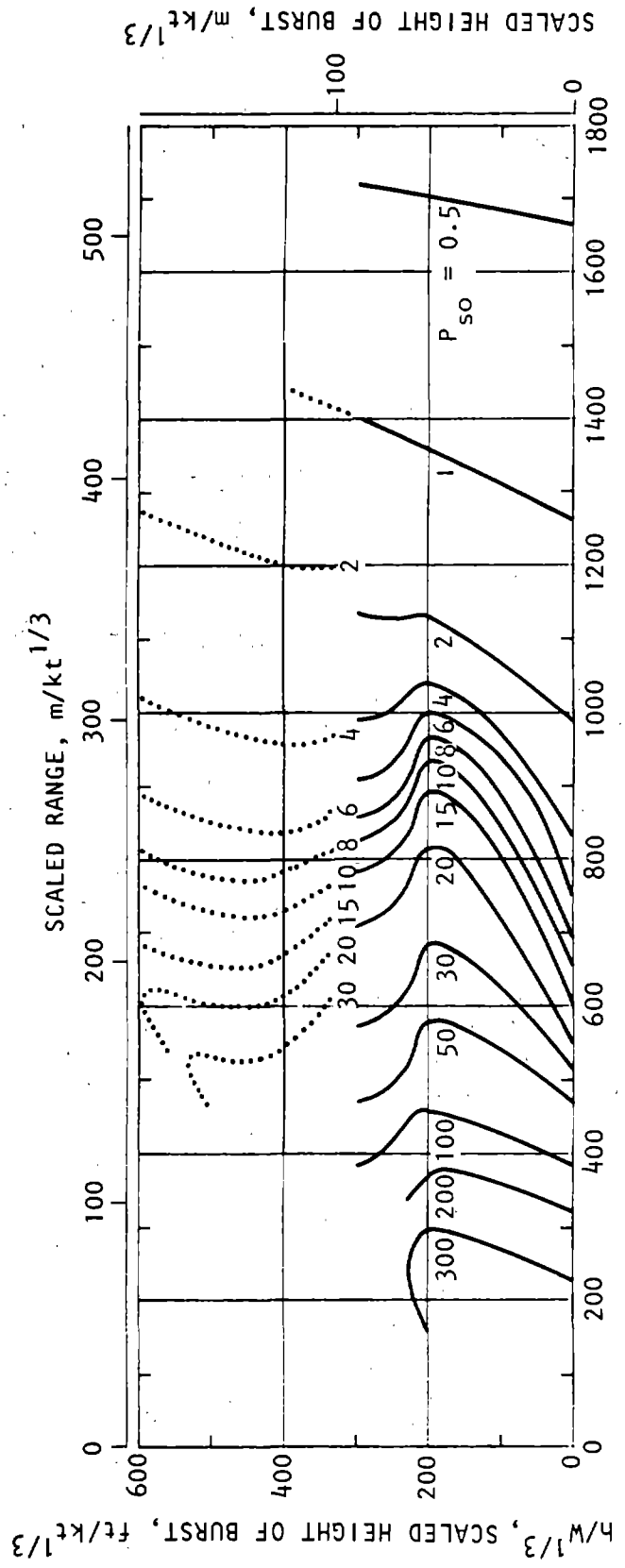

Figure 7–18. Peak Dynamic Pressure at a Surface with Heavy Dust Conditions (DNA, 1972)
(Dotted sections are taken from figure 7–17, for Light-Dust Conditions.)

7-4. Overpressure positive phase duration.

a. The positive phase duration, that is, the time that the overpressure remains positive, is relatively insensitive to HOB or range. Reasonably accurate mathematical representations of the positive phase durations presented in figures 7-19 and 7-20 may be achieved by interchanging the variables on the ordinate with the variables on the family of curves and replotting the data as shown in figures 7-21 and 7-22. Equations of the latter forms of the positive phase durations are

$$\frac{D_p^+}{W^{1/3}} = C_{o_i} + C_{D_i} \log \frac{R}{W^{1/3}} \quad R_{i-1} \leq R < R_i$$

$$i = 1, 2, \ldots, N \qquad (7\text{-}9)$$

for a scaled HOB of 200 ft/kt$^{1/3}$ (61 m/kt$^{1/3}$) or

$$\frac{D_p^+}{W^{1/3}} = C_{o_i} + C_{D_i} \frac{R}{W^{1/3}} \quad R_{i-1} < R < R_i$$

$$i = 1, 2, \ldots, N \qquad (7\text{-}10)$$

for other selected scaled HOBs. In equations 7-9 and 7-10, D_p^+ is the positive overpressure duration in sec, W is yield in kt, R is range in ft, and C_o and C_D are constants.

b. It is recommended that the mean values of the positive phase durations be extracted from figures 7-19 and 7-20 by interpolating the plotted data presented in table 7-3.

c. The uncertainty of the positive phase duration for equation 7-9 is to be computed from:

$$\Omega^2_{D_p^+} = \Omega_f^2 + \frac{W^{2/3}}{D_p^{+2}}\left\{\left[C_o^2 + C_D^2 \log^2 R/W^{1/3}\right]\Omega_c^2 + 0.189\, C_D^2 \Omega_R^2 + \frac{1}{9}\left[C_D\,(0.434 - \log R/W^{1/3}) - C_o\right]^2 \Omega_W^2\right\} \qquad (7\text{-}11)$$

and for Equation 7-10:

$$\Omega^2_{D_p^+} = \Omega_f^2 + \frac{1}{D_p^{+2}}\left\{\left[W^{2/3}C_o^2 + R^2 C_D^2\right]\Omega_c^2 + \frac{W^{2/3}}{9} C_o^2 \Omega_W^2 + R^2\, C_D^2\, \Omega_R^2\right\} \qquad (7\text{-}12)$$

where Ω_f is the uncertainty of the functional form of equations 7-9 and 7-10, Ω_c is the uncertainty of the coefficients, and Ω_R is the uncertainty of the scaled range. The value of the constants in equations 7-9 through 7-11 are presented in table 7-3. Assume $\Omega_f \approx 0.2$ and $\Omega_c = 0.1$ for $D_p^+/W^{1/3} < 0.25$ s/kt$^{1/3}$ or $\Omega_c = 0.17$ for $D_p^+/W^{1/3} > 0.25$ s/kt$^{1/3}$ (which is predicated on the use of equation 2-17 where n = 2 and R = 1.4 or R = 2, respectively).

7-5. Dynamic pressure positive phase duration.

a. Dynamic pressure positive phase durations are not as readily defined as the over-pressure positive phase durations. The usual practice is to modify the positive phase of the overpressure by certain factors. Thus, the dynamic pressure positive phase is approximated by

$$\frac{D_u^+}{W^{1/3}} = C_{o_i} + C_{D_i}\, R/W^{1/3},\ R_{i-1} \leq R < R_i$$

$$i = 1, 2, \ldots, N \qquad (7\text{-}13)$$

from figure 7-23, which is recast from figures 7-24 and 7-25 where C_o and C_D are constants. The dynamic positive phase duration D_u^+ has units of sec, W is the yield in kt, and R is the range in ft.

b. The mean values of the positive phase should be extracted from figures 7-24 and 7-25 by interpolating the plotted data.

c. The uncertainty of the dynamic pressure positive phase duration is computed from

$$\Omega^2_{D_u^+} = \Omega_f^2 + \frac{1}{D_u^{+2}}\left\{\left[W^{2/3}\, C_o^2 + R^2\, C_D^2\right]\Omega_c^2 + \frac{W^{2/3}}{9} C_o^2 \Omega_W^2 + R^2\, C_D^2\, \Omega_R^2\right\} \qquad (7\text{-}14)$$

where Ω_f is the uncertainty of the functional forms of equation 7-13, Ω_c is the uncertainty of the coefficients of the equation, Ω_R is the uncertainty of the range, etc. The values of the coefficients are presented in table 7-4. Assume $\Omega_f \approx 0.2$ and $\Omega_c = 0.07$ for $D_u^{+1/3} \leq 0.35$ s/kt$^{1/3}$, and $\Omega_c = 0.17$ for $D_u^+/W^{1/3} > 0.35$ s/kt$^{1/3}$ (from equation 2-17 where n = 2 and R = 1.3 and R = 1.5, respectively).

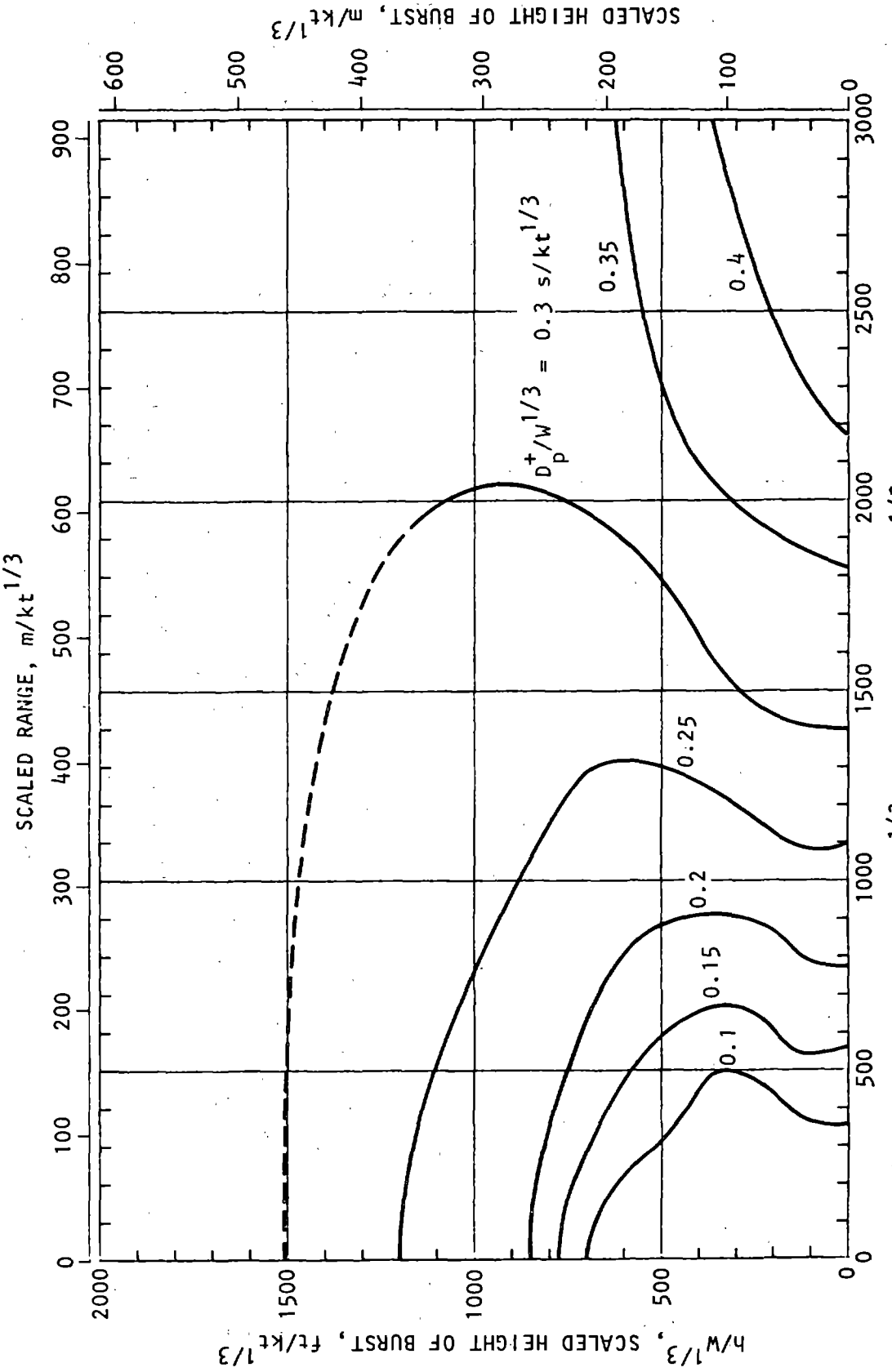

Figure 7–19. Duration of Positive Overpressure at a Near-Ideal Surface (DNA, 1972)

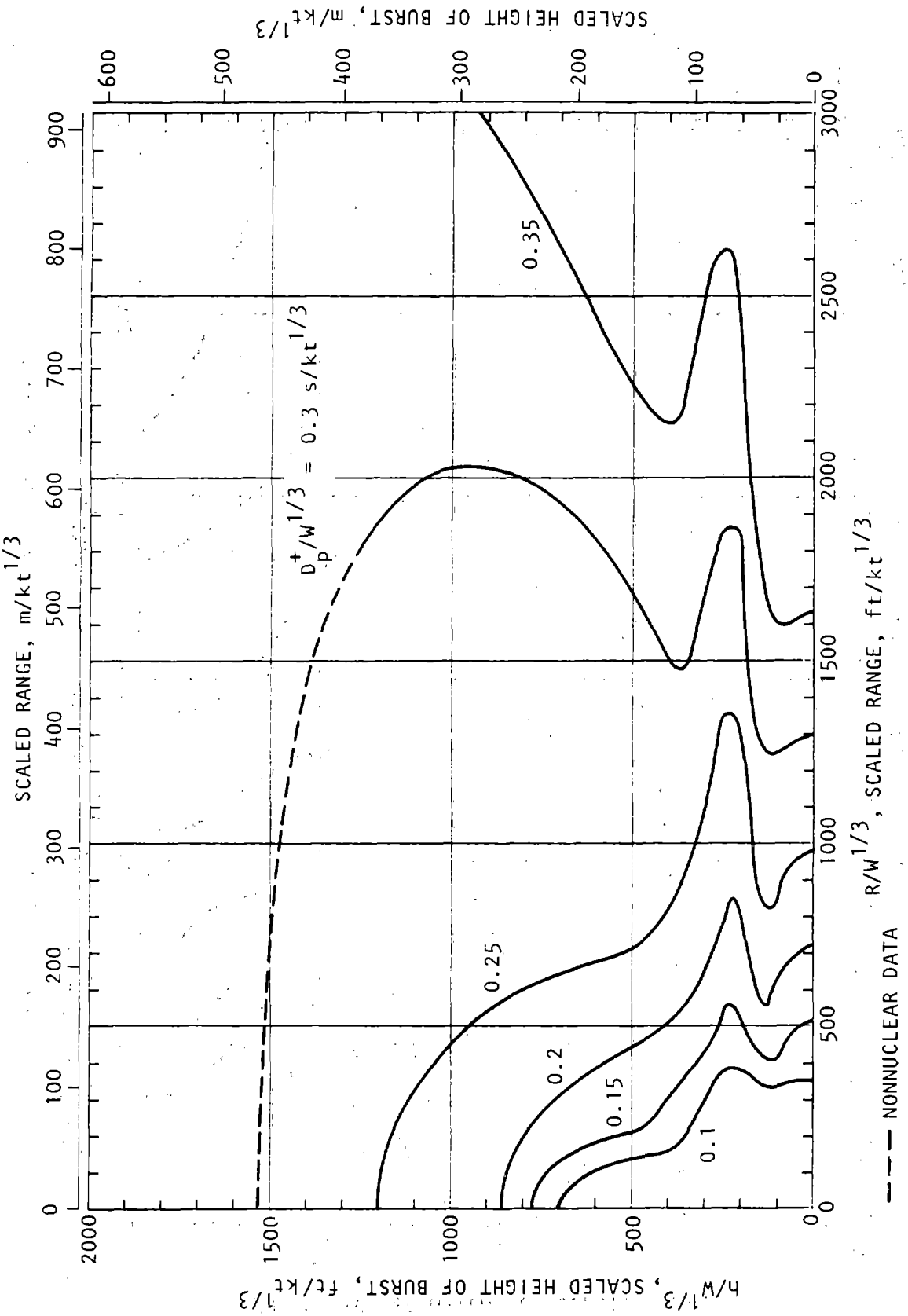

Figure 7–20. Duration of Positive Overpressure at a Thermally Nonideal Surface (DNA, 1972)

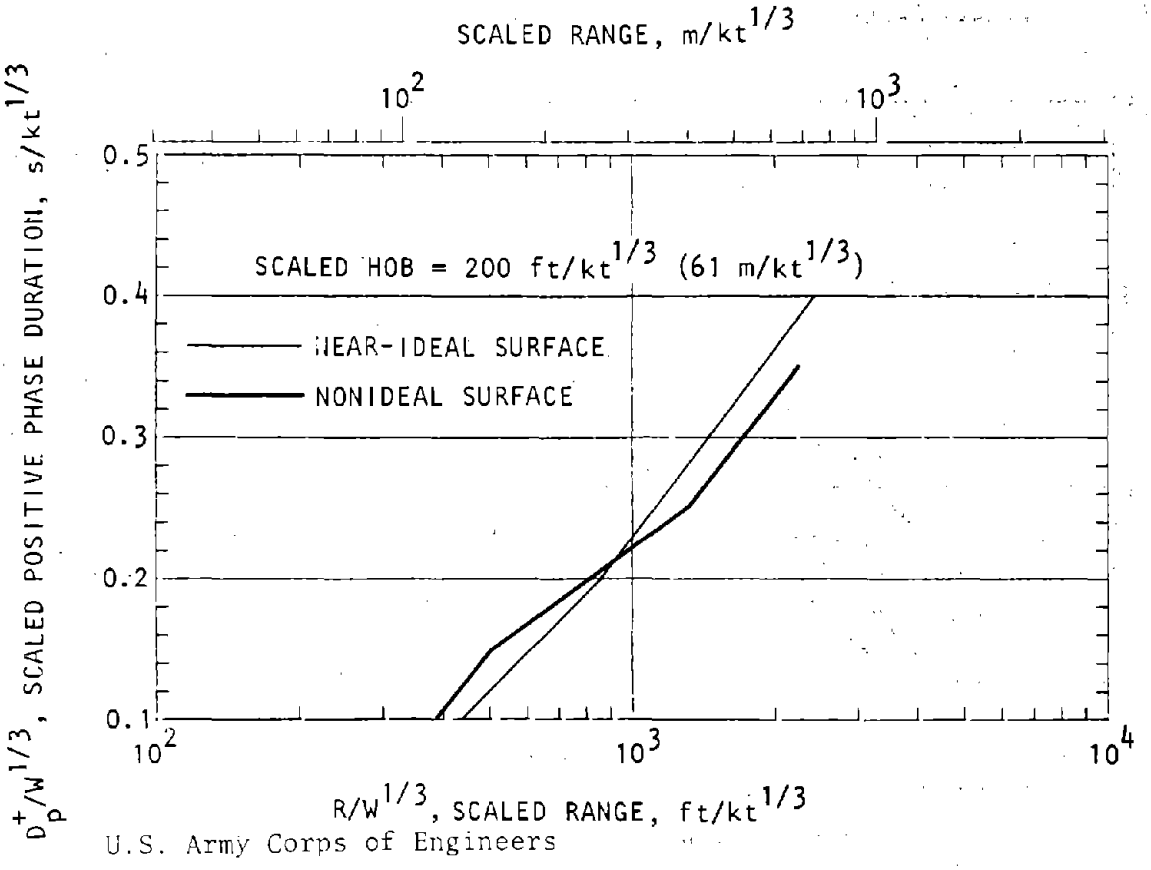

Figure 7-21. Duration of Positive Overpressure at the Surface

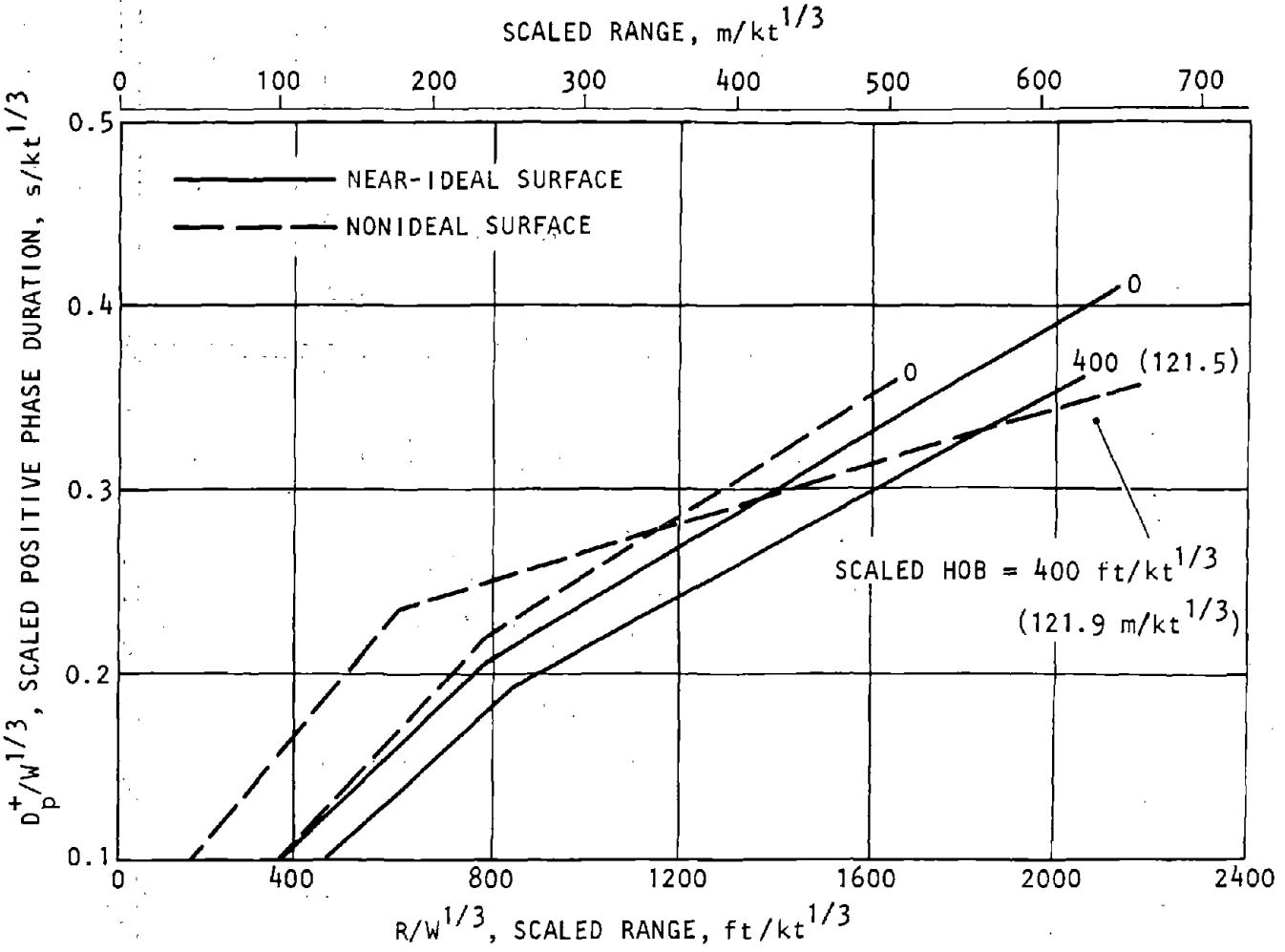

U.S. Army Corps of Engineers

Figure 7–22. Duration of Positive Overpressure at the Surface

Table 7-3. Parameters for Positive Phase Duration

Scaled HOB		Scaled Range			
$ft/kt^{1/3}$	$(m/kt^{1/3})$	$ft/kt^{1/3}$	$(m/kt^{1/3})$	C_o	C_D
Near-Ideal Surface					
0	(0)	300 to 750	(91 to 229)	1.25×10^{-2}	2.50×10^{-4}
		750 to 2150	(229 to 655)	8.89×10^{-2}	1.48×10^{-4}
200	(61)	440 to 860	(134 to 262)	-8.08×10^{-1}	3.44×10^{-1}
		860 to 2450	(262 to 747)	-9.12×10^{-1}	3.79×10^{-1}
400	(122)	450 to 850	(137 to 259)	-6.58×10^{-3}	2.37×10^{-4}
		850 to 2075	(259 to 632)	7.65×10^{-2}	1.37×10^{-4}
Nonideal Surface					
0	(0)	350 to 780	(107 to 238)	7.89×10^{-3}	2.63×10^{-4}
		780 to 1650	(238 to 503)	1.03×10^{-1}	1.49×10^{-4}
200	(61)	380 to 500	(116 to 152)	-9.84×10^{-1}	4.20×10^{-1}
		500 to 1300	(152 to 396)	-5.00×10^{-1}	2.41×10^{-1}
		1300 to 2300	(396 to 701)	-1.01×10^{0}	4.03×10^{-1}
400	(122)	150 to 600	(46 to 183)	5.50×10^{-2}	3.00×10^{-4}
		600 to 2150	(183 to 655)	1.90×10^{-1}	7.42×10^{-5}

U.S. Army Corps of Engineers

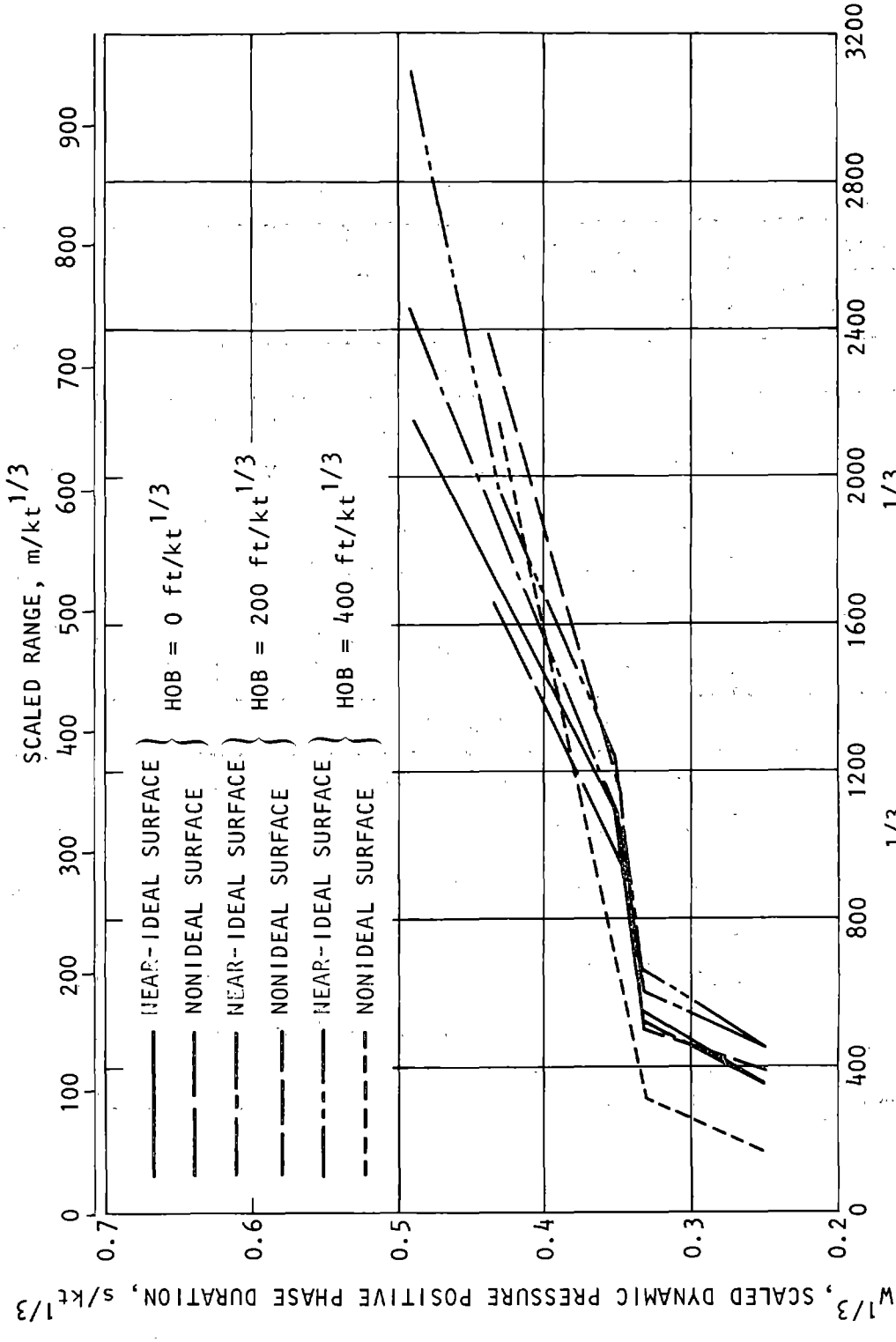

Figure 7-23. Duration of Positive Dynamic Pressure at the Surface

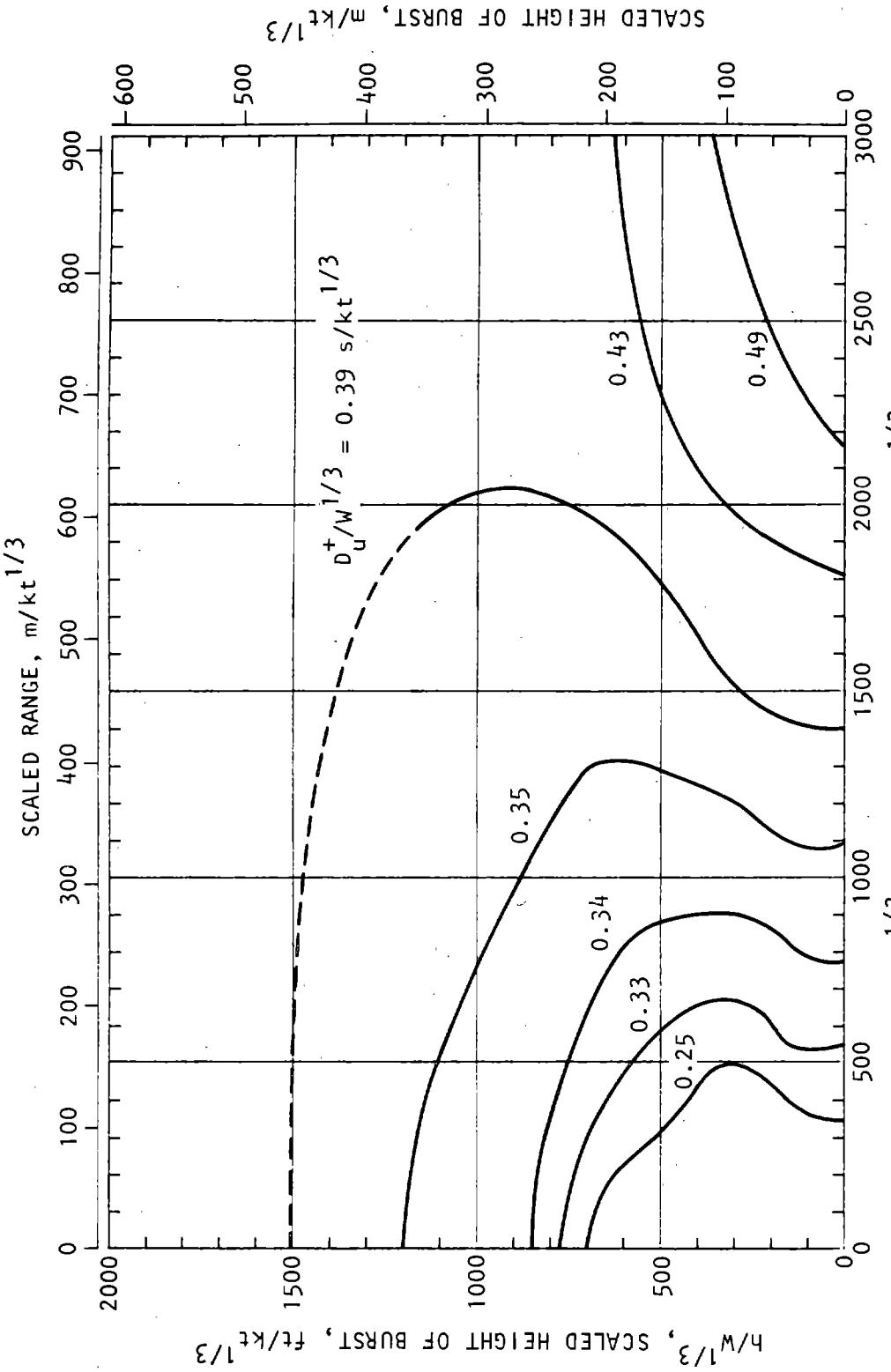

Figure 7-24. Duration of Positive Dynamic Pressure at a Dust-Free or Light-Dust Surface (DNA, 1972)

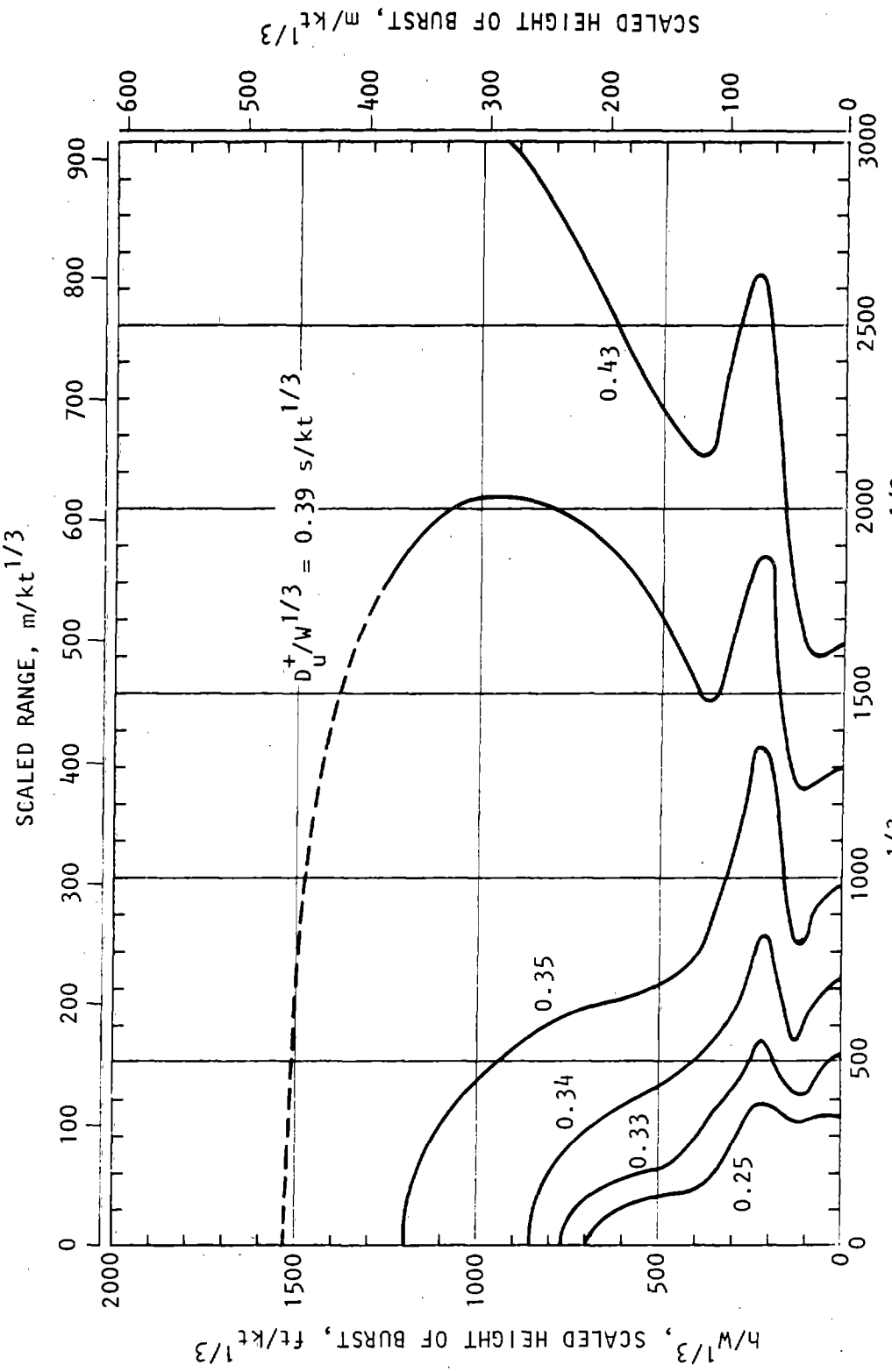

Figure 7–25. Duration of Positive Dynamic Pressure at a Heavy-Dust Surface (DNA, 1972)

Table 7-4. Parameters for Dynamic Pressure Positive Phase Duration

Scaled HOB		Scaled Range		
$ft/kt^{1/3}$	$(m/kt^{1/3})$	$ft/kt^{1/3}$	$(m/kt^{1/3})$	C_o	C_D
Near-Ideal Surface				
0	(0)	350 to 550	(107 to 168)	0.11	0.00040
		550 to 1100	(168 to 335)	0.31	0.000036
		1100 to 2150	(335 to 655)	0.20	0.00013
200	(61)	450 to 600	(137 to 183)	0.01	0.00053
		600 to 1100	(183 to 335)	0.31	0.000040
		1100 to 2450	(335 to 747)	0.24	0.00010
400	(122)	450 to 650	(137 to 198)	0.07	0.00040
		650 to 1250	(198 to 381)	0.31	0.000033
		1250 to 2000	(381 to 610)	0.22	0.00011
		2000 to 3100	(610 to 945)	0.32	0.000055
Nonideal Surface				
0	(0)	350 to 500	(107 to 152)	0.063	0.00053
		500 to 975	(152 to 297)	0.31	0.000042
		975 to 1650	(297 to 503)	0.23	0.00012
200	(61)	400 to 500	(122 to 152)	0.29	0.00080
		500 to 1200	(152 to 366)	0.32	0.000029
		1200 to 2400	(366 to 732)	0.27	0.000067
400	(122)	150 to 300	(46 to 91)	0.17	0.00053
		300 to 2150	(91 to 655)	0.31	0.000054

U.S. Army Corps of Engineers

7-6. Pressure waveforms.

a. General. Under ideal conditions, i.e., airblast propagating across snow, ice, or water, the overpressure and dynamic waveforms can be characterized by the curves presented in figures 7-26 and 7-27, where the peak pressure and positive phase durations are obtained from the data presented in paragraphs 7-2 through 7-5. Under nonideal conditions, such idealized waveforms will not apply, since a number of factors act to distort and modify the blast shape. Among these are:

- Location of the precursor formation region
- Height of a structure relative to the location of the regular and Mach reflection regions
- Effect of rain, fog, or snow
- Terrain features
- Weapon design

This document addresses only the precursor formations since this probably will predominate for surface structures. Most structures will be located below the triple point and will be designed for worst-case conditions (clear day) over the actual terrain. The terrain (topography) must be considered in determining the actual waveforms. Exposed structures locally convert free-field dynamic pressure to overpressure; the degree and areal extent of conversion depend on size and orientation of the structures (DNA, 1972; GETEMPO, 1972 reports.)

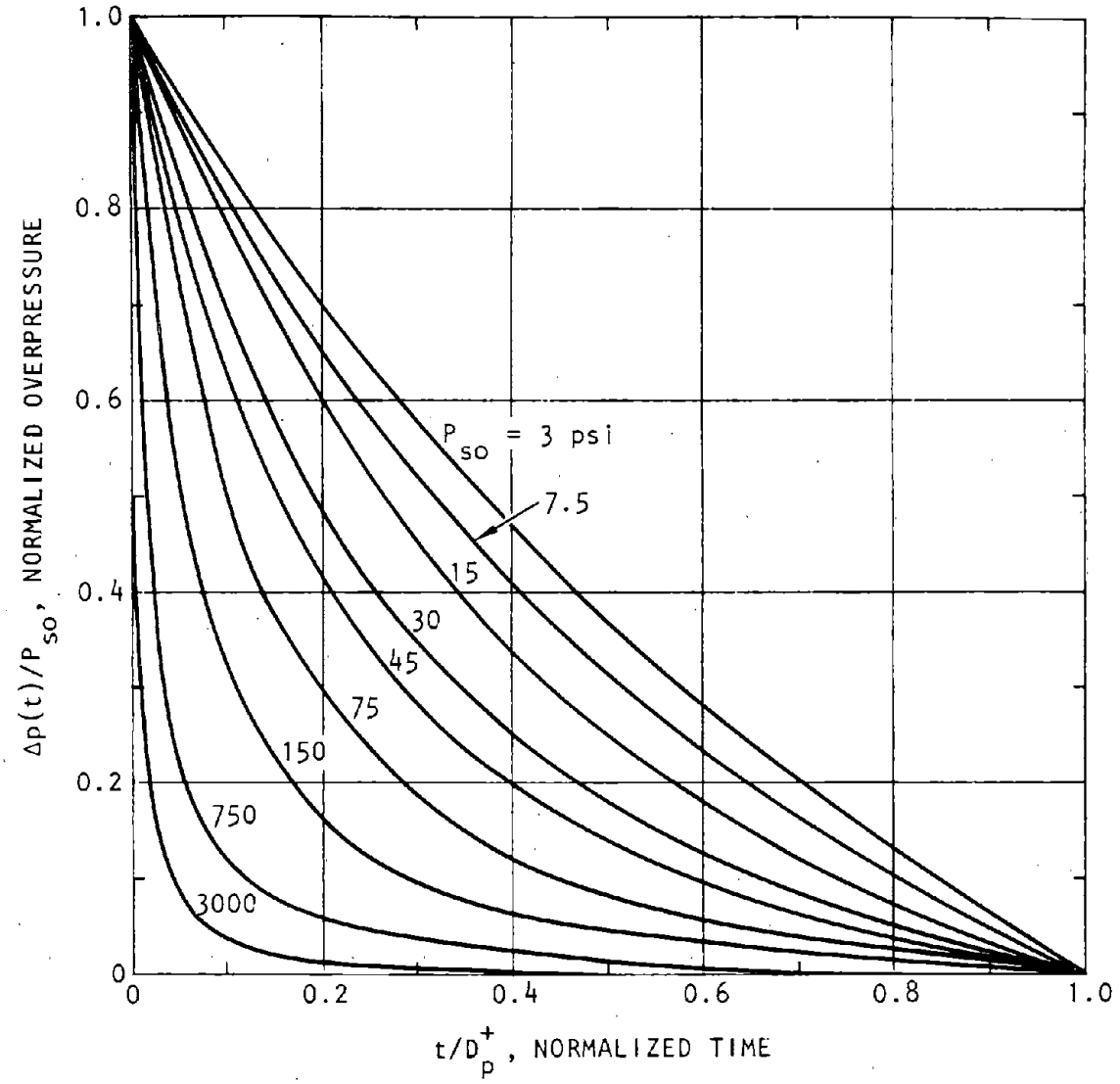

Figure 7–26. Positive Overpressure Waveforms for an Ideal Shock Wave in a Standard Sea Level Atmosphere (DNA, 1972)

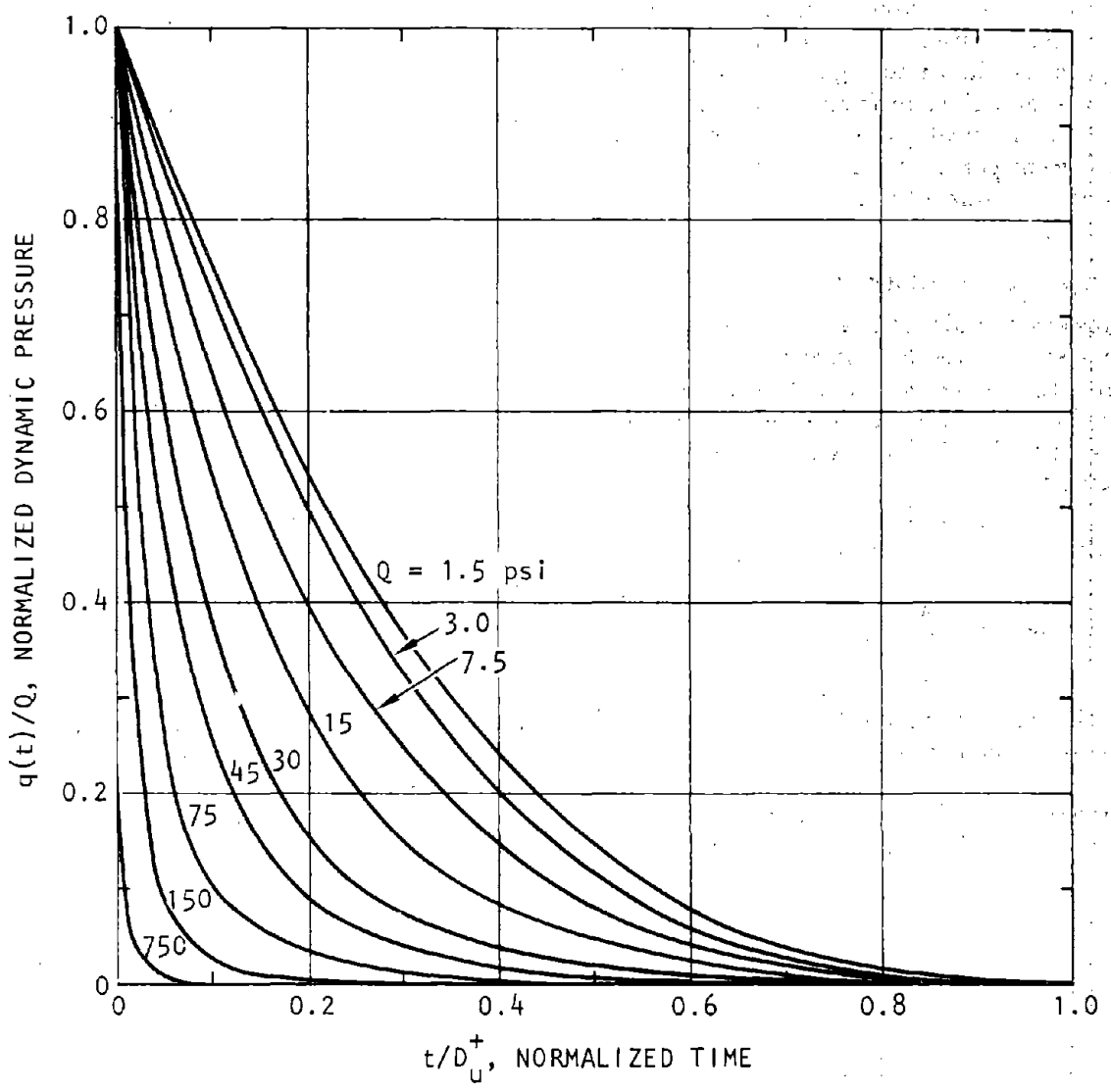

Figure 7–27. Positive Dynamic Pressure Waveforms for an Ideal Shock Wave in a Standard Sea Level Atmosphere (DNA, 1972)

b. Precursor effect—overpressure. Waveforms are classified in terms of the state of precursor formation as the five general types shown in figures 7-28. The type of waveform for a given situation is to be estimated from the data presented in figure 7-29. The peak values of the pulse, the positive phase duration and the impulse should be obtained from the data presented in paragraphs 7-2, 7-4, and 7-7 (GETEMPO, 1972).

c. Precursor effect—dynamic pressure. Dynamic pressure waveforms are also categorized as the five general types as shown in figure 7-30. The appropriate type for a given problem is estimated from figure 7-29. Actual peak dynamic pressures should be obtained from paragraph 7-3, and the positive phase should be obtained from paragraph 7-5 (GETEMPO, 1972).

7-7. Overpressure impulse.

a. Overpressure impulse at the surface is primarily a function of slant range. Reasonably accurate equations of the impulse data presented in figures 7-31 and 7-32 (which show parametric representations of impulse as functions of HOB and ground range) can be represented by

$$\frac{I}{W^{1/3}} = C_1 + C_2 \frac{R}{W^{1/3}} + C_3 \exp\left(C_5 \frac{R}{W^{1/3}}\right) + C_4 \exp\left(C_6 \frac{R}{W^{1/3}}\right) \qquad (7\text{-}15)$$

where I is the impulse in psi-s, W is yield in kt, and R is range in ft. The symbols C_1 through C_6 denote constants.

b. The mean values for overpressure impulse can be obtained directly from figures 7-31 and 7-32 for near-ideal and nonideal surfaces, respectively, or from figures 7-33 and 7-34, or from equation 7-15 in conjunction with the data in table 7-5. It is recommended that the mean values be obtained from figures 7-31 and 7-32 by interpolation.

c. The uncertainty of the overpressure impulse corresponding to equation 7-15 is

$$\begin{aligned}\Omega_I^2 = \Omega_f^2 + \frac{1}{I^2}\Bigg\{&\Big[C_1^2 W^{2/3} + C_2^2 R^2 + C_3^2 W^{2/3} \exp(2C_5 R/W^{1/3}) \\ &+ C_4^2 W^{2/3} \exp(2C_6 R/W^{1/3})\Big]\Omega_c^2 \\ &+ \frac{W^{2/3}}{9}\Bigg[C_1 - \frac{C_3 C_5 R \exp(C_5 R/W^{1/3})}{W^{1/3}} \\ &+ C_3 \exp(C_5 R/W^{1/3}) \\ &- \frac{C_4 C_6 R \exp(C_6 R/W^{1/3})}{W^{1/3}} + C_4 \exp(C_6 R/W^{1/3})\Bigg]^2 \Omega_W^2 \\ &+ R^2\Big[C_2 + C_3 C_5 \exp(C_5 R/W^{1/3}) \\ &+ C_4 C_6 \exp(C_6 R/W^{1/3})\Big]^2 \Omega_R^2\Bigg\} \qquad (7\text{-}16)\end{aligned}$$

where Ω_f is the uncertainty of equation 7-15, Ω_c is the uncertainty of the coefficients, Ω_R is the uncertainty of the ground range, and so forth. Assume $\Omega_f = 0$ and $\Omega_c = 0.1$ (using equation 2-17 where $n = 2$ and $R = 1.5$).

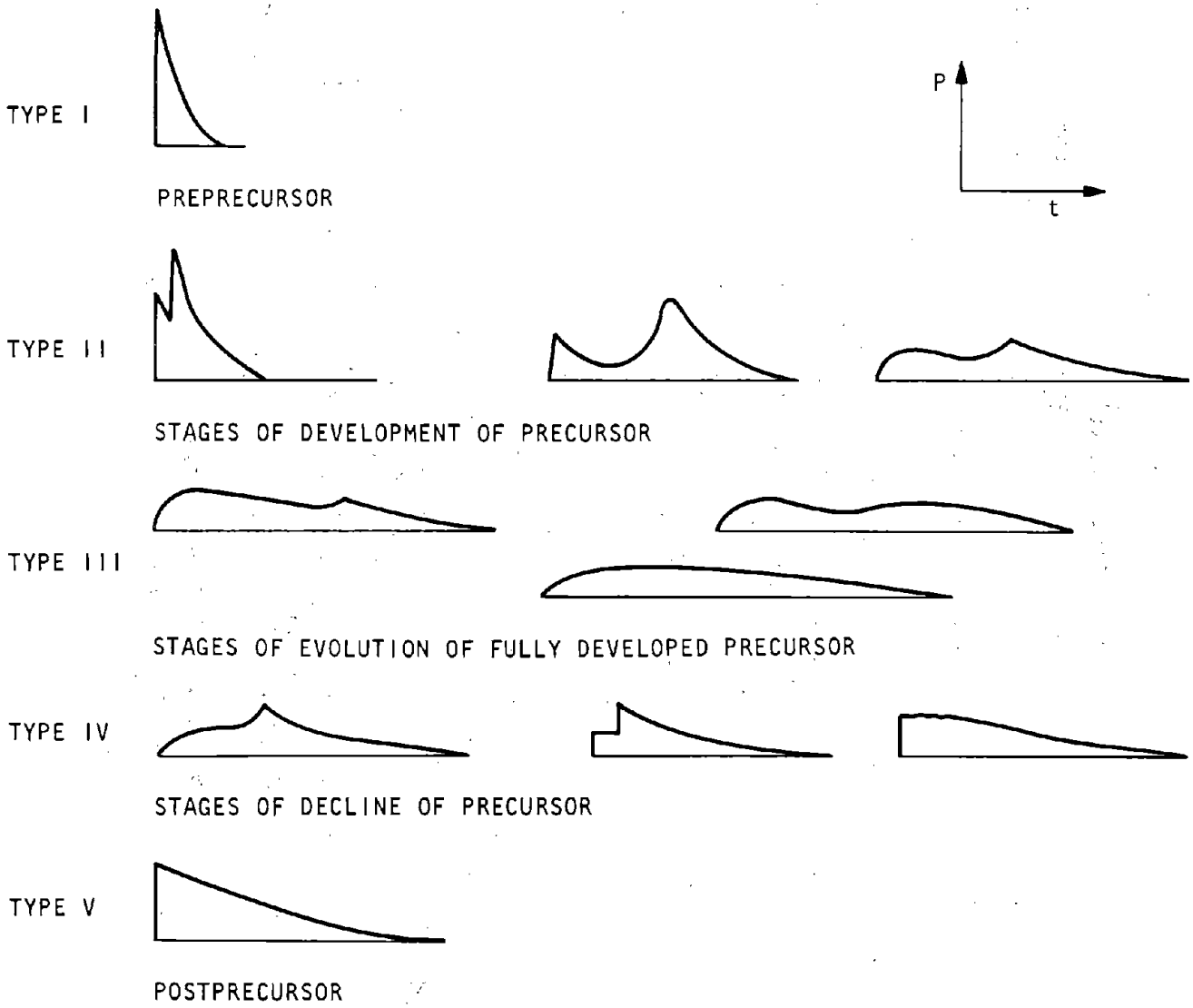

Figure 7–28. Typical Sequence of Overpressure Waveforms over Thermally Nonideal Surfaces (DNA, 1972)

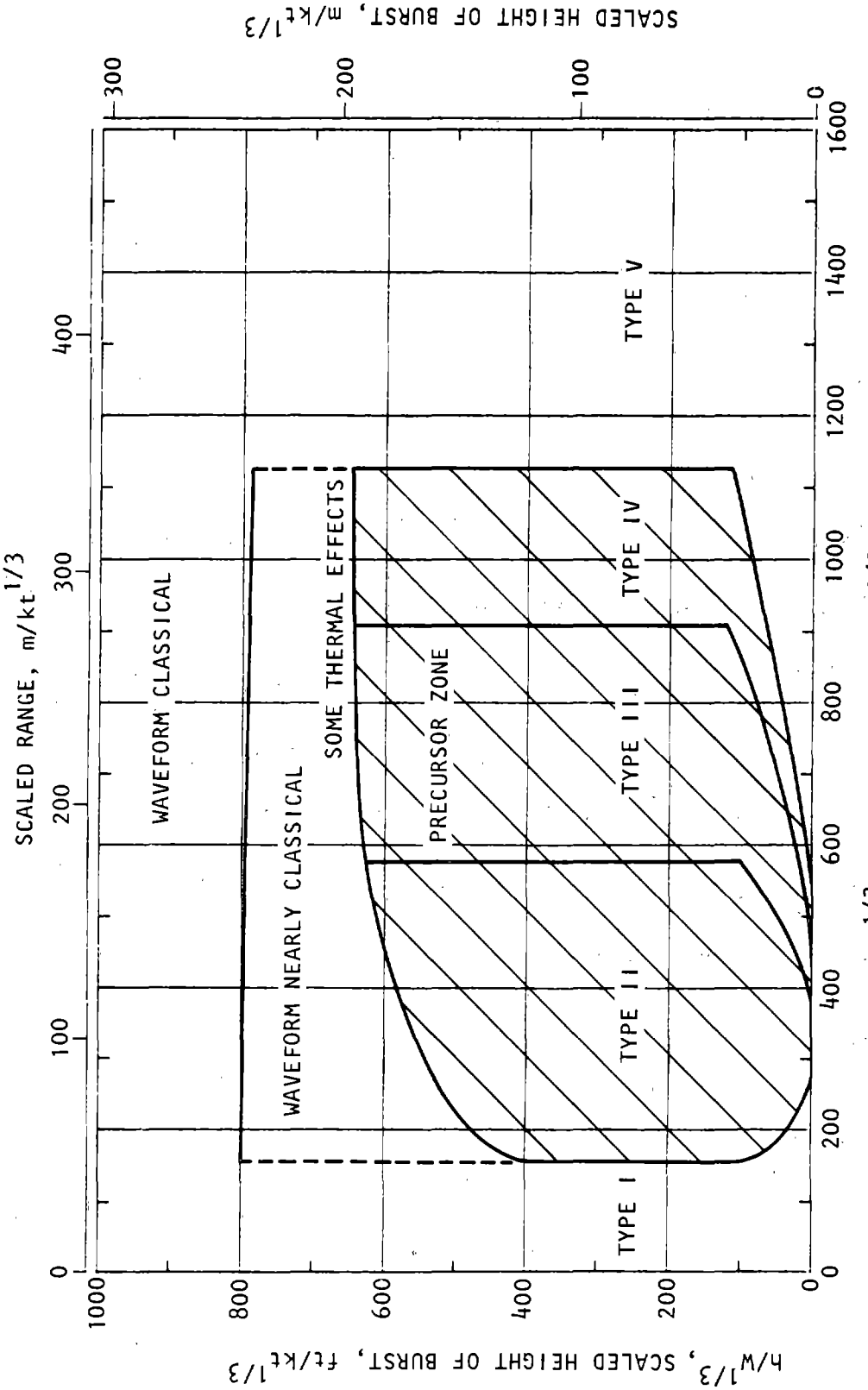

Figure 7–29. Type of Overpressure Waveform Developed over a Thermally Nonideal Surface (DNA, 1972)

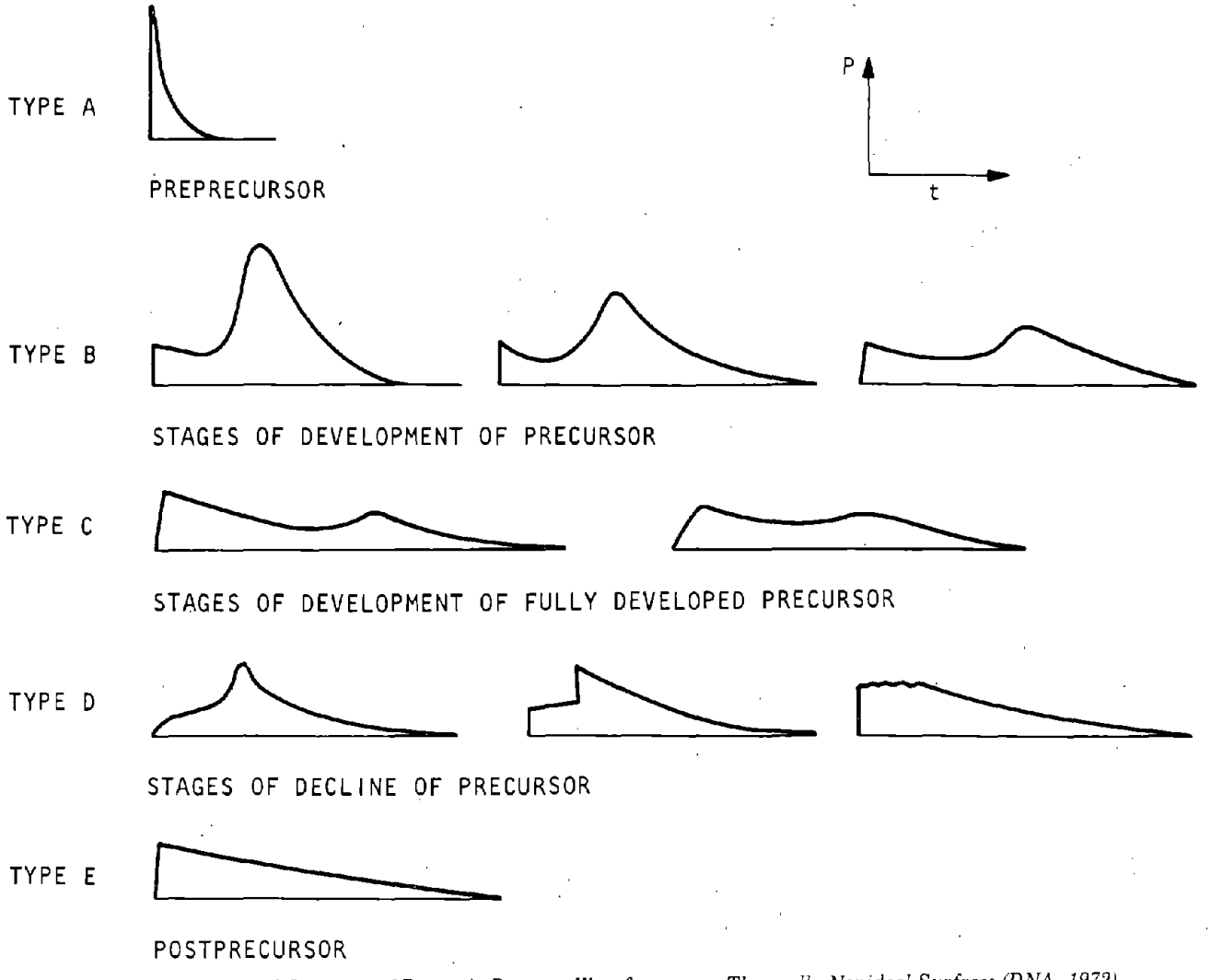

Figure 7-30. Typical Sequence of Dynamic Pressure Waveforms over Thermally Nonideal Surfaces (DNA, 1972)

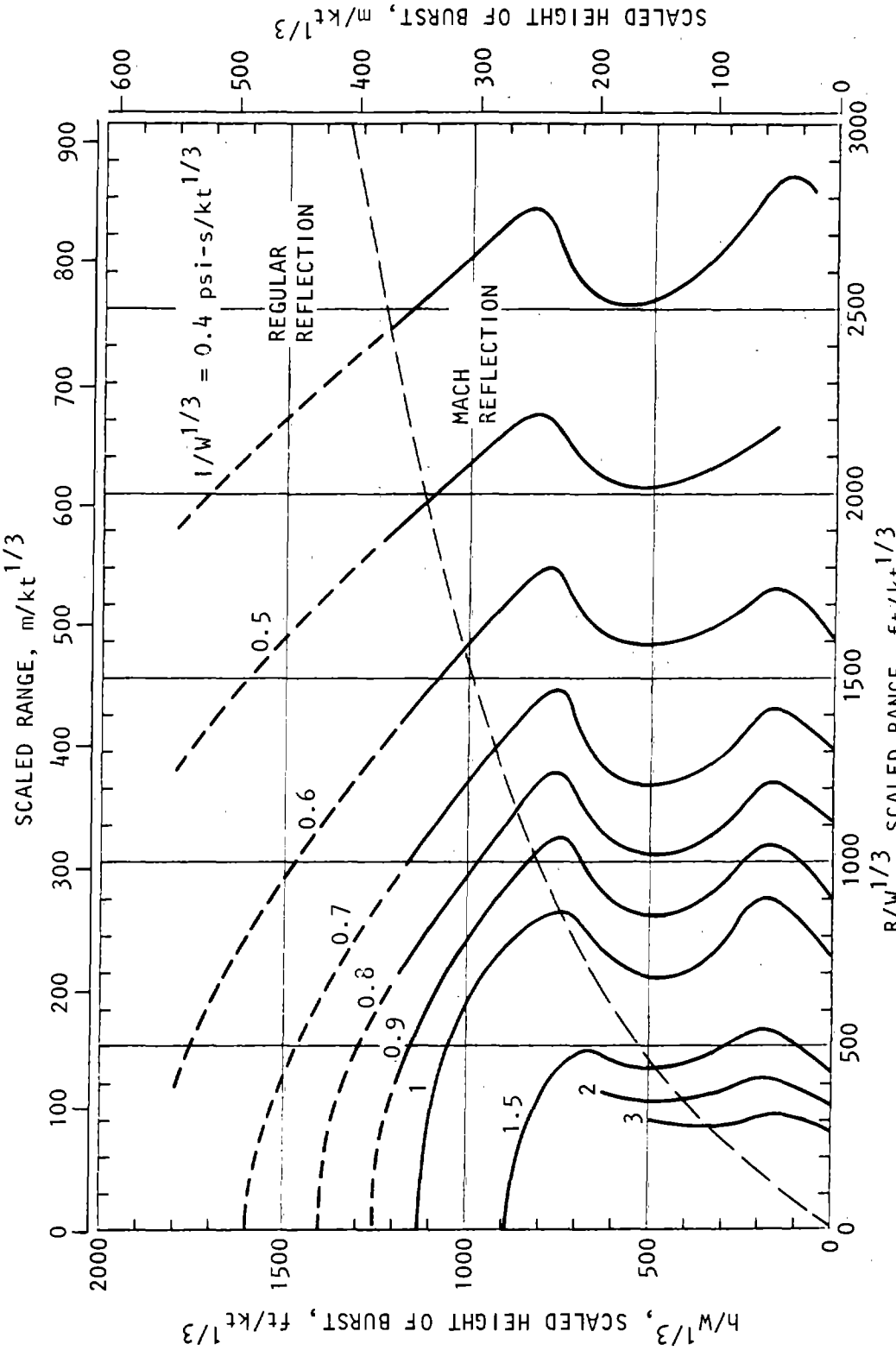

Figure 7–31. Positive Overpressure Impulse at a Near-Ideal Surface (DNA, 1972)

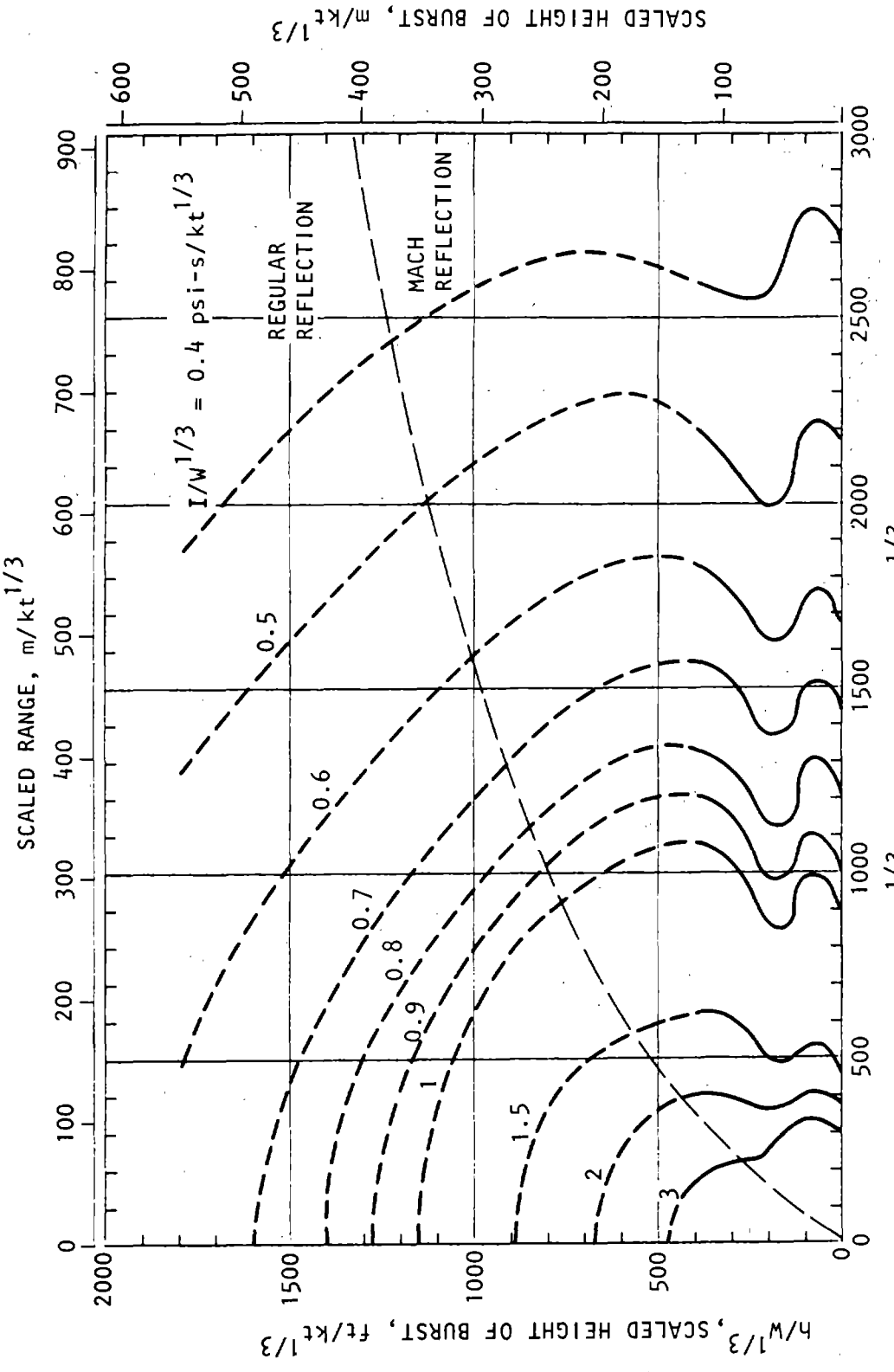

Figure 7-32. Positive Overpressure Impulse at a Thermally Nonideal Surface (DNA, 1972)

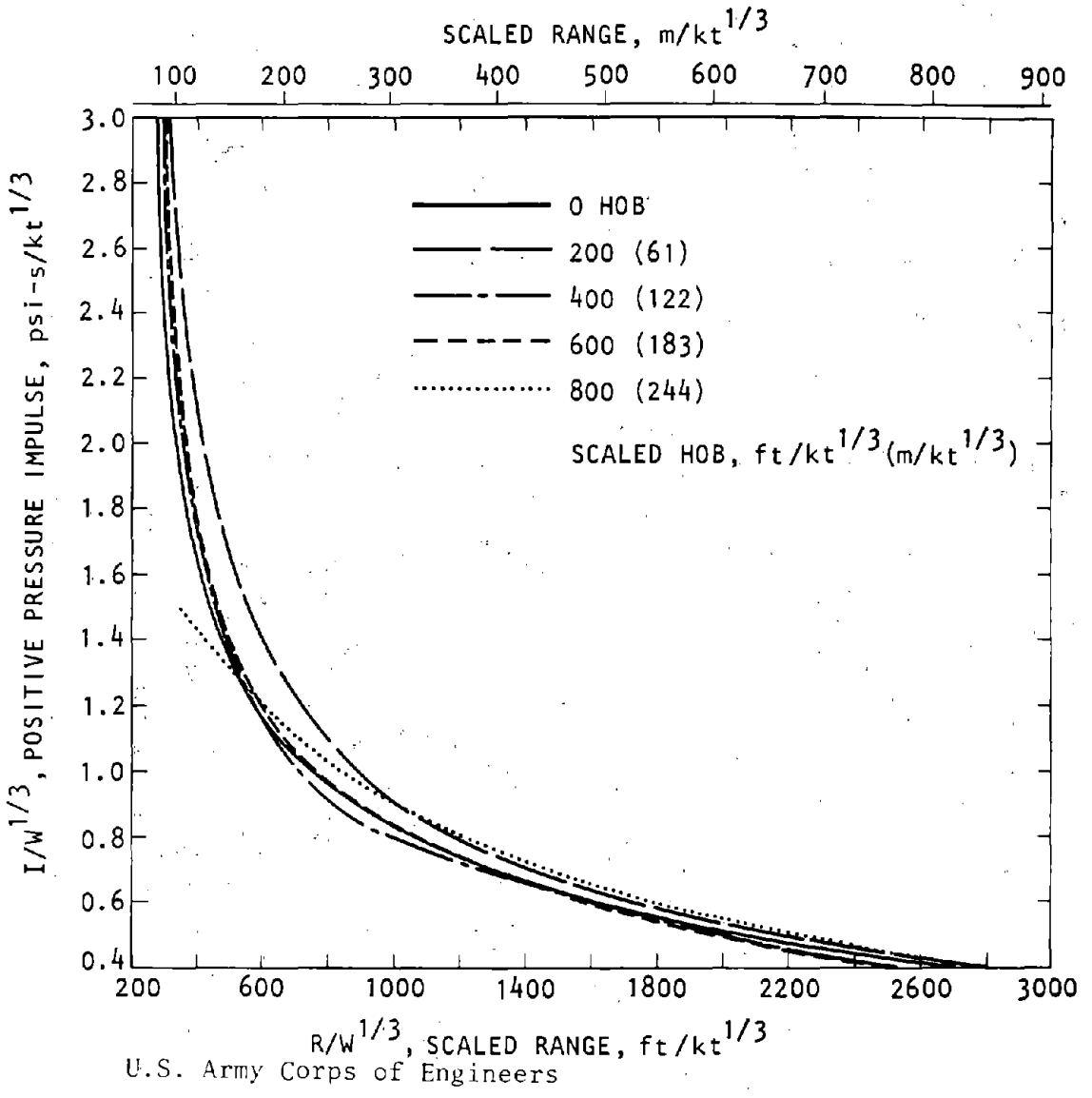

Figure 7-33. Positive Overpressure Impulse at a Near-Ideal Surface different burst heights

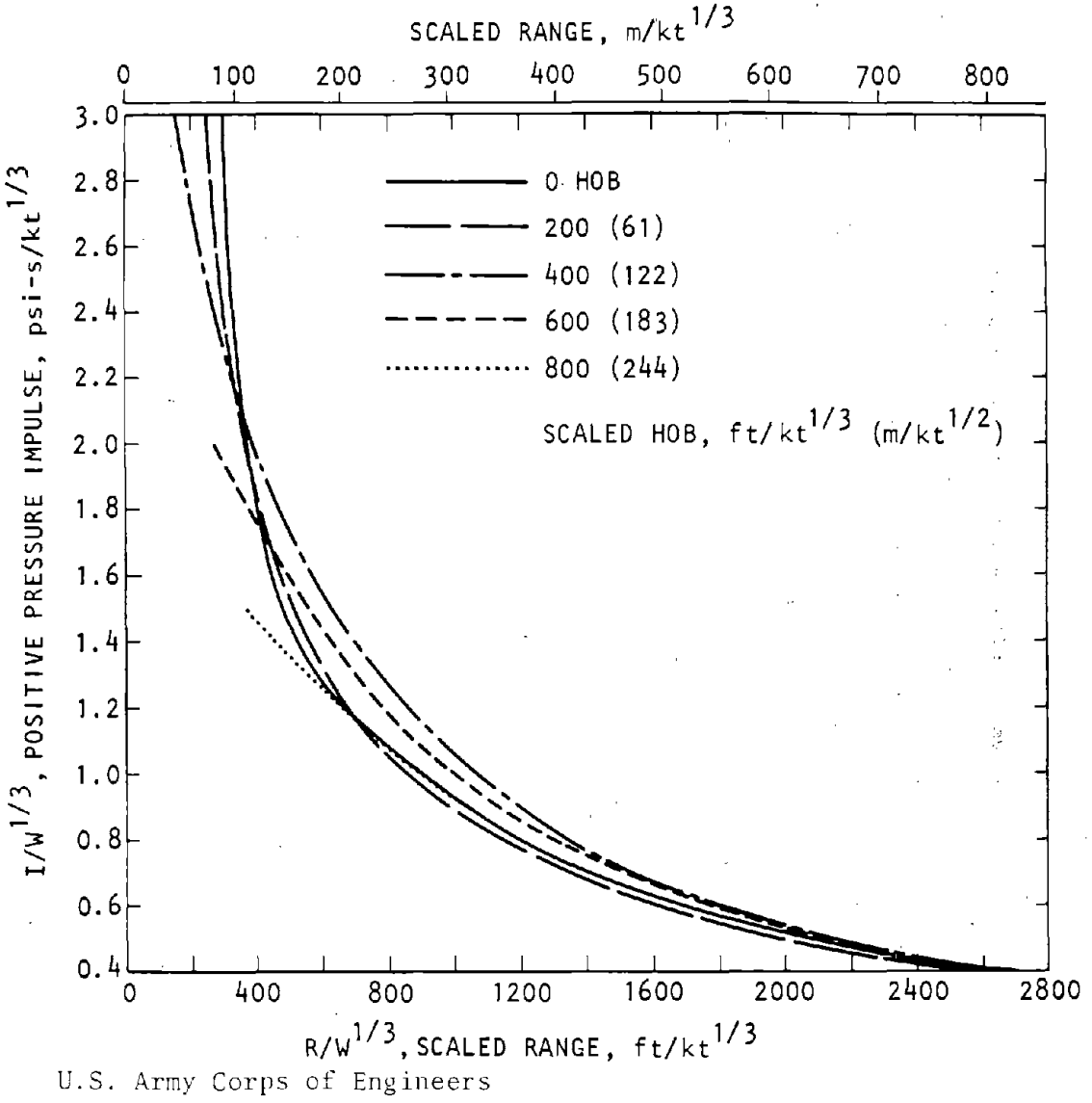

Figure 7-34. Positive Overpressure Impulse at a Nonideal Surface different burst heights

Table 7-5. Values of Constants for Overpressure Impulse Functions

Scaled HOB		Constants					
$ft/kt^{1/3}$	$(m/kt^{1/3})$	C_1	C_2	C_3	C_4	C_5	C_6
Near-Ideal Surface							
0	(0)	7.510×10^{-1}	-1.336×10^{-4}	6.628×10^{1}	1.486×10^{0}	-1.374×10^{-2}	-1.912×10^{-3}
200	(61)	7.735×10^{-1}	-1.360×10^{-4}	7.010×10^{1}	2.526×10^{0}	-1.377×10^{-2}	-2.176×10^{-3}
400	(122)	8.994×10^{-1}	-1.958×10^{-4}	9.629×10^{1}	2.321×10^{0}	-1.506×10^{-2}	-3.129×10^{-3}
600	(183)	8.160×10^{-1}	-1.677×10^{-4}	3.382×10^{1}	1.404×10^{0}	-1.090×10^{-2}	-2.098×10^{-3}
800	(244)	5.922×10^{-1}	-8.990×10^{-5}	5.019×10^{6}	1.258×10^{0}	-5.090×10^{-2}	-1.130×10^{-3}
Nonideal Surface							
0	(0)	-2.400×10^{1}	1.981×10^{-3}	4.716×10^{1}	2.556×10^{1}	-1.112×10^{-2}	-1.086×10^{-4}
200	(61)	4.379×10^{-1}	-4.422×10^{-5}	9.865×10^{0}	1.631×10^{0}	-7.918×10^{-3}	-1.191×10^{-3}
400	(122)	7.415×10^{-1}	-1.450×10^{-4}	1.737×10^{0}	2.151×10^{0}	-5.937×10^{-3}	-1.559×10^{-3}
600	(183)	3.395×10^{-1}	1.219×10^{-5}	0	2.283×10^{0}	8.611×10^{-3}	-1.235×10^{-3}
800	(244)	-1.811×10^{1}	3.228×10^{-3}	-1.958×10^{-2}	2.015×10^{1}	1.376×10^{-3}	-2.387×10^{-4}

U.S. Army Corps of Engineers

CHAPTER 8
AIRBLAST-INDUCED GROUND SHOCK

8-1. Gross phenomenology.

a. At near-surface locations, airblast-induced ground shock can cause outright structural failure of facilities or the failure or malfunction of internal systems. To achieve survival, whether by burial or other hardening techniques, the facility designer must have knowledge of the intensity of the ground-shock environment and of the waveforms.

b. The basic variables affecting the intensity of the ground-shock environment are:

- Weapon design
- Weapon yield
- Burst elevation
- Slant range
- Earth material properties

The larger the yield, the lower the HOB, the smaller the ground impedance, and the closer the facility to the surface, the more severe will be the airblast-induced ground-shock environment.

c. The airblast signal produced by a near-surface nuclear explosion causes ground-shock signals to be formed as the shock front expands. Near the surface in the high overpressure region, the ground-shock signal is a sequence of events represented as the combination of (1) a downward, outward motion from initial loading by the overhead airblast overpressure, and (2) a later upward, outward motion from release of the overhead overpressure and from motion induced by overpressure closer in but delayed by transmission through the ground. The first resembles the airblast overpressure in pulse shape and duration, the pulse shape modifying with depth. The second contribution, termed a "run-up" contribution because the effects are delayed by travel time through the medium, comes from the intense overpressure occurring in the region near GZ and the subsequent complex of motions known as directly induced ground shock.

d. At more distance points, outrunning motion occurs in which the signal in the ground outraces the air shock on the surface. The motion is characterized by an upward and outward surge and often exhibits an oscillatory nature. In addition to these contributions, there may also be crater-induced motion, which is most pronounced near the crater and diminishes with increasing range.

e. In the region between the ground surface and a depression angle of about 30 deg below the surface, the response is arbitrarily termed airblast-induced ground shock regardless of the origin of the motion. See figure 9-1 to visualize delineations made in this volume.

8-2. Ground Response.

For convenience, airblast-induced ground response is usually segregated into two regimes—superseismic and outrunning. In the superseismic region, the speed of the overpressure shock front is greater than the shock speed in the ground. The ground-shock signal appears to be attached to and dragged along by the overpressure shock front traveling across the surface. In the outrunning region, the ground-shock signals arrive first, "outrunning" the overpressure shock front.

8-3. Superseismic peak soil response.

a. Peak soil acceleration. Peak horizontal and vertical accelerations are directly related to the peak overpressure at the surface, modified by the soil properties and the depth. The vertical component is given by Sauer (1964) and Crawford et al. (1974) as

$$a_V = k_o \frac{P_{so}}{C_o \gamma} Z^n \qquad (8\text{-}1a)$$

or

$$a_V = \frac{k_o Z^n}{C_o \gamma} 10^{A + B \log R/W^{1/3} + C \log^2 R/W^{1/3}}$$

where

a_V = Vertical soil acceleration, g
P_{so} = Overpressure, psi
C_o = Soil seismic sound speed, ft/s
γ = In situ soil density, lb/ft^3
Z = Depth, ft
R = Range, ft
W = Yield, kt
A, B, C, n, k_o = Constants

The horizontal component of soil acceleration may be taken as

$$a_H = \begin{cases} a_V \dfrac{C_o}{\sqrt{U^2 - C_o^2}}, & C_o \leq U/\sqrt{2} \\ a_V, & C_o > U/\sqrt{2} \end{cases} \qquad (8\text{-}1b)$$

where U = overhead airblast shock speed, ft/s (see fig. 29 in Brode, 1964)

b. Peak soil velocity. Peak vertical and horizontal velocities are represented by

$$u_V = 0.11\ f(Z,W,C_L)\ P_{so}^{0.896} \qquad (8\text{-}2a)$$

or

$$u_V = 0.11\, f(Z,W,C_L)\, 10^{A' + B' \log R/W^{1/3} + C' \log^2 R/W^{1/3}}$$

and

$$u_H = D(R/W^{1/3})^m \qquad (8\text{–}2b)$$

where

u_V = Vertical soil particle velocity, ft/s
u_H = Horizontal soil particle velocity, ft/s

$$f(Z,W,C_L) = \frac{11\, C_L W^{1/3}}{1115\, Z + 11\, C_L W^{1/3}}$$

C_L = Compressional wave speed of soil under load, ft/s

A′, B′, C′, D, m are constants

Equations 8–2 are adaptations of the work presented by Sauer (1964) and Murrell (1974). Note that the horizontal particle velocity does not attenuate with depth.

c. Peak soil displacement. The peak vertical and horizontal displacements are (Sauer, 1964)

$$d_V = f(Z,W,C_L)\left\{13\, P_{so}^{0.4}\frac{W^{1/3}}{C_o} + 280\frac{P_{so} - 40}{C_o^2}W^{1/3}\right\}, \text{ in.} \qquad (8\text{–}3a)$$

$$d_H = d_V/3, \text{ in.} \qquad (8\text{–}3b)$$

where the variables have been previously defined. Equations 8–3 may be converted to range via the relationship

$$\log P_{so} = A + B \log R/W^{1/3} + C \log^2 R/W^{1/3} \qquad (8\text{–}4)$$

d. Peak soil stress. The peak stress in the soil is computed from equations 8–2 via the relationships

$$\sigma_V = \frac{\varrho C_L u_V}{144}, \text{ psi} \qquad (8\text{–}5a)$$

$$\sigma_H = \frac{\nu}{1-\nu}\varrho_V, \text{ psi} \qquad (8\text{–}5b)$$

where

$$\varrho = \frac{\gamma}{g}\frac{\text{lb sec}^2}{\text{ft}^4}$$

g = 32.2 ft/sec^2
ν = Poisson's ratio

e. Constants in mean and uncertainty calculations of peak soil response. For peak accelerations (eqs. 8–1, peak velocities (eqs. 8–2), peak displacements (eqs. 8–3 and 8–4), and peak stress (eqs. 8–5), use the following constants to calculate mean values:

$$k_o = \begin{cases} 1.72 \times 10^5 \\ 4.36 \times 10^6 \end{cases} \qquad n = \begin{cases} -0.4\ , & 1 \leq Z \leq 20 \text{ ft} \\ -1.48\ , & Z > 20 \text{ ft} \end{cases}$$

A	= 11.87	A′	= 10.64
B	= –5.26	B′	= –4.71
C	= 0.543	C′	= 0.487
D	= 2.72×10^5		
m	= –2.09		

In calculating uncertainties at *f, g, h,* and *i* below, find $\Omega_{P_{so}}$ from equation 7–2 and assume the following value:

$\Omega_f \approx 0.13$
$\Omega_g \approx 0.09$
$\Omega_h \approx 0.24$
$\Omega_k \approx 0.13$
$\Omega_m \approx 0.10$

f. Uncertainty of peak soil accelerations. Using the values from *e* above, calculate uncertainties of vertical and horizontal accelerations:

$$\Omega^2_{a_V} = \begin{cases} \Omega_f^2 + \Omega_{P_{so}}^2 + \Omega_{C_o}^2 + \Omega_\gamma^2 + n^2\Omega_Z^2 \\ \text{or} \\ \Omega_f^2 + \Omega_{C_o}^2 + \Omega_\gamma^2 + n^2\Omega_Z^2 \\ \quad + \left[B + 2C \log R/W^{1/3}\right]^2\left[\frac{\Omega_W^2}{9} + \Omega_R^2\right] \end{cases} \qquad (8\text{–}6a)$$

$$\Omega^2_{a_H} = \begin{cases} \Omega_f^2 + \Omega_{P_{so}}^2 + \Omega_\gamma^2 + n^2\Omega_Z^2 + \dfrac{1}{(U^2 - C_o^2)^2} \\ \quad \left[U^4\Omega_U^2 + C_o^4\Omega_{C_o}^2\right],\ C_o \leq U/\sqrt{2} \\ \text{or} \\ \Omega_f^2 + \Omega_\gamma^2 + n^2\Omega_Z^2 + \dfrac{1}{(U^2 - C_o^2)^2}\left[U^4\Omega_U^2 + C_o^4\Omega_{C_o}^2\right] \\ \quad + \left(B + 2C \log R/W^{1/3}\right)^2\left(\dfrac{\Omega_W^2}{9} + \Omega_R^2\right), \\ \quad C_o \leq U/\sqrt{2} \\ \Omega^2_{a_V},\ C_o > U/\sqrt{2} \end{cases} \qquad (8\text{–}6b)$$

g. Uncertainty of peak soil velocities. Using values from *e* above, calculate uncertainties of vertical and horizontal peak velocities:

$$\Omega^2_{u_V} = \begin{cases} \Omega^2_g + \left[\dfrac{1115\,Z}{1115\,Z + 11\,C_L W^{1/3}}\right]^2 \left[\dfrac{\Omega^2_W}{9} + \Omega^2_{C_L} + \Omega^2_Z\right] \\ \quad + 0.803\Omega^2_{P_{so}} \\ \text{or} \\ \Omega^2_g + \left[\dfrac{1115\,Z}{1115\,Z + 11\,C_L W^{1/3}}\right]^2 \left[\Omega^2_{C_L} + \Omega^2_Z\right] \\ \quad + \left[B' + 2C' \log R/W^{1/3}\right]^2 \Omega^2_R \\ \quad + \left[\dfrac{1115\,Z}{1115\,Z + 11\,C_L W^{1/3}} - B'\right. \\ \quad \left. - 2C' \log R/W^{1/3}\right]^2 \Omega^2_W \end{cases} \qquad (8\text{–}7a)$$

$$\Omega^2_{u_H} = \Omega^2_h + m^2\left[\Omega^2_R + \frac{\Omega^2_W}{9}\right] \qquad (8\text{–}7b)$$

h. Uncertainty of peak soil displacements. Using values from *e* above, calculate uncertainties of vertical and horizontal peak displacements:

$$\Omega^2_{d_V} = \Omega^2_k + \left[\frac{1115\,Z}{1115\,Z + 11\,C_L W^{1/3}}\right]^2 \left[\Omega^2_{C_L} + \Omega^2_Z\right] + \left[\frac{2230\,Z + 11\,C_L W^{1/3}}{1115\,Z + 11\,C_L W^{1/3}}\right]^2 \frac{\Omega^2_W}{9} + \left[\frac{5.2\,P^{0.4}_{so}\,C_o + 280\,P_{so}}{13\,P^{0.4}_{so}\,C_o + 280(P_{so} - 40)}\right]^2 \Omega^2_{P_{so}} \qquad (8\text{–}8a)$$

$$\Omega^2_{d_H} = \Omega^2_{d_V} \qquad (8\text{–}8b)$$

These equations may be expressed in terms of range and yield by utilizing equation 7–2.

i. Uncertainty of peak soil stress. Using values in *e* above, calculate uncertainties of vertical and horizontal peak stresses:

$$\Omega^2_{\sigma_V} = \Omega^2_m + \Omega^2_\gamma + \Omega^2_{C_L} + \Omega^2_{u_V} \qquad (8\text{–}9a)$$

$$\Omega^2_{\sigma_H} = \Omega^2_{\sigma_V} + \Omega^2_\nu \qquad (8\text{–}9b)$$

8–4. Superseismic peak rock response.

a. Peak rock acceleration. The peak horiontal and vertical accelerations in rock are described by equations 8–1.

b. Peak rock velocity and displacement. Utilizing an adaptation of work performed by Cooper (1973), the peak horizontal and vertical particle velocities and displacements can be represented by equations of the form:

$$u_V = \left[A_V \frac{W^{2/3}}{R^2} - A'_V \frac{ZW^{1/3}}{R^2}\right] C_L \qquad (8\text{–}10a)$$

$$u_H = \left[A_H \frac{W^{2/3}}{R^2} - A'_H \frac{ZW^{1/3}}{R^2}\right] C_L \qquad (8\text{–}10b)$$

and

$$d_V = \left[B_V \frac{W^{4/3}}{R^3} - B'_V \frac{ZW}{R^3}\right] \qquad (8\text{–}11a)$$

$$d_H = \left[B_H \frac{W^{4/3}}{R^3} - B'_H \frac{ZW}{R^3}\right] \qquad (8\text{–}11b)$$

where A_V, A_H, A'_V, A'_H, B_V, B_H, B'_V, and B'_H are constants and the other variables have definitions as previously defined.

c. Peak rock stress. The peak horizontal and vertical stresses are identical to the definitions presented in equation 8–5.

d. Mean peak rock response. The mean peak horizontal and vertical accelerations are evaluated by using equations 8–1 (variables redefined for rock where necessary) with the values presented in paragraph 8–3*e*. The corresponding velocities and displacements are obtained from equations 8–10 and 8–11 where the values of the constants from the data presented in table 8–1 should be used. The mean peak horizontal and vertical stress may be obtained from equation 8–5 where the proper mean values for the properties of particular rocks are considered.

e. Uncertainty of rock response. Equations 8–6 and 8–9 may be utilized to compute the uncertainty of rock acceleration and stress. The values of Ω_f and Ω_m presented in paragraph 8–3*e* are still applicable. The computation of velocity and displacement uncertainties produces

$$\Omega^2_{u_V} = \Omega^2_P + 4\Omega^2_R + \left[2 + \frac{A'_V C_L Z W^{1/3}}{R^2 u_V}\right] \frac{\Omega^2_W}{9} + \left[\frac{A'_V C_L Z W^{1/3}}{u_V R^2}\right]^2 \Omega^2_Z + \Omega^2_{C_L} \qquad (8\text{–}12a)$$

$$\Omega^2_{u_H} = \Omega^2_P + 4\Omega^2_R + \left[2 + \frac{A'_H C_L Z W^{1/3}}{R^2 u_H}\right]^2 \frac{\Omega^2_W}{9} + \left[\frac{A'_H C_L Z W^{1/3}}{u_H R^2}\right]^2 \Omega^2_Z + \Omega^2_{C_L} \qquad (8\text{–}12b)$$

Table 8-1. Mean Parameters for Calculation of Velocity and Displacement Due to Airblast on Rock

A_H =	144	A_H' =	0	, $0 \leq Z/W^{1/3} \leq 31$ ft/kt$^{1/3}$
	424		2.16	, $31 < Z/W^{1/3} \leq 61$ ft/kt$^{1/3}$
A_V =	193	A_V'' =	1.57	, $0 \leq Z/W^{1/3} \leq 31$ ft/kt$^{1/3}$
	134		0.62	, $31 < Z/W^{1/3} \leq 61$ ft/kt$^{1/3}$
B_H =	5.03×10^6	B_H' =	0	, $0 \leq Z/W^{1/3} \leq 31$ ft/kt$^{1/3}$
	7.82×10^6		8.99×10^4	, $31 < Z/W^{1/3} \leq 61$ ft/kt$^{1/3}$
B_V =	5.03×10^6	B_V' =	8.99×10^4	, $0 \leq Z/W^{1/3} \leq 31$ ft/kt$^{1/3}$
	3.35×10^6		3.59×10^4	, $31 < Z/W^{1/3} \leq 61$ ft/kt$^{1/3}$

U.S. Army Corps of Engineers

$$\Omega_{D_V}^2 = \Omega_q^2 + 9\Omega_R^2 + \left[4 + \frac{B_V' ZW}{R^3 d_V}\right]^2 \Omega_W^2 + \left[\frac{B'_V ZW}{R^3 d_V}\right]^2 \Omega_Z^2 \qquad (8\text{-}13a)$$

$$\Omega_{D_H}^2 = \Omega_q^2 + 9\Omega_R^2 + \left[4 + \frac{B_H' ZW}{R^3 d_H}\right]^2 \Omega_W^2 + \left[\frac{B_H' ZW}{R^3 d_H}\right]^2 \Omega_Z^2 \qquad (8\text{-}13b)$$

where $\Omega_p \approx 0.36$ and $\Omega_q \approx 0.36$.

8-5. Superseismic coil and rock waveforms.

a. Soil waveforms. According to the data presented by Murrell (1974), vertical velocities at a constant range maintain a relatively constant waveform but decrease in amplitude with depth. Conversely, at a constant depth, the vertical velocities undergo distinct changes in both waveform and amplitude with variations in range. Horizontal velocities qualitatively display the same type of behavior although they are markedly different in character than their vertical counterparts.

(1) Typical examples taken from Murrell (1974) have been normalized and are presented at various ranges for the vertical velocity in figure 8-1 and for the horizontal velocity in figure 8-2. The data generally apply at all depths in the superseismic region.

(2) Parenthetically, it is noted in figure 8-2 that outrunning motion appears at the 340 ft/kt$^{1/3}$ range and is characterized by the rolling motion after a time of about 1.0 s/kt$^{1/3}$. The outrunning is well developed at the 535 and 680 ft/kt$^{1/3}$ ranges. The amplitudes presented in paragraph 8-3 apply to the motion prior to the time of the arrival of the outrunning motion. After the outrunning motion occurs, the amplitudes of paragraph 8-6 will apply. The reader is encouraged to study Murrell (1974) prior to constructing waveforms having the generalized waveform characteristics of figures 8-1 and 8-2 but adjusted to match the amplitude statistics presented in paragraphs 8-3 and 8-6.

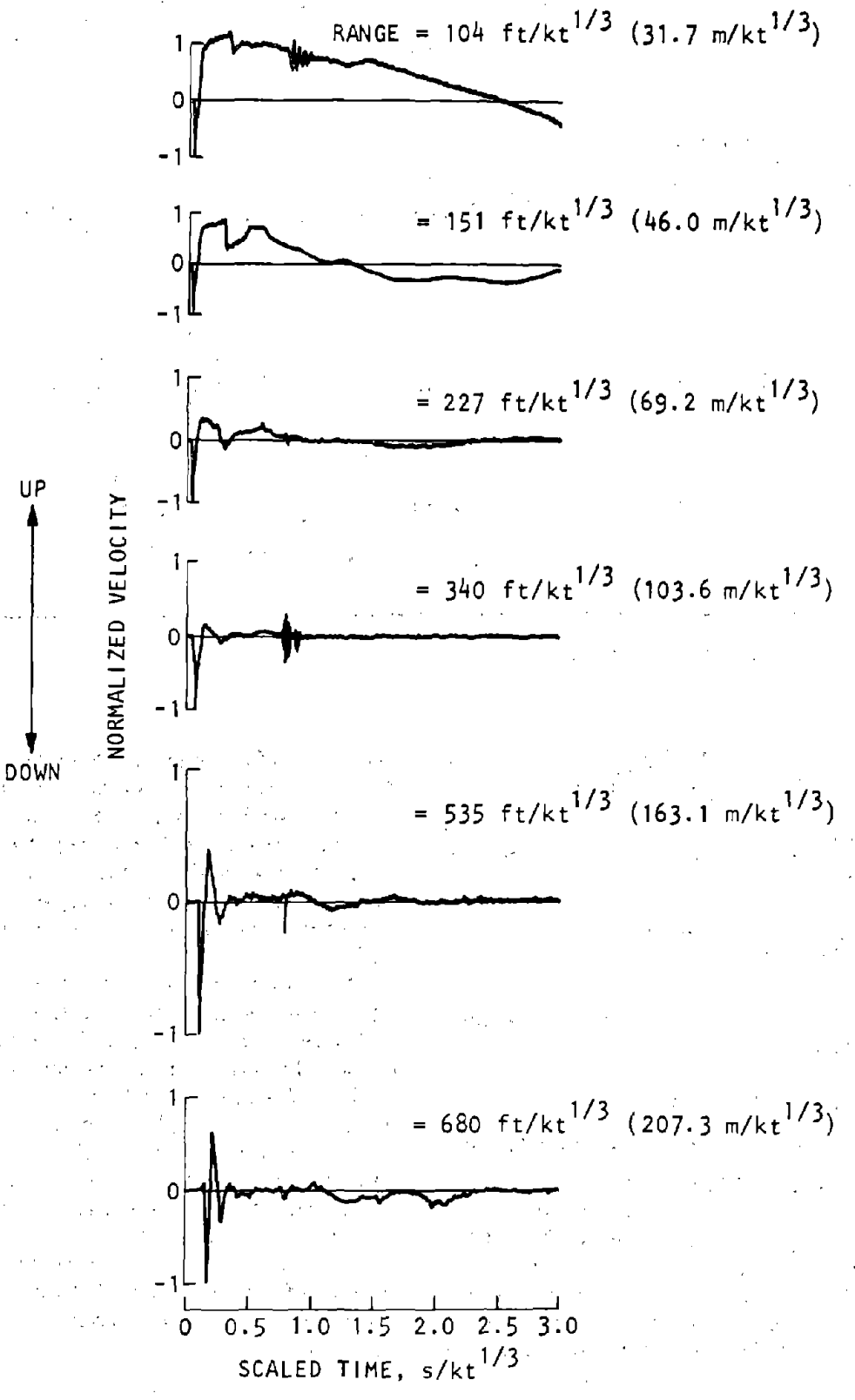

Figure 8–1. Vertical Velocity Waveforms for Soils at All Depths (Adapted from Murrell, 1974)

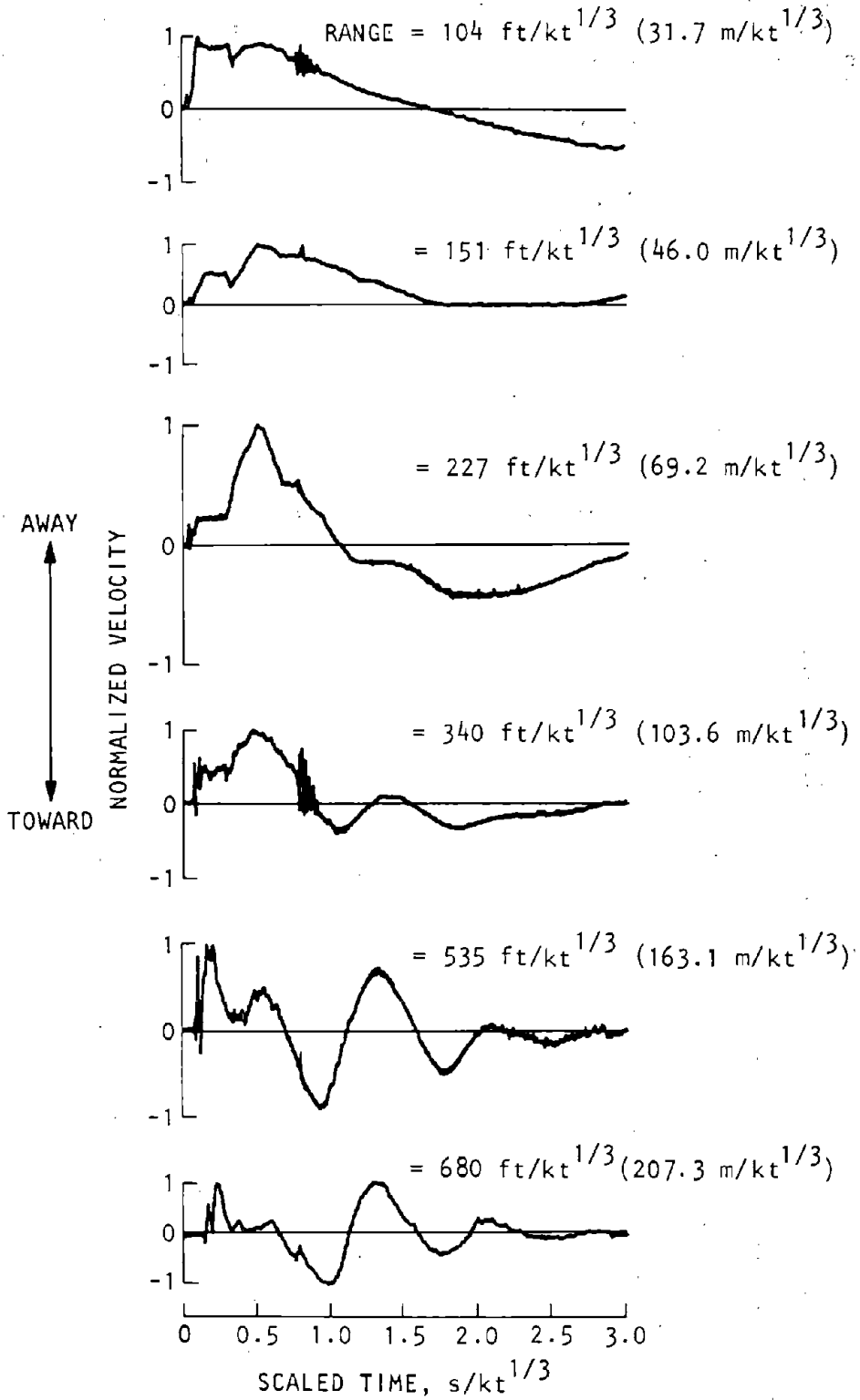

Figure 8–2. Horizontal Velocity Waveforms for Soils at All Depths (Adapted from Murrell, 1974)

b. Rock waveforms. Utilizing normalized data from Murrell-Carleton (1973), figures 8–3 and 8–4 present selections of vertical velocity histories at various scaled ranges but at the constant specified scaled depths. It is noted that at a given range, the depth influences the character of the waveforms (in contrast to the data presented in *a* above in which depth plays a minor role in modifying velocity signatures in soil). Conversely, figure 8–5 presents normalized horizontal velocity histories for a selection of scaled ranges and for all depths of interest. The reader should study Murrell-Carleton (1973) prior to adapting the data in figures 8–3 through 8–5 to suit his own needs. Derived signatures should be compatible with the peak amplitude data presented in paragraph 8–4 above for airblast-induced response in rock.

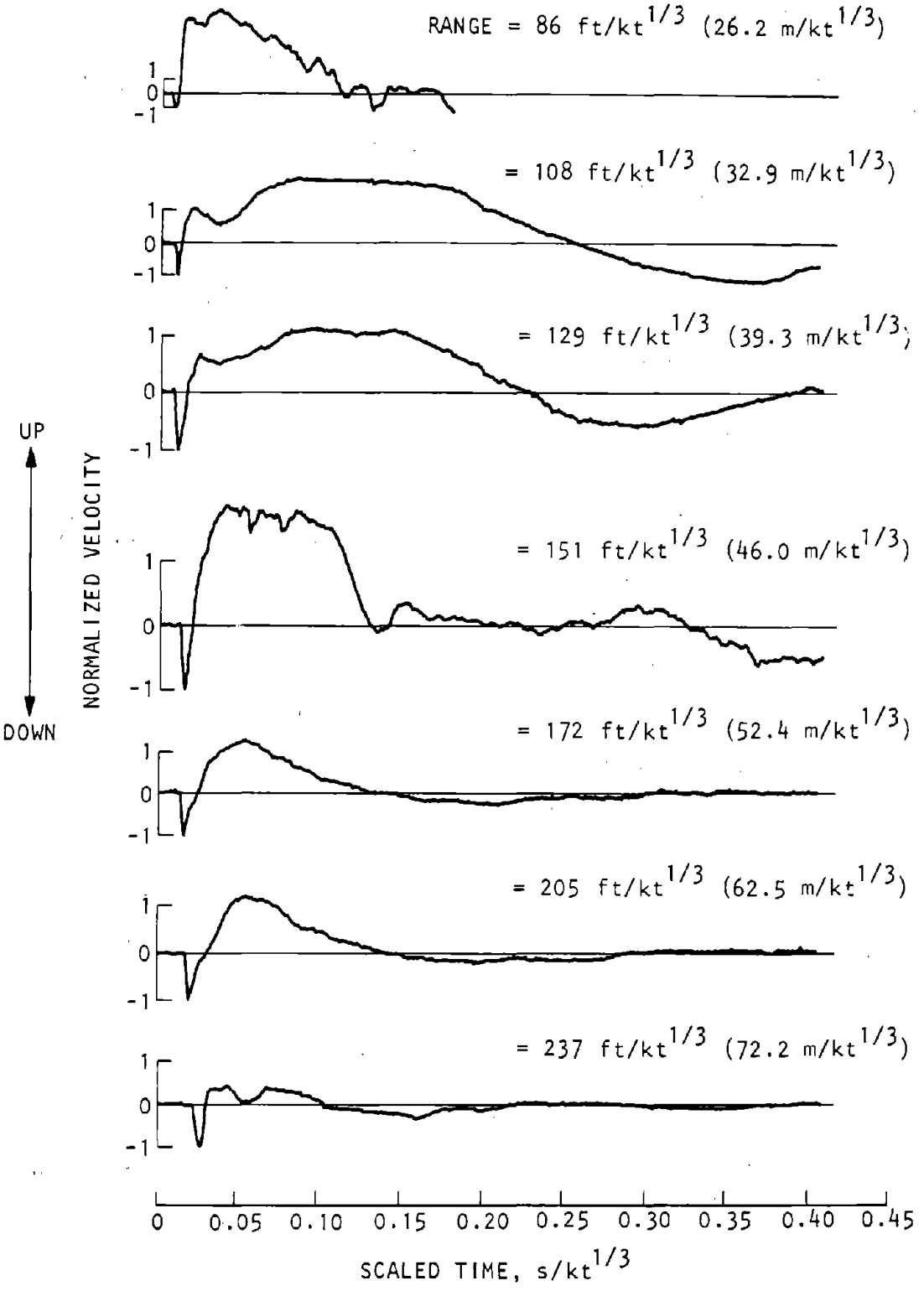

Figure 8–3. Vertical Velocity Waveforms for Rock, Scaled Depth of 4.3 ft/kt$^{1/3}$ (1.31 m/kt$^{1/3}$) (Adapted from Murrell-Carleton, 1973)

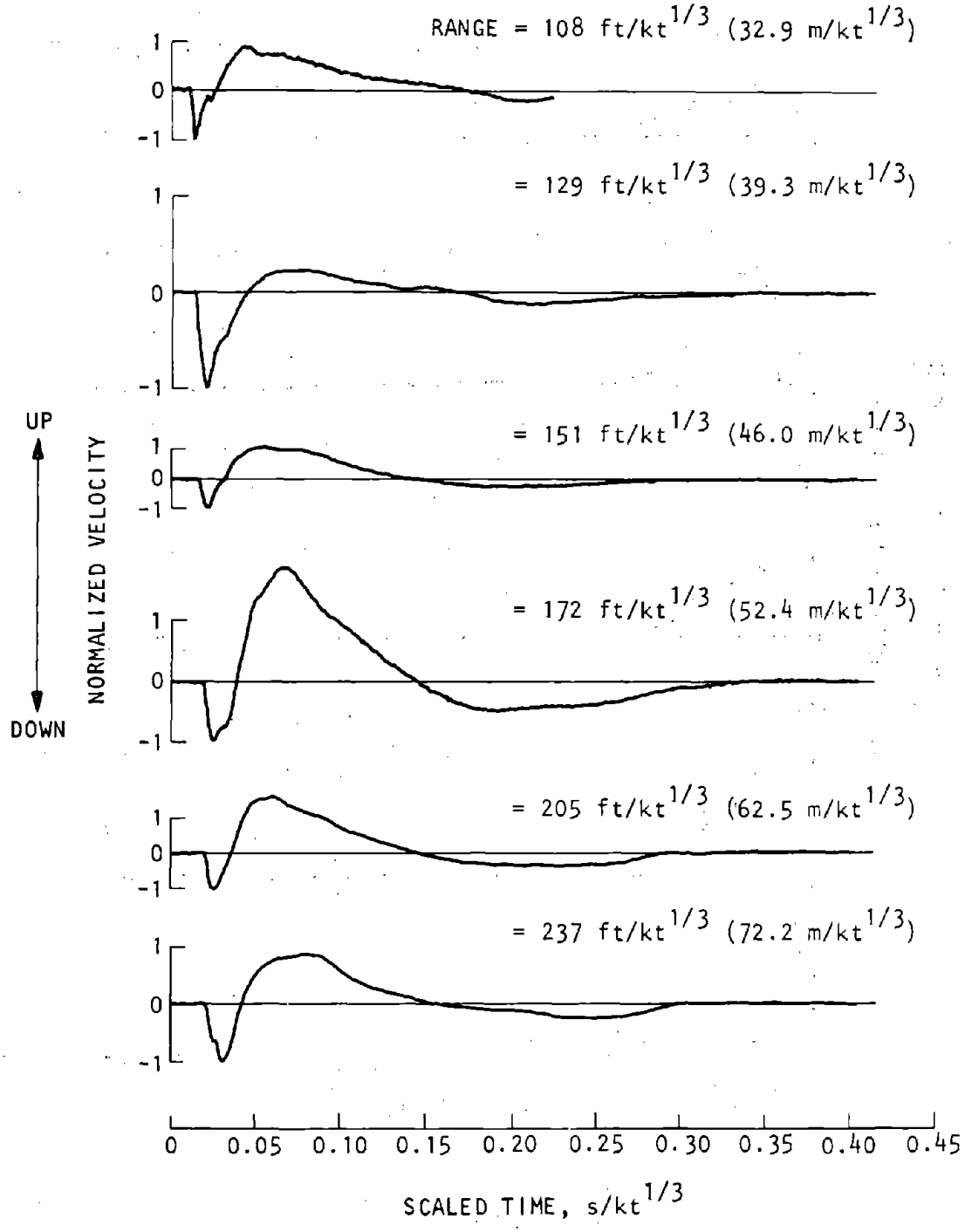

Figure 8–4. Vertical Velocity Waveforms for Rock, Scaled Depths Below 38.8 ft/kt$^{1/3}$ (11.83 m/kt$^{1/3}$) (Adapted from Murrell-Carleton, 1973)

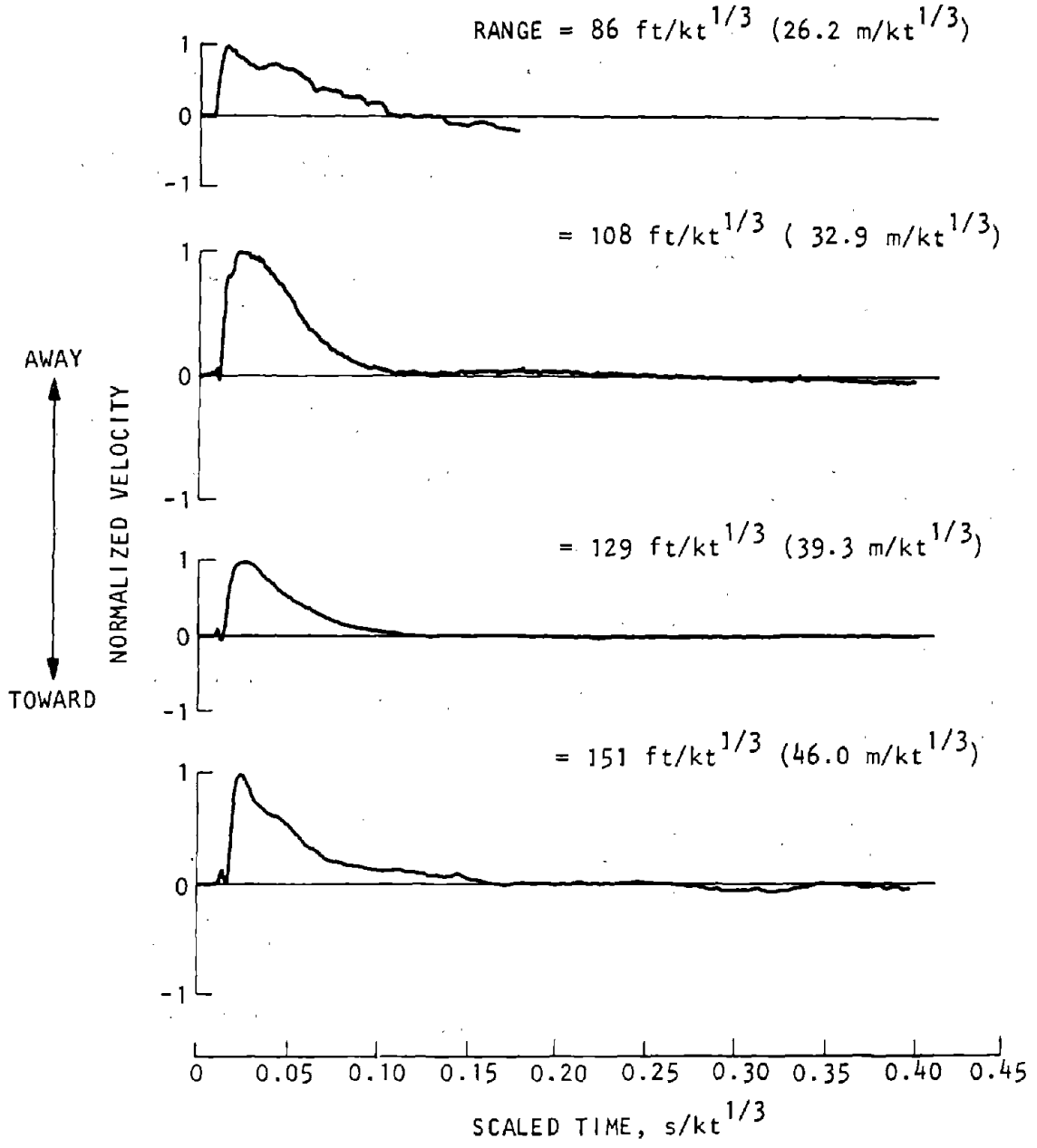

(a)

Figure 8-5. Horizontal Velocity Waveforms for Rock for All Depths (Adapted from Murrell-Carleton, 1973) (1 of 2)

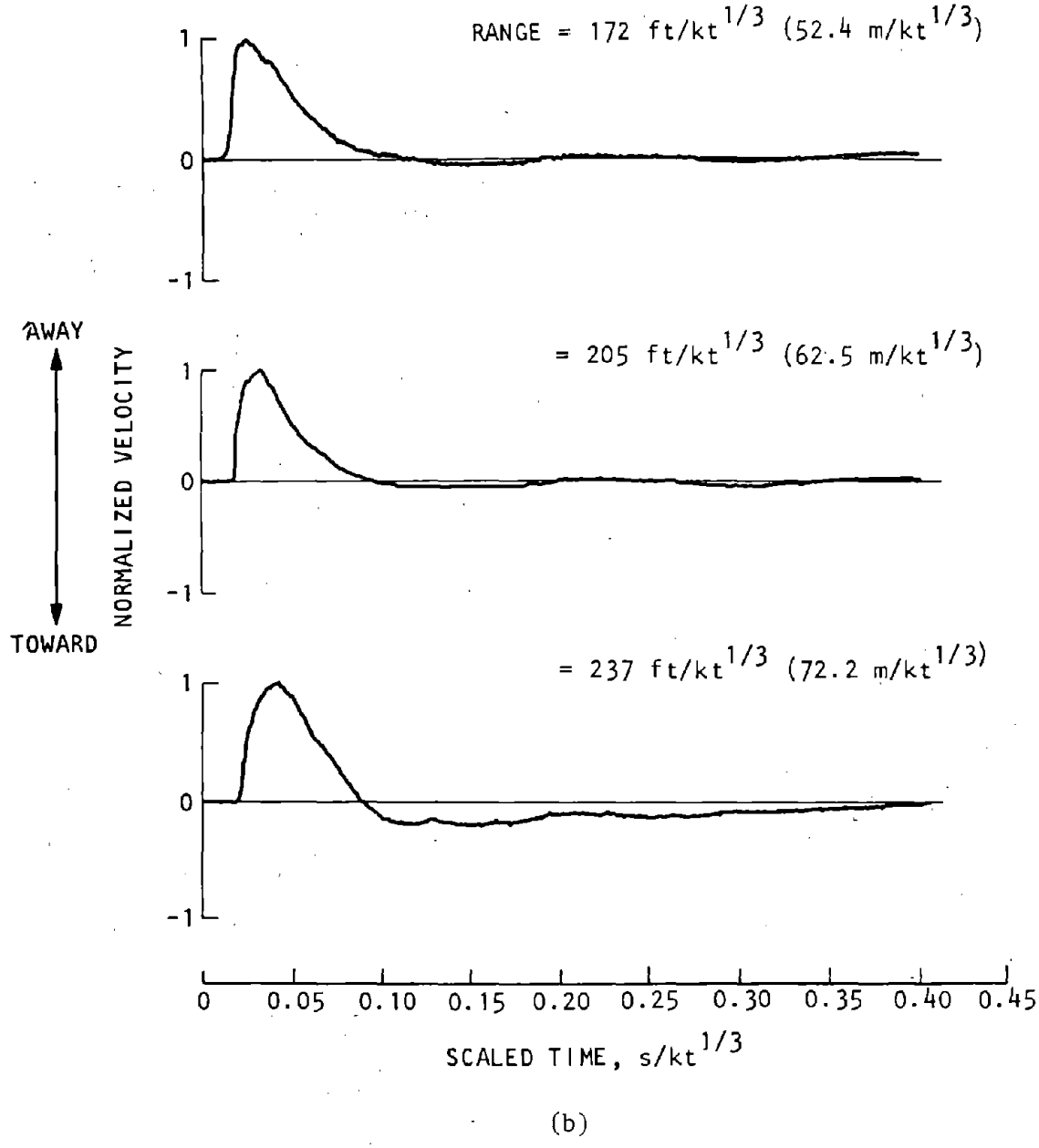

(b)

Figure 8-5. Horizontal Velocity Waveforms for Rock for All Depths (Adapted from Murrell-Carleton, 1973) (2 of 2)

8-6. Outrunning peak ground response.

a. Peak ground acceleration. Peak vertical and horizontal outrunning accelerations (adapted from Sauer, 1964) are given by:

$$a_V = \frac{k_o Z^n}{C_o}(R/W^{1/3})^m \qquad (8\text{–}14a)$$

$$a_H = a_V \qquad (8\text{–}14b)$$

where

a_V = Vertical acceleration, g's
a_H = Horizontal acceleration, g's
R = Range, ft
W = Yield, kt
Z = Depth, ft
C_o = Seismic velocity, ft/s
k_o, n, m are constants

b. Peak ground velocity. Equations for the calculation of peak vertical and horizontal oscillating outrunning particle velocities designated as u_m and applicable at all near-surface depths of interest in design can be represented by the equation

$$u_m = C\,(R/W^{1/3})^r \qquad (8\text{–}15)$$

where

u_m = Peak oscillatory outrunning velocity, ft/s

c. Peak ground displacements. Peak vertical and horizontal out-running displacements for all near-surface depths (adapted from Sauer, 1964) are given by

$$\delta_V W^{1/3} = D(R/W^{1/3})^s \qquad (8\text{–}16a)$$

$$\delta_H = \delta_V \qquad (8\text{–}16b)$$

where

δ_V = Vertical displacement, in.
δ_H = Horizontal displacement, in.
D, s are constants

d. Mean peak ground response. Equations 8–14 and 8–16 may be evaluated for their mean values from the quantities:

$$k_o = \begin{cases} 3 \times 10^{14} \\ 3.75 \times 10^{15} \\ 1.5 \times 10^{10} \\ 1.88 \times 10^{11} \end{cases} \qquad n = \begin{cases} -0.44 \\ -1.35 \\ -0.44 \\ -1.35 \end{cases}$$

$$m = \begin{cases} -3.5, & 150 \leq R/W^{1/3} \leq 800, & 1 \leq Z \leq 16 \\ -3.5, & 150 \leq R/W^{1/3} \leq 800, & Z > 16 \\ -2.0, & 800 < R/W^{1/3} \leq 3000, & 1 \leq Z \leq 16 \\ -2.0, & 800 < R/W^{1/3} \leq 3000, & Z > 16 \end{cases}$$

D = 6400
s = –1.98

The mean peak values for the parameters in equation 8–15 are presented in table 8–2 (Higgins, 1975). For convenience, the data in table 8–2 are cross referenced to the appropriate figure (Higgins, 1975). The ratio of the initial peak, u_1, to the oscillatory peak, u_m, is presented in figure 8–6 as a function of scaled range.

e. Uncertainty of peak acceleration. The uncertainties of equation 8–14 for peak outrunning accelerations are:

$$\Omega^2_{a_V} = \Omega^2_f + \Omega^2_{C_o} + n^2\Omega^2_Z + m^2\Omega^2_R + \frac{m^2}{9}\Omega^2_W \qquad (8\text{–}17a)$$

$$\Omega_{a_H} = \Omega_{a_V} \qquad (8\text{–}17b)$$

where $\Omega_f \approx 0.8$.

f. Uncertainty of peak velocity. The uncertainty associated with the amplitude of the oscillatory component of the vertical outrunning ground shock or for the maximum horizontal motion for contact or near-surface bursts is

$$\Omega^2_{u_m} = \Omega^2_g + r^2\Omega^2_R + \frac{r^2}{9}\Omega^2_W \qquad (8\text{–}18)$$

where Ω_g is the uncertainty of equation 8–15. The values of Ω_g are presented in table 8–2 in which the data scatter in (Higgins, 1975) is assumed to be log-normally distributed. The uncertainty, Ω_{u_1}, of the initial peak vertical velocity u_1 (depicted in figure 8–7) is given by

$$\Omega^2_{u_1} = \Omega^2_h + r^2\Omega^2_R + \frac{r^2}{9}\Omega^2_W \qquad (8\text{–}19)$$

where the values of Ω_h are presented in table 8–3 from data presented in (Higgins, 1975).

g. Uncertainty of peak displacement. The uncertainties of the displacements in equations 8–16 are

$$\Omega^2_{\delta_V} = \Omega^2_k + s^2\Omega^2_R + \frac{(1-s)^2}{9}\Omega^2_W \qquad (8\text{–}20a)$$

$$\Omega_{\delta_H} = \Omega_{\delta_V} \qquad (8\text{–}20b)$$

where $\Omega_k \approx 0.6$.

Table 8-2. Values of Parameters for Calculating Outrunning Mean Ground Shock Velocity and Associated Uncertainties (Adapted from Higgins, 1975)

Direction	Material	Coefficient C	Exponent r	Higgins Figure No. in 1975 Reference	Uncertainty Ω_{g_i}
Vertical u_m	Wet clay/shale	1.33×10^3	-1.2	32	0.36
	Dry clay/shale	3.91×10^2	-1.05	34	0.60
	Sand/sandstone	3.91×10^2	-1.05	35	0.48
	Tonalite	1.15×10^3	-1.2	33	0.60
	Clay	3.08×10^3	-1.35	36	0.40
Horizontal u_m	Wet clay/shale	5.41×10^4	-1.8	50	0.60
	Dry clay/shale	2.57×10^4	-1.65	52	0.30
	Sand/sandstone	2.79×10^5	-1.95	53	0.36
	Tonalite	2.69×10^4	-1.7	51	0.50
	Clay	5.66×10^3	-1.4	54	0.36

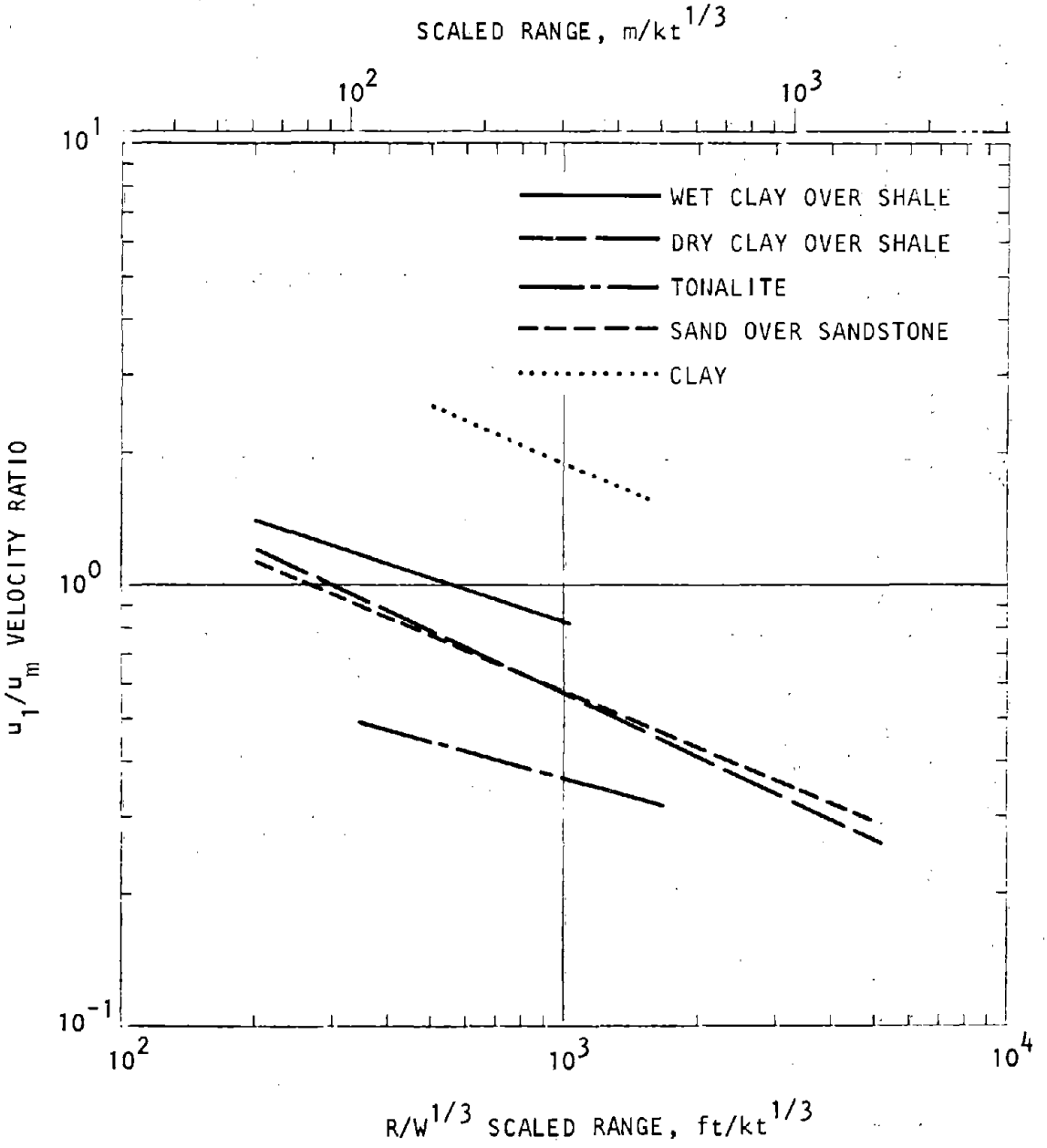

Figure 8–6. Ratios of Initial to Oscillatory Peak Particle Velocities

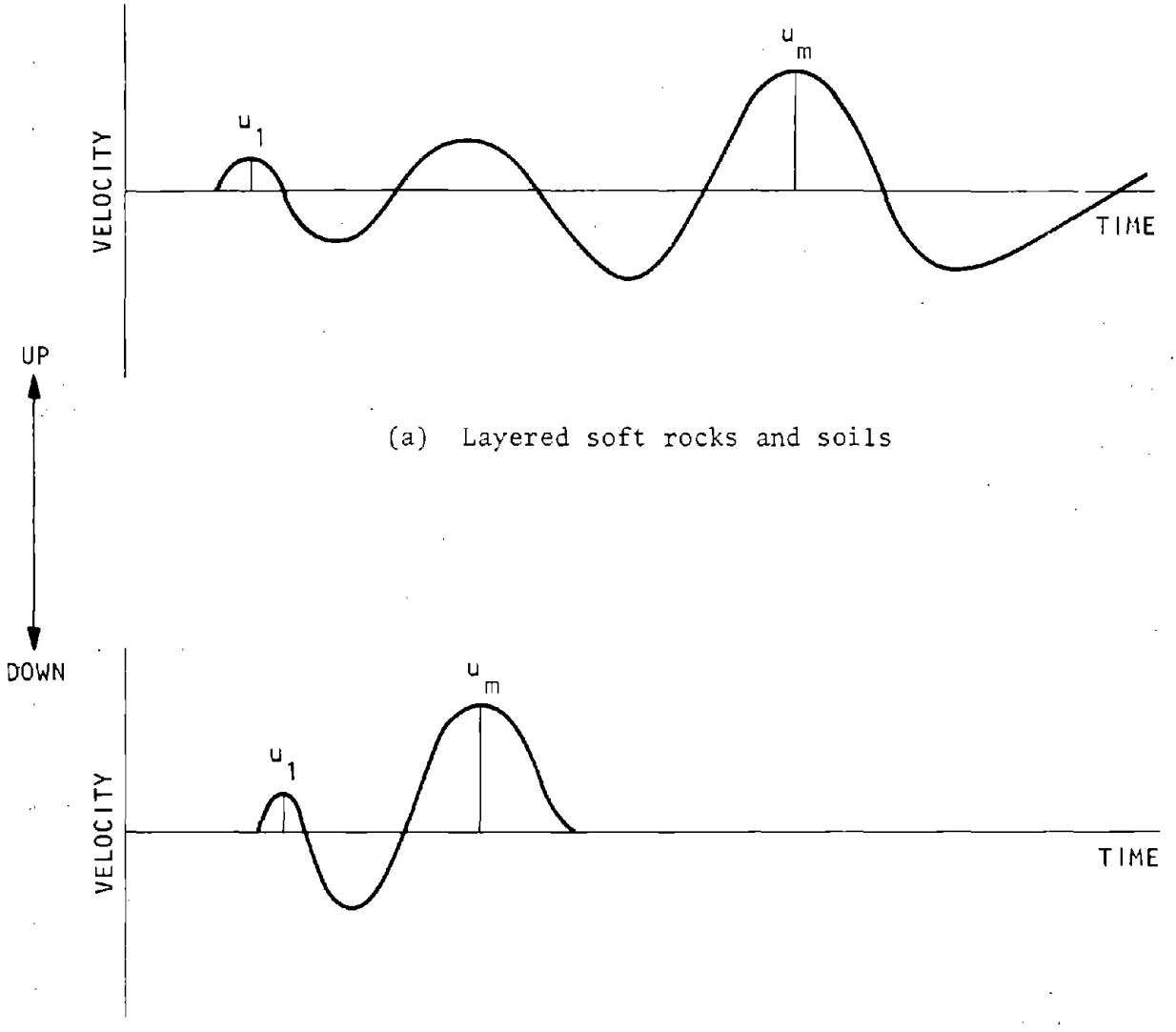

(a) Layered soft rocks and soils

(b) Homogeneous rocks and soils

Figure 8-7. Characteristic Vertical Outrunning Waveforms (Adapted from Higgins, 1975)

Table 8-3. Uncertainties of the Initial Peak Velocity

Geology	Uncertainty Ω_h
Wet clay over shale	0.18
Dry clay over shale	0.37
Sand over sandstone	0.32
Tonalite	0.33
Clay	0.16

U.S. Army Corps of Engineers

8-7. Outrunning waveforms.

a. Velocity. Outrunning is a complicated phenomenon that is not easily described by simple waveforms. Nevertheless, over the years, certain waveform characteristics have been identified that describe the principal elements of the velocity signature. The reader will be required to adapt the signatures recommended below to the amplitudes presented in paragraph 8-6.

b. Vertical. Figure 8-7(a) presents the recommended waveform for vertical outrunning motion in layered soft rock and soil sites. Figure 8-7(b) shows the recommended waveform for homogeneous sites.

c. Horizontal. Horizontal velocity waveforms vary continuously with range, and, near the crater, with depth as well. Composite waveforms in figure 8-7 are more difficult to develop. Figure 8-8 presents typical waveforms for wet and dry clays over shale, and sands over sandstones. These data are presented for three crater-volume scale ranges based on apparent crater volumes. Refer to (Higgins, 1975) for definition of time scales. The reader may also obtain some guidance from paragraph 8-5*a* on how outrunning develops. Consult chapter 12 for the computation of crater volumes.

8-8. Height of burst effects.

a. Correction factors. Detonation at positive heights of burst will alter overpressure and initial coupling of energy to the ground, hence the airblast-induced ground shock in the superseismic region. To a first approximation, HOB-corrected accelerations and velocities can be obtained by applying HOB peak overpressure correction factors; displacements can be modified by applying the HOB-correction factors for the overpressure positive-phase impulse.

b. Velocity, acceleration, and stress. The velocity, acceleration, and stress amplitudes characterized in equations 8-1, 8-2, 8-5, and 8-10 must be adjusted for HOB effects. At any scaled range in these equations, the ratio of the overpressure at the appropriate scaled HOB to the overpressure for a contact burst from chapter 7 establishes a correction factor used to adjust the peak velocity, acceleration, and stress. Thus,

$$a_{(HOB)} = \frac{P_{so(HOB)}}{P_{so(o)}} a_{(o)} \qquad (8\text{-}21)$$

where

$a_{(HOB)}$ = Acceleration for a particular HOB and range
$P_{so(HOB)}$ = Overpressure at that same HOB and range, from chapter 7
$P_{so(o)}$ = Overpressure at that same range for a contact burst, from chapter 7
$a_{(o)}$ = Acceleration at that same range for a contact burst, from equation 8-1.

and

$$u_{(HOB)} = \frac{P_{so(HOB)}}{P_{so(o)}} u_{(o)} \qquad (8\text{-}22)$$

$$\sigma_{(HOB)} = \frac{P_{so(HOB)}}{P_{so(o)}} \sigma_{(o)} \qquad (8\text{-}23)$$

where

$u_{(HOB)}$, $\sigma_{(HOB)}$ = Velocity and stress for a particular HOB
$u_{(o)}$, $\sigma_{(o)}$ = Velocity and stress at that same range for a contact burst using equations 8-2, 8-5, and 8-10

c. Displacement. The peak displacement data of equations 8-3 and 8-11 also must be adjusted for HOB effects. At any scaled range in these equations,

the ratio of the impulse at the appropriate scaled HOB to the impulse for a contact burst establishes a factor that is to be used to adjust the peak displacement. Thus,

$$d_{(HOB)} = \frac{I_{(HOB)}}{I_{(o)}} d_{(o)} \qquad (8\text{–}24)$$

where

$d_{(HOB)}$ = Displacement at a particular HOB and range

$I_{(HOB)}$ = Impulse at that same HOB and range, from chapter 7

$I_{(o)}$ = Impulse at that same range for a contact burst, from chapter 7

$d_{(o)}$ = Displacement at that same range for a contact burst, from equations 8–3 and 8–11

The ratio of $I_{(HOB)}/I_{(o)}$ as a function of range and HOB is presented in table 8–4.

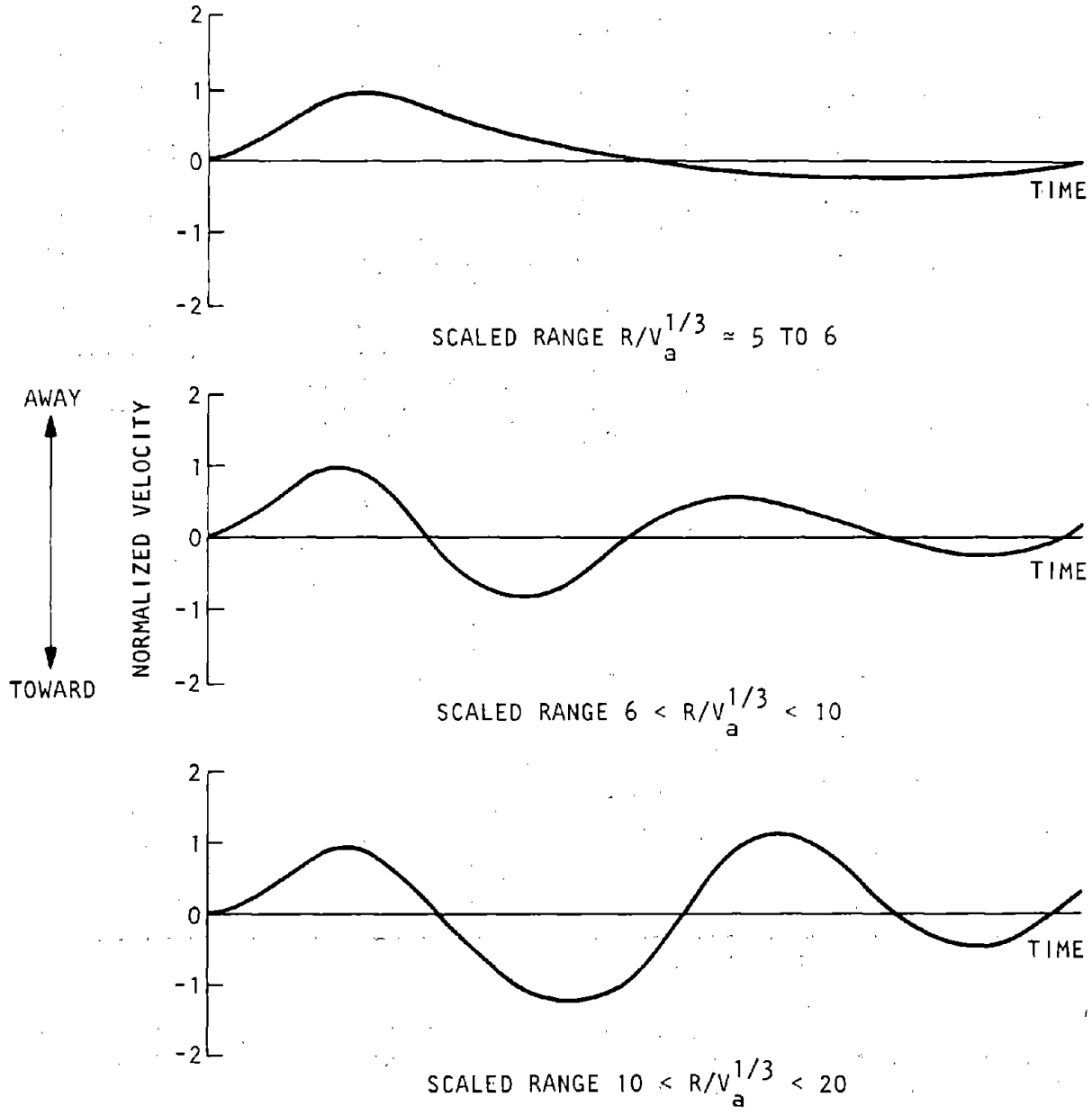

Figure 8–8. Normalized Horizontal Velocities for Clay over Shale and Sand over Sandstone Sites (Adapted from Higgins, 1975)

Table 8–4. Impulse $I_{(HOB}/I_{(o)}$ for Displacement Computation

Scaled Range ft/kt$^{1/3}$ (m/kt$^{1/3}$)	HOB ft/kt$^{1/3}$ (m/kt$^{1/3}$)		
	200(61)	400(122)	600(188)
	Near-Ideal Surface		
300 (91)	1.2	1.1	1.4
400 (122)	1.3	1.0	1.1
600 (183)	1.2	1.0	1.0
800 (244)	1.2	1.1	1.0
1000 (305)	1.1	1.0	1.0
1250 (381)	1.1	1.0	1.0
1500 (457)	1.0	1.0	1.0
2000 (610)	1.1	1.0	1.0
	Nonideal Surface		
300 (91)	0.8	0.8	-
400 (122)	1.0	1.1	1.1
600 (183)	1.0	1.2	1.2
800 (244)	1.0	1.2	1.2
1000 (305)	1.0	1.2	1.2
1250 (381)	1.0	1.1	1.1
1500 (457)	1.0	1.1	1.1
2000 (610)	0.9	1.0	1.0
2500 (762)	0.9	1.0	1.0

U.S. Army Corps of Engineers

d. Uncertainty. For all practical purposes, the uncertainties associated with acceleration, velocity, and displacement are equivalent to those established for contact bursts, as defined in paragraphs 8–3*f, g, h* for soils, and paragraph 8–4*e* for rock.

CHAPTER 9
CRATER-INDUCED GROUND SHOCK

9-1. Gross phenomenology.

a. Direct coupling of weapon energy from near-surface, contact, and shallow underground bursts drives shock waves through the ground and leads to crater formation. The relative importance of airblast-induced signals, unloading signals from the ground surface, and signals resulting from crater formation depends on the location of the facility relative to ground zero (GZ). As shown in figure 9-1, the region between 45 deg (0.79 rad) and 30 deg (0.52 rad) is influenced by composite signals of both airblast-induced and crater-induced shock waves. In the central conical region below depression angles of ~45 deg, crater-induced signals are dominant and are the subject of this chapter.

b. The basic variables affecting the intensity and duration of the crater-induced ground shock are:

- Weapon design
- Weapon yield
- Burst elevation or burial
- Properties of the site media (rock, soil)
- Slant range to the facility (or any other point of interest)

c. Crater-induced ground shock can be predicted from (1) mathematical simulation, (2) scaling and extrapolation of near-surface burst data, and (3) scaling and extrapolation of fully contained burst data. Method 3 currently offers the most credible basis for estimating the crater-induced ground shock environment and its uncertainty. In this method, underground nuclear ground-shock environments from near-surface (contact or shallow-buried) nuclear bursts are estimated from the ground-shock data of fully contained bursts. The regions for which these data apply include the crater-induced region in figure 9-1 and, with some reservations, the composite region as well.

d. Of importance to design of facilities are ground-shock intensity and time histories and their pulse shape. These features are delineated in paragraphs 9-2 and 9-3.

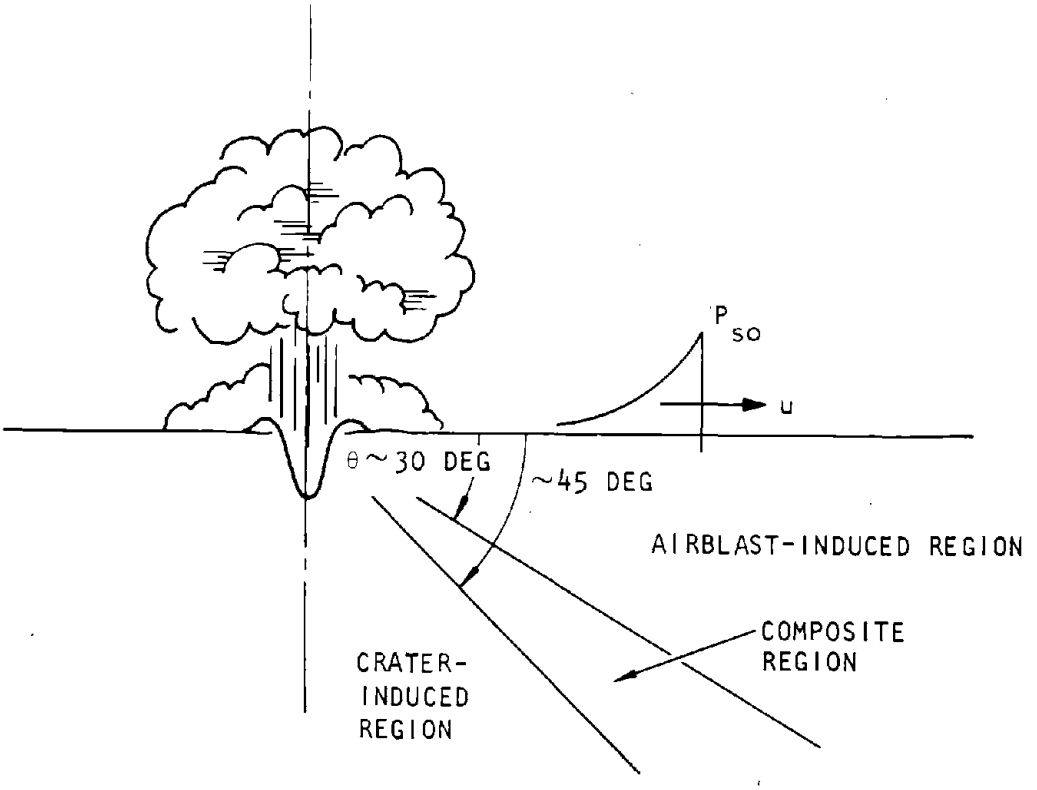

U.S. Army Corps of Engineers

Figure 9-1. Regions of Ground Shock

9-2. Ground-shock intensity.

a. Decay curves for peak acceleration, velocity, and displacement are presented in the general form (Perret-Bass, 1975).

$$aW_e^{1/3} = C_a \left(\frac{R}{W_e^{1/3}}\right)^{n_a} \quad (9\text{-}1a)$$

$$u = C_u \left(\frac{R}{W_e^{1/3}}\right)^{n_u} \quad (9\text{-}1b)$$

$$\delta W_e^{1/3} = C_\delta \left(\frac{R}{W_e^{1/3}}\right)^{n_\delta} \quad (9\text{-}1c)$$

where

a, u, δ = Peak acceleration (g), particle velocity (ft/s), displacement (in)
C,n = Site geology parameters (see table 9-1)
R = Slant range from GZ (ft)
W_e = Effective weapon yield (kt)

b. In using equations 9-1, which pertain to fully contained bursts, a weapon-yield correction is necessary to convert to the ground-shock response for near-surface bursts. This correction utilizes the equation

$$\frac{W_e}{W} = \left[1 + \alpha\frac{z}{W^{1/3}} + \beta\frac{z^2}{W^{2/3}} + \gamma\frac{z^3}{W} + \xi\frac{z^4}{W^{4/3}} + \ldots\right] \Gamma_m, \frac{z}{W^{1/3}} < 20 \text{ ft/kt}^{1/3} \quad (9\text{-}2)$$

where W_e and W are the effective and true yields in kt; z is depth ($z > 0$) or height of burst in ft; α, β, γ, and ξ are coefficients of HOB/DOB influence and Γ_m accounts for scaling of deep-buried bursts to contact bursts as a function of site material properties and the ground motion parameter of interest.

c. The mean peak of the crater-induced ground shock environment is calculated from equations 9-1 and 9-2, using values of the site-dependent coefficients and exponents presented in table 9-1. The values of the coefficients in equation 9-2 are presented in tables 9-2 and 9-3.

d. The uncertainties associated with the crater-induced ground shock for deeply buried systems are

$$\Omega_a^2 = \Omega_{f_a}^2 + \Omega_{C_a}^2 + \frac{(1+n_a)^2}{9}\Omega_{W_e}^2 + n_a^2\,\Omega_R^2 \quad (9\text{-}3a)$$

$$\Omega_u^2 = \Omega_{f_u}^2 + \Omega_{C_u}^2 + \frac{n_u^2}{9}\Omega_{W_e}^2 + n_u^2\,\Omega_R^2 \quad (9\text{-}3b)$$

$$\Omega_\delta^2 = \Omega_{f_\delta}^2 + \Omega_{C_\delta}^2 + \frac{(1-n_\delta)^2}{9}\Omega_{W_e}^2 + n_\delta^2\,\Omega_R^2 \quad (9\text{-}3c)$$

where Ω_f are the uncertainties of the functional forms of the decay laws, Ω_C are the uncertainties of the coefficients, and so forth. Assume $\Omega_f \approx 0.05$ and compute Ω_{C_a} from equation 2-18 where L_2 and L_1 are the upper and lower bounds on the data at any given slant range in figures 9-2 through 9-5. Similarly, compute Ω_{C_u} and Ω_{C_δ} from figures 9-6 through 9-9, and 9-10 through 9-13, respectively. Assume n = 1.65.

e. The uncertainties associated with the yield correction presented in equation 9-2 are

$$\Omega_{W_e}^2 = \Omega_f^2 + \frac{\Gamma_m^2}{W_e^2}\Big\{W^2\Big[1 + 2\alpha z/3W^{1/3} + \beta z^2/3W^{2/3} - \xi z^4/3W^{4/3}\Big]^2\Omega_W^2 + z^2\Big[\alpha^2W^{4/3} + \beta^2z^2W^{2/3} + \gamma^2z^4 + \xi^2z^6W^{-2/3}\Big]^2\Omega_C^2 + z^2\Big[\alpha W^{2/3} + 2\beta zW^{1/3} + 3\gamma z^2 + 4\xi z^3/W^{1/3}\Big]^2\Omega_z^2\Big\} + \Omega_{\Gamma_m}^2 \quad (9\text{-}4)$$

where Ω_f is the uncertainty of equation 9-2, Ω_W is the uncertainty in the yield, Ω_C are the uncertainties of the coefficients, and so forth. Assume $\Omega_f = \Omega_C = \Omega_{\Gamma_m} \approx 0.2$.

Table 9-1. Mean Values of Parameters for Calculations of Direct-Induced Ground Motion (equation 9-1)

Parameter	Geology	Coefficient C_a	Exponent n_a	Range ft/kt$^{1/3}$	Range (m/kt$^{1/3}$)
$aW_e^{1/3}$ (g·k$^{1/3}$ Eq. (9-1a)	Alluvium	2.15×10^{14}	-5.78	66-262	(20-80)
	Alluvium	6.02×10^{5}	-2.13	197-1148	(60-350)
	Dry tuff	1.42×10^{13}	-4.77	131-492	(40-150)
	Dry tuff	7.55×10^{5}	-1.92	328-1641	(100-500)
	Wet tuff	9.58×10^{8}	-2.61	98-1969	(30-600)
	Hard rock	1.09×10^{13}	-4.35	131-656	(40-200)
	Hard rock	1.46×10^{8}	-2.32	295-7218	(90-2200)
		C_u	n_u		
u(ft/s) Eq. (9-1b)	Alluvium	2.91×10^{9}	-3.27	98-492	(30-150)
	Alluvium	6.03×10^{3}	-1.16	328-1148	(100-350)
	Dry tuff	7.66×10^{6}	-1.98	131-1641	(40-500)
	Wet tuff	1.66×10^{6}	-1.56	98-1969	(30-600)
	Hard rock	5.50×10^{6}	-1.72	131-7218	(40-2200)
		C_δ	n_δ		
$\delta/W_e^{1/3}$ (in/kt$^{1/3}$) Eq. (9-1c)	Alluvium	5.02×10^{7}	-3.04	131-492	(40-150)
	Alluvium	3.27×10^{2}	-1.11	328-1148	(100-350)
	Dry tuff	2.04×10^{6}	-2.20	328-1641	(100-500)
	Wet tuff	4.39×10^{7}	-2.63	164-1969	(50-600)
	Hard rock	3.20×10^{5}	-1.88	230-7218	(70-2200)

U.S. Army Corps of Engineers

Table 9-2. Factors in Calculating HOB/DOB Effective Yield (equation 9-2)

Coefficient	Value
α	3.39×10^{-2}
β	-3.33×10^{-4}
γ	2.36×10^{-7}
ξ	-1.19×10^{-8}

U.S. Army Corps of Engineers

Table 9-3. Factors Γ_m to Account for Geological Properties (equation 9-2)

Geology	Acceleration and Velocity	Displacement
Alluvium	0.04	0.0025
Tuff	0.04	0.0025
Hard rock	0.04	0.01

U.S. Army Corps of Engineers

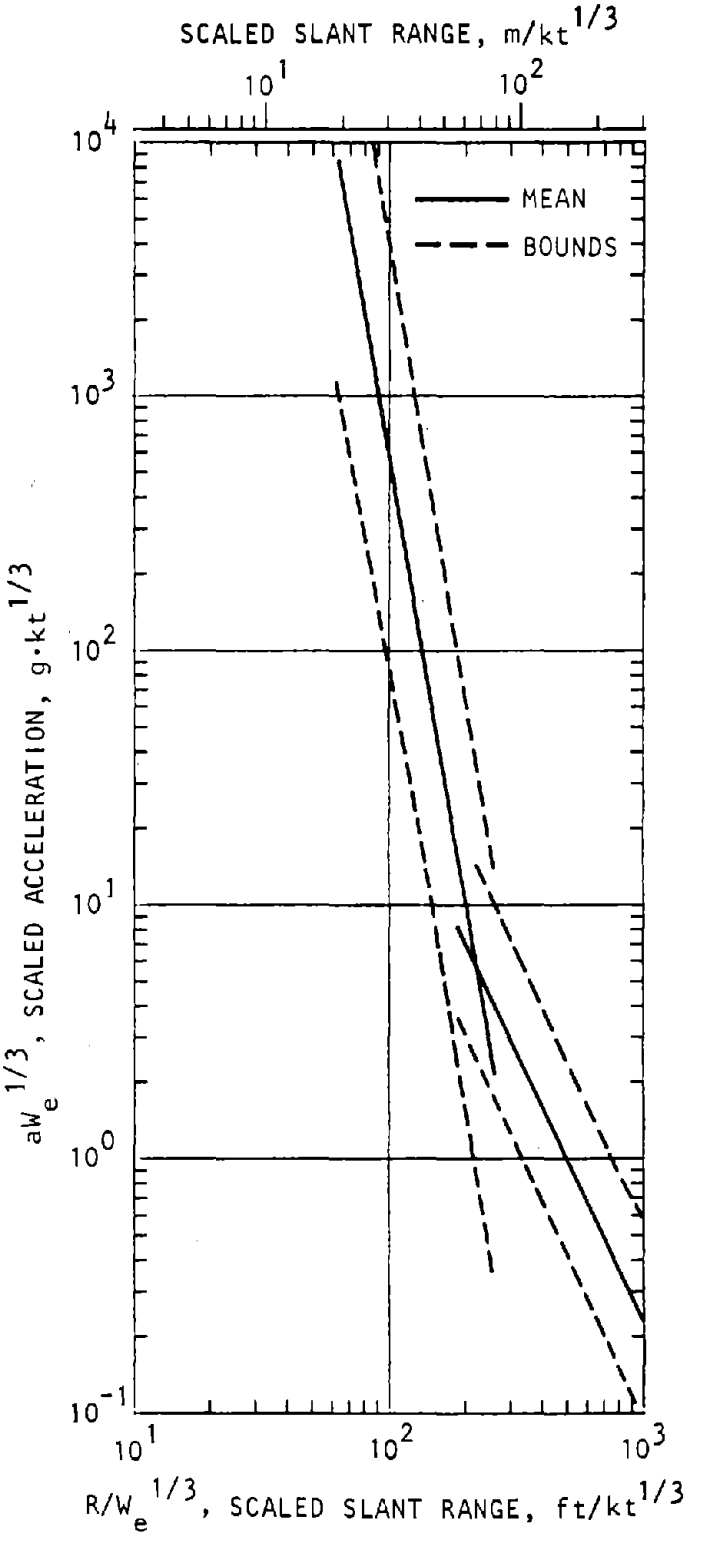

Figure 9-2. Attenuation of Scaled Acceleration—Dry Alluvium (Perret-Bass, 1975)

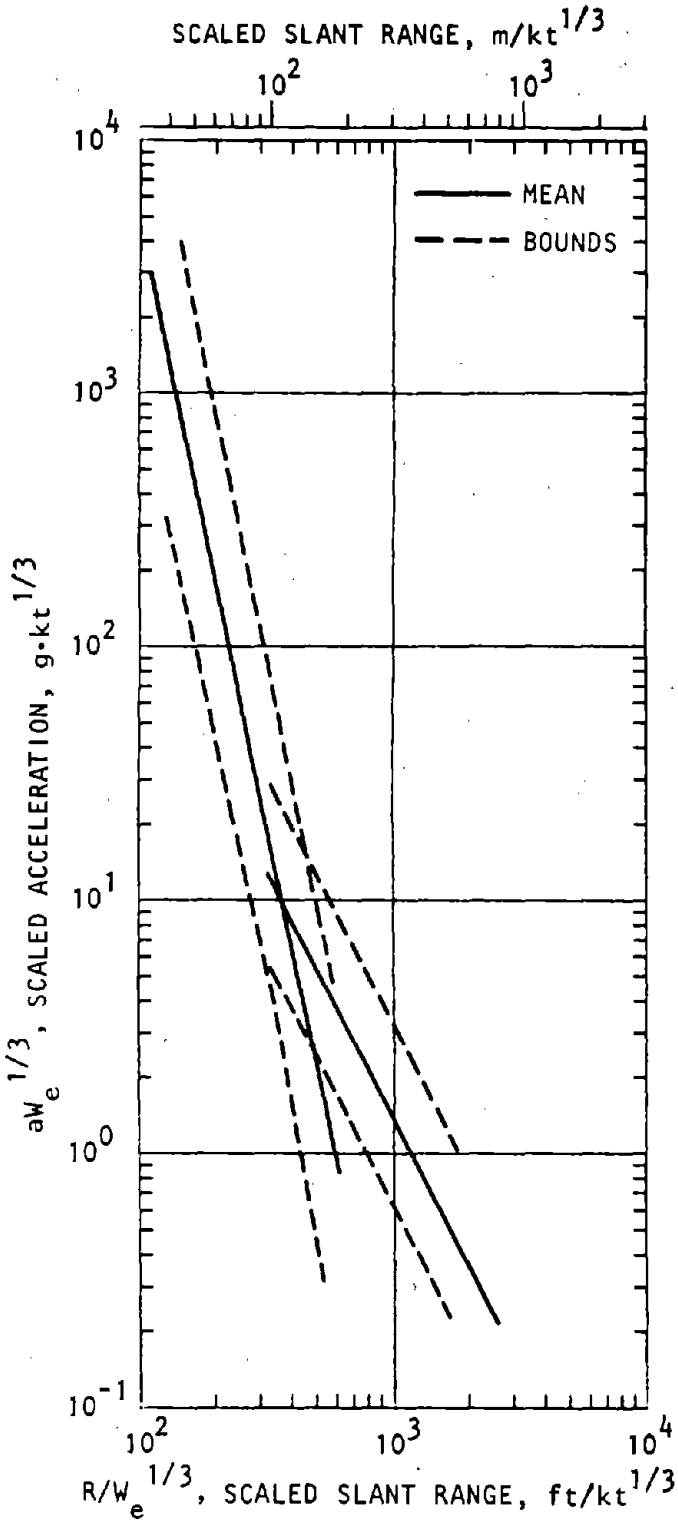

Figure 9-3. Attenuation of Scaled Acceleration—Dry Tuff (Perret-Bass, 1975)

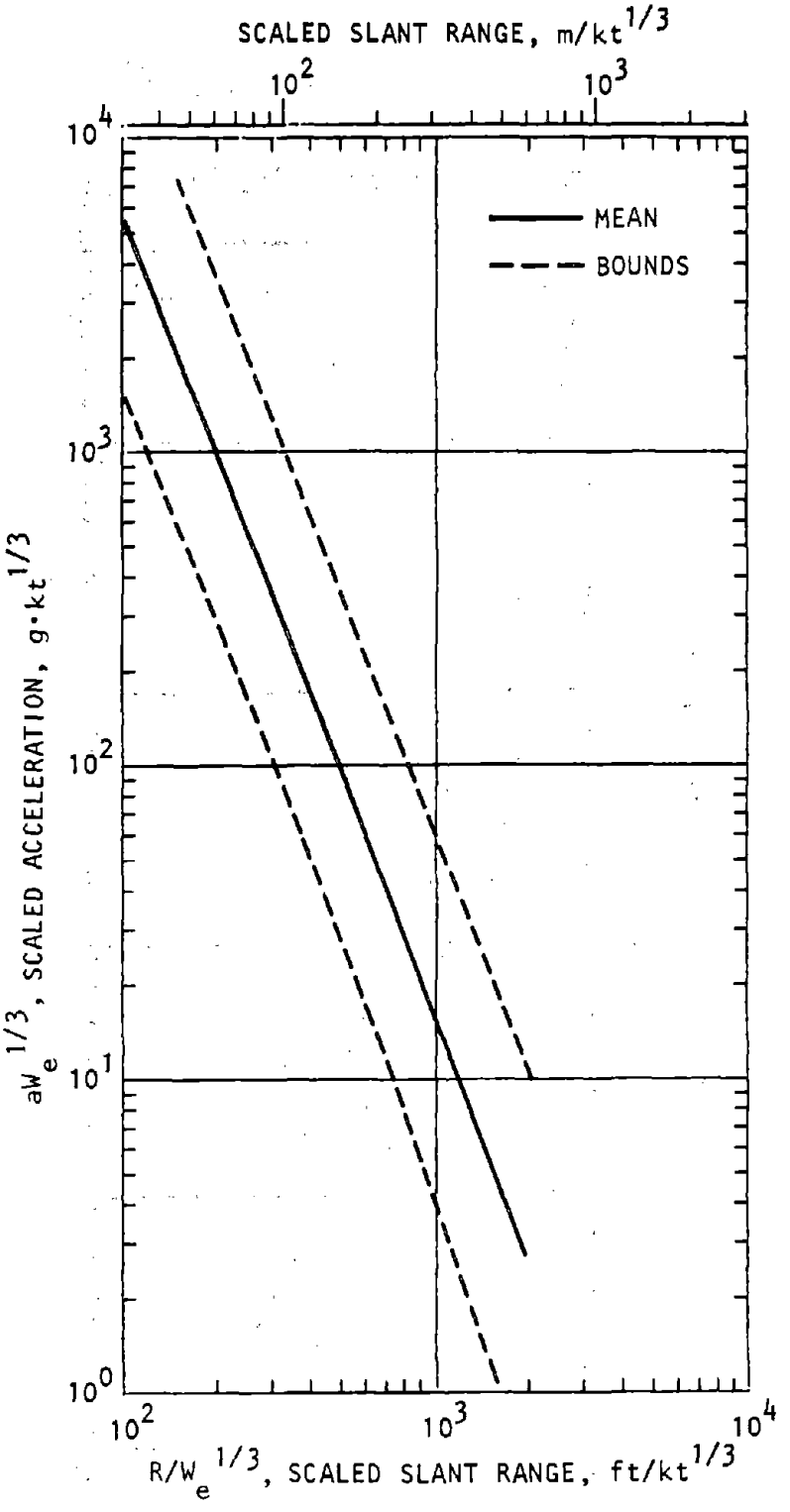

Figure 9–4. Attenuation of Scaled Acceleration—Wet Tuff (Perret-Bass, 1975)

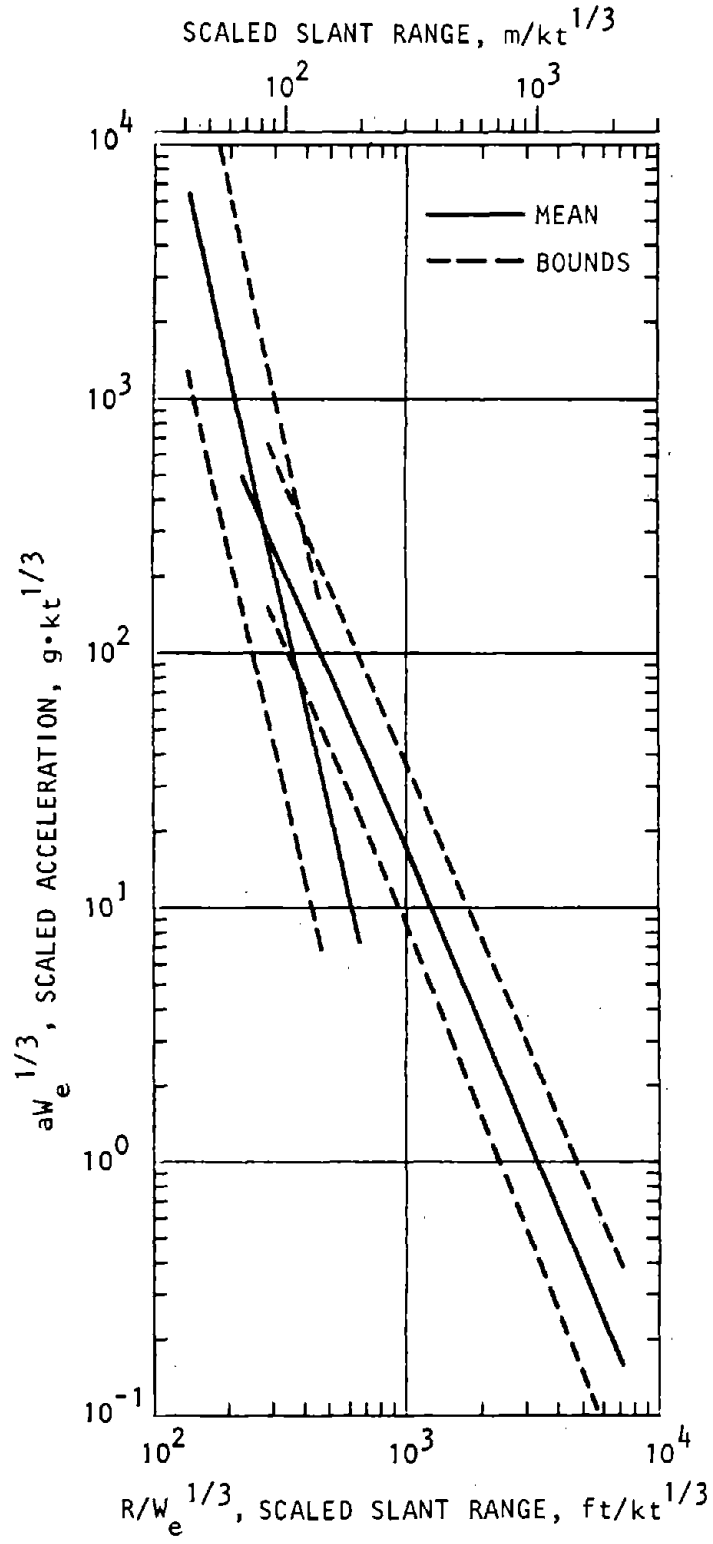

Figure 9–5. Attenuation of Scaled Acceleration—Hard Rock (Perret-Bass, 1975)

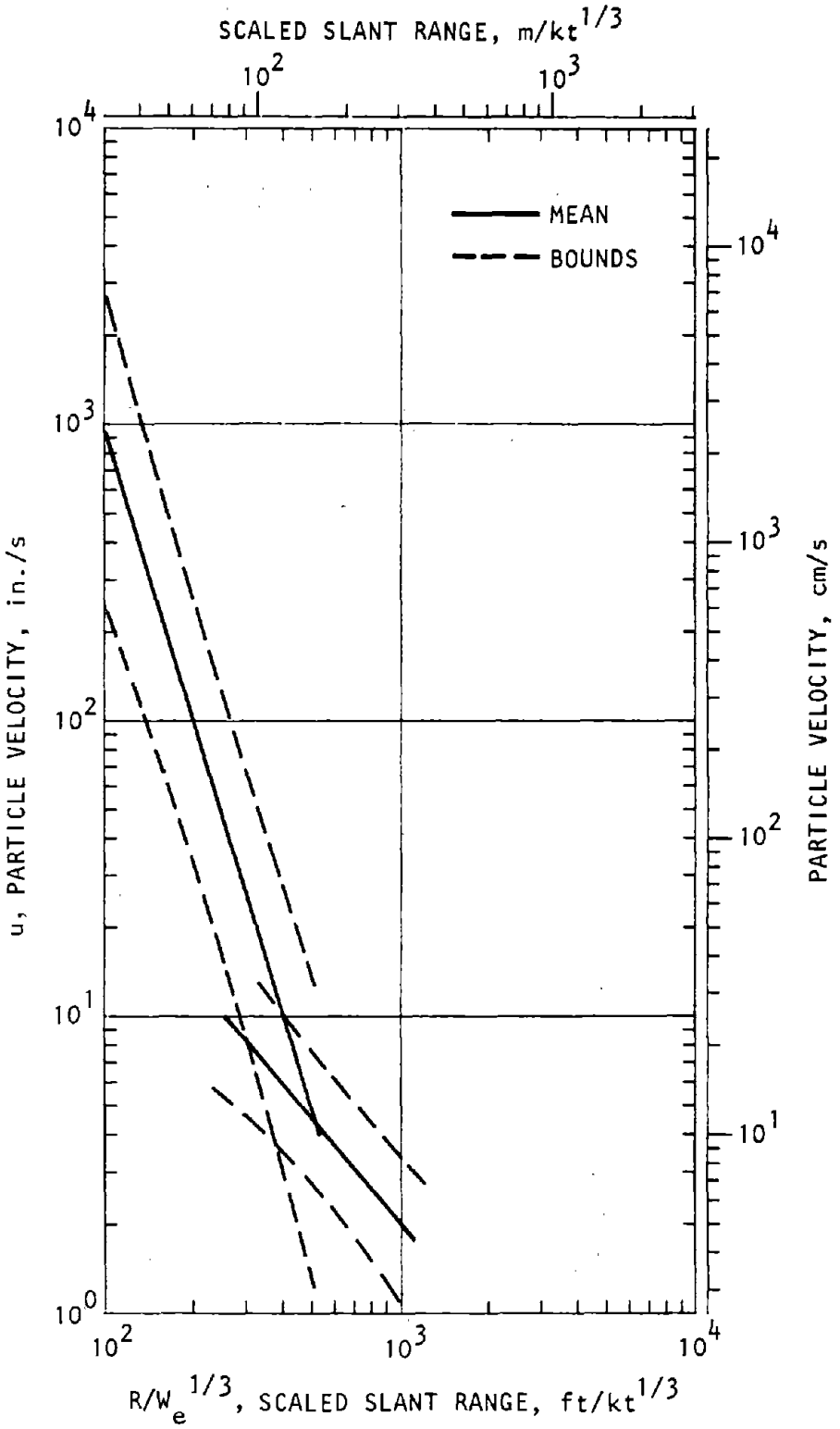

Figure 9–6. Attenuation of Particle Velocity—Dry Alluvium (Perret-Bass, 1975)

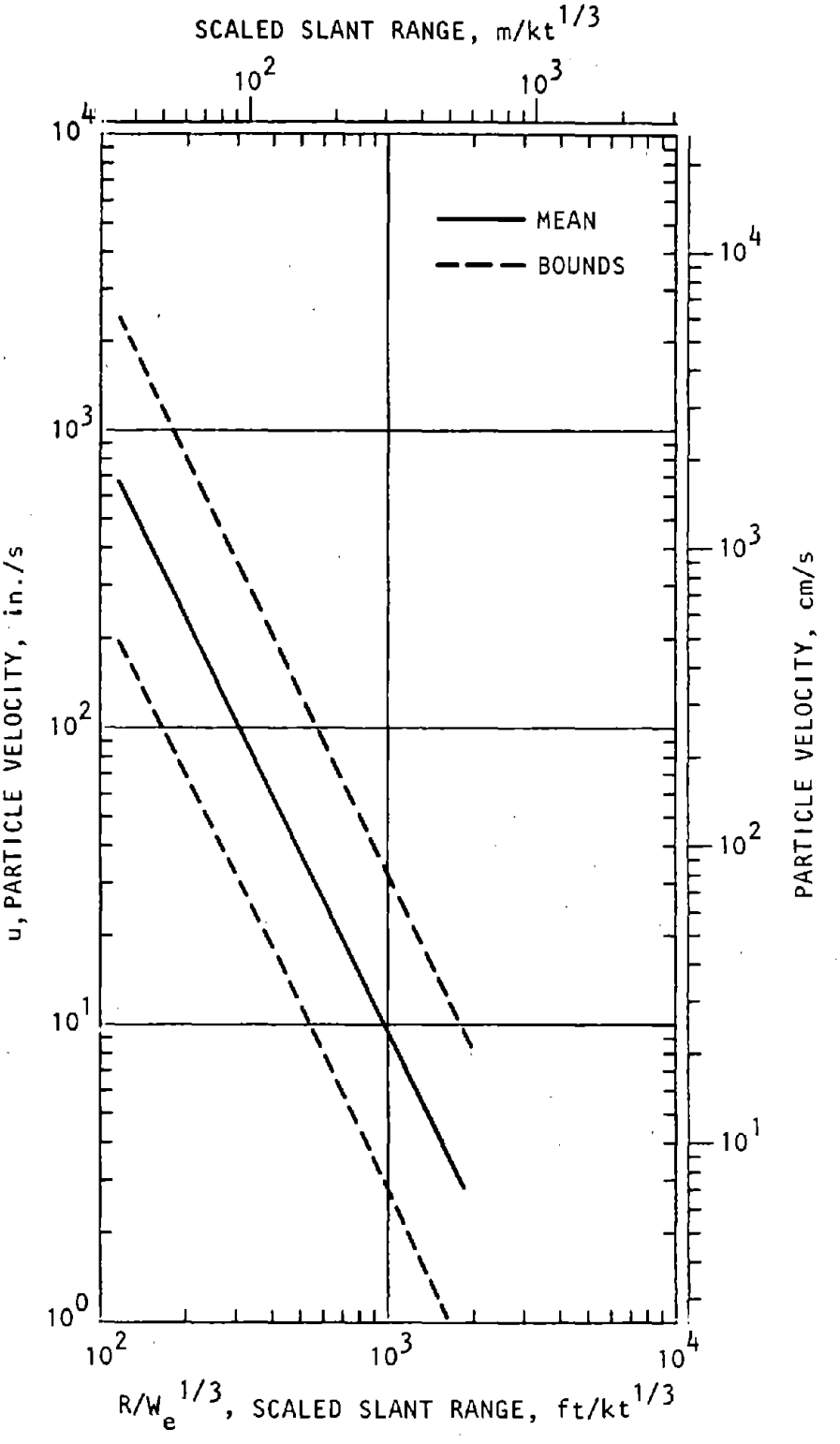

Figure 9–7. Attenuation of Particle Velocity—Dry Tuff (Perret-Bass, 1975)

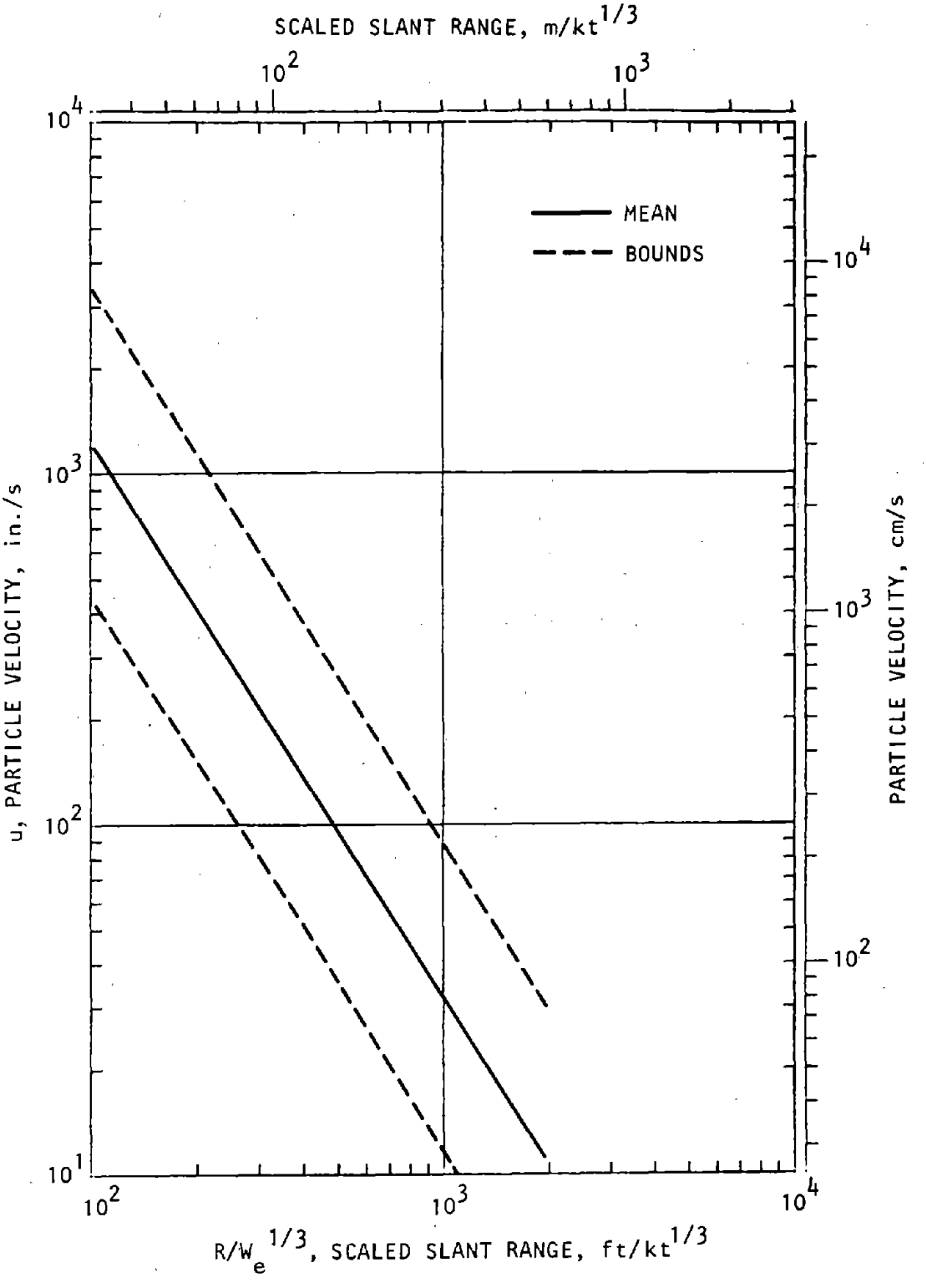

Figure 9–8. Attenuation of Particle Velocity—Wet Tuff (Perret-Bass, 1975)

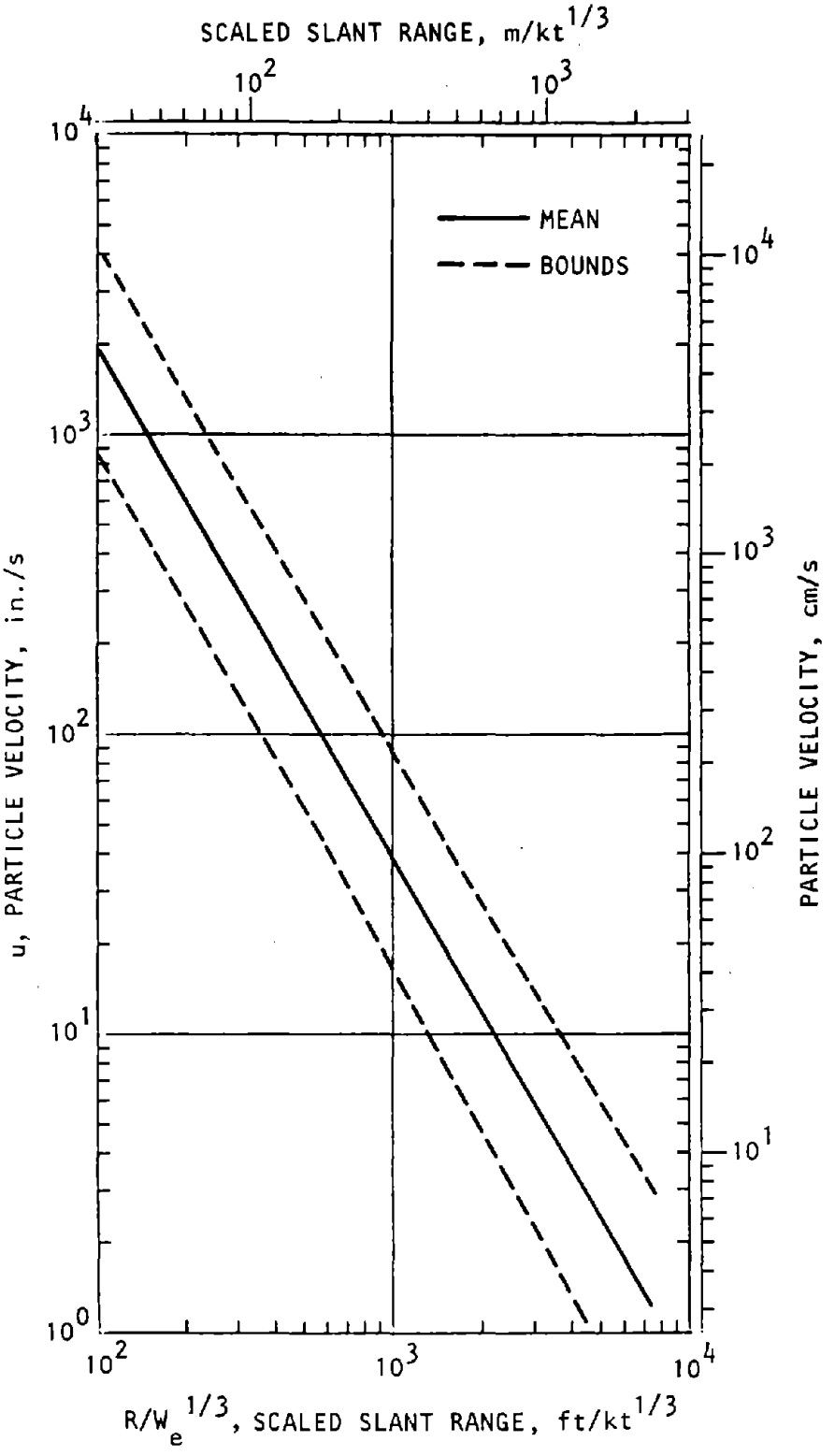

Figure 9–9. Attenuation of Particle Velocity—Hard Rock (Perret-Bass, 1975)

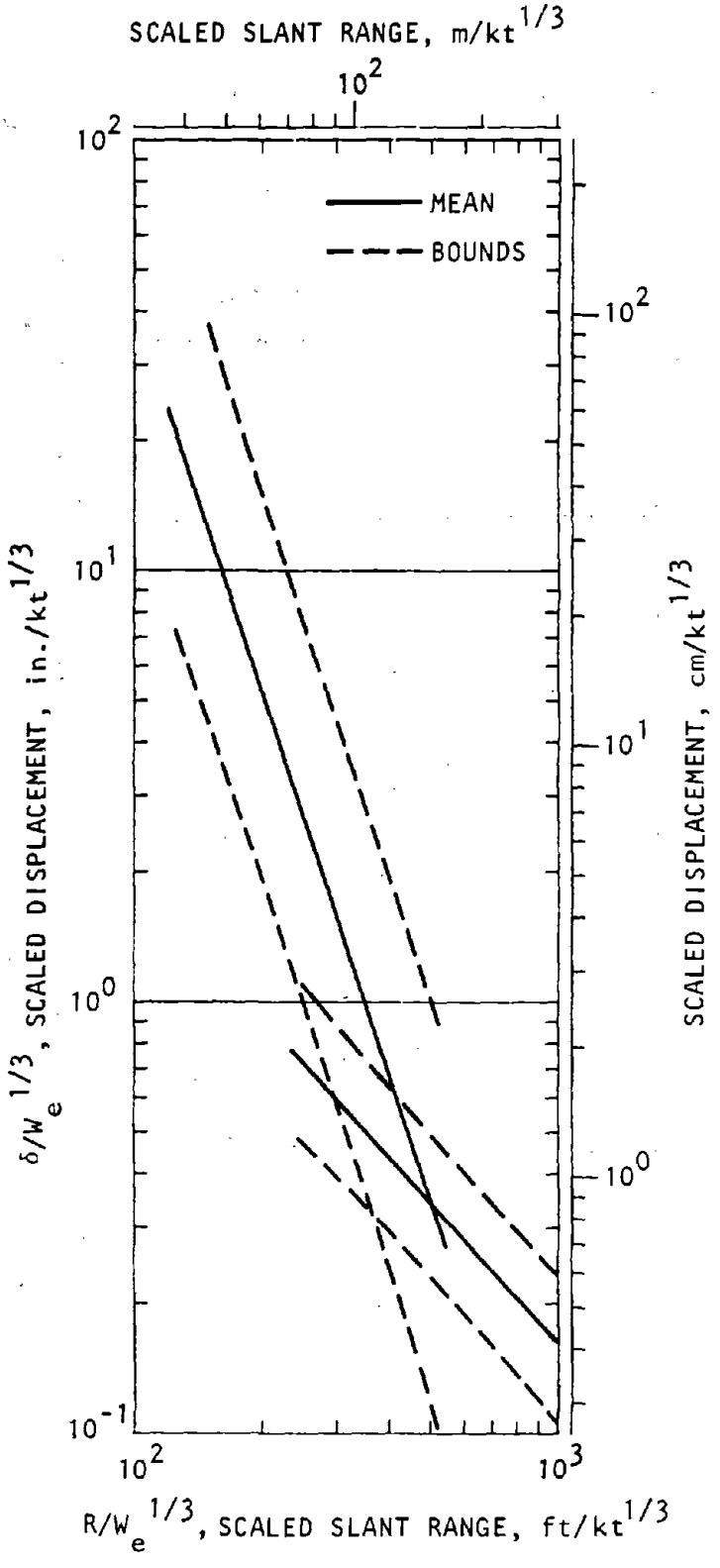

Figure 9-10. Attenuation of Scaled Displacement—Dry Alluvium (Perret-Bass, 1975)

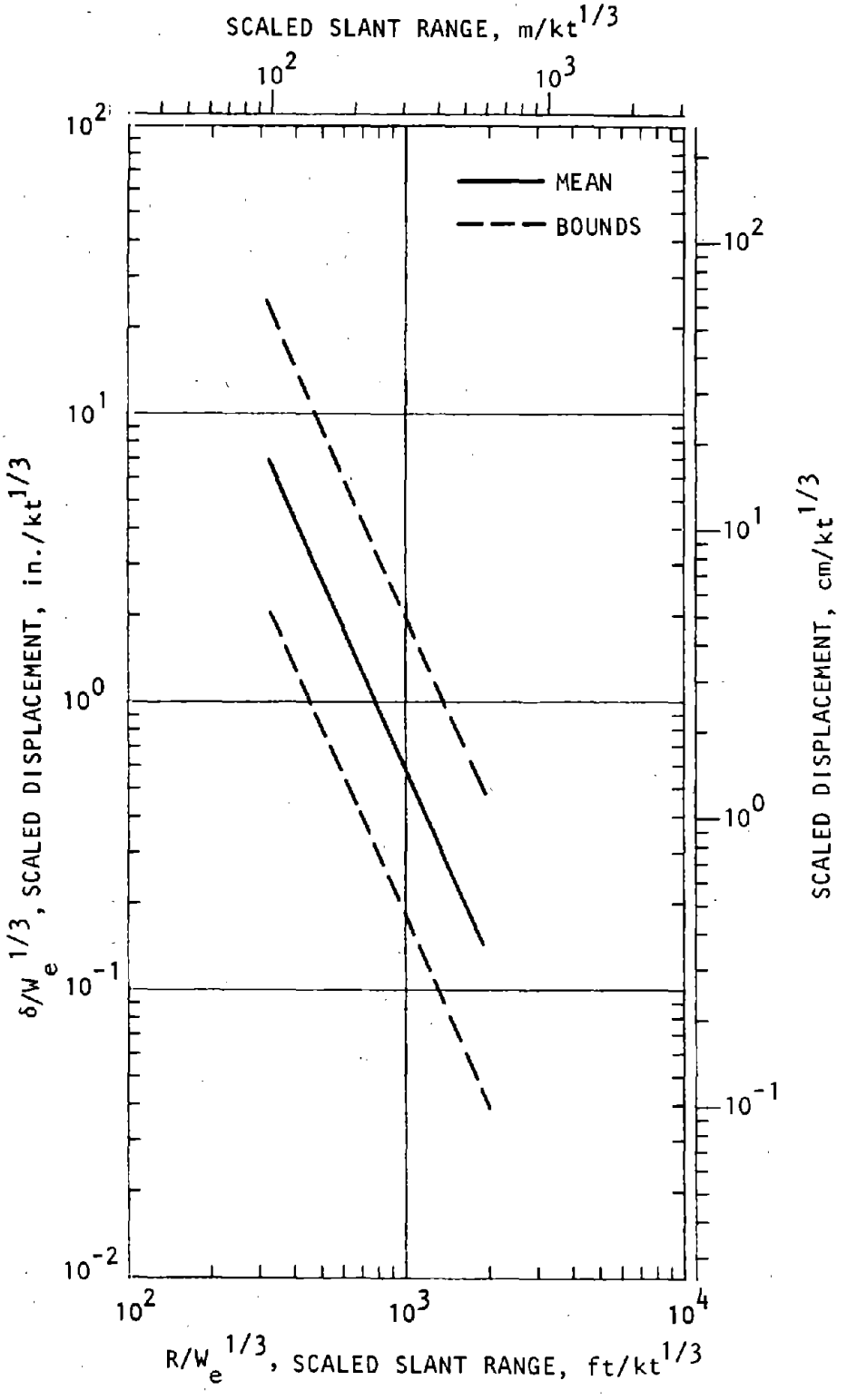

Figure 9–11. Attenuation of Scaled Displacement—Dry Tuff (Perret-Bass, 1975)

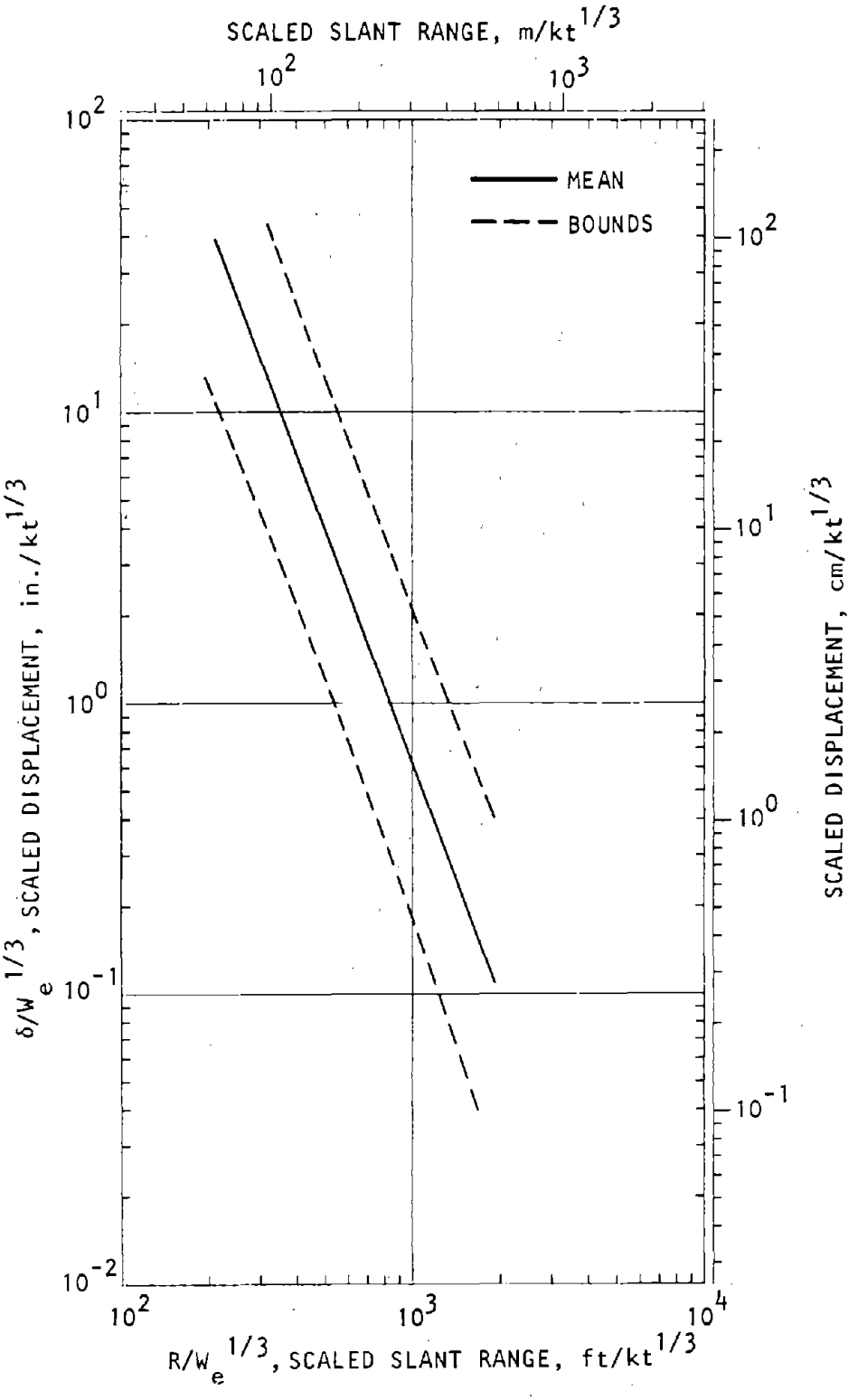

Figure 9-12. Attenuation of Scaled Displacement—Wet Tuff (Perret-Bass, 1975)

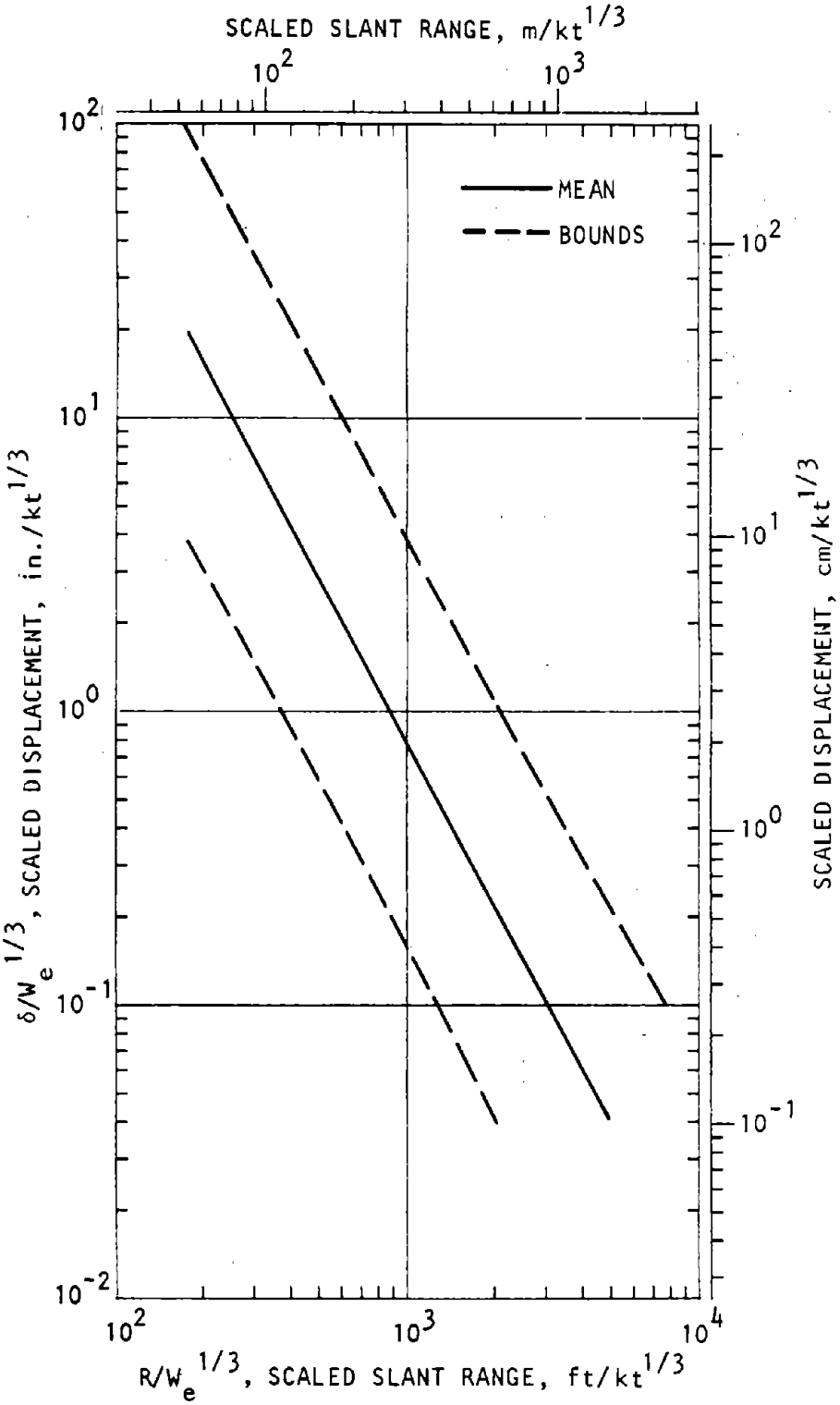

Figure 9-13. Attenuation of Scaled Displacement—Hard Rock (Perret-Bass, 1975)

9-3. Pulse Shapes

a. Ground-shock histories are required for the analysis of some aspects of system survivability. For underground locations that are below a declination angle of 30 deg, it is assumed that particle velocity can be represented by simple triangles, as defined in figure 9-14*a*. The corresponding acceleration and displacement plots are shown in figure 9-14*b* and 9-14*c*. The symbols in the figure are defined as follows:

a = Peak acceleration from equation 9-1a, g
δ = Peak displacement from equation 9-1c, ft
$t_f = 2t_+$, sec
$t_r = \frac{u}{32.2\ a}$ = rise time, sec
t_+ = Positive phase duration = $2\delta/u$, sec
t_- = Negative phase time = $4t_+$, sec
u = Peak velocity from equation 9-1b, ft/sec
u_n = Peak negative velocity = u/m, ft/sec

$$m = \begin{cases} \dfrac{3}{a + b\dfrac{R}{W_e^{1/3}} + c\left(\dfrac{R}{W_e^{1/3}}\right)^2} & \dfrac{R}{W_e^{1/3}} \leq 261 \text{ ft/kt}^{1/3} \\ 3 & \dfrac{R}{W_e^{1/3}} > 261 \text{ ft/kt}^{1/3} \end{cases} \qquad (9\text{-}5)$$

b. The mean pulse shape is derived by utilizing the above relationships and the data in table 9-1. Also utilize

$a = 0.694$
$b = -7.05 \times 10^{-3}$
$c = 3.15 \times 10^{-5}$

c. The uncertainty of a, u, and δ are presented in equation 9-3 and in conjunction with equation 9-4. In addition, assume that

$$\Omega^2_{t_+} = \Omega^2_\delta + \Omega^2_u$$

$$\Omega^2_{t_f} = \Omega^2_{t_+}$$

$$\Omega^2_{t_r} = \Omega^2_u + \Omega^2_a$$

$$\Omega^2_{t_-} = \Omega^2_{t_+}$$

$$\Omega^2_{u_n} = \Omega^2_u + \Omega^2_m$$

$$\Omega_m \approx 0.2 + \Omega^2_R + \frac{1}{9}\Omega^2_{W_e} \qquad (9\text{-}6)$$

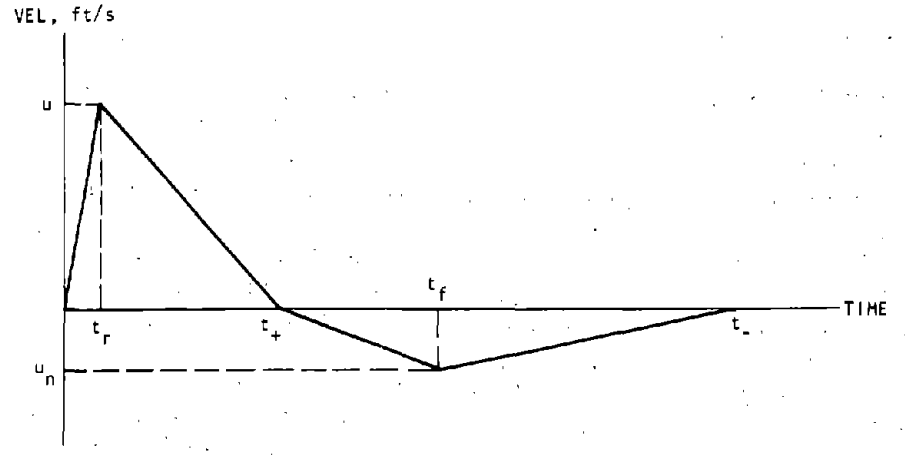

(a) Velocity

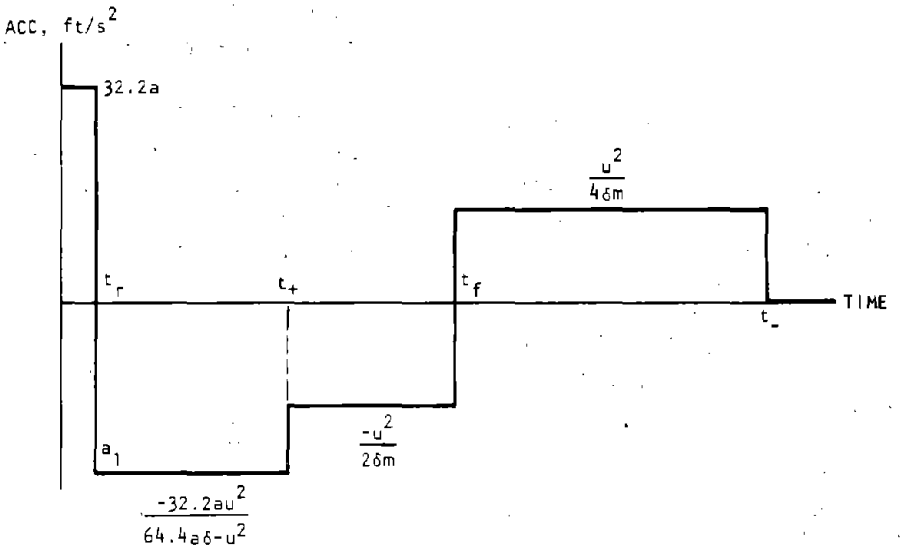

(b) Acceleration

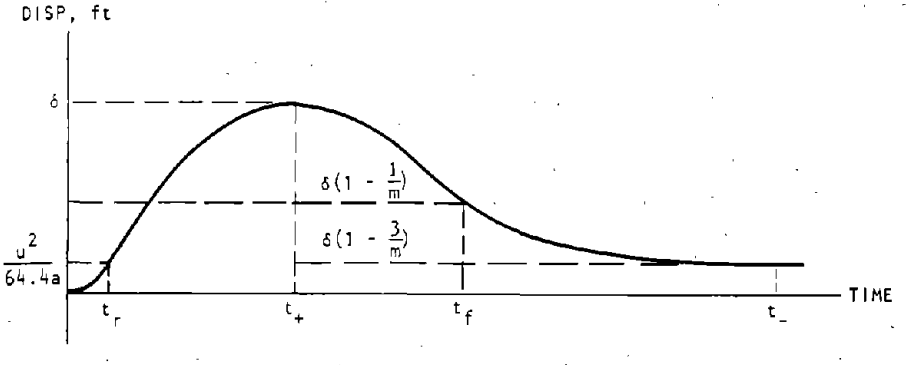

(c) Displacement

U.S. Army Corps of Engineers

Figure 9–14. Pulse Shape Parameters

CHAPTER 10
CRATER

10-1. Gross phenomenology.

a. A crater is formed when a nuclear weapon is detonated below ~ 35 ft/kt$^{1/3}$ (~ 10.7 m/kt$^{1/3}$). The significant features of the crater include the apparent crater (i.e., the visible contour), the true crater as defined by the limits of dissociation of the natural material, ejecta that falls back into the true crater, a rupture zone in which cracking and crushing occurs, a plastic zone (or displacement zone in rock) in which significant permanent deformation occurs, and the ejecta that, along with ground deformation, form the crater lip. These zones are depicted in figure 10–1.

b. The basic variables affecting the cratering phenomenon are:

- Weapon design
- Weapon yield
- HOB/DOB
- Site condition (stratification, water-table elevation, etc.)
- Material properties (principally shear strength)

The greater the yield, the greater will be the DOB (or the lesser the HOB), or the weaker the site medium, the larger the crater volume. The crater will be flatter the higher the burst or the weaker the site medium. Crater size increases with DOB up to the optimum cratering DOB ($\approx$131 ft/kt$^{1/3}$, or 40 m/kt$^{1/3}$). Further increases of DOB reduce crater size.

c. Currently, crater dimensions are estimated by scaling from the cratering data obtained during the atmospheric nuclear tests (perhaps a score of cratering events) and from the large number of atmospheric HE tests conducted with charges weighing from a few grams to 500 tons. The credibility of mathematically simulated craters has not been generally established; the prediction methods described in this volume do not include these data. Moreover, fairly recent data from the AEWES, DNA-PR-0012, Phase 2 and DNA-PR-0028, Phase 3 (1976, 1977), which included cratering experiments in soils with a high water content, have not been included in this manual since the results were reported after the manual was prepared.

d. The volume of material excavated by a nuclear blast is of little direct concern to designers except as it relates to the formation of ejecta material which produces an impact phenomenon and buildup of ejecta on the ground surface beyond the crater lip. It also contributes to the formation of the dust cloud. These subjects are discussed in Chapters 11, 12, and 13. A detailed derivation of crater volume is presented in Chapter 12. A system cannot survive if its original position places it within the crater proper or even somewhat beyond the crater. Moreover, only very simple, compact, inherently rugged facilities can be expected to survive in the contiguous rupture zone. The crater (crater proper and crater rupture zone) produced by a single, relatively small-yield weapon poses a threat to a near-surface facility. The crater produced by a single super-yield weapon, a laydown pattern of weapons, or a sequential detonation of weapons delivered to a single point poses a threat to a deep-underground facility. The facility designer will thus need to know the dimensions and uncertainties of the true crater, the rupture zone, and the plastic zone under the three patterns of attack.

10-2. Single burst.

a. True crater. The true crater is estimated from the apparent crater dimensions shown in figures 10–2 through 10–5 for a variety of soils and rocks. The generalized equations for the apparent crater dimensions are

$$\left.\begin{aligned} R_a &= \alpha' W^{1/3} + \beta' z + \gamma' z^3 W^{-2/3} \\ D_a &= \alpha W^{1/3} + \beta z + \gamma z^3 W^{-2/3} \end{aligned}\right\} \text{ft}, \left|\frac{z}{W^{1/3}}\right| < 16.4$$

and

$$\left.\begin{aligned} R_a &= A' W^{1/3} + B' z + C' z^2 W^{-1/3} \\ D_a &= A W^{1/3} + B z + C z^2 W^{-1/3} \end{aligned}\right\} \text{ft}, 16.4 < \frac{z}{W^{1/3}} < 100 \qquad (10\text{–}1)$$

and the true crater dimensions are

$$R_t = \phi R_a$$

$$D_t = \phi D_a \qquad (10\text{–}2)$$

where R is radius, D is depth, z is HOB/DOB (all in feet, positive for DOB and negative for HOB), and W is weapon yield (in kilotons). The quantities α, β, γ, ϕ, A, B, and C are defined below.

(1) The mean true crater radius and depth are calculated from equations 10–1 and 10–2 using the values presented in table 10–1.

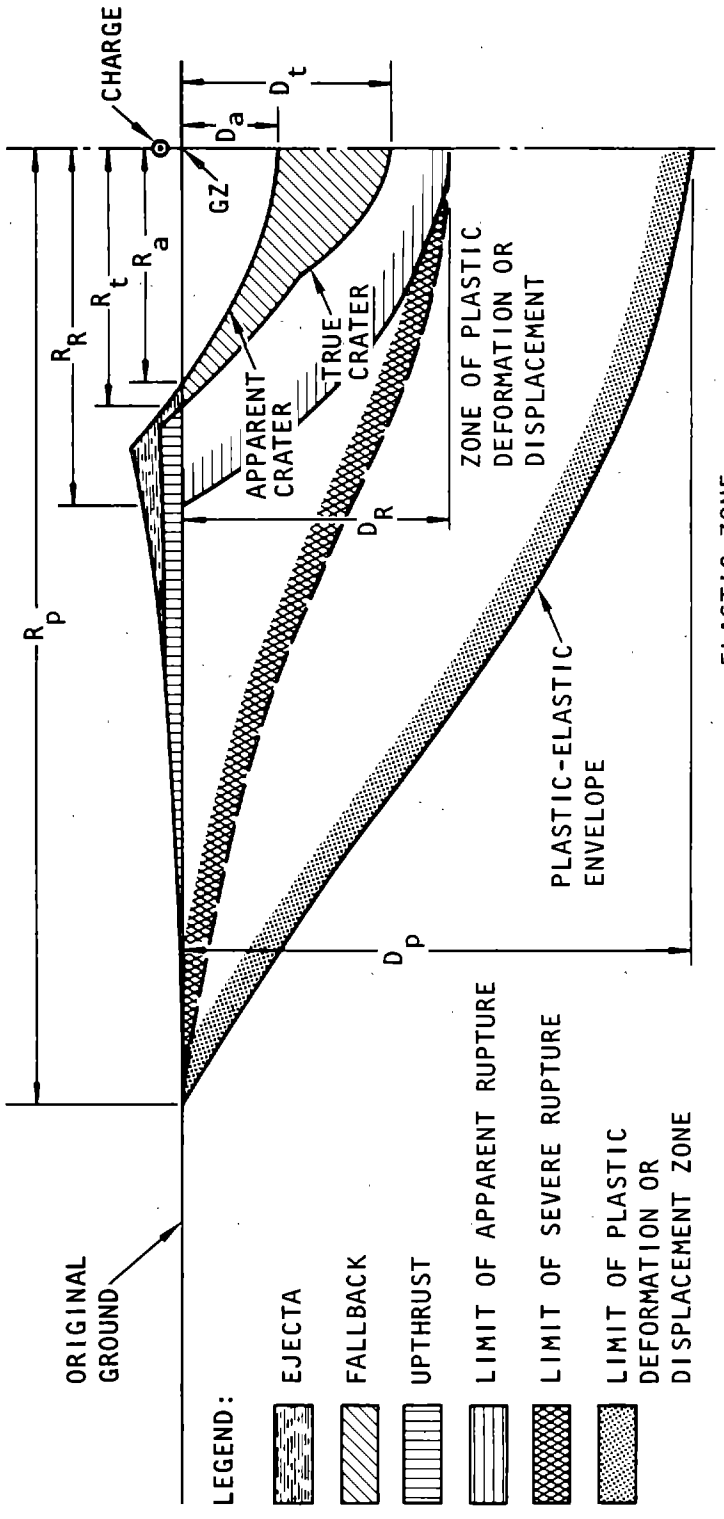

Figure 10-1. Typical Crater from a Near-Surface Explosion (Rooke et al., 1974)

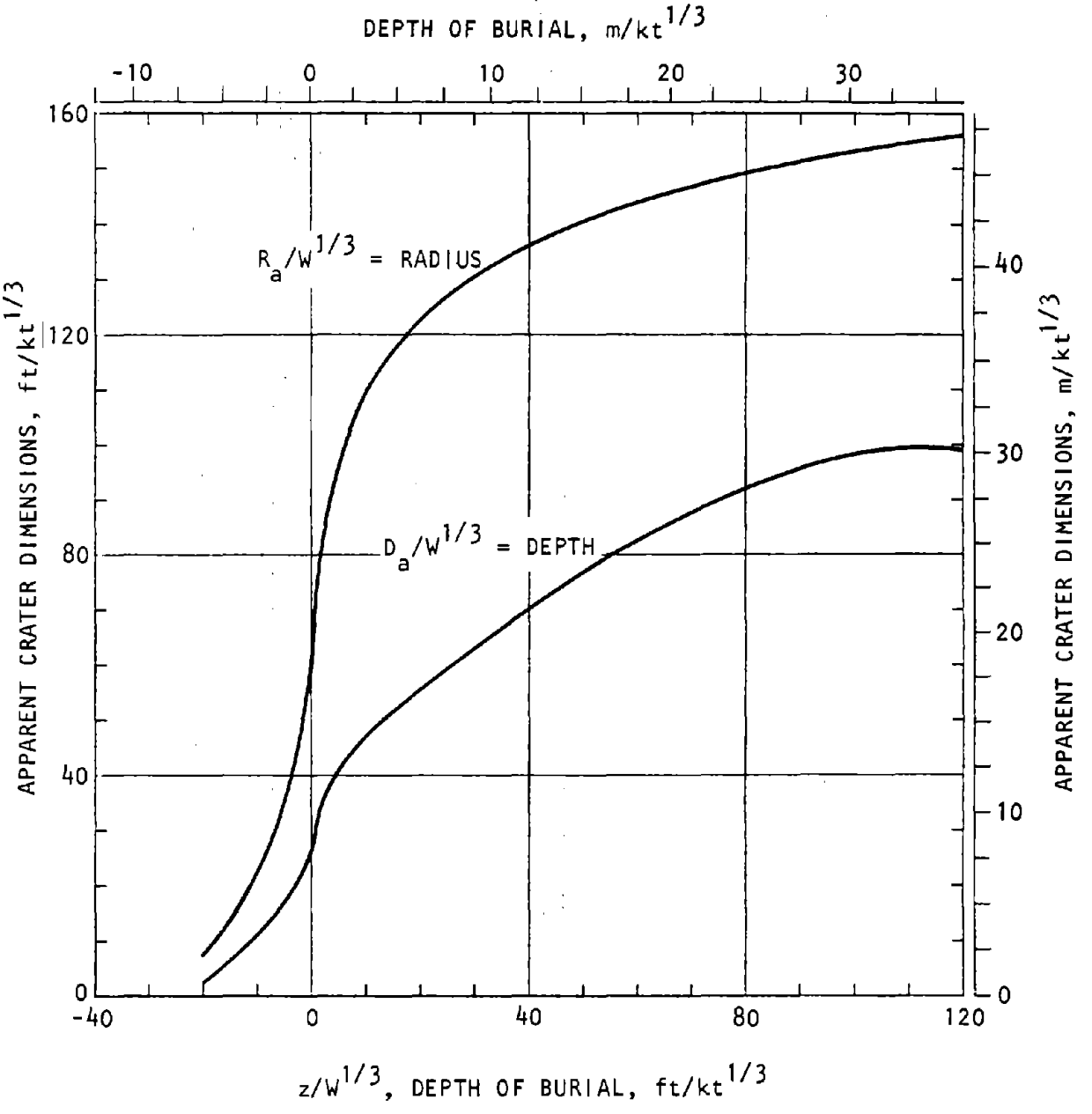

Figure 10-2. Apparent Crater Dimension for Dry Soil or Soft Rock (≤10% Water Content), (DNA, 1972)

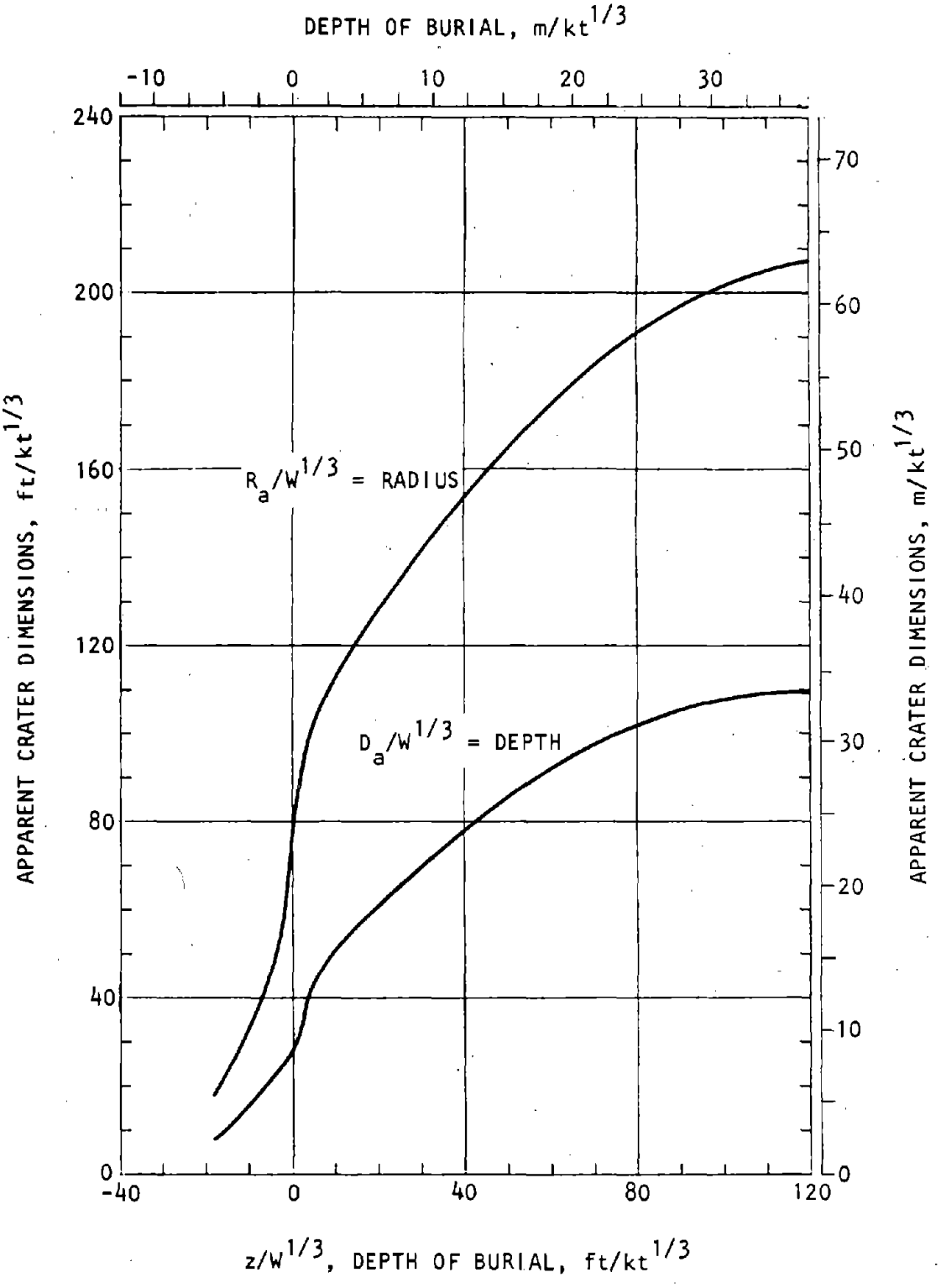

Figure 10–3. Apparent Crater Dimensions for Wet Soil or Soft Rock (>10% Moisture Content), (DNA, 1972)

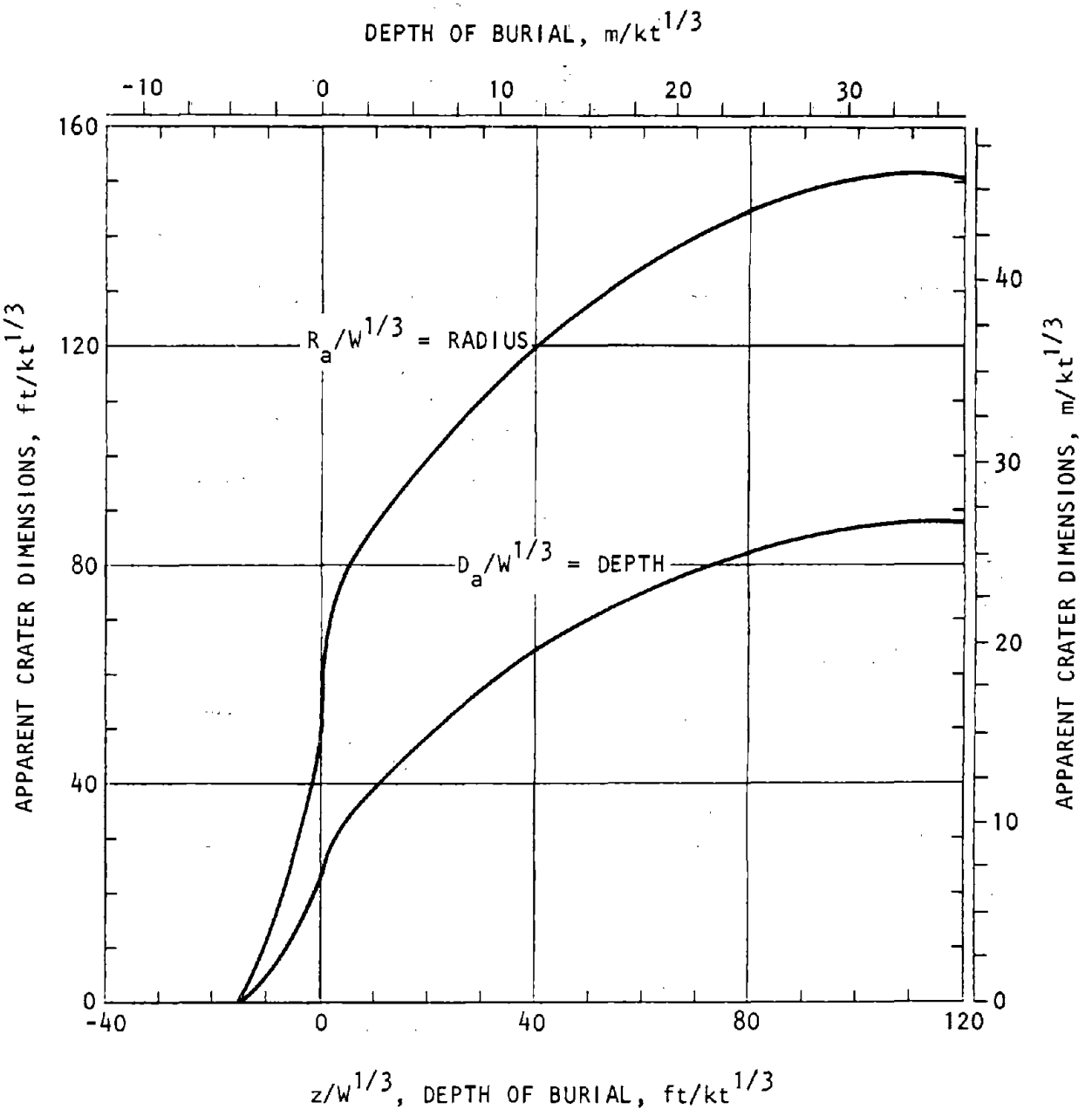

Figure 10–4. Apparent Crater Dimensions for Dry Hard Rock (≤3% Moisture Content), (DNA, 1972)

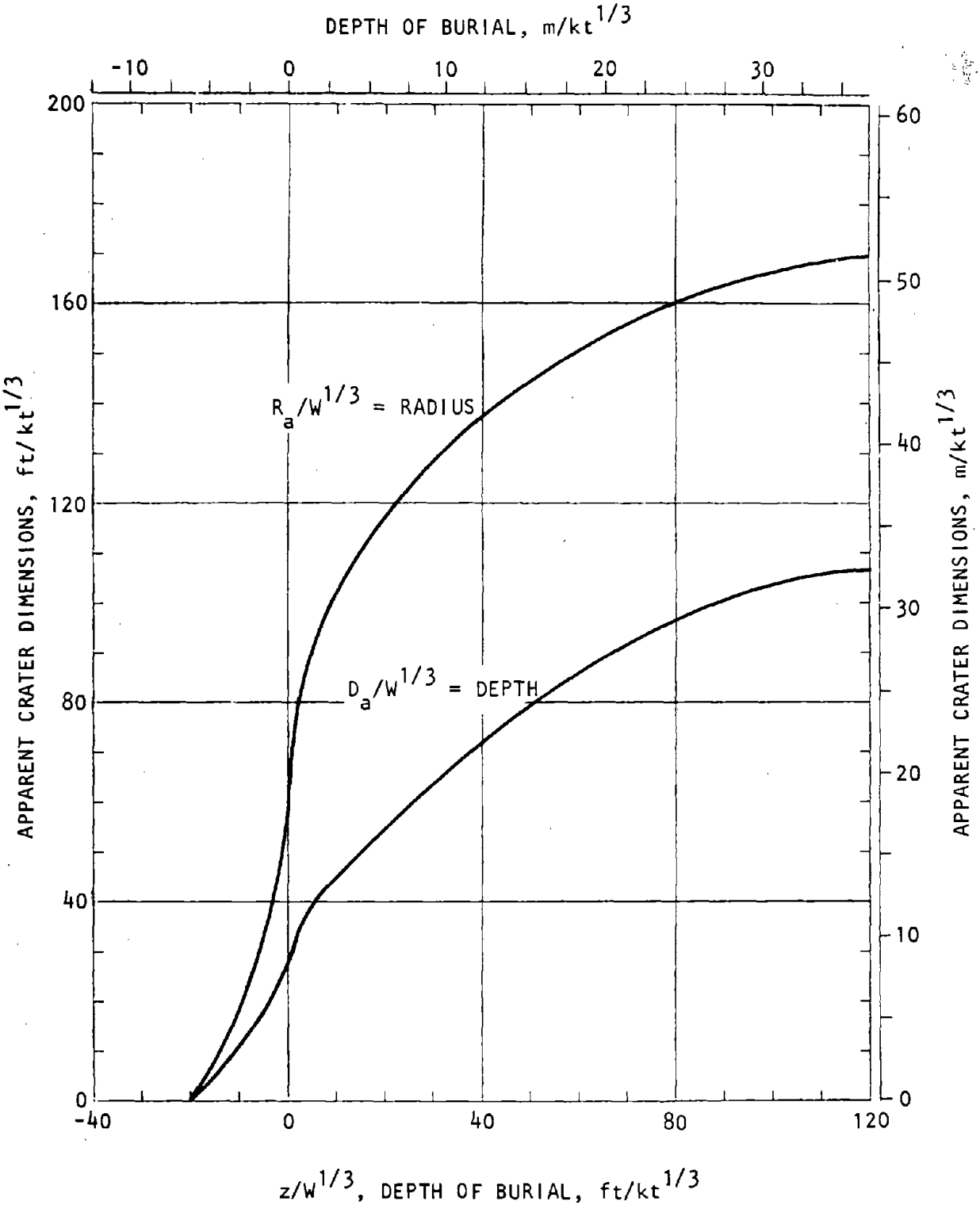

Figure 10–5. Apparent Crater Dimensions for Wet Hard Rock (>3% Moisture Content), (DNA, 1972)

(2) The uncertainties associated with the true crater dimensions are

$$\Omega^2_{R_t} = \Omega^2_g + \Omega^2_\phi + \Omega^2_{R_a}$$
$$\Omega^2_{D_t} = \Omega^2_g + \Omega^2_\phi + \Omega^2_{D_a} \qquad (10\text{–}3)$$

where

$$\Omega^2_{R_a} = \Omega^2_f + \frac{1}{R_a^2}\left\{\left[\alpha'^2 W^{2/3} + \beta'^2 z^2 + \gamma'^2 z^6 W^{-4/3}\right]\Omega^2_{C_o} + z^2(\beta' + 3\gamma' z^2 W^{-2/3})^2\,\Omega^2_z + \frac{W^{2/3}}{9}(\alpha' - 2\gamma' z^3 W^{-1})^2\,\Omega^2_W\right\},$$
$$\left|\frac{z}{W^{1/3}}\right| < 16.4 \qquad (10\text{–}4a)$$

and

$$\Omega^2_{R_a} = \Omega^2_f + \frac{1}{R_a^2}\left\{\left[A'^2 W^{2/3} + B'^2 z^2 + C'^2 z^4 W^{-2/3}\right]\Omega^2_{C_o} + z^2(B' + 2C' z W^{-1/3})^2\,\Omega^2_z + \frac{W^{2/3}}{9}(A' - C' z^2 W^{-2/3})^2\,\Omega^2_W\right\},$$
$$16.4 < \frac{z}{W^{1/3}} < 100 \qquad (10\text{–}4b)$$

In these equations Ω_f is the uncertainty associated with the functional form of R_a, and Ω_{C_o} is the uncertainty associated with the constants in the equations. Assume that $\Omega_f \approx 0.36$, $\Omega^2_g + \Omega^2_\phi \approx 0.01$; assume that $\Omega_{C_o} = 0.07$ for reasonably homogeneous sites and 0.12 for layered sites or for sites where a water table intersects the crater. These uncertainties were obtained from equation 2–17 where n = 2 and R = 1.35 for the former case (homogeneous) and R = 1.67 for the latter (layered). The calculation of Ω^2_D parallels equation 10–4 where the notation R_a is replaced by D_a.

b. Rupture zone. The rupture zone is also estimated from the apparent crater, and its dimensions are

$$R_R = \theta\phi R_a$$
$$D_R = \theta'\phi D_a \qquad (10\text{–}5)$$

Values of θ, θ', and ϕ are defined below.

(1) The mean rupture zone radius and depth are calculated from the values presented in table 10–1 and equations 10–1, 10–2, and 10–5.

(2) The uncertainties associated with the rupture zone are

$$\Omega^2_{R_R} = \Omega^2_g + \Omega^2_\theta + \Omega^2_\phi + \Omega^2_{R_a}$$
$$\Omega^2_{D_R} = \Omega^2_g + \Omega^2_{\theta'} + \Omega^2_\phi + \Omega^2_{D_a} \qquad (10\text{–}6)$$

where Ω_θ, $\Omega_{\theta'}$, and Ω_ϕ are the uncertainties of the coefficients in equation 10–5, and Ω_{R_a} and Ω_{D_a} are defined in *a* (2) above. Assume that $\Omega^2_g + \Omega^2_\theta + \Omega^2_\phi = \Omega^2_g + \Omega^2_{\theta'} + \Omega^2_\phi \approx 0.05$.

c. Plastic or displacement zone. The plastic zone (for soils) and the displacement zone (for rocks) are estimated from the apparent crater, and their dimensions are

$$R_p = \Gamma\phi R_a$$
$$D_p = \Gamma'\phi D_a \qquad (10\text{–}7)$$

Values of Γ and Γ' are given below.

(1) The mean plastic or displacement zone radius and depth are calculated from the values presented in table 10–1 and equations 10–1, 10–2, and 10–7.

(2) The uncertainties associated with the plastic or displacement zone are

$$\Omega^2_{R_P} = \Omega^2_g + \Omega^2_\Gamma + \Omega^2_\phi + Q^2_{R_a}$$
$$\Omega^2_{D_P} = \Omega^2_g + \Omega^2_{\Gamma'} + \Omega^2_\phi + \Omega^2_{D_a} \qquad (10\text{–}8)$$

where Ω_Γ, $\Omega_{\Gamma'}$, and Ω_ϕ are the uncertainties in equation 10–7, and Ω_{R_a} and Ω_{D_a} are defined in *a* (2) above. Assume that $\Omega^2_g + \Omega^2_\Gamma + \Omega^2_\phi = \Omega^2_g + \Omega^2_{\Gamma'} + \Omega^2_\phi \approx 0.05$.

10–3. Multiple, pattern burst.

Close spacing of charges (less than 1.4 single-charge crater radii) enhance both radius and depth of cratering. Figure 10–6 shows the enhancement of single-charge crater dimensions obtained by reducing the spacing between charges in a row-charge at optimum DOB. The enhancement is proportional to $1/\sqrt{s}$ where s is the charge spacing in ft. As the charge spacing decreases, the optimum DOB for each charge must be increased by the enhancement factor in figure 10–6 in order to achieve these results. Since the enemy may not be able to achieve penetration to the optimum DOB, figure 10–6 is an upper bound. Nevertheless, it is recommended that the enhanced crater dimensions be taken as

$$R'_a = ER_a \qquad D'_a = E'D_a$$
$$R'_t = ER_t \qquad D'_t = E'D_t$$
$$R'_R = ER_R \qquad D'_R = E'D_r$$
$$R'_p = ER_p \qquad D'_p = E'D_p \qquad (10\text{–}9)$$

Table 10-1. Mean Value of Parameters (equations 10-1 & 10-2)

Site	Parameter																
	α'	β'	γ'	α	β	γ	A'	B'	C'	A	B	C	ϕ	θ	θ'	Γ	Γ'
Dry Soil or Dry Soft Rock	48.6	4.7	-7.43×10^{-5}	22.3	1.9	-2.42×10^{-7}	-3.43×10^{-3}	7.75×10^{-1}	1.09×10^{2}	-3.43×10^{-3}	9.50×10^{-1}	3.74×10^{1}	1.4	2.0	1.5	6.0	3.0
Dry Hard Rock	39.0	6.3	-3.80×10^{-6}	17.4	2.5	-1.21×10^{-6}	-5.94×10^{-3}	1.35	7.44×10^{1}	-4.06×10^{-3}	9.50×10^{-1}	3.16×10^{1}	1.4	2.0	3.0	4.0	4.0
Wet Soil or Wet Soft Rock	65.0	4.2	-5.57×10^{-7}	24.6	1.9	-2.23×10^{-7}	-6.25×10^{-3}	1.68	9.80×10^{1}	-4.69×10^{-3}	1.13	4.14×10^{1}	1.4	2.0	1.5	6.0	3.0
Wet Hard Rock	45.9	4.4	-6.13×10^{-7}	22.3	1.7	-1.30×10^{-7}	-5.31×10^{-3}	1.25	9.41×10^{1}	-4.69×10^{-3}	1.18	3.14×10^{1}	1.4	2.0	3.0	4.0	4.0

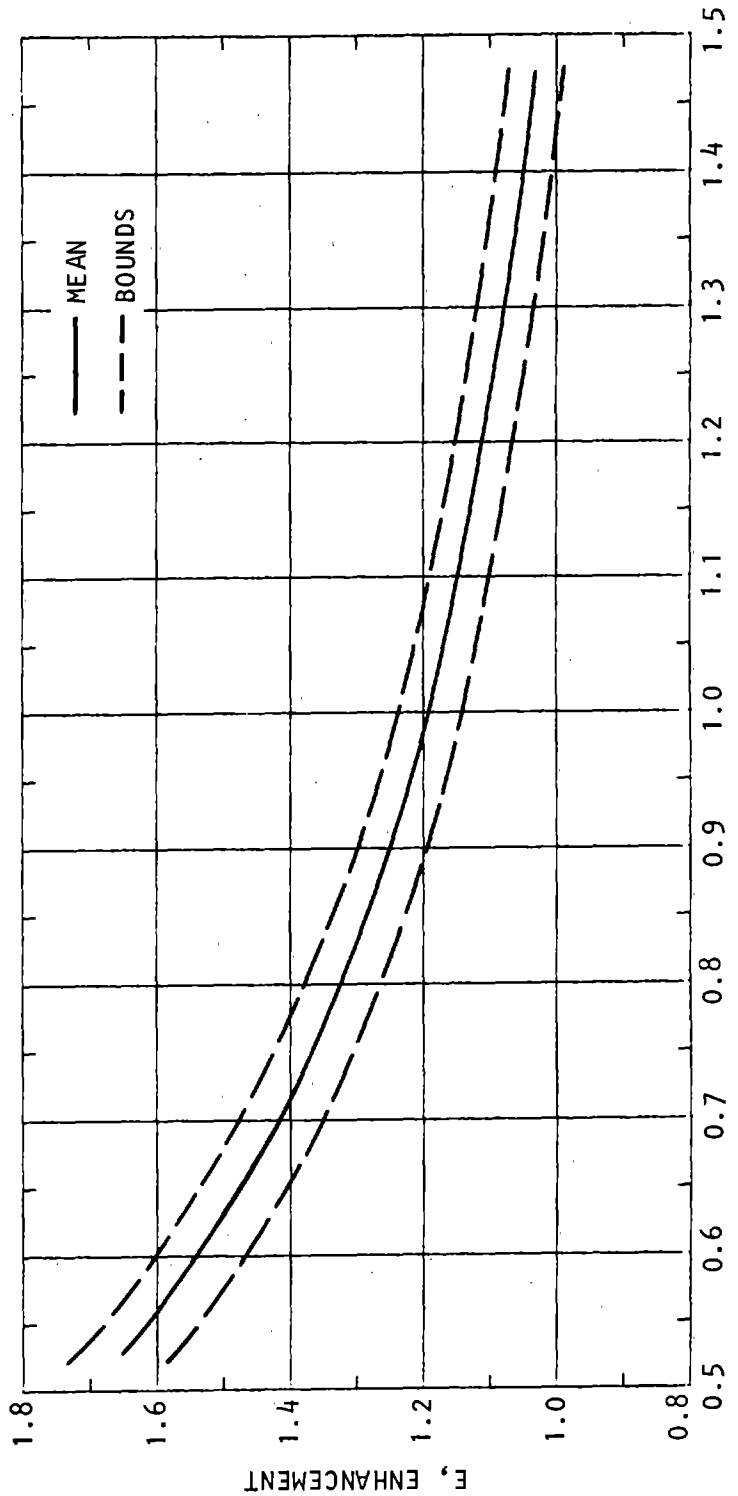

Figure 10-6. Enhancement of Single-Charge Apparent Crater Dimensions in a Row Crater as a Function of Charge Spacing at Optimum DOB in Soil (Rooke et al., 1974)

where the enhancement factors are of the form

$$E = A(s/R_a)^{1/2} \qquad (10\text{–}10a)$$

Similar equations apply to the depth dimensions, i.e.,

$$E' = A(s/D_a)^{1/2} \qquad (10\text{–}10b)$$

a. Use the mean value of the data range presented in figure 10–6 to determine the mean enhancement factor. This occurs when A = 1.2 in equation 10–10.

b. The uncertainties associated with equations 10–9 and 10–10 are

$$\begin{aligned}
\Omega^2_{R'_a} &= \Omega^2_f + \Omega^2_A + \tfrac{1}{4}\Omega^2_s + \tfrac{1}{4}\Omega^2_{R_a} \\
\Omega^2_{R'_t} &= \Omega^2_{R'_a} + \Omega^2_\phi \\
\Omega^2_{R'_R} &= \Omega^2_{R'_t} + \Omega^2_\theta \\
\Omega^2_{R'_P} &= \Omega^2_{R'_a} + \Omega^2_\Gamma + \Omega^2_\phi
\end{aligned} \qquad (10\text{–}11a)$$

where Ω_f is the uncertainty of equations 10–9, and Ω_A is the uncertainty of the constant in equation 10–10. Assume $\Omega_f \approx 0.04$ and calculate Ω_A from figure 10–6 and equation 2–17 where n = 2 and L_2 and L_1 are the upper and lower bounds on the data at any selected burst spacing. Similarly, the uncertainties of the crater depths are calculated from

$$\begin{aligned}
\Omega^2_{D'_a} &= \Omega^2_f + \Omega^2_A + \tfrac{1}{4}\Omega^2_s + \Omega^2_{D_a} \\
\Omega^2_{D'_t} &= \Omega^2_{D'_a} + \Omega^2_\phi \\
\Omega^2_{D'_R} &= \Omega^2_{D'_t} + \Omega^2_\theta \\
\Omega^2_{D'_P} &= \Omega^2_{D'_a} + \Omega^2_\Gamma + \Omega^2_\phi
\end{aligned} \qquad (10\text{–}11b)$$

10–4. Repeated attack (nail driving).

a. Repeated attack, sometimes called "nail driving," is the successive firing of shots in the center of craters formed by preceding shots to enhance cratering. Bounds of the true crater data for tests in rock are shown in figure 10–7. These data are represented by equations of the form

$$E'' = A + BN \qquad (10\text{–}12)$$

and the enhanced dimensions are

$$\begin{aligned}
R''_t &= E''R_t = E''\phi R_a \\
D''_t &= E''D_t = E''\phi D_a
\end{aligned} \qquad (10\text{–}13)$$

where E″ is the increase in true crater dimensions and N is the number of successive shots. The parameters A and B are defined in *b* below.

b. The mean increase in true crater dimensions can be obtained from figure 10–7 or from equations 10–12 and 10–13, with the constants defined in table 10–2.

c. The uncertainties of the true crater dimensions from the nail-driving attack are

$$\begin{aligned}
\Omega^2_{R''_t} &= \Omega^2_f + (A^2 + B^2N^2)\left(\frac{R_t}{R''_t}\right)^2 \Omega^2_{C_R} + \frac{N^2B^2}{R''^2_t}\Omega^2_N + \Omega^2_{R_t} \\
\Omega^2_{D''_t} &= \Omega^2_f + (A^2 + B^2N^2)\left(\frac{D_t}{D''_t}\right)^2 \Omega^2_{C_D} + \frac{N^2B^2}{D''^2_t}\Omega^2_N + \Omega^2_{D_t}
\end{aligned} \qquad (10\text{–}14)$$

where Ω_f is the uncertainty of the form of equation 10–13, Ω_{C_R} and Ω_{C_D} are the uncertainties of the nail-driving enhancement factors applied to the radius and diameter, respectively. Assume $\Omega_f \approx 0.2$ and calculate Ω_{C_R} and Ω_{C_D} from equation 2–17 where n = 2 and L_2 and L_1 are the upper and lower bounds on the enhancement factors in figure 10–7 for any selected number of shots.

10–5. Crater volume.

Crater volumes in homogeneous and in layered geologies are calculated in chapter 12, where the depth of burial by crater ejecta is defined.

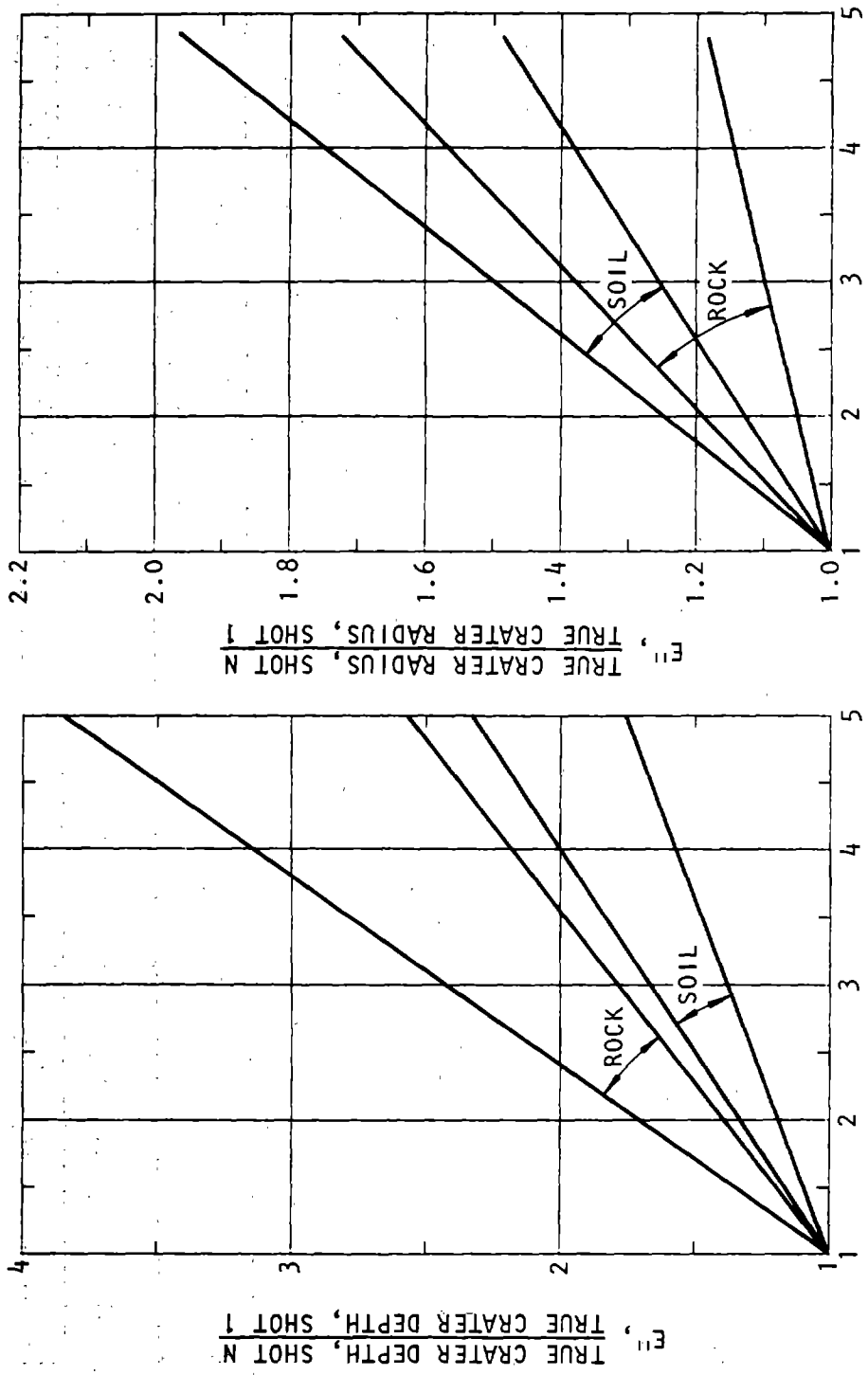

Figure 10-7. Enhancement in True-Crater Dimensions for Nail-Driving (Rooke et al., 1974)

Table 10-2. Parameters for Increase of True Crater Dimensions Due to Nail Driving

Geology	Dimension	A	B
Rock	Radius	0.88	0.12
	Depth	0.45	0.55
Soil	Radius	0.81	0.19
	Depth	0.99	0.01

U.S. Army Corps of Engineers

CHAPTER 11
EJECTA/DEBRIS IMPACT

11-1. Gross phenomenology.

a. Material is thrown out of the crater region as a part of the unloading process following the initial strong shock driven into the ground by the explosion. Ejected particles produced by a near-surface burst extend over a range from the crater lip to remote points. Discrete particles are thus part of the crater formation, extending through the continuous ejecta coverage, on out into the discontinuous region. The resulting projectiles of debris create the ejecta/debris impact hazard and may pose a substantial threat to exposed structures. (Projectiles may also result from fragmented structures and trees between the point of interest and ground zero, GZ. These are of secondary importance and are not treated here.) Ejecta impact encompasses the problems of estimating the initial mass of ejecta and the size of its consequent particles, the number of impacting particles, their incoming velocity and angle, and their distribution. Designers must also consider the damage potential of ejecta impact in its timing relative to other nuclear weapon effects.

b. The basic variables affecting the number, size, velocity, and angle of approach of the impacting ejecta/debris projectiles at target points are:

- Range to GZ
- Weapon yield
- Weapon design
- Height of burst
- Geology
- Target elevation

11-2. Ejected mass and particle size.

a. The effects of ejecta impact are determined from calculations of total ejected mass, number of impact particles, mean maximum particle size and number, and mean impact velocities and angles. Using the data of Post (1974) and Crawford et al. (1974) state that the total ejected mass can be calculated from the apparent crater mass with the equation

$$M_t/M_a = AW^n \tag{11-1}$$

where

M_a = Apparent ejecta weight, lb
M_t = Total ejecta weight, lb
W = Yield, kt
A,n = Constants depending on geologic properties

Since

$$M_a = \gamma_p V_a \tag{11-2}$$

where

V_a = Apparent crater volume, ft^3

it follows that

$$M_t = A\gamma_p W^n V_a \tag{11-3}$$

In turn, the maximum particle weight at any range (from unpublished work by Post) is determined from the total weight to be

$$m_m = BM_t^m R_s^\alpha \text{ , lb} \tag{11-4a}$$

where the particle configuration is assumed to be spherical, that is,

$$m_m = \pi a_m^3 \gamma_p/6 \tag{11-4b}$$

Therefore, the maximum particle diameter is

$$a_m = 1.241\ \gamma_p^{(M-1)/3} B^{1/3} A^{m/3} W^{mn/3} R_s^{\alpha/3} V_a^{m/3} \text{ , ft} \tag{11-5}$$

where

R = Range, ft
R_s = $R/V_a^{1/3}$
B,m,n,α = Constants

b. The mean value for equations 11-1 through 11-5 can be obtained from the values of the constants presented below:

$$A = \begin{cases} 1.08 \text{ (hard rock)} \\ 0.54 \text{ (other geologies)} \end{cases} \qquad n = \begin{cases} -0.0477 & W \geq 1 \text{ kt} \\ 0 & W < 1 \text{ kt} \end{cases}$$

$B = 0.1094$
$m = 0.8$
$\alpha = -1.644$

c. The uncertainty associated with equation 11-5 is

$$\Omega^2_{a_m} = \Omega_f^2 + \frac{(m-1)^2}{9}\Omega^2_{\gamma_p} + \frac{(mn)^2}{9}\Omega_W^2 + \frac{\alpha^2}{9}\Omega_R^2 + \left(\frac{m}{3} - \frac{\alpha}{9}\right)^2 \Omega_V^2 \tag{11-6}$$

where $\Omega_f = 0.36$ and $\Omega_{\gamma_p} = 0.05$. ($\Omega^2_{V_a}$ is defined in ch. 12.)

11-3. Number of impact particles.

a. It is useful to express the number of particles equal to or greater than a specified size that will occur at a specified range from GZ. Such an equation is of the form

$$I = \frac{KsD_e}{(s-3)} \quad \frac{a_m^{s-3} - a_o^{s-3}}{a_m^s} \qquad (11\text{-}7)$$

where

I = Number of particles per unit area (ft^2) greater in size than a_o (ft) (an arbitrary particle size) but less than a_m (ft)
s = Constant depending on geology
$K = \frac{6\gamma}{\pi\gamma_p}$
γ = Postattack unit weight of ejecta, lb/ft^3

Equation 11-7 was derived by Post (again, in unpublished work) based on a review of empirical data; it implicitly contains the range parameter from the variables D_e and a_m where D_e is the continuous ejecta depth, as defined in chapter 12.

b. The mean number of impacting particles per unit area is obtained from equation 11-7. For $a_o \geq 4$ in.,

$$s = \begin{cases} 0.00147 \text{ for unconsolidated alluvial soil} \\ 0.5 \text{ for hard rock, cohesive soils, or layered geologies} \end{cases}$$

c. An estimate of the uncertainty associated with equation 11-7 is given by

$$\Omega_I^2 = \Omega_f^2 + \Omega_{D_e}^2 + \frac{1}{4}\left(\frac{a_o^{-2.5} - 6a_m^{-2.5}}{a_o^{-2.5} - a_m^{-2.5}}\right)^2 \Omega_{a_m}^2 \qquad (11\text{-}8)$$

where $\Omega_f \approx 0.2$, Ω_{a_m} is obtained from equation 11-6, and Ω_{D_e} is presented in equation 12-2.

11-4. Particle impact velocities and angles.

a. Computational and experimental evidence support the adoption of a model of ejecta trajectories based on the assumption that particles are ejected at a random elevation angle θ and at a velocity dependent on size, and that the trajectory is determined by gravity and aerodynamic drag forces. Analysis of the trajectories obtained from calculations have led to the simplified description of impact velocity reported by Crawford et al. (1974):

$$v_i = \mathscr{A}\left(\frac{R}{\sin 2\theta}\right)^{1/2} \exp(-R/R_o) \quad , \quad R \leq R_o/2$$

$$= \mathscr{B}\left(\frac{a_o\gamma_p}{C_D}\right)^{1/2} \quad , \quad R > R_o/2 \qquad (11\text{-}9)$$

where

V_i = Impact velocity, ft/sec
C_D = Drag coefficient of particles
R = Range from GZ, ft
γ_p = Preattack density of ejecta, lb/ft^3
$R_o = \frac{90a_o\gamma_p}{C_D} \sin 2\theta$, ft
a_o = Arbitrary particle diameter, ft
θ = Ejection elevation angle, deg
$\mathscr{A}, \mathscr{B}$ = Constants

b. At an arbitrary range, the incoming particle size may be selected in the range $a_o \leq a_m$ where a_m is obtained from equation 11-5. The ejection elevation angle is assumed to be distributed between 15 deg and 75 deg, but strongly concentrated near 45 deg, as shown in figure 11-1. The drag coefficient is assumed to lie between 0.3 and 1.2, with a mean value of 0.6. The mean impact velocity is computed from equation 11-9 where $\mathscr{A} = 5.673$ and $\mathscr{B} = 23.08$.

c. The uncertainty in the impact velocity is given by

$$\Omega_{V_i}^2 = \begin{cases} \Omega_f^2 + \left(\frac{1}{2} - \frac{R}{R_o}\right)^2 \Omega_R^2 + 2\theta^2\left(\frac{R}{R_o} - 1\right)^2 \left(\cot^2 2\theta\right)\Omega_\theta^2 \\ \quad + \left(\frac{R}{R_o}\right)^2 \Omega_{\gamma_P}^2 + \left(\frac{R}{R_o}\right)^2 \Omega_{C_D}^2 \quad , \quad R \leq R_o/2 \\ \Omega_f^2 + \frac{1}{4}\Omega_{\gamma_P}^2 + \frac{1}{4}\Omega_{C_D}^2 \quad , \quad R > R_o/2 \end{cases} \qquad (11\text{-}10)$$

where $\Omega_f = 0.36$ and $\Omega_{C_D} = \Omega_\theta = 0.3$.

11-5. Impact damage potential.

a. Impact damage potential can be measured in terms of particle kinetic energy (momentum), expected target penetration, or expected crater volume. For hardened facility applications, use the damage measures—penetration or crater volume. Penetration has been examined as a continuing part of armor/armor-piercing projectile development and, more recently, as part of the safety program for nuclear power reactor development. Available data for projectiles striking concrete targets are utilized to extrapolate the effect of rock fragments striking similar targets.

b. The penetration depth, d, is adapted from ASCE (1976):

$$d = \begin{cases} 0.04\, F_D (KN\gamma_p)^{1/2}\, a_o^{1.1} V_i^{0.9} \quad , \quad d/a_o \leq 2 \\ 2 \times 10^{-6}\, F_D KN\gamma_p a_o^{1.2} V_i^{1.8} \quad , \quad d/a_o > 2 \end{cases} \qquad (11\text{-}11)$$

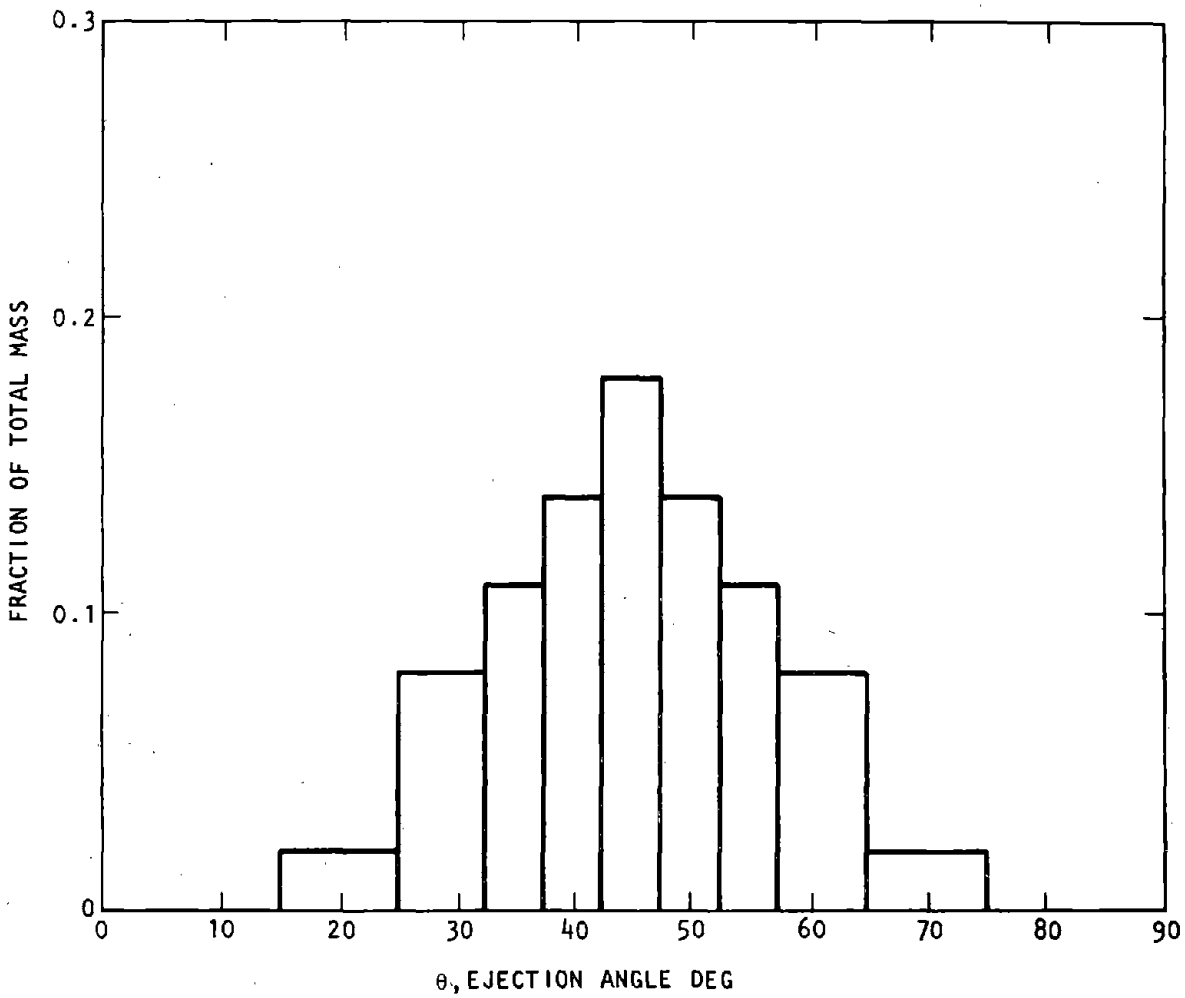

Figure 11-1. Ejection Angle Distribution for High-Yield Surface Bursts (Seebaugh, 1975)

where

F_D = Particle deformability factor
$\approx \begin{cases} 0.7 \text{ for hard rock} \\ 0.25 \text{ for soft rock or alluvium} \end{cases}$

K = Concrete penetrability index = $\frac{180}{\sqrt{f'_c}}$

f'_c = Ultimate compressive strength of concrete, psi

N = Particle nose shape factor ≈ 1.0

a_o = Arbitrary particle diameter $\leq a_m$, in.

V_i = from equation 11-9 based on particle size a_o, ft/sec

γ_p = Preattack particle density, lb/in.^{3}

The estimate of penetration crater volume is based on an assumed conical crater depth d and radius 2.5d

$$V_{crater} = 6.5\ d^3 \qquad (11\text{-}12)$$

c. The uncertainty associated with equation 11-11 is

$$\Omega_d^2 = \Omega_f^2 + \begin{cases} \Omega_{F_D}^2 + \frac{1}{4}\Omega_K^2 + \frac{1}{4}\Omega_N^2 + \frac{1}{4}\Omega_{\gamma_p}^2 + 0.8\Omega_{V_i}^2, \\ d/a_o \leq 2 \\ \left(\frac{d - a_o}{d}\right)^2 \left[\Omega_{F_D}^2 + \Omega_K^2 + \Omega_N^2 + \Omega_{\gamma P}^2 \right. \\ \left. + 3.24\,\Omega_{V_i}^2\right], \ d/a_o > 2 \end{cases} \qquad (11\text{-}13)$$

where $\Omega_f \approx 0.5$, $\Omega_{F_D} \approx 0.25$, $\Omega_K = \frac{1}{2}\Omega_{f'_c}^2$, $\Omega_N \approx 0.15$, $\Omega_{\gamma P} = 0.05$, and Ω_{V_i} is obtained from equation 11-10. The quantity $\Omega_{f'_c}$ is the uncertainty of the unconfined compressive strength of concrete.

CHAPTER 12
EJECTA/DEBRIS DEPTH

12-1. Gross phenomenology.

a. To prevent burial of a facility and interruption of its function or to plan active removal of debris, the designer must know the expected depth of debris, in addition to the expected particle size distribution delineated in chapter 11. Deposition of crater ejecta as surface debris becomes significant when the height of burst is less than 35 ft/kt$^{1.3}$ (10.7 m/kt$^{1/3}$). The depth of debris in the region of continuous coverage of the ground depends on range from ground zero (GZ) and varies (usually unpredictably) with azimuth, probably the result of fracture patterns and inhomogeneities in the medium. Outside the continuous region (greater than five crater radii), the debris consists of separated discrete particles unlikely to bury the facility. The amount of ejecta threatening burial of a facility depends on the crater volume and is addressed in this chapter for both homogeneous and layered geologies.

b. The basic variables effecting the ejecta thickness at a point on the ground are:

- Range to GZ
- Weapon yield
- Weapon design
- Height of burst or depth of burst
- Geology

Ejecta depth is enhanced by large yields, reduced ranges, weapon penetration, and certain geological features described below.

12-2. Debris depth.

a. The depth of crater ejecta debris from a near-surface burst is related to the apparent crater volume. (See chapter 10 for calculation of apparent depth and radius.) In turn, the crater volume is implicitly dependent on weapon yeild, height of burst, weapon type, and geology (Post, 1974). The scaled debris depth as a function of scaled range can be represented by an equation of the form

$$\frac{D_e}{V_a^{1/3}} = A \exp\left(\alpha \frac{R}{V_a^{1/3}}\right) + B \exp\left(\beta \frac{R}{V_a^{1/3}}\right) \qquad (12\text{-}1)$$

where

D_e = Average ejecta thickness, ft
V_a = Apparent crater volume, ft^3
R = Range from ground zero, ft
A, B, α, and β are constants

b. The mean average ejecta debris depth is calculated from equation 12–1 where the constants have the values:

A	B	α	β
0.75	0.017	–2.3	–0.423

Equation 12–1 is plotted in figure 12–1 as the median value with uncertainty bounds. These data are applicable for depths of burst less than 17 ft/kt$^{1/3}$ (5 m/kt$^{1/3}$) and for most of the layered geologies encountered within the continental United States. Equation 12–1 should be multiplied by the quantities in table 12–1 for the other geologies shown therein. The mean apparent crater volumes are calculated from the procedures presented in paragraph 12–3 below.

c. The uncertainty associated with equation 12–1 is

$$\Omega_{D_e}^2 = \Omega_f^2 + \frac{1}{9D_e^2}\left[D_e - A\alpha R e^{\alpha R/V_a^{1/3}} - B\beta R e^{\beta R/V_a^{1/3}}\right]^2 \Omega_{V_a}^2 + \frac{R^2}{D_e^2}\left[\alpha A e^{\alpha R/V_a^{1/3}} + \beta B e^{\beta R/V_a^{1/3}}\right]^2 \Omega_R^2 \qquad (12\text{-}2)$$

where Ω_f is the uncertainty of the functional form of equation 12–1, Ω_{V_a} is the uncertainty of the apparent crater volume, etc. Calculate Ω_f from equation 2–20 where L_1 and L_2 are the lower and upper bounds from figure 12–1, multiplied by $V_a^{1/3}$. The uncertainty of V_a is obtained from paragraphs *a* (2) and *a* (3) below.

12-3. Crater volumes.

a. Homogeneous geologies. Normalized apparent crater volumes are presented for both "high-yield" and "low-yield" nuclear devices. These terms from Cooper (1971) refer to "hot" devices having a high yield-to-mass ratio and to "cold" devices having a low yield-to-mass ratio. The relationship of volume to different ranges of HOB/DOB are also considered for both high-yield and low-yield devices. Typical cratering efficiencies are shown in table 12–2 for half-buried HE charges.

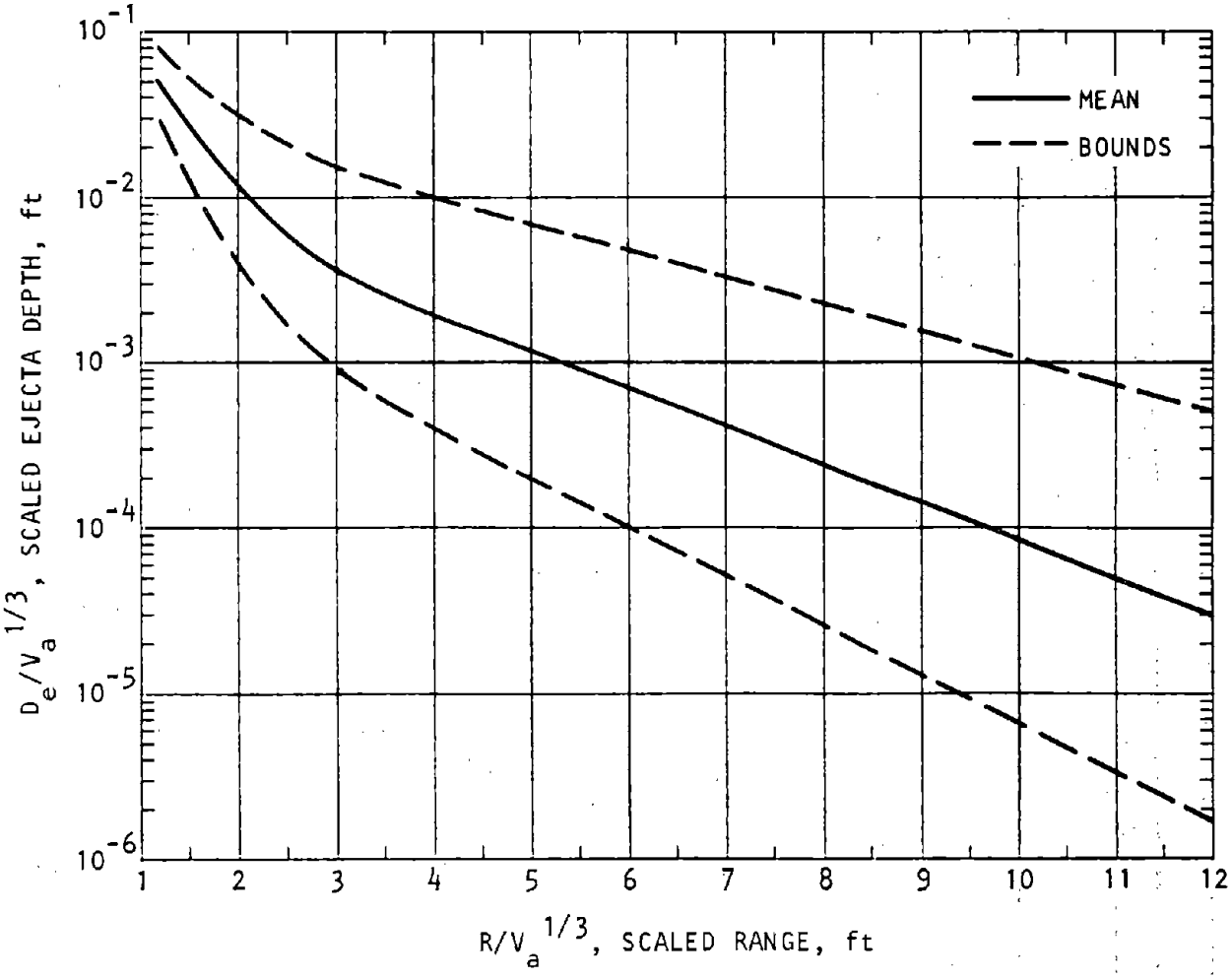

Figure 12–1. Ejecta Depth Prediction Curves for Nuclear Events, $1 \leq R/V^{1/3} \leq 12$ (Post, 1974) (1 of 2)

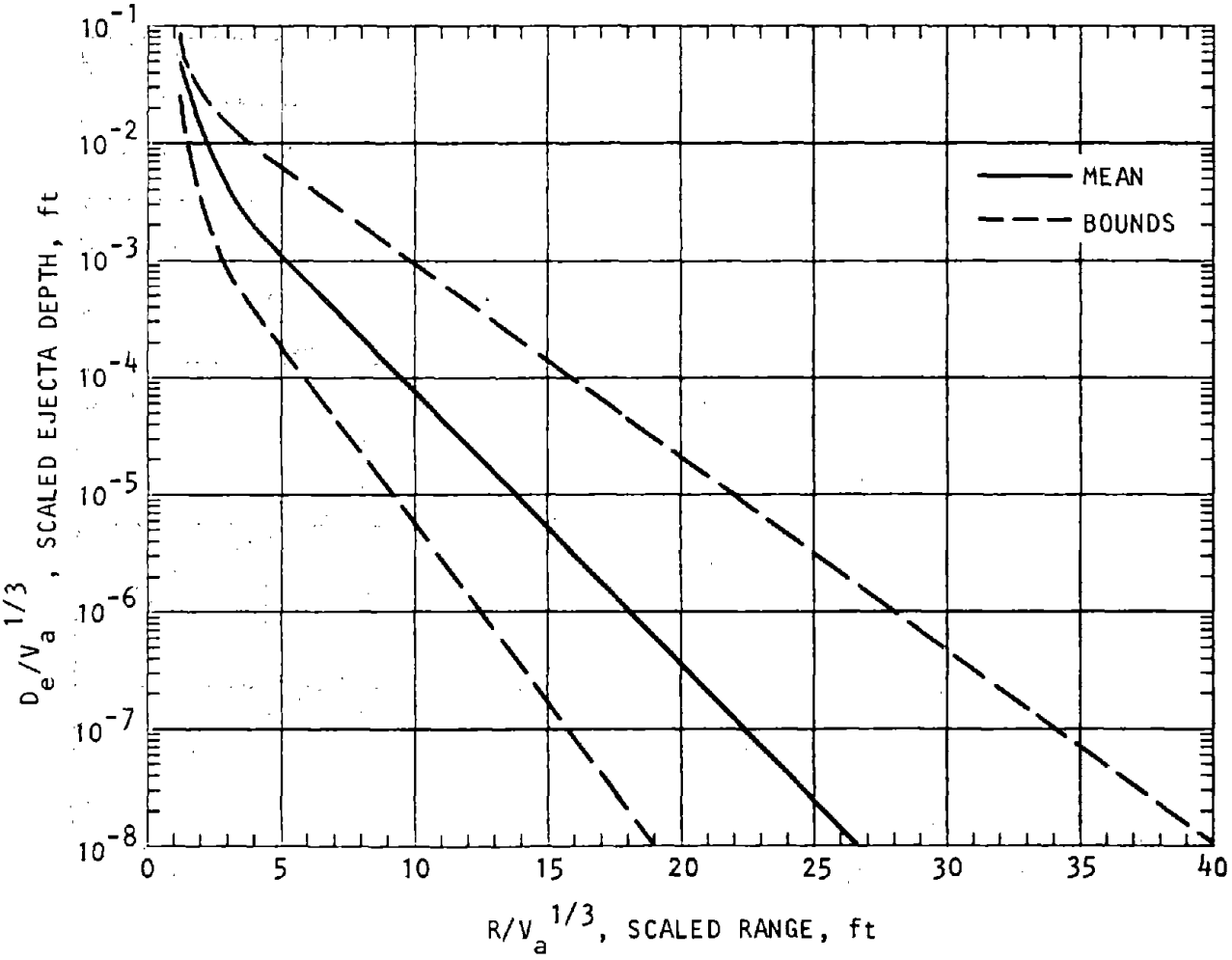

Figure 12–1. Ejecta Prediction Curves for Nuclear Events, $0 \leq R/V^{1/3} \leq 40$ (Post, 1974) (2 of 2)

Table 12-1. Geology Correction Factors

Medium	Correction Factor
Hard Rock	2.0
Porous Rock	0.75

U.S. Army Corps of Engineers

Table 12-2. Normal Cratering Efficiencies E_o for Half-Buried HE Charges (Post, 1974)

Idealized Geology	E_o ft^3/kt
Wet Soil	4×10^6
Wet Soft Rock	2×10^6
Dry Soil	1.4×10^6
Dry Soft Rock	1.0×10^6
Hard Rock	0.6×10^6

(1) The mean apparent nuclear crater volumes for $100 < W < 10$ kt can be described by the following:

"High-yield" weapons:

$$V_a/V_o = 0.04\ e^{-55.1H_s} \qquad H_s \geq 0.002$$
$$V_a/V_o = 0.05\ e^{-166\ H_s} \qquad 0 \leq H_s \leq 0.002$$
$$V_a/V_o = 4.07\ (0.0033 + D_s)^{0.77} \qquad 0 \leq D_s \leq 0.02 \qquad (12\text{–}3)$$

"Low-yield" weapons:

$$V_a/V_o = 4.39\ (D_s + 0.0216)^{0.88} \qquad 0 \leq D_s < 0.055$$
$$V_a/V_o = 4.07\ (0.0033 + D_s)^{0.77} \qquad 0.055 \leq D_s < 0.2 \qquad (12\text{–}4)$$

where

H_s = HOB/$V_o^{1/3}$
D_s = DOB/$V_o^{1/3}$
V_o = $W_T E_o$
E_o = Cratering efficiency in ft^3/kt
W = Yield in kt

in which HOB and DOB are both expressed in ft. For yields greater than 10 kt, the DOB cases of equations 12–3 and 12–4 should be replaced by the following:

"High-yield" weapons:

$$V_a/V_o = 4.07\ W^a\left[0.0033 + D_s W^{a/3}\right]^{0.77} \qquad 0 \leq D_s < 0.2 \qquad (12\text{–}5)$$

"Low-yield" weapons:

$$V_a/V_o = 4.39\ W^a\left[D_s W^{a/3} + 0.0216\right]^{0.88} \qquad 0 < D_s \leq 0.055$$
$$V_a/V_o = 4.07\ W^a\left[D_s W^{a/3} + 0.0033\right]^{0.77} \qquad 0.055 < D_s \leq 0.2 \qquad (12\text{–}6)$$

where $a = -0.3\ D_s W^{0.02}$

(2) The uncertainties associated with equations 12–3 and 12–4 are specified as

$$\Omega^2_{V_a} = \Omega^2_f + \left[1 - \frac{\gamma H_s}{3}\right]^2 \Omega^2_{V_o} + H_s^2 \gamma^2 \Omega^2_{HOB} \qquad (12\text{–}7)$$

for the HOB conditions and

$$\Omega^2_{V_a} = \Omega^2_f + \left[1 - \frac{\gamma D_s}{3(A + D_s)}\right]^2 \Omega^2_{V_o} + \frac{\gamma^2 D_s^2}{(A + D_s)^2} \Omega^2_{DOB} \qquad (12\text{–}8)$$

for the DOB conditions. The values of the constants A and γ are defined as:

Assumed Condition	*Values of Constants* A	γ
"High-yield" weapons		
$H_s \geq 0.002$	–	–55.1
$0 \leq H_s < 0.002$	–	–166.0
$0 \leq D_s < 0.02$	0.0033	0.77
"Low-yield" weapons		
$0 \leq D_s < 0.055$	0.0216	0.88
$0.055 \leq D_s < 0.2$	0.0033	0.77

The quantity Ω_f is the uncertainty of equations 12–3 and 12–4, Ω_{HOB} is the uncertainty of the HOB, etc. Assume $\Omega_f \approx 0.2$ and let

$$\Omega^2_{V_o} = \Omega^2_W + \Omega^2_{E_o} \qquad (12\text{–}9)$$

where $\Omega_{E_o} = 0.3$ based on the use of equation 2–20 for an uncertainty band of ± 50% on the data presented in table 12–2.

(3) An approximation of the uncertainties associated with equations 12–5 and 12–6 is

$$\Omega^2_{V_a} = \Omega^2_f + \left[\frac{\gamma a D_s W^{a/3}}{3(A + D_s W^{1/3})} + a\right]^2 \Omega^2_W + \left[\frac{\gamma D_s W^{a/3}}{(A + D_s W^{1/3})}\right]^2 \Omega^2_{DOB} + \left[1 - \frac{\gamma D_s W^{a/3}}{3(A + D_s W^{1/3})}\right]^2 \Omega^2_{V_o} \qquad (12\text{–}10)$$

where Ω_f is the uncertainty of equations 12–5 and 12–6 and Ω_{V_o} is the uncertainty of V_o. The constants for the various conditions are:

Assumed Condition	*Value of Constants* A	γ
"High-yield" bursts:	0.0033	0.77
"Low-yield" bursts:		
$0 < D_s \leq 0.055$	0.0216	0.88
$0.055 < D_s < 0.2$	0.0033	0.77

Assume $\Omega_f \approx 0.2$ and use equation 12–9 to compute Ω_{V_o}.

b. Layered geologies. Apparent crater volumes can be determined for layered geologies from the equation

$$\frac{V_a - V_L}{V_U - V_L} = 1 - \exp\left(-5.4d/V_a^{1/3}\right) \qquad (12\text{–}11)$$

where

d = Layer thickness in ft

V_U = Crater volume (at the HOB or DOB of interest) when $d = \infty$

V_L = Crater volume (at the HOB or DOB of interest) when $d = 0$

Equation 12–11 can be written for a layered site of n different materials via the recursive equations:

$$\left(V_{n-1,n} - V_n\right) \Big/ \left(V_{n-1} - V_n\right) = 1 - \exp\left[-5.4d_{n-1}\left(V_{n-1,n}\right)^{1/3}\right] \qquad (12\text{–}12a)$$

$$\left(V_{n-2,n-1,n} - V_{n-1,n}\right) \Big/ \left(V_{n-2} - V_{n-1,n}\right) = 1 - \exp\left[-5.4d_{n-2}\left(V_{n-2,n-1,n}\right)^{1/3}\right] \qquad (12\text{–}12b)$$

$$\left(V_{1,2,\ldots,n-1,n} - V_{2,\ldots,n-1,n}\right) \Big/ \left(V_1 - V_{2,\ldots,n-1,n}\right) = 1 - \exp\left[-5.4d_1\left(V_{1,2,\ldots n-1,n}\right)^{1/3}\right] \qquad (12\text{–}12n)$$

Equations 12–12 must be solved sequentially, beginning with the first equation and working upward through n materials.

(1) For convenience, the mean for equations 12–12 coupled with the equations and figures discussed in previous subparagraphs are presented in figures 12–2 through 12–6 for a few interesting geologies. In figures 12–2 through 12–4, cratering efficiencies can be determined for three different geological conditions. Based on these cratering efficiencies, the mean ejecta-debris depth can be calculated from figure 12–5 for airblast pressures of 600 and 1000 psi and in figure 12–6 for a larger selection of overpressures. (Refer to figure 7–10 to determine overpressure/range relationship.)

(2) The uncertainty of ejecta depth for layered sites should be calculated from equation 12–2. Equation 12–2 in turn requires the uncertainty Ω_{V_a}. Depending on the HOB or DOB and the yield and type of weapon involved, Ω_{V_a} should be determined from one of equations 12–7 through 12–10 (omitting equation 12–9, which is used to compute the uncertainty of V_0). Equations 12–7, 12–8, and 12–10 require a value of V_0. It is recommended that V_0 be calculated from the applicable condition in equations 12–3 through 12–6 by iterating the value of V_0 until the ratio V_a/V_0 on the left-hand side of the equation is compatible with the right-hand side that involves scaled HOB's and DOB's.

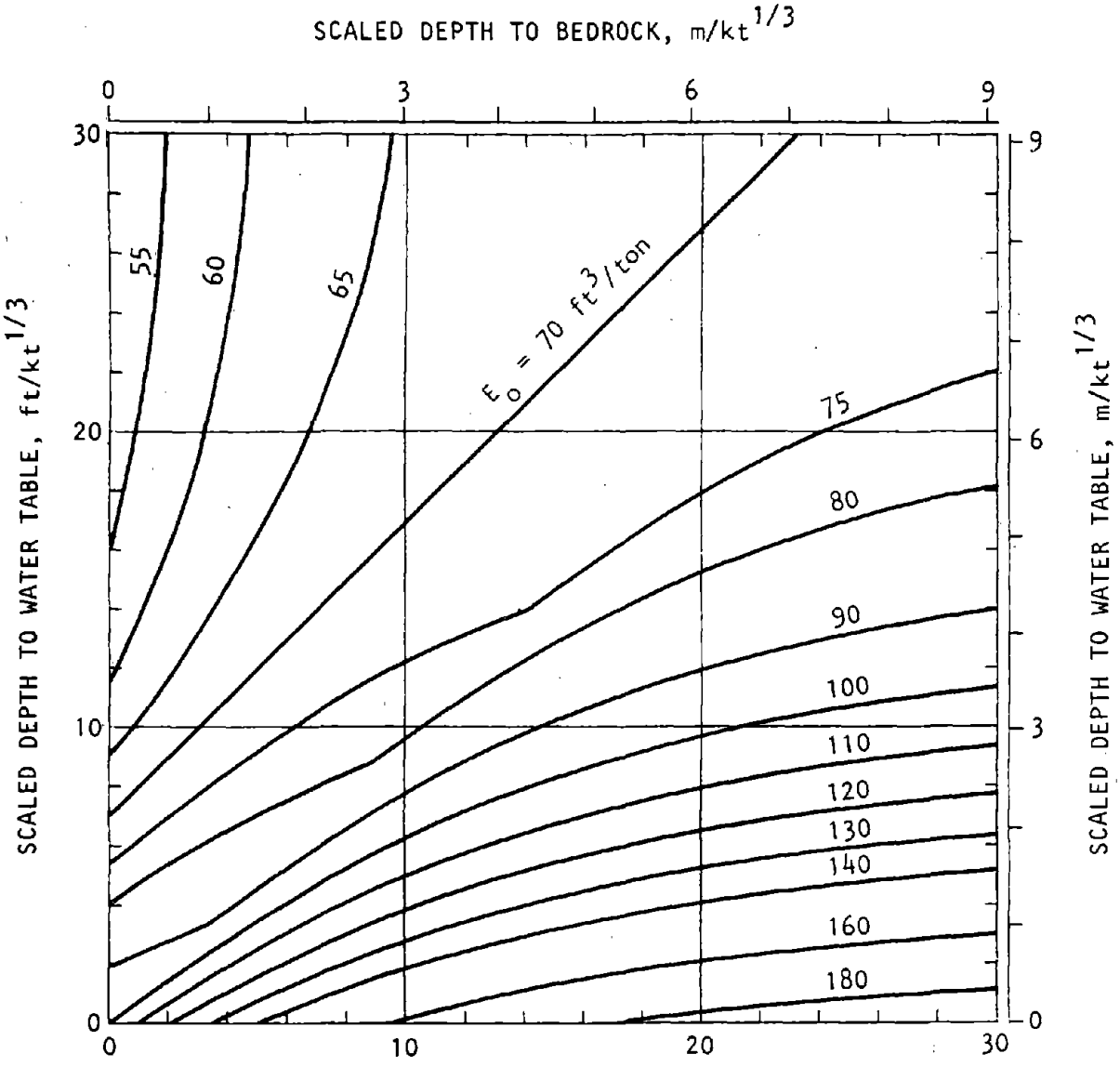

Figure 12-2. High-Yield Nuclear Surface-Burst Cratering Efficiencies in Layered Geologies, Soil over Soft Rock (Shale or Sandstone) with a Water Table (Post, 1974)

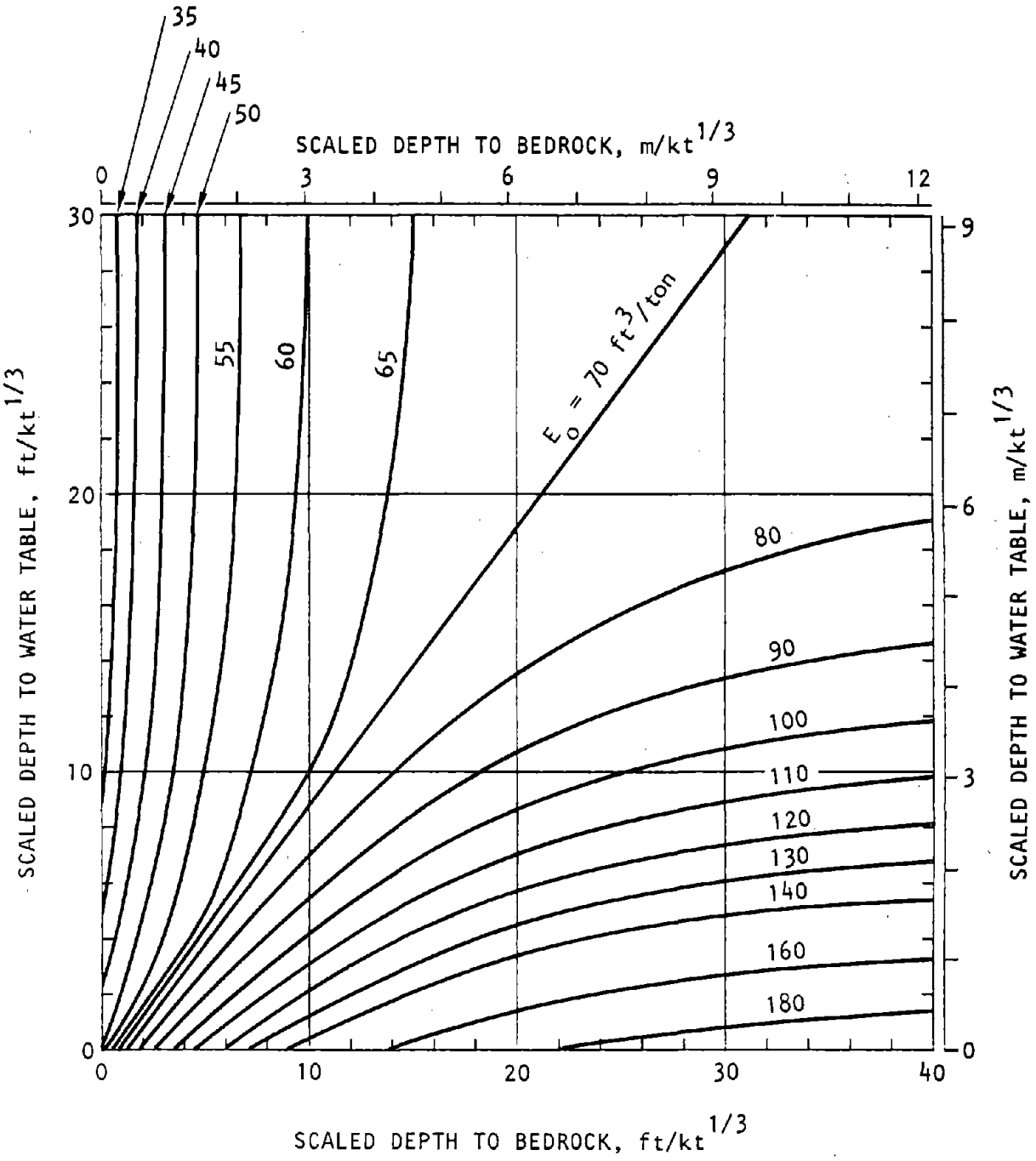

Figure 12-3. High-Yield Nuclear Surface-Burst Cratering Efficiencies in Layered Geologies, Soil over Hard Rock (Limestone) with a Water Table (Post, 1974)

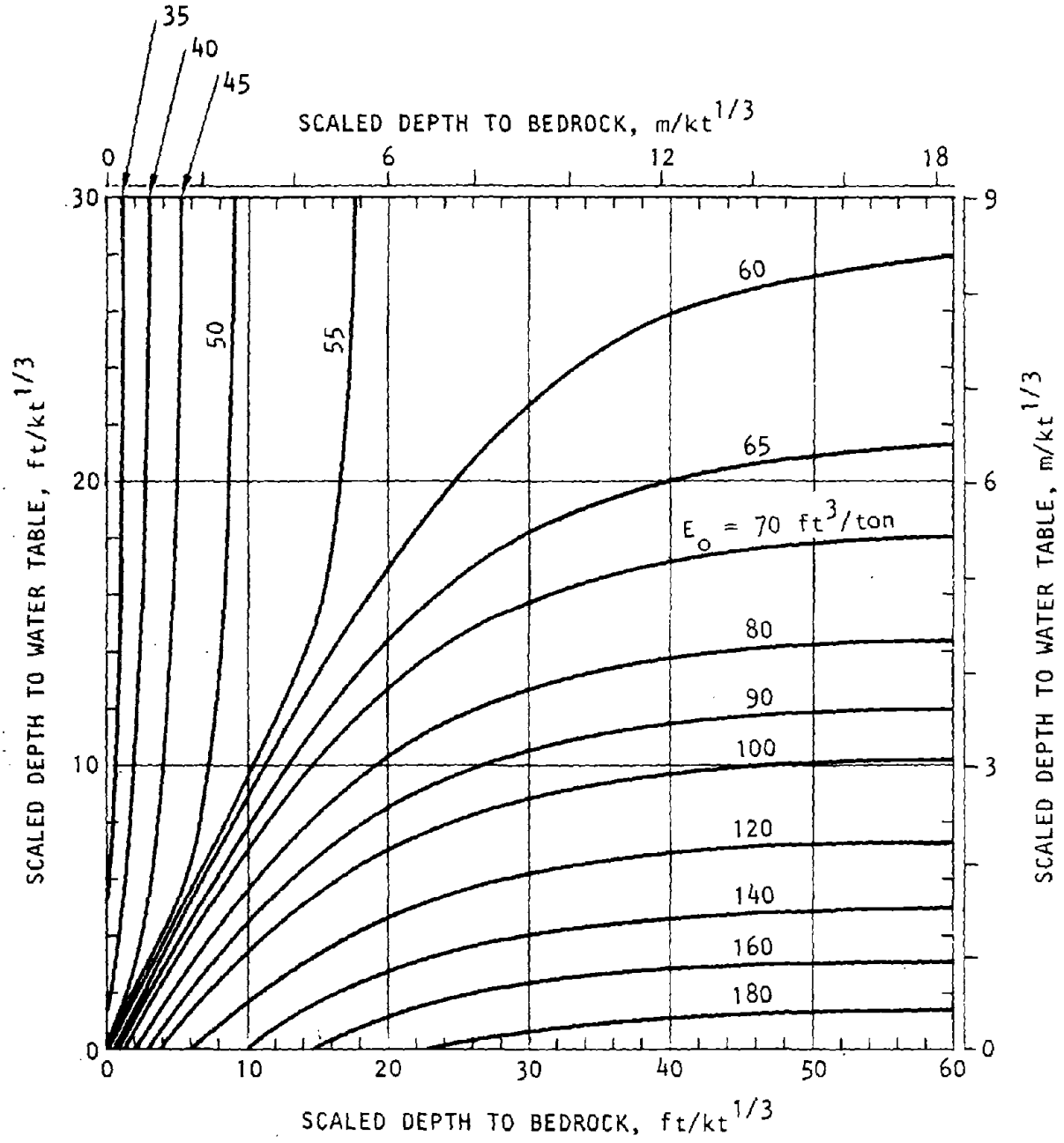

Figure 12–4. High-Yeild Nuclear Surface-Burst Cratering Efficiencies in Layered Geologies, Alluvial Soil over Hard Rock Baser with a Water Table (Post, 1974)

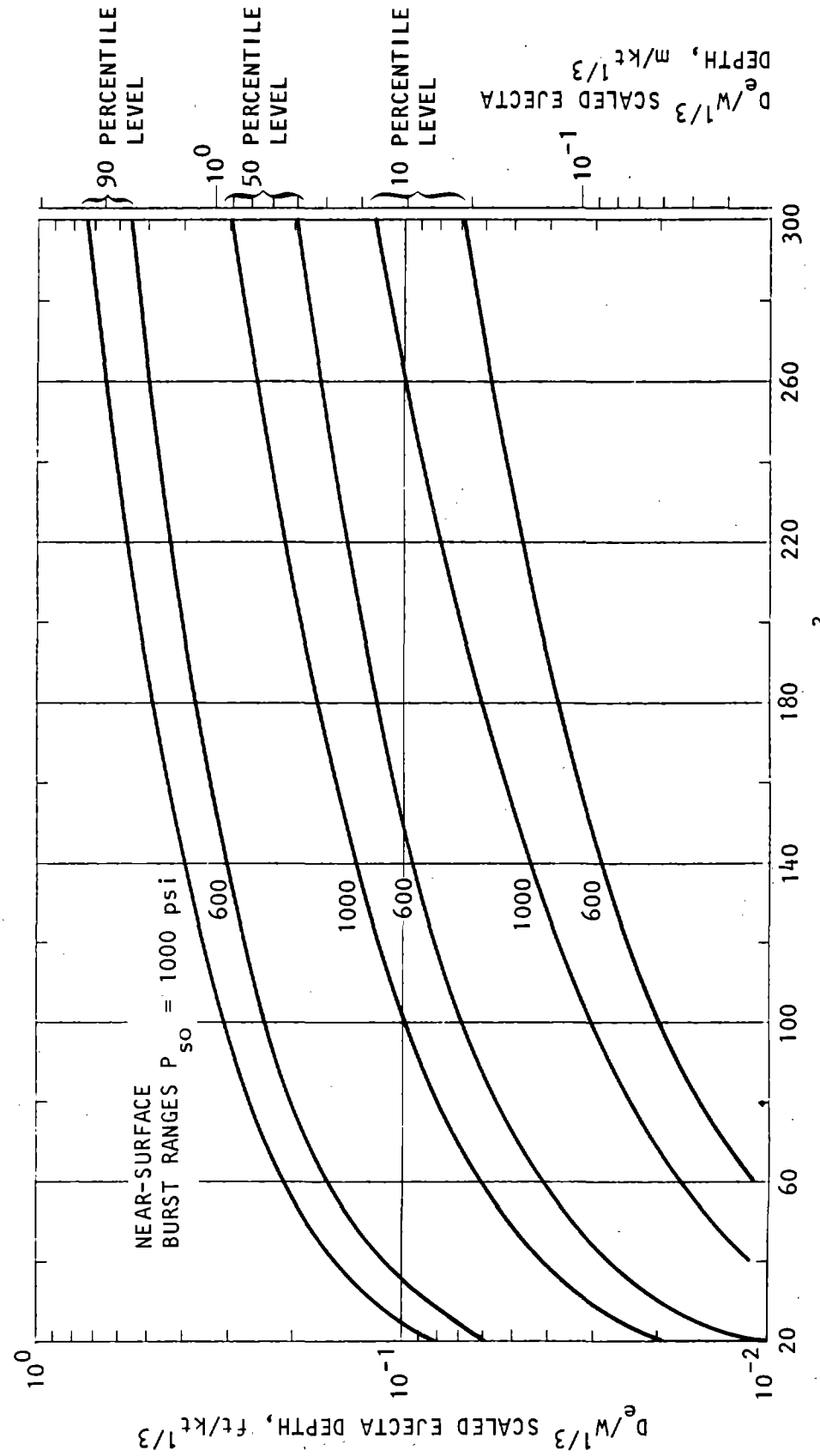

Figure 12-5. Scaled Ejecta Depth Vs. Cratering Efficiency at 600- and 1000-psi Levels (Post, 1974)

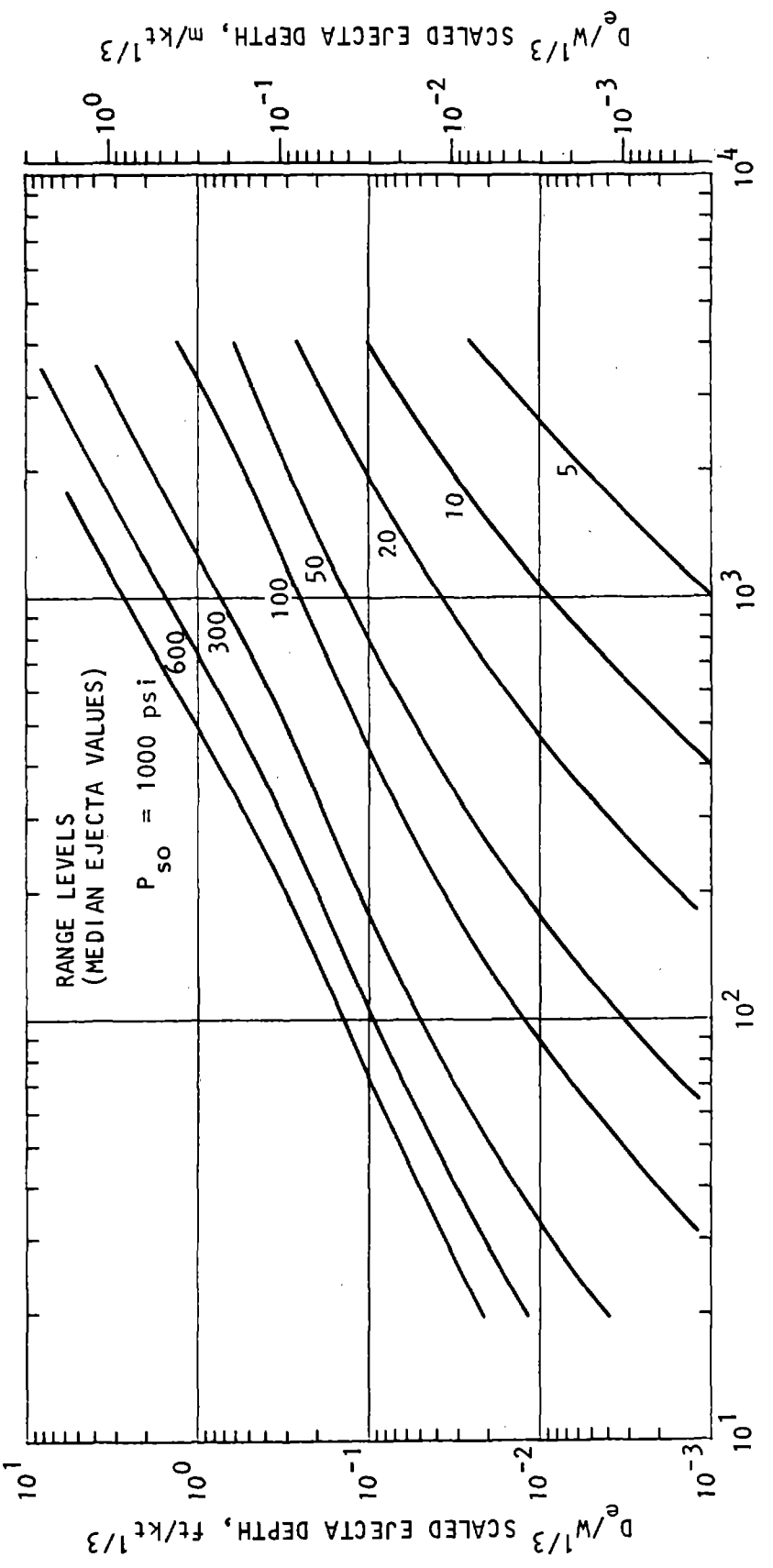

Figure 12–6. Scaled Median Ejecta Depth vs. Cratering Efficiency at Varying psi Levels Post, 1974)

CHAPTER 13
DUST

13-1. Gross phenomenology.

a. Dust is lofted into the air by the deposition of the initial radiation on the ground surface, by the cratering process, by the outward sweep of the airblast across the ground surface, and by the inward sweep of the afterwinds produced by the rising fireball. The lofted dust is quickly partitioned into a low-lying or base surge cloud and a high-altitude or ejecta dust cloud.

b. Only recently have dust clouds been accorded attention by the nuclear weapon effects community. The material presented in this chapter is a synthesis of the literature on the subject (see, for example, Young, 1965; Tewes, 1970; Crawford, 1970; Allison, 1971; Swatosh, 1971; Powers, 1975).

c. The basic variables affecting the potential destructiveness of the free-field dust environment received at a ground surface location of interest here are:

- Weapon yield
- Burst elevation
- Dustiness of the ground surface
- Dustiness of the crater ejecta
- Prevailing winds
- Height of temperature inversion (mixing depth)

Dust effects increase with larger weapon yields, lower heights of burst, dustier ground surfaces, calmer winds, or lower inversion bases.

d. Personnel will rapidly become incapacitated if they breathe the heavily dust-laden air. Appropriate design measures must be taken either to remove the dust from the air or to allow for functioning in a sealed facility. Knowledge of two aspects of the dust cloud are required to implement dust removal measures or button-up procedures:

Particle-size distribution vs. time
Load vs. time

For calculations the ground-surface dust and the ejecta dust are treated separately as though they formed two noninteracting clouds.

13-2. Base-surge dust cloud.

a. Cloud model. The model of the base-surge dust cloud is developed on the assumption that it is instantaneously formed and initially centered at the weapon aim-point. The model is configured as a right circular cylinder of constant radius R and constant height H and in which the initial dust concentration throughout the cloud, ψ_o, undergoes no dilution or diffusion of the cloud with the surrounding air but decreases in concentration due to vertical settlement of the dust particles. The cloud will move horizontally at the prevailing wind velocity.

(1) The cloud radius is given by

$$R = R_1 W^n \tag{13-1}$$

where

R = Cloud radius, m
R_1 = Cloud radius for a 1 Mt burst, m
W = Weapon yield, Mt
n = Constant

(2) The mean radius is obtained from equation 13-1 where R_1 = 3000 m and n = 0.4.

(3) The uncertainty associated with the radius R is

$$\Omega_R^2 = \Omega_f^2 + \Omega_{R_1}^2 + n^2\Omega_W^2 \tag{13-2}$$

where Ω_f is the uncertainty associated with the functional form of R, Ω_{R_1} is the uncertainty parameter associated with R_1, etc. Assume $\Omega_f \approx 0.2$ and $\Omega_{R_1} = 0.2$.

(4) The cloud height is given by

$$H = H_1 W^m \tag{13-3}$$

where

H = Cloud height, m
H_1 = Cloud height for a 1 Mt burst, m
m = Constant

(5) The mean height is obtained from equation 13-3 where H_1 = 100 meters and m = 0.2.

(6) The uncertainty associated with the height H is

$$\Omega_H^2 = \Omega_f^2 + \Omega_{H_1}^2 + m^2\Omega_W^2 \tag{13-4}$$

Assume $\Omega_f \approx 0.2$, $\Omega_{H_1} = 0.2$.

b. Initial dust concentration. Assume that the top ξ meter of dust cover is uniformly dispersed into the cloud. Accordingly, the initial dust concentration is

$$\psi_o = \frac{\xi\varrho}{H} \tag{13-5}$$

where

ξ = Thickness of dust layer on the earth's surface that is dispersed into the cloud, m
ϱ = Density of the in-situ earth layer, g/m^3
ψ_o = Initial dust concentration, g/m^3
H = Dust cloud height (eq. 13-3)

(1) The mean initial dust concentration is obtained from equation 13-5 where ξ = 0.5 m or whatever depth applies to a particular site, and $\bar{\varrho} = 1.0 \times 10^6$ g/m^3.

(2) The uncertainty associated with the initial dust concentration is

$$\Omega^2_{\psi_o} = \Omega^2_f + \Omega^2_\xi + \Omega^2_\varrho + \Omega^2_H \qquad (13\text{–}6)$$

where $\Omega^2_f \approx 0.4$, $\Omega_\xi \approx 0.4$, and $\Omega_\varrho = 0.2$.

c. Vertical settlement speed. The vertical settlement speed of a dust particle is

$$V = \begin{cases} \infty & , \quad a > 1000\ \mu m \\ V_o\left(\dfrac{a}{1000}\right) & , \quad 100 \leqslant a \leqslant 1000\ \mu m \\ V'_o\left(\dfrac{a}{100}\right)^{3.0} & , \quad 10 \leqslant a \leqslant 100\ \mu m \\ 0 & , \quad a < 10\ \mu m \end{cases} \qquad (13\text{–}7)$$

where

a = Particle diameter, μm
V_o, V'_o = Settling speeds for a 1000 μm and 100 μm particle, respectively, m/s

The meaning of $V = \infty$ for $a > 1000\ \mu m$ is that particle sizes larger than 1000 μm are not lofted.

(1) The mean vertical settlement speed of a particle of diameter a is obtained from equation 13–7 where $V_o = 55$ m/s and $V'_o = 5.5$ m/s. Mean settlement speed is plotted in figure 13–1.

(2) The uncertainty associated with the settlement speed is

$$\Omega^2_V = 0.13 \qquad (13\text{–}8)$$

d. Wind transport. Assume that the cloud is transported as a rigid body by the prevailing wind. Assume that the cloud is initially centered above ground zero and thereafter moves with the prevailing wind. Use local wind statistics (contact the National Weather Records Center, operated by the Environmental Services Administration at Ashville, NC, for meteorological data) to determine transport speed and direction of the cloud. Track all clouds that originate in the general vicinity of the point of interest to develop probabilities of their passing over the point of interest. Appropriately account for the "contribution" of each cloud.

e. Particle size vs. time. With the passage of time, progressively smaller and smaller particles settle out of the cloud. In effect, the cloud progressively exhibits a finer distribution of dust. At time

$$t_a = \begin{cases} 0 & , \quad a > 1000\ \mu m \\ \dfrac{H_1 W^{0.2}}{V_o\left(\dfrac{a}{1000}\right)} & , \quad 100 \leqslant a \leqslant 1000\ \mu m \\ \dfrac{H_1 W^{0.2}}{V'_o\left(\dfrac{a}{100}\right)^3} & , \quad 10 \leqslant a \leqslant 100\ \mu m \\ \infty & , \quad a < 10\ \mu m \end{cases} \qquad (13\text{–}9)$$

only particles smaller than diameter a are in the cloud.

(1) The mean value t_a is obtained from equation 13–9 where the mean value of H and V are obtained from *a* (5) and *c* (1) above, respectively. The mean value of equation 13–9 is plotted in figure 13–2.

(2) The uncertainty associated with t_a is

$$\Omega^2_{t_a} = \Omega^2_f + \Omega^2_H + \Omega^2_V \qquad (13\text{–}10)$$

where Ω_H and Ω_V are calculated from equations 13–4 and 13–8. Assume $\Omega_f \approx 0.36$.

f. Load vs. time. The dust load that is entrained into the facility is of critical importance to the designers. The load is determined by integrating the product of the dust concentration and the air-intake-volume rate over the elapsed time of interest:

$$L = \int_{a_1}^{a_2} \int_o^t \psi(a,t)\phi(t)dtda \qquad (13\text{–}11)$$

where

L = Dust load, g
t = Time, s
ϕ = Air-intake-volume rate, m^3/s
ψ = Dust concentration at an arbitrary time t, g/m^3
a_1, a_2 = Size of smallest and largest particles in cloud, m

For the assumption of a constant air-intake-volume rate and of a particle diameter distribution of a^{-4}, the

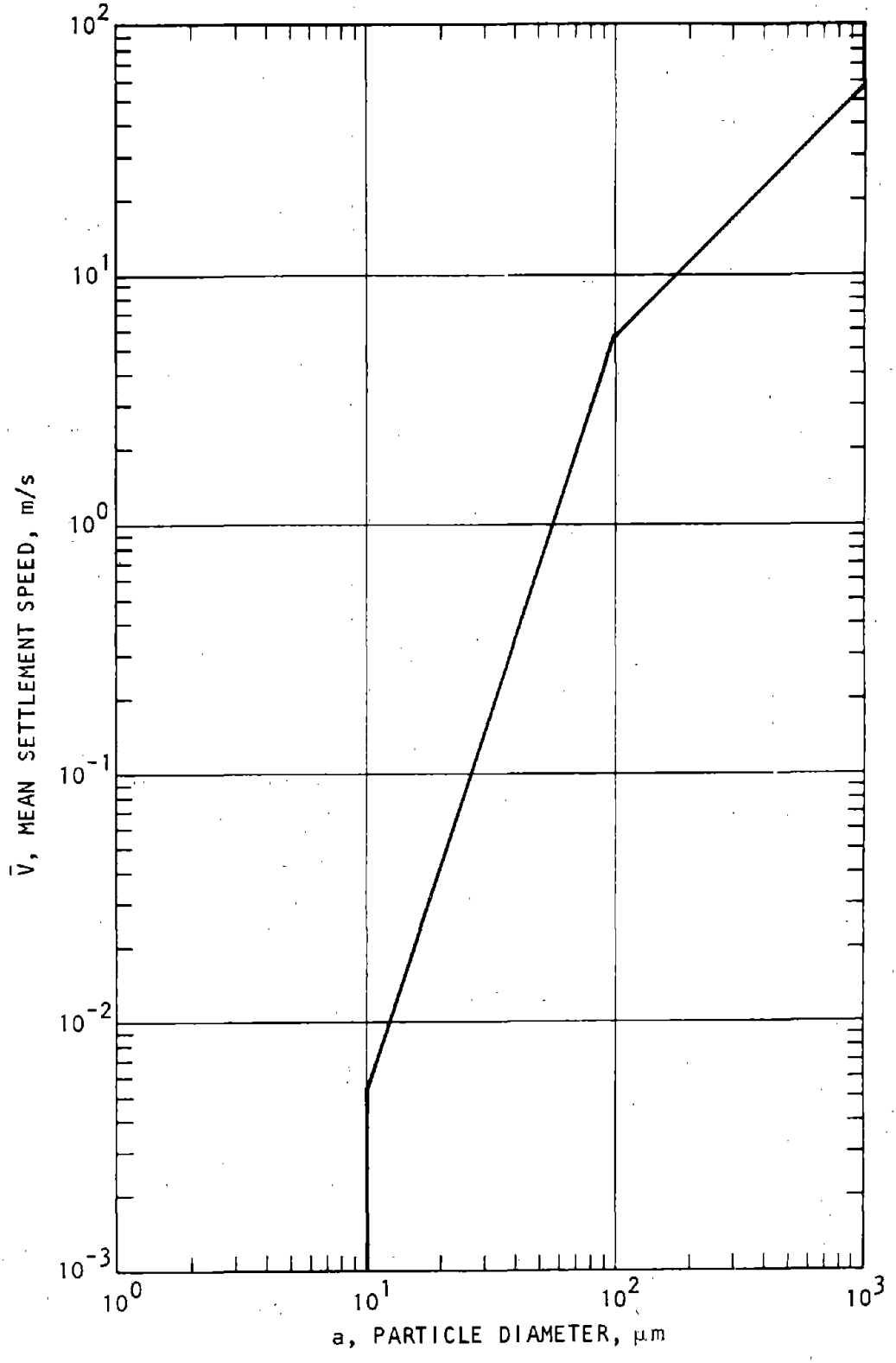

Figure 13–1. Mean Vertical Settlement Speed of Dust Particles.

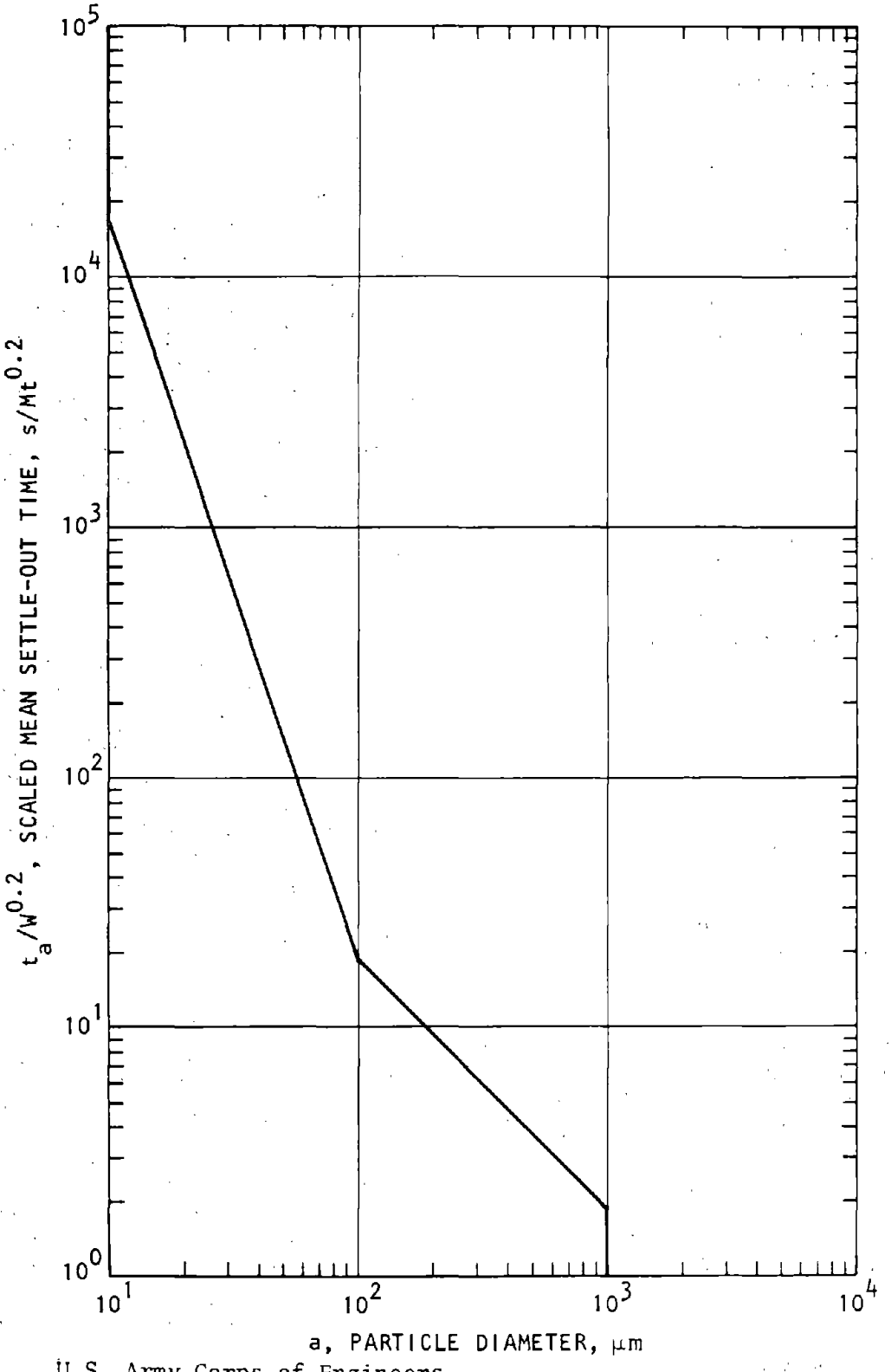

Figure 13–2. Mean Settle-Out Time of Dust Particles—Base Surge

load attributable to particles of diameters $a_1 \leqslant a \leqslant a_2$ is

$$L = \int_{a_1}^{a_2}\int_{0}^{t_1} \psi(a,t)\phi(t)dtda + \int_{a_1}^{a_*}\int_{t_1}^{t_2} \psi(a,t)\phi(t)dtda + \int_{a_1}^{a_{**}}\int_{t_2}^{t_3} \psi(a,t)\phi(t)dtda + \int_{a_1}^{a_o}\int_{t_3}^{t} \psi(a,t)\phi(t)dtda \quad (13\text{–}12)$$

where

$$a_* = \frac{a_2 H}{V_o t}, \text{ m}$$

$$a_{**} = 10\, a_o \left(\frac{H}{V_o' t}\right)^{1/3}, \text{ m}$$

a_o = Smallest particle that settles, m

$$t_1 = \frac{H}{V_o}, \text{ s}$$

$$t_2 = \frac{10H}{V_o}, \text{ s}$$

$$t_3 = \frac{1000\ H}{V_o'}, \text{ s}$$

$$\psi = \frac{\varrho\xi}{aH\ell n(a_2/a_1)}, \text{ g/m}^4$$

(1) The mean load is obtained from equation 13–12 by substituting the appropriate mean values for variables where a_1 = 1 μm a_2 = 1000 μm.

(2) The uncertainty associated with the load L is

$$\Omega_L^2 = \Omega_f^2 + \Omega_\varrho^2 + \Omega_\xi^2 + \Omega_H^2 + \Omega_\phi^2 \quad (13\text{–}13)$$

where $\Omega_f \approx 0.4$, $\Omega_\varrho = 0.2$, $\Omega_\xi = 0.4$, and Ω_H is calculated from equation 13–4.

13–3. Ejecta dust cloud.

a. Cloud model. The ejecta dust cloud model assumes that the cloud instantaneously reaches a height equal to the base of the upper atmosphere temperature inversion (H′) and remains at that height, and that it instantaneously reaches a radius equal to twice the apparent crater radius and thereafter expands radially according to the equation

$$v = v_a\left(\frac{2R_a}{R'}\right)^2 \quad (13\text{–}14)$$

where R_a = apparent crater radius, m; R′ = cloud radius at time t, m; v = cloud radial surge velocity at R′, m/s; v_a = cloud initial radial surge velocity, m/s. The cloud is also assumed to be initially centered at the weapon aim-point and has a uniform initial dust concentration throughout the cloud, ψ_o', which undergoes no dilution or diffusion of the cloud with the surrounding air, except for the horizontal expansion stated in equation 13–14. The cloud maintains a uniform, horizontal dust concentration at all times but the dust concentration decreases due to vertical settlement of the dust particles. The cloud moves horizontally at the prevailing wind velocity.

b. Radius. The cloud radius is

$$R' = (8R_a^3 + 12v_aR_a^2t)^{1/3} \quad (13\text{–}15)$$

where

R_a = Apparent crater radius, m
R′ = Cloud radius at time t, m
t = Time, s
v_a = Cloud initial radial surge velocity, m/s

(1) The mean cloud radius at time t is obtained from equation 13–15 where the mean value of R_a is defined in chapter 10 and V_a = 200 m/s. The cloud will stabilize when the mean surge velocity is very small compared to the mean prevailing wind velocity.

(2) The uncertainty associated with the cloud radius at time t is

$$\Omega_{R'}^2 = \Omega_f^2 + \Omega_{v_a}^2 + \Omega_{R_a}^2 \quad (13\text{–}16)$$

where Ω_f is the uncertainty associated with the functional form of R′, Ω_{v_a} is the uncertainty associated with v_a, etc. Assume $\Omega_f \approx 0.36$ and $\Omega_{v_a} = 0.36$. Refer to chapter 10 for calculation of Ω_{R_a}.

c. Height. The cloud height is equal to the height of the base of the temperature inversion. The mean height (based on a one-year interval) and the uncertainty parameter of the inversion base can be determined from weather statistics.

d. Initial dust concentration. Assume that a fraction of the earth material that comprised the apparent crater volume is uniformly dispersed into the initial ejecta dust cloud. Accordingly, the initial dust concentation is

$$\psi_o' = \frac{f_{HL}f_{1000}V_a\gamma}{\pi(2R_a)^2H'} \quad (13\text{–}17)$$

where

f_{HL} = Fraction of the ejecta dust which is partitioned into the dust cloud
= 0.5 - HOB/500 , $-250 < HOB < 250$ $m/Mt^{1/3}$

f_{1000} = Fraction of the crater ejecta comprising 1000 μm diameter particles and smaller

HOB = Scaled height of burst, $m/Mt^{1/3}$

H′ = Height of the inversion layer above the ground surface, m

V_a = Apparent crater volume, m^3

γ = In situ earth density, g/m^3

(1) The mean initial dust-concentration is obtained from equation 13–17 where the mean values of V_a and R_a are defined in chapter 10. Mean values of f_{1000} and H′ are site specific.

(2) The uncertainty associated with the initial dust-concentration is

$$\Omega^2_{\psi'_0} = \Omega^2_{f_{\psi'}} + \Omega^2_{f_{HL}} + \Omega^2_{f_{1000}} + \Omega^2_{V_a} + \Omega^2_{\gamma} + \Omega^2_{R_a} + \Omega^2_{H'} \qquad (13\text{–}18)$$

where

$$\Omega^2_{f_{HL}} + \Omega^2_{f_f} + \left(\frac{HOB/500}{0.5 - HOB/500}\right)^2 \Omega^2_{HOB} \qquad (13\text{–}19)$$

and in which $\Omega_{f_{\psi'}} \approx 0.36$, $\Omega_{\gamma} = 0.17$, and $\Omega_{f_f} \approx 0.36$.

e. Vertical settlement speed. Paragraph 13–2*c* (for base-surge dust) is applicable.

f. Wind transport. Paragraph 13–2*d* is applicable. However, remember that the ejecta dust cloud radius is not constant but is increasing with time as defined in the model *a* above.

g. Particle size vs. time. Paragraph 13–2*e* is applicable when H is replaced by H .

h. Load vs. time. The form of equations 13–11 and 13–12 remain unchanged; however, utilize the following values of the parameters:

$$a_* = \frac{a_2 H'}{V_o t}, \text{ m}$$

$$a_{**} = \frac{a_2}{10}\left(\frac{H'}{V_o t}\right)^{1/3}, \text{ m}$$

$$t_1 = H'/V_o, \text{ s}$$

$$t_2 = 10\ H'/V_o, \text{ s}$$

$$t_3 = 1000\ H'/V'_o, \text{ s}$$

$$\psi = \frac{f_{HL}\ f_{1000}\ V_a \gamma}{\pi a H'\ R_a^2 \left(8 + \frac{12\ v_a t}{R_a}\right)^{1/3} \ln a_2/a_1}$$

$$R_a = 1.2\ V_a^{1/3}$$

$$f_{1000} = \frac{\ln (a_2/a_1)}{\ln (a_\ell/a_1)}$$

(1) The mean value of the ejecta dust cloud is obtained from equation 13–12 when a_ℓ = largest lofted ejecta particle ≈ 18 m, a_1 = 1 μm, a_2 = 1000 μm.

(2) The uncertainty associated with the ejecta dust cloud is

$$\Omega^2_L = \Omega^2_f + \Omega^2_{HL} + \Omega^2_H + \Omega^2_{\gamma} + \frac{1}{9}\Omega^2_{V_a} \qquad (13\text{–}20)$$

where $\Omega_f \approx \Omega_{HL} = 0.36$, $\Omega_{H'} \approx 0$, $\Omega_{\gamma} = 0.05$, and Ω_{V_a} is obtained from equations 12–9 or 12–10.

CHAPTER 14
FIRESTORM

14-1. Gross phenomenology.

a. A firestorm, which can develop from the uniting of the many small fires started by the thermal radiation pulse, represents the most violent type of mass fire. The thermal convection column and strong ground-level winds blowing inward restrict growth of the fire, but intensify the burning. Firewhirls or fire cyclones may develop during the intensified burning phase. Full development of a firestorm can occur in an hour; burnout may not occur for several hours.

b. A firestorm results in oxygen depletion, elevation of ground and air temperatures (several hundred K), reduced or enhanced atmospheric pressures, and massive air pollution. Appropriate design measures must be taken, either to alter the site fuel-density characteristics sufficiently to reduce the probability of a firestorm to a safe level, or to provide the facility with heat shields and semi-closed-cycle ventilation, life support, and combustion air systems for the duration of the firestorm. The designer must know the density of the site fuel, the types of fuel, and the conditions that will ignite the fire in the thermal radiation environment (chap. 6).

c. After a nuclear burst, the likelihood that a firestorm will develop is a function of:

- Weapon yield
- Burst elevation
- Slant range
- Weather conditions
- Fuel density and kindling type

The first three factors primarily affect ignition through their influence on incident radiant energy (see paragraph 6-2, Radiant Exposure). The other factors account for the availability and condition of fuel.

14-2. Weather conditions.

Firestorms can occur in the dry season and if wind velocities are less than 8 ft/s (2.4 m/s), a calm wind. Climatological data of a facility site are required to estimate need for protection and level of protection against firestorms.

14-3. Fuel density.

a. Conditions. Prerequisites for a firestorm are:

- Gross area aflame > 300 acres
- Net fueled area ÷ gross area > 25 percent
- Firebreaks < 50 ft wide
- Fuel density (based on gross area) > 175 tons/acre
- Sufficient kindling/tinder available so that 10 cal/cm^2 of incident nuclear radiation will cause ignition

A near-surface burst of > 10 kt will produce 10 cal/cm^2 (4.184×10^5 J/m^2) radiation intensity at sufficient distances to ignite 300 acres for virtually all dry-season preattack conditions.

b. Spontaneous ignition. Spontaneous ignition of kindling occurs when the incident energy density exceeds specific values. Thus when

$$Q_t > Q_0 \qquad (14\text{-}1)$$

ignitions will occur; if the conditions specified in *a* above are present, the fire will become a firestorm. The value of Ω_t in equation 14-1 is obtained from equation 6-16 in chapter 6 of this manual for a time of t_{max} as defined below. The value of Ω_0 is also determined below.

(1) Ignition thresholds for dry kindling materials are expressed with equations of the form (Kerr, 1971)

$$Q_0 = -K_1 \frac{\varrho cL}{a}\left(\tau - K_2\right)^n + \frac{K_3 H_c t_{max}}{a} \qquad (14\text{-}2)$$

where

Q_0 = Ignition threshold radiant exposure, cal/cm^2

ϱc = Volumetric heat capacity, cal/°C/cm^3

L = Thickness of the material, cm

a = Absorptivity of material

$\tau = \dfrac{\sqrt{\alpha t_{max}}}{L}$

α = Thermal diffusibility of the material, cm^2/s

H_c = Critical irradiance, cal/cm^2/s

t_{max} = Time to maximum temperature $\approx 0.032\ W^{0.5}$, s/kt$^{1/2}$

W = Weapon yield, kt

K_1, K_2, K_3, and n are constants

For moist fuels, equation 14-2 is modified by the factor $1 + h\sqrt{\varrho L}$ so that

$$Q_{0_m} = \left(1 + h\sqrt{\varrho L}\right)Q_0 \qquad (14\text{-}3)$$

where h = relative humidity in percent.

(2) Mean values for parameters related to wildland fuels are presented in table 14–1 for use in equations 14–2 and 14–3. In addition, the following restrictions prevail:

$$K_1 = \begin{cases} -750, \\ -2250, \\ -1522, \end{cases} \quad K_2 = \begin{cases} 1, \\ 0, \\ 0, \end{cases} \quad K_3 = \begin{cases} 0, \\ 0, \\ 2.6, \end{cases}$$

$$n = \begin{cases} 1, & \tau < 0.25 \\ 1, & 0.25 < \tau < 0.52 \\ 0.4, & \tau \geq 0.52 \end{cases}$$

The value of H_c is generally not a fixed value for all fuels but is dependent on the opacity and geometry. However, a value of 0.4 cal/cm^2/s (1.7×10^4 J/m^2/s) can be used in lieu of specific values measured in the laboratory.

(3) The uncertainty associated with equation 14–2 can be reasonably expressed by

$$\Omega^2_{Q_0} = \Omega^2_f + \frac{K_1^2(\varrho c)^2 \Gamma^{2n}}{Q^2_0 a^2} \left\{ 2L^2 + L^2 \left[\frac{n}{\Gamma L} - 1 \right]^2 + \left[L - \frac{K_3 H_c t_{max}}{K_1 \varrho c \Gamma^n} \right]^2 + t^2_{max} \left[\frac{n}{2\Gamma} \sqrt{\frac{\alpha}{t_{max}}} - \frac{K_3 H_c}{\Gamma^n K_1 \varrho c} \right]^2 + \frac{\alpha n^2 t_{max}}{4\Gamma^2} + \frac{K_2^2 L^2 n^2}{\Gamma^2} + \frac{2K_3^2 H_{c\,max}^2 t^2_{max}}{(\varrho c)^2 K_1^2 \Gamma^{2n}} \right\} \Omega_{C_o} \qquad (14\text{–}4)$$

in which $\Gamma = \dfrac{\sqrt{\alpha t_{max}}}{L} - K_2$

and where Ω_f is the uncertainty of the functional form of equation 14–2 or 14–3, Ω_{K_1} is the uncertainty of the constant K_1. For moist kindling, and to a first approximation, the uncertainty associated with equation 14–3 is

$$\Omega^2_{Q_{0m}} = \Omega^2_{Q_0} + \frac{\varrho h^2 Q_0^2 L}{\Omega^2_{0_m}} \left(\frac{\Omega^2_{C_o}}{2} + \Omega^2_h \right) \qquad (14\text{–}5)$$

where $^2_{Q_0}$ is taken from equation 14–4 and Ω_h is the uncertainty of the value of the humidity.

(4) Using existing experimental data, it is not practical to evaluate the various uncertainties associated with the various parameters in equations 14–2 and 14–3. Instead, it is recommended that the calculated values for Q_0 and Q_{0_m} be increased by the factor 1.15 and that $\Omega_f \approx 0.2$ be used based on the data presented in table 14–2, in which the mean and standard deviation (exclusive of the wheat-straw data) were used to estimate the bias and scatter between calculated and experimental data. Assume $\Omega_{C_o} \approx 0.2$.

Table 14-1. Physical and Thermal Properties of Wild Land Fuels (Kerr, 1971)

Fuel Materials	Thermal Diffusivity, α $10^{-3}\ \frac{cm^2}{s}$	ρcL $10^{-3}\ \frac{cal}{^oC \cdot cm^2}$	Absorptivity,* a Dimensionless	$(\rho L)^{1/2}$ $\frac{g^{1/2}}{cm}$
Grasses and Other Fine Fuels				
Horsehair lichen (*Alectoria jubata*)	1.90	0.39	0.4	9.75×10^{-4}
Cheatgrass seedpod (*Bromus tectorum*)	2.12	0.33	0.3	1.11×10^{-3}
Wiregrass (*Aristrida stricta*)	1.88	1.41	0.5	2.8×10^{-3}
Desert stipa (*Stipa* spp.)	1.98	1.11	0.4	2.8×10^{-3}
Cheatgrass leaves (*Bromus tectorum*)	2.35	0.82	0.3	2.7×10^{-3}
Harding grass (*Phalaris tuberosa* var *stenoptera*)	2.10	1.76	0.5	3.5×10^{-3}
Sedge (*Carex geyeri*)	1.96	2.60	0.5	5.2×10^{-3}
Wheat straw (*Triticum* spp.)	2.14	3.89	0.6	6.5×10^{-3}
Cheatgrass stalks (*Bromus tectorum*)	2.12	5.73	0.3	1.9×10^{-2}
Hardwood and Shrub Leaves				
Beech (*Fagus* spp.)	2.10	1.05	0.6	1.76×10^{-3}
Chestnut oak (*Q. montana*)	2.12	2.00	0.8	2.5×10^{-3}
Scarlet oak (*Q. coccinea*)	1.92	3.19	0.8 0.7	4.0×10^{-3} 4.6×10^{-3}
Lauraceae-S.E. Asia (*Lauraceae* spp.)	2.03	3.04	0.7	4.3×10^{-3}
Litsea (*Litsea* spp.)	2.16	2.18	0.6	3.6×10^{-3}
Rhododendron (*Rhododendron catawbiense*)	1.97	3.75	0.8	4.7×10^{-3}
Madrone (*Arbutus menziesii*)	2.04	3.79	0.8 0.6	4.7×10^{-3} 6.3×10^{-3}
Arrowleaf balsam root (*Balsamorhiza sagittata*)	2.37	2.02	0.7	2.9×10^{-3}
Oregon grape (*Berberis repans*)	2.15	3.16	0.6	5.3×10^{-3}
Service berry (*Amelanchier* spp.)	2.14	3.36	0.6	5.6×10^{-3}
Messmate stringybark (*Eucalyptus obliqua*)	1.92	5.57	0.8	7.0×10^{-3}
Conifer Leaves and Needles				
Western larch (*Larix occidentalis*)	1.90	4.1	0.7	5.9×10^{-3}
Redwood (*Sequoia sempervirens*)	2.06	5.79	0.8	7.2×10^{-3}
Western red cedar (*Thuja plicata*)	2.06	6.15	0.8	7.7×10^{-3}
Chamise (*Adenostoma fasciculatum*)	2.14	5.78	0.6	9.6×10^{-3}
Douglas-Fir (*Pseudotsuga menziesii*)	1.94	9.75	0.8	12.2×10^{-3}
Shortleaf pine (*Pinus echinata*)	1.96	9.05	0.8	11.3×10^{-3}
Lodgepole pine (*Pinus contorta*)	1.94	10.4	0.8	13.0×10^{-3}
Coulter pine (*Pinus coulteri*)	2.03	9.12	0.8	11.4×10^{-3}
Ponderosa pine (*Pinus ponderosa*)	1.96	10.6	0.8	1.32×10^{-2}
Engelmann spruce (*Picea engelmannii*)	1.93	12.4	0.7	1.8×10^{-2}

*When two values are given in this column and the one following it, the lower value of the absorptivity (and hence the larger value of $\rho cL/a$) are for newly fallen leaves. All other values are for weathered materials. Few of these absorptivities have actually been measured. Most are estimated from the appearance of the material.

Table 14-2. Comparison of Weapon-Test Data with Predictions Based on Correlation Model (Kerr, 1971)

			Materials																
			Horsehair Lichen		Cheatgrass		Desert Needlegrass		Wheatstraw		Beech Leaves, Weathered		Madrona, Weathered		Coulter Pine Needles		Ponderosa Pine Needles		
			Ignition Thresholds, cal/cm^{-2}																
Weapon Test	Yield, kt	t_{max}, s	Test Data*	Calc. Values	Test Data*	Calc. Values**	Test Data*	Calc. Values**	Test Data*	Calc. Values	Test Data*	Calc. Values	Test Data*	Calc. Values	Test Data*	Calc. Values‡	Test Data*	Calc. Values§	**
Buster																			
Easy	31	0.190					3.7 (4)	7.5	4.6 (6)	9.5							11.1 (7)	10.4	9.6
Snapper																			
3	31	0.185	5 (7.9)	5.1	4.3 (7.1)	5.2	3.0 (#)	8.3	>8.9 (6.3)	9.6	3.4† (9.5)	5.2	6.1 to 7.3 (9.0)	8.3	7.3 to 8.9 (7.4)	9.6	7.3 to 8.9 (7.4)	10.4	9.7
4	19	0.155	5.3 (14)	5.7	6.6 (10.6)	5.4			8.2 (10.1)	9.8	5.3 (13.6)	5.4	5.3 to 6.6 (11.9)	8.6	10.8 (11.4)	9.6	8.2 to 10.8 (12.6)	10.8	9.9
Upshot/Knothole																			
4	11	0.103															4.8 (5.4)	9.4	6.8
9	26	0.179															6.3 to 7.7 (4.4)	9.5	8.8
10	15	0.138															9.5 (5.8)	9.2	8.0

* Estimated moisture contents (expressed as percent of dry weight) are given in parentheses.
** Calculated values are based on finest particles.
† Possibly a spurious value. Other samples located to receive exposures up to 7.3 cal cm^{-2} didn't ignite.
(#) Unknown but assumed to be 8% for purposes of calculation.
‡ Based on average thickness of needles
§ Based on thinnest needles

CHAPTER 15
RESIDUAL NUCLEAR RADIATION

15-1. Gross phenomenology.

a. Radiation emitted later than one minute after detonation is defined as residual. Residual radiation is composed of fission-product reactions and neutron reactions from fallout and of the neutron-induced gamma rays discussed in chapter 3. Fallout is the most significant contribution for most burst conditions of interest; it is separated into the early phase (which settles within 24 hr) and the delayed phase (which settles after 24 hr). Early fallout has military significance because exposure to such fallout may debilitate humans—they must be protected during those periods when the radiation intensity poses a threat. The design requires both dose rate and accumulated dose (Glasstone, 1977). Neutron-induced soil activity (chap. 3) should be considered for burst elevations less than 75 $ft/kt^{0.35}$.

b. Effects of residual nuclear radiation depend on:
- Weapon design
- Weapon yield
- Burst elevation
- Range
- Climatic conditions
- Soil composition

15-2. Early fallout.

a. Air bursts. Except for the phenomenon of rain-out (para. 15-4), dispersion of radioactive debris from an air burst before it reaches the ground is usually sufficient to preclude a hazard of military significance.

b. Surface bursts. Deposited radioactivity during the first day after detonation of a surface burst can extend for several hundred miles. Dose-rate contours for the environment one hour after burst over ideal surfaces can be prepared, as shown in figure 15-1, from the data presented in figures 15-2 through 15-11. For reasonably level terrain, the values given in these figures should be multiplied by 0.7; rough and hilly terrain requires the data to be multiplied by a factor of 0.5 to 0.6. The effective wind is the average of the net wind vectors at the top and bottom of the stabilized cloud, as defined in figures 15-12 and 15-13. The net wind vectors should be obtained from a plot of the wind vectors (hodograph) as a function of altitude (fig. 15-14, for example). The hodograph should be plotted for equal increments of altitude. The net wind vectors are the vectors extending from zero elevation to the points on the hodograph corresponding to the top and bottom of the stabilized cloud. For example, the net wind vectors and effective wind for a typical blast are superimposed on the hodograph of figure 15-14.

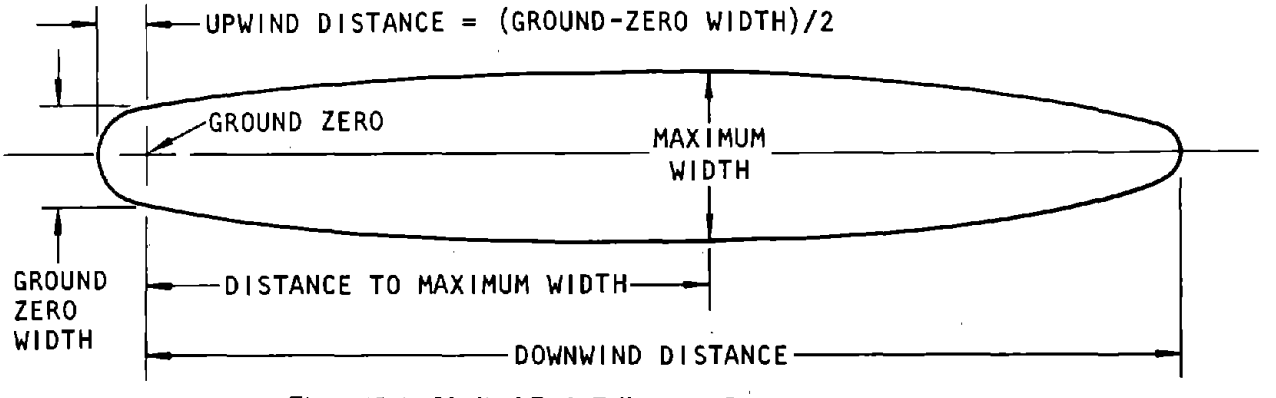

Figure 15-1. Idealized Early Fallout Dose-Rate Contour (DNA, 1972)

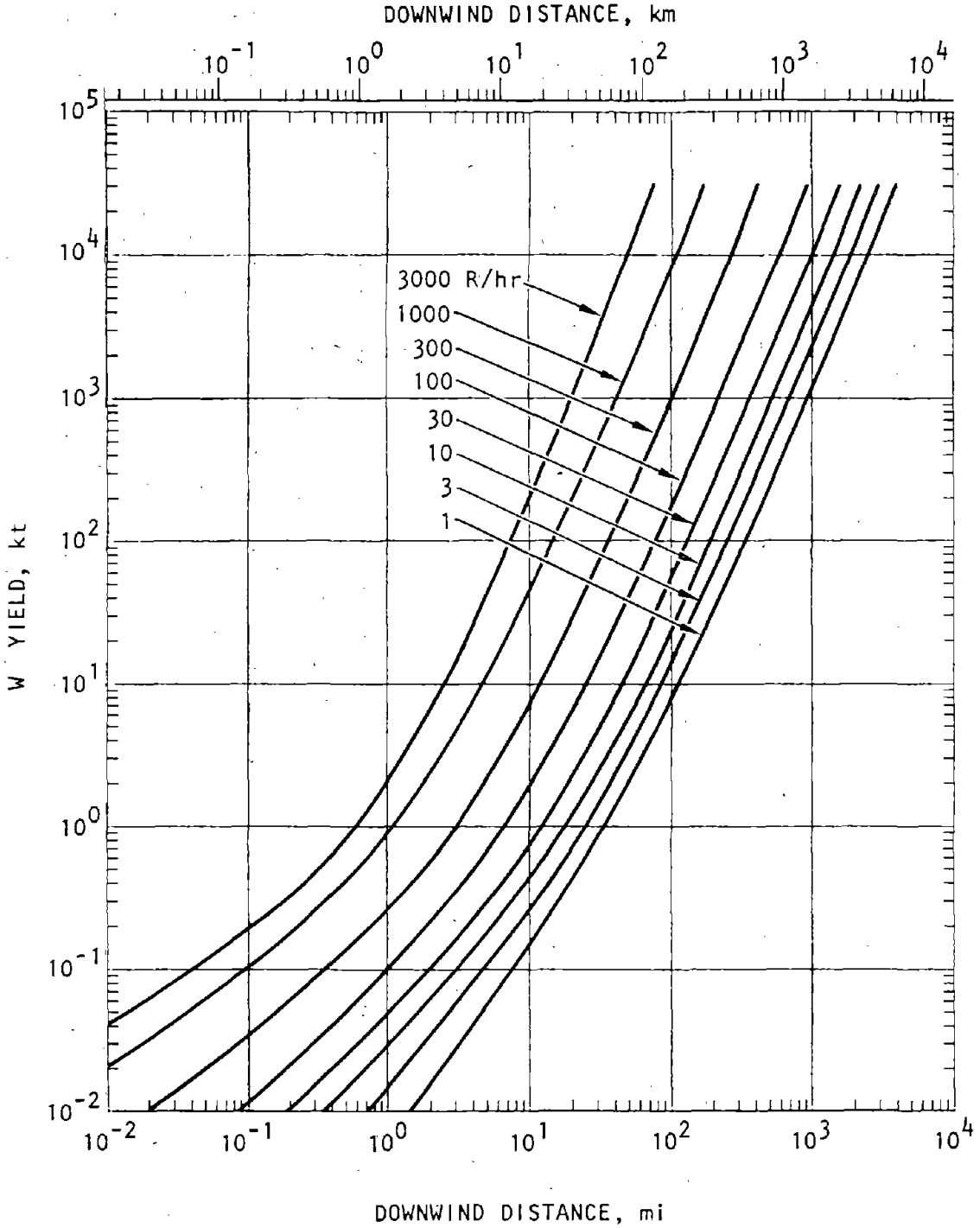

Figure 15-2. Downwind Distance and Fallout Radiation at t = 1 Hr After Burst as a Function of Yield, 10-Knot Effective Wind (DNA, 1972)

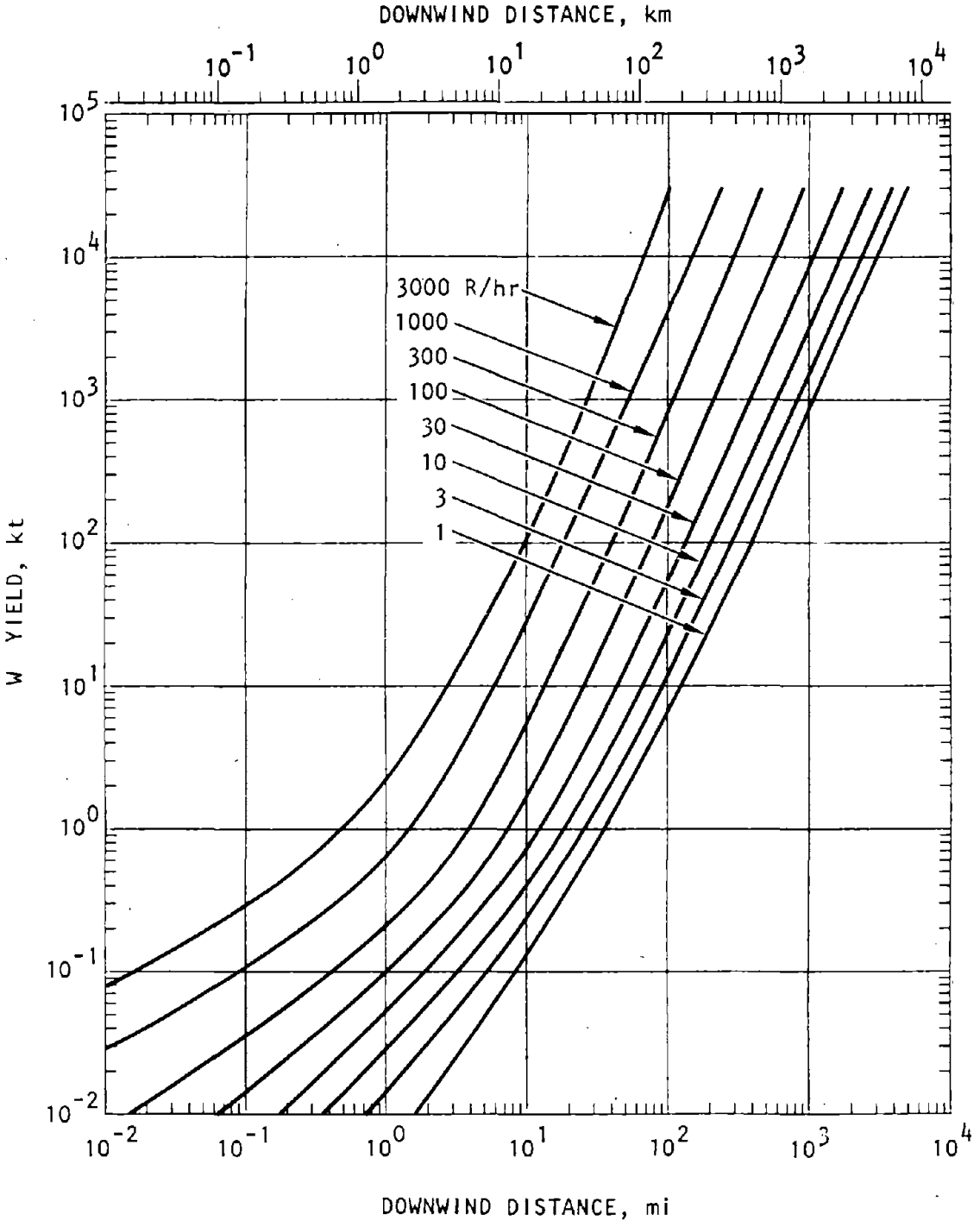

Figure 15–3. Downwind Distance and Fallout Radiation at t = 1 Hr After Burst as a Function of Yield, 20-Knot Effective Wind (DNA, 1972)

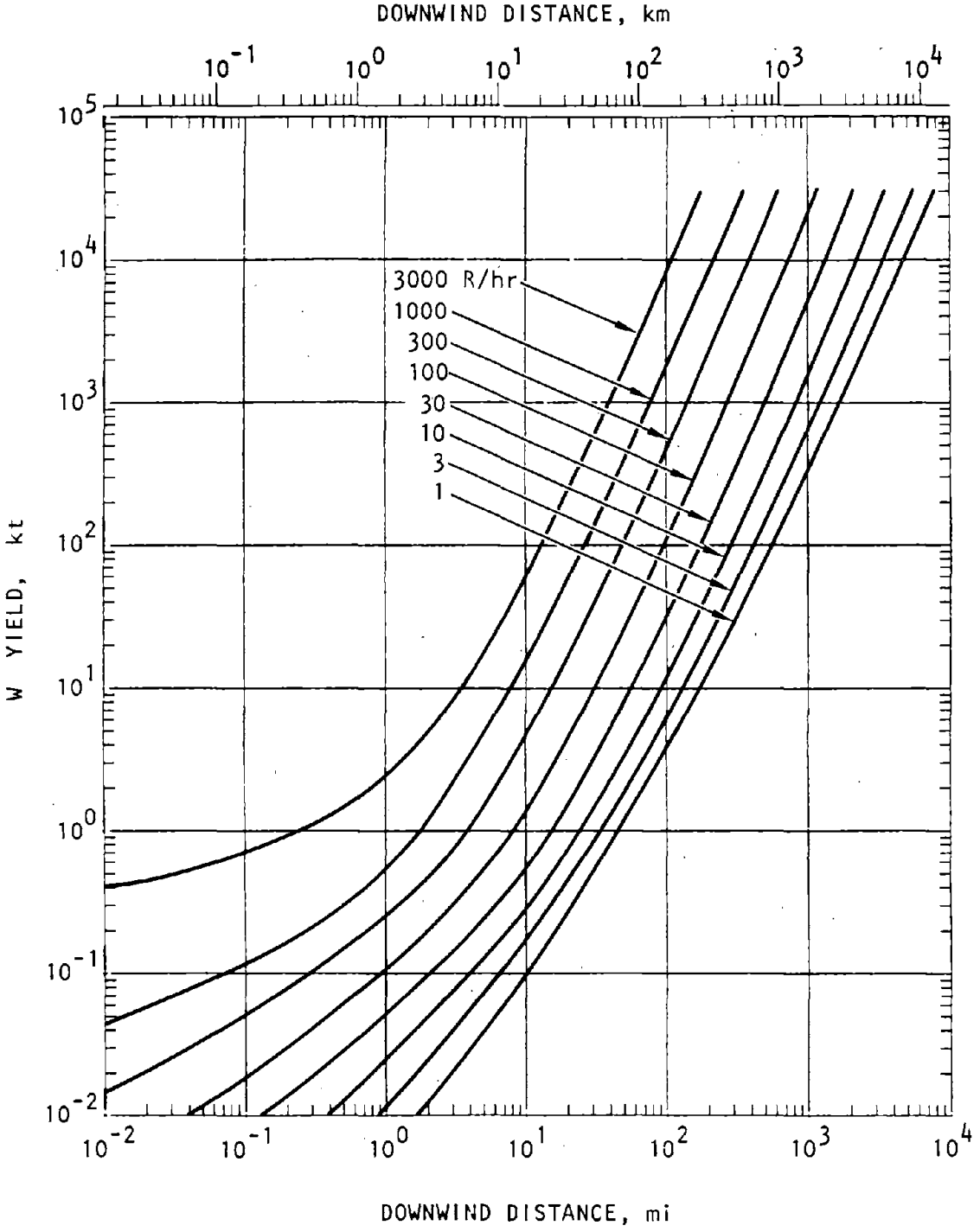

Figure 15–4. Downwind Distance and Fallout Radiation at t = 1 Hr After Burst as a Function of Yield, 40-Knot Effective Wind (DNA, 1972)

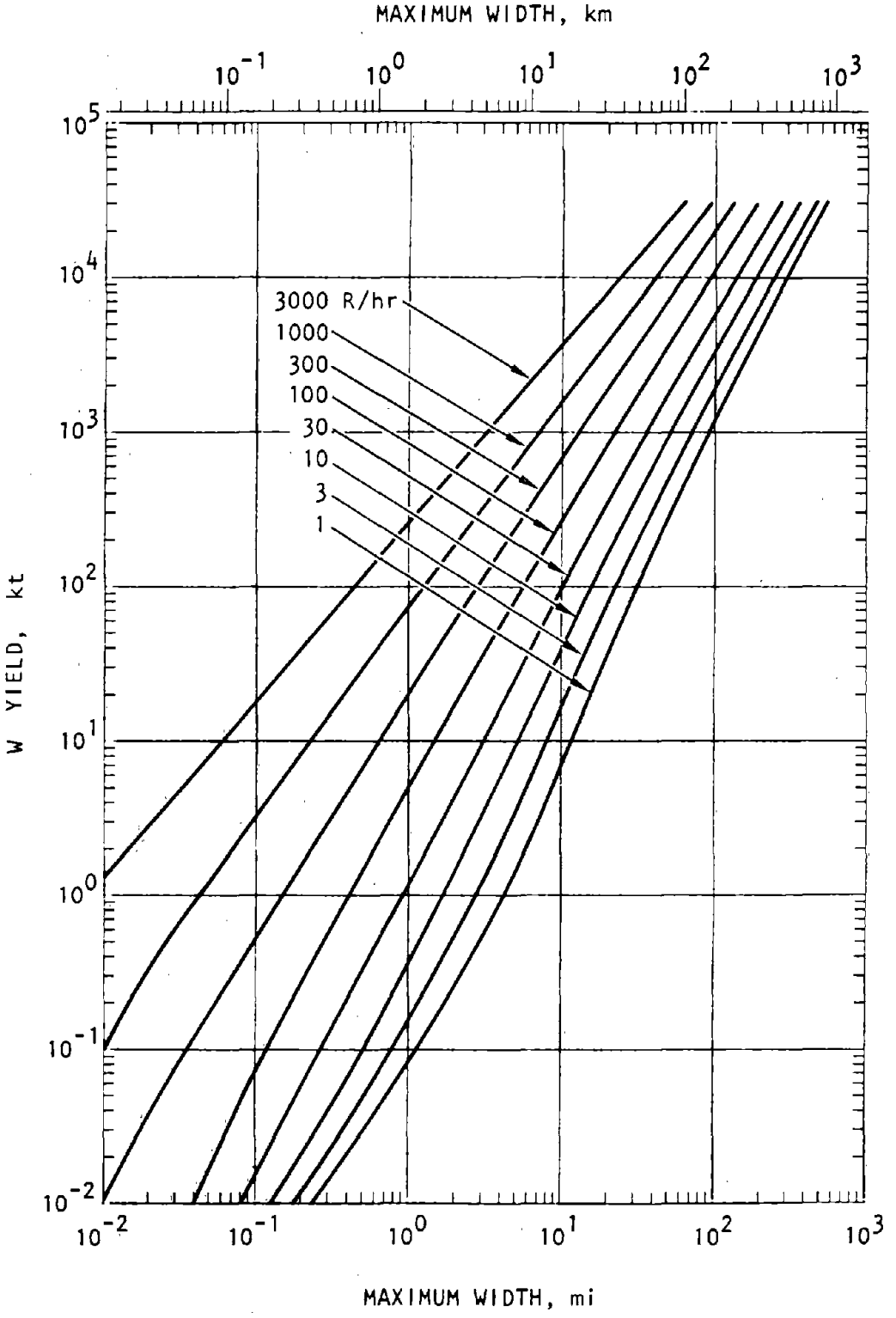

Figure 15–5. Maximum Width and Fallout Radiation at t = 1 Hr After Burst as a Function of Yield, 10-Knot Effective Wind (DNA, 1972)

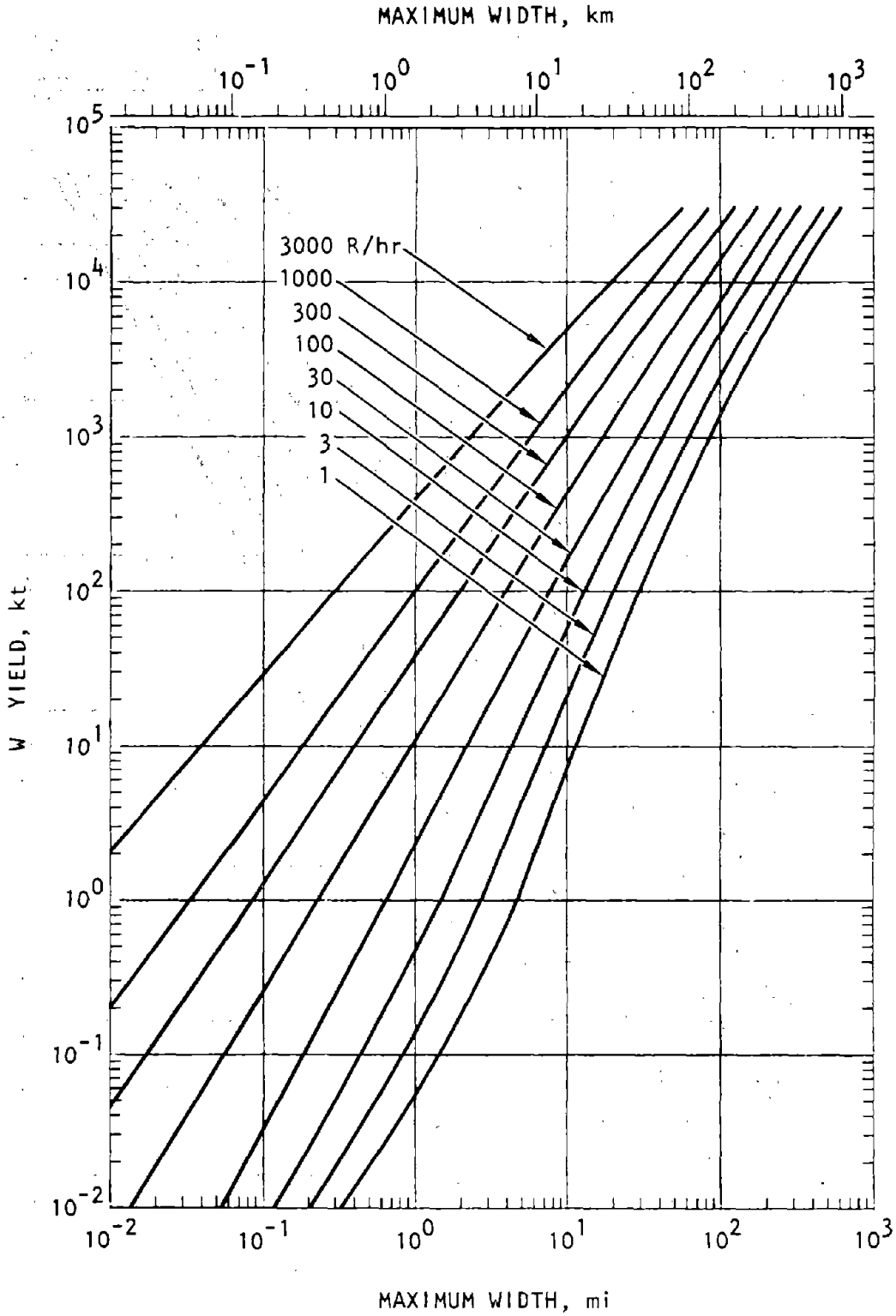

Figure 15–6. Maximum Width and Fallout Radiation at t = 1 Hr After Burst as a Function of Yield, 20-Knot Effective Wind (DNA, 1972)

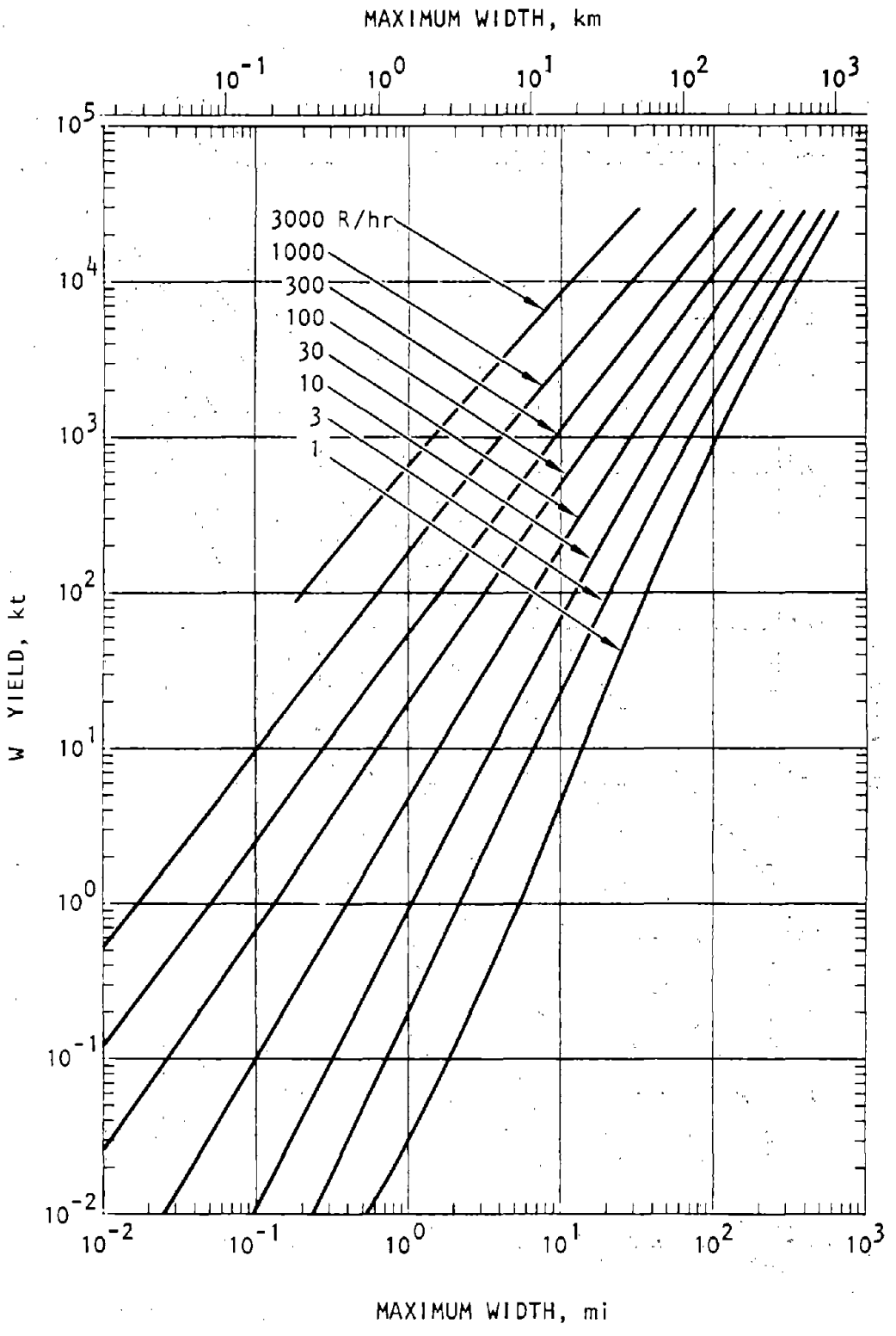

Figure 15–7. Maximum Width and Fallout Radiation at t = 1 Hr After Burst as a Function of Yield, 40-Knot Effective Wind (DNA,

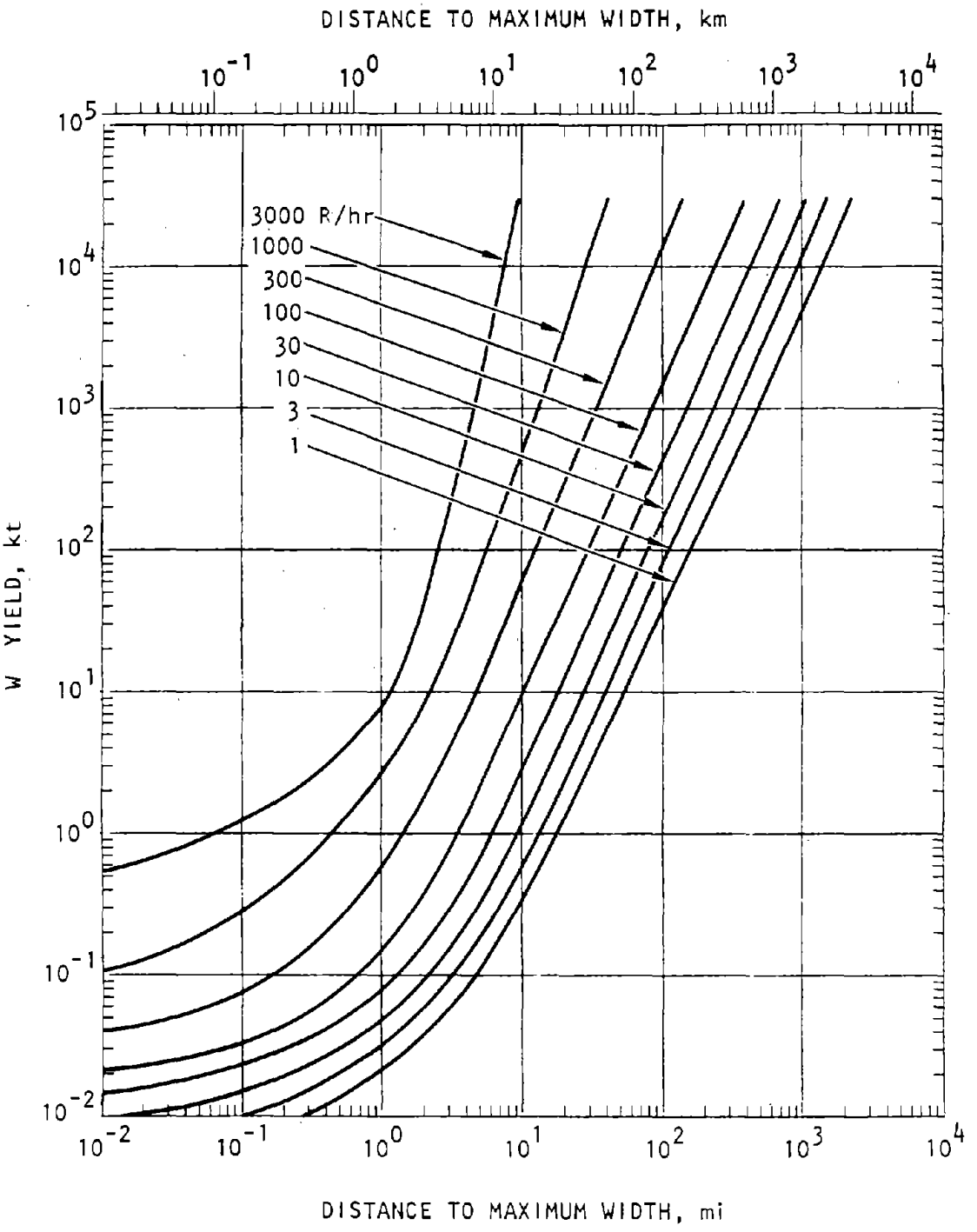

Figure 15-8. Distance to Maximum Width and Fallout Radiation at t = 1 Hr After Burst as a Function of Yield, 10-Knot Effective Wind (DNA, 1972)

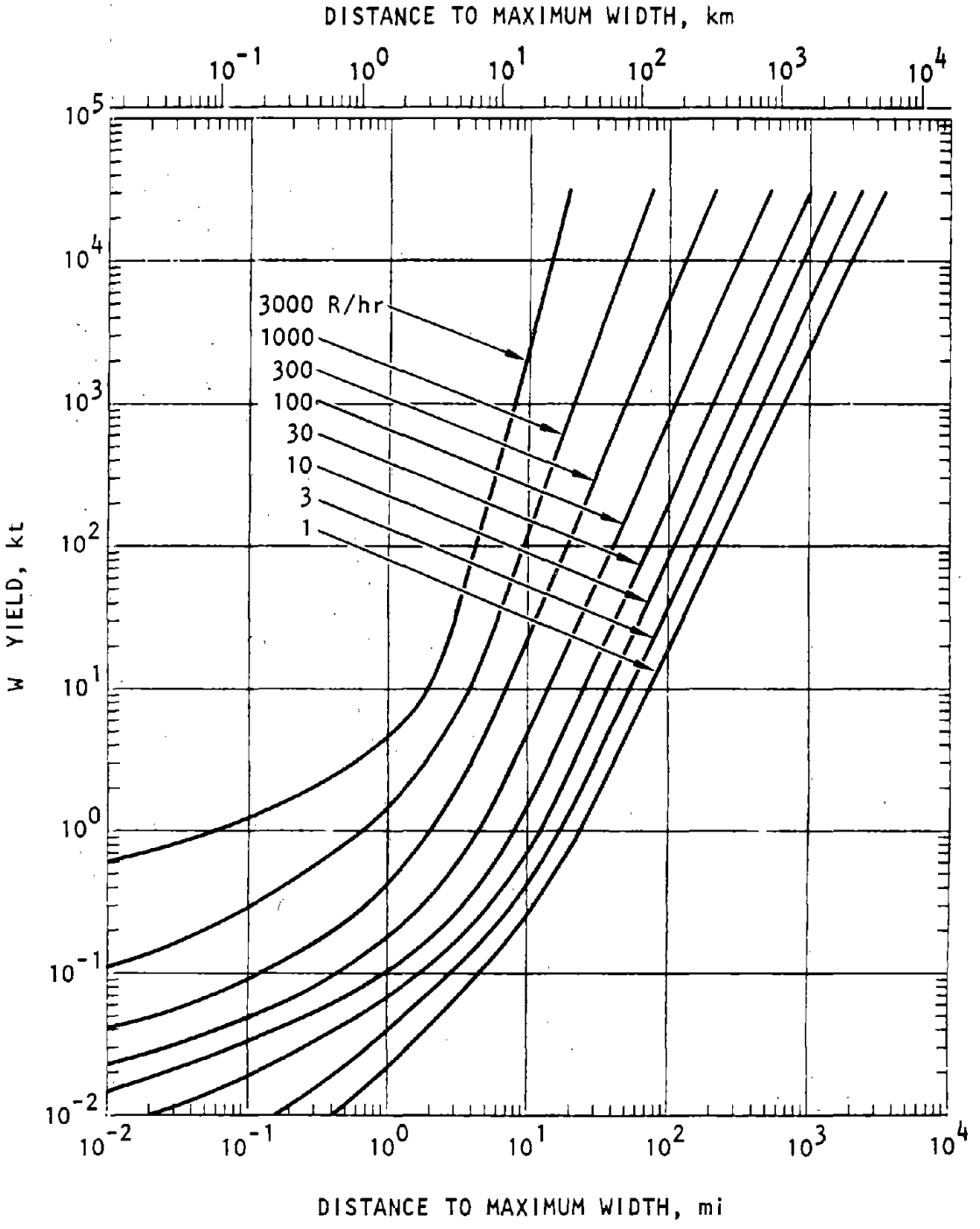

Figure 15–9. Distance to Maximum Width and Fallout Radiation at t = 1 Hr After Burst as a Function of Yield, 20-Knot Effective Wind (DNA, 1972)

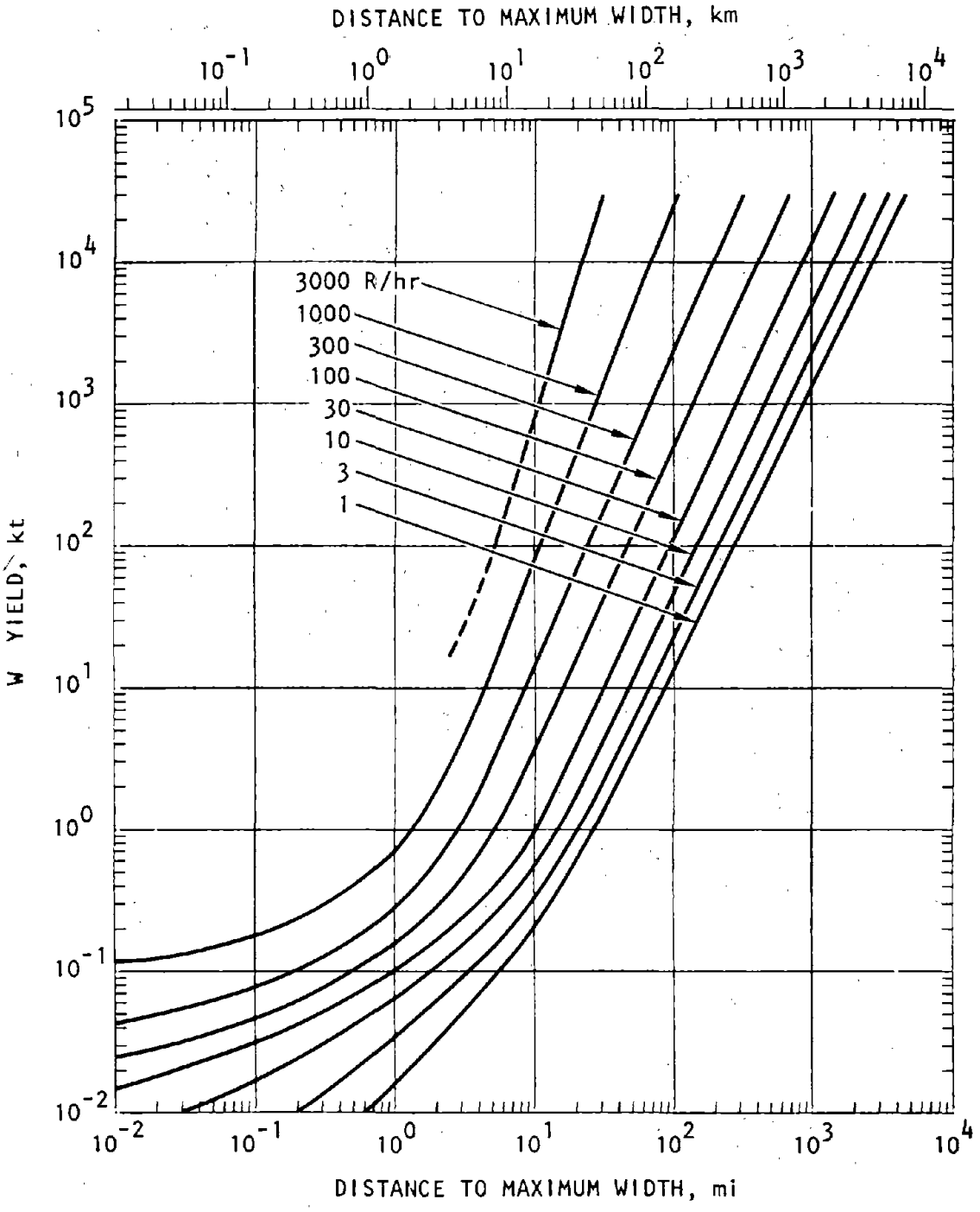

Figure 15–10. Distance to Maximum Width and Fallout Radiation at t = 1 Hr After Burst as a Function of Yield, 40-Knot Effective Wind (DNA, 1972)

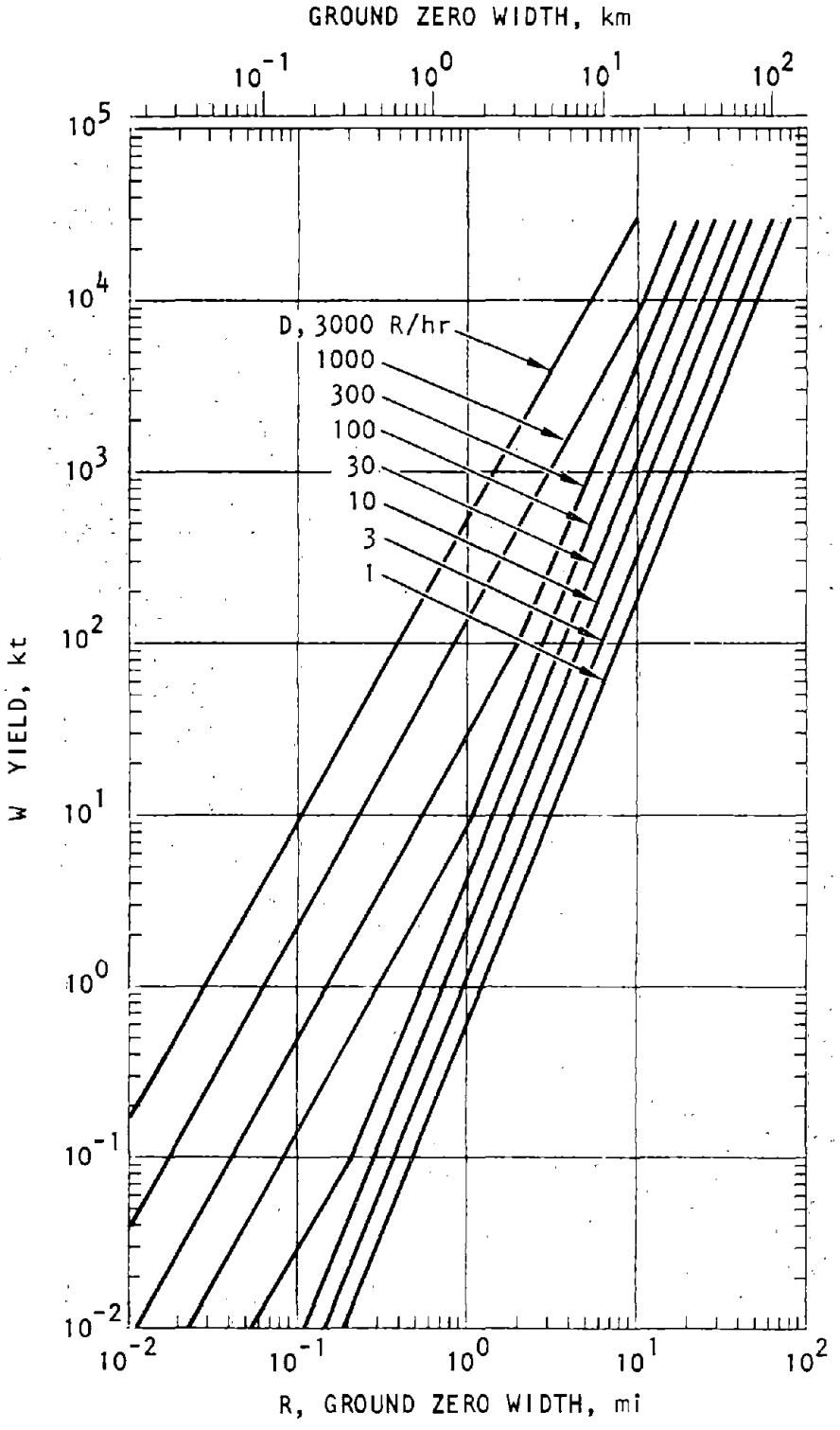

Figure 15–11. Ground Zero Width and Fallout Radiation at t = 1 Hr After Burst as a Function of Yield (DNA, 1972)

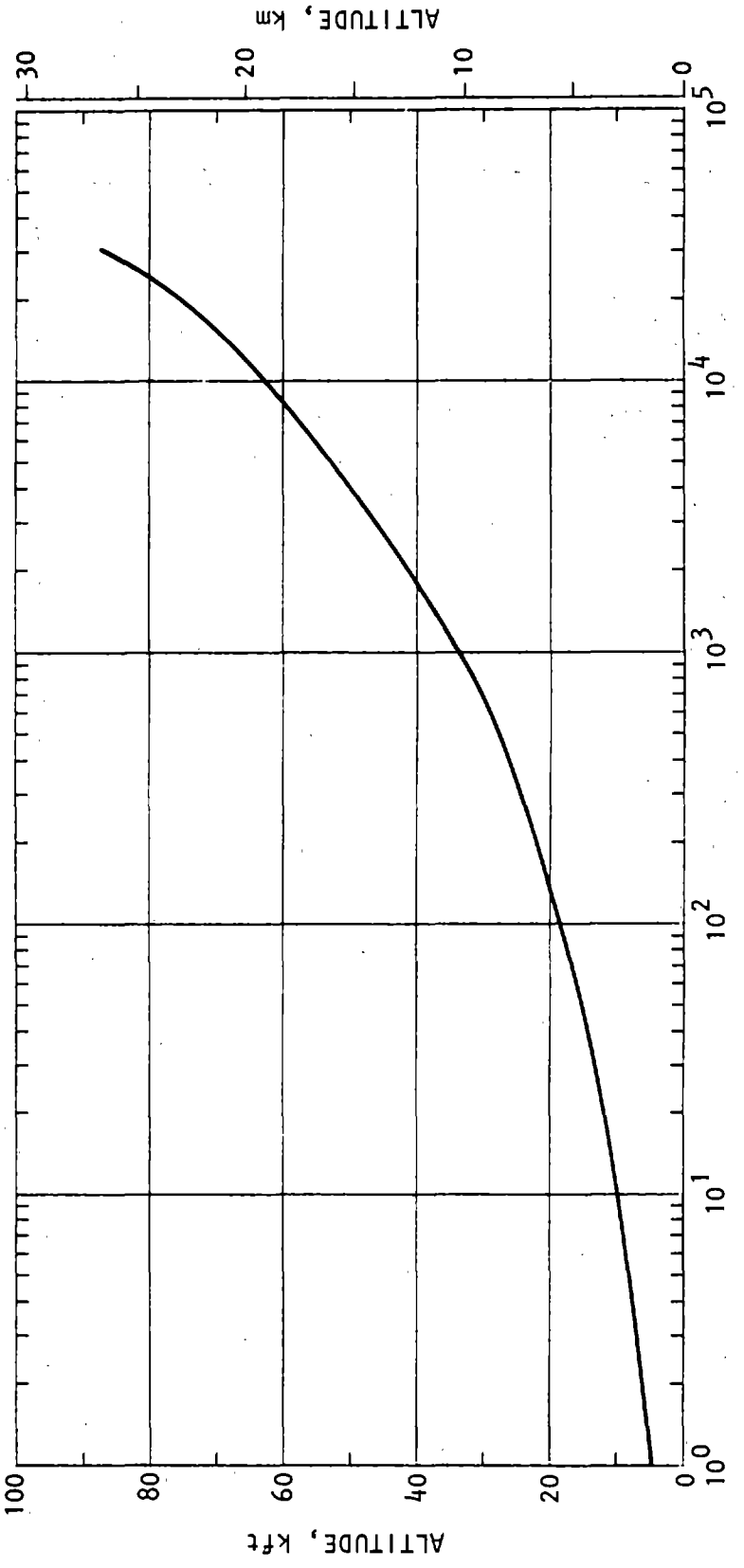

Figure 15-12. Height of the Stabilized Cloud Bottom as a Function of Yield (DNA, 1972)

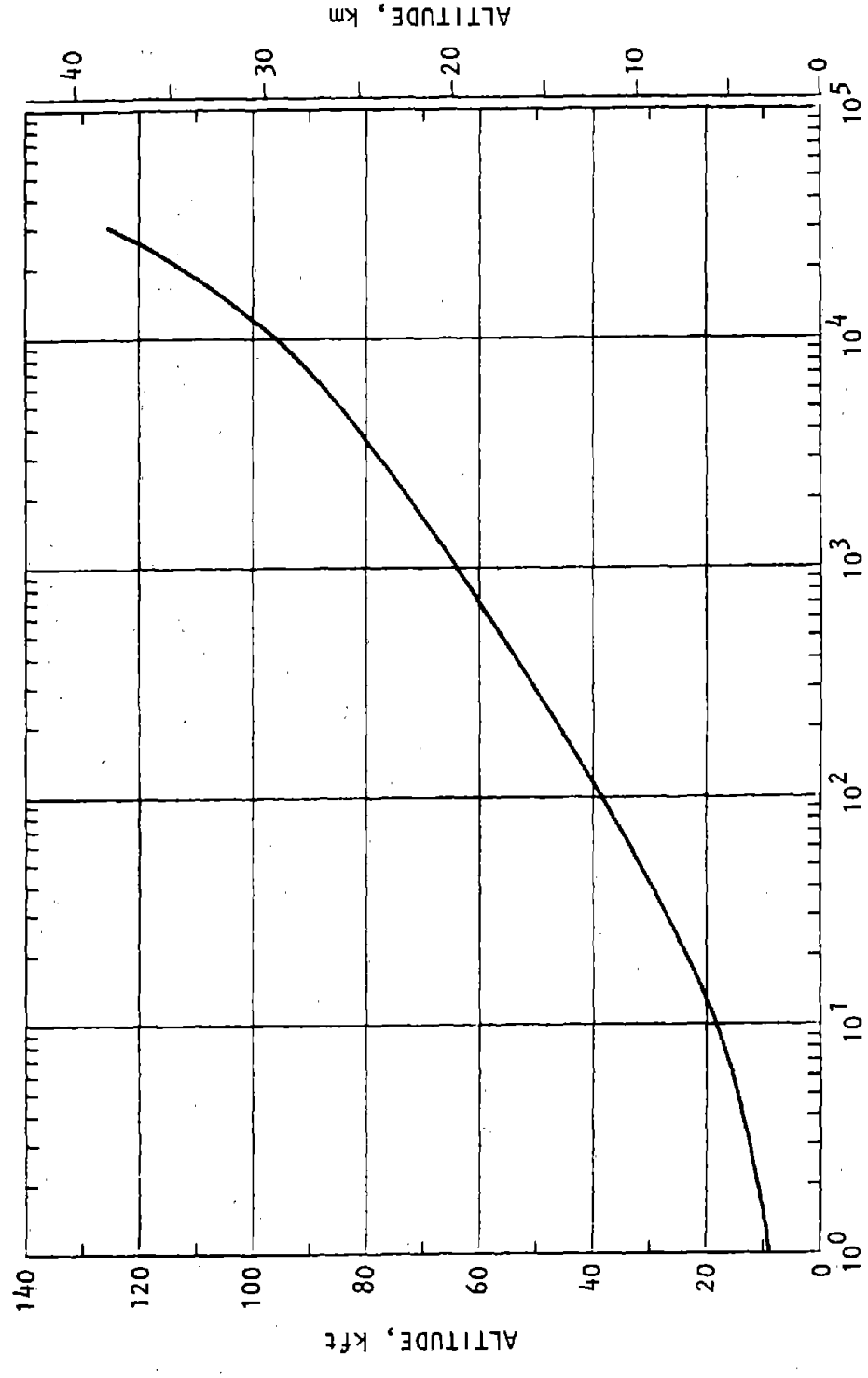

Figure 15–13. Height of the Stabilized Cloud Top as a Function of Yield (DNA, 1972)

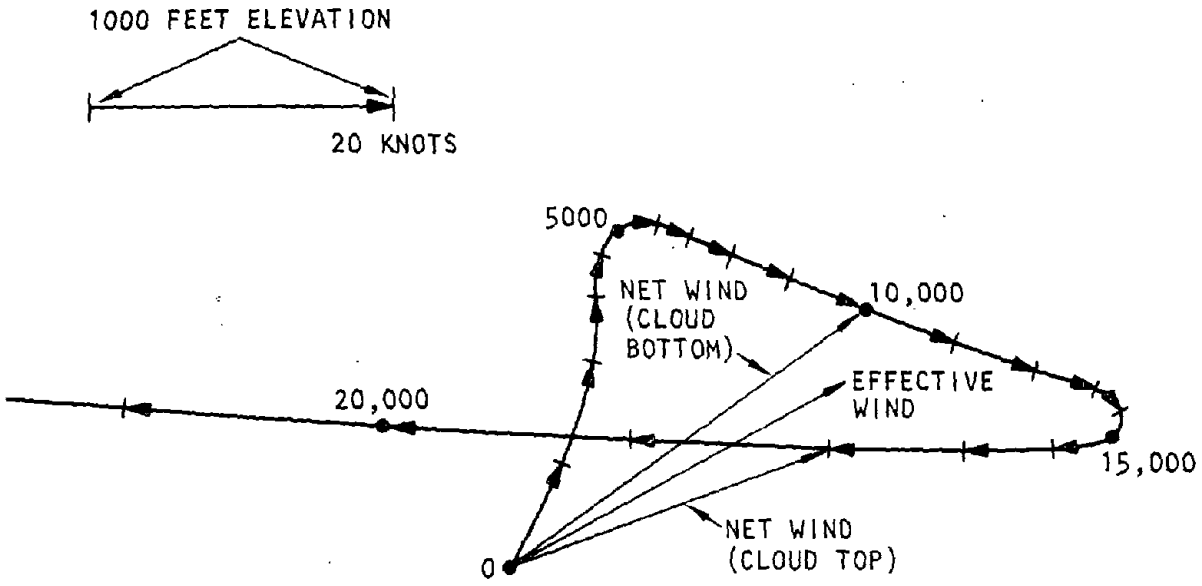

Figure 15-14. Typical Hodograph of a Vertical Wind Structure

c. Transition height bursts. For burst heights between the surface and the scaled height 100 ft/kt$^{1/3}$ (30.5 m/kt$^{1/3}$), fallout contamination will be a variable problem. The elevations below which fallout should be considered are presented in figure 15-15. An estimate of the dose rate should be obtained by multiplying the data in figures 15-2 through 15-11 by the adjustment factors presented in figure 15-16. For bursts in the upper one-quarter of the transition zone, the neutron-induced soil activity described in paragraph 3-3*f* represents a significant contribution to the residual radiation environment that must be considered in addition to the fallout.

15-3. Late fallout

a. Decay rate. The decay rate of radioactivity normalized to the quantitative data of radiation dose rates presented in figures 15-2 through 15-11 is summarized in figure 15-17 for any time after detonation. The total dosage that will be accumulated for exposure starting one hour after burst can be calculated from figure 15-18 and the one-hour dose rate data of figures 15-2 through 15-11.

b. Mean decay rate. For practical purposes, the fallout radiation can be assumed to obey the $t^{-1.2}$ law in which the dosage rates at t = 1 hour are modified by the factor $t^{-1.2}$ to obtain the dosage rates at an arbitrary time.

15-4. Precipitation effects.

In inclement weather, air bursts (which usually produce residual radiation effects of negligible military significance) may cause dangerous contamination on the ground. The effect is called precipitation scavenging, or rain-out, and its importance depends on whether the burst occurs before or during precipitation; on the weapon yield, size and shape of the nuclear cloud, and radioactive decay rate; on the rain cloud size and type and duration of precipitation; and on the effects of precipitation on the contamination after it reaches the ground. Specific details regarding precipitation effects should be obtained from the DNA (1972) report.

15-5. Uncertainty.

a. The data presented can be considered only a guide for estimating residual contamination. The greatest uncertainty originates with the weather itself. Therefore, the degree of surface residual radioactive contamination is largely dependent on precipitation and wind conditions during and after detonation. Other effects that should be considered are weapon yield and HOB.

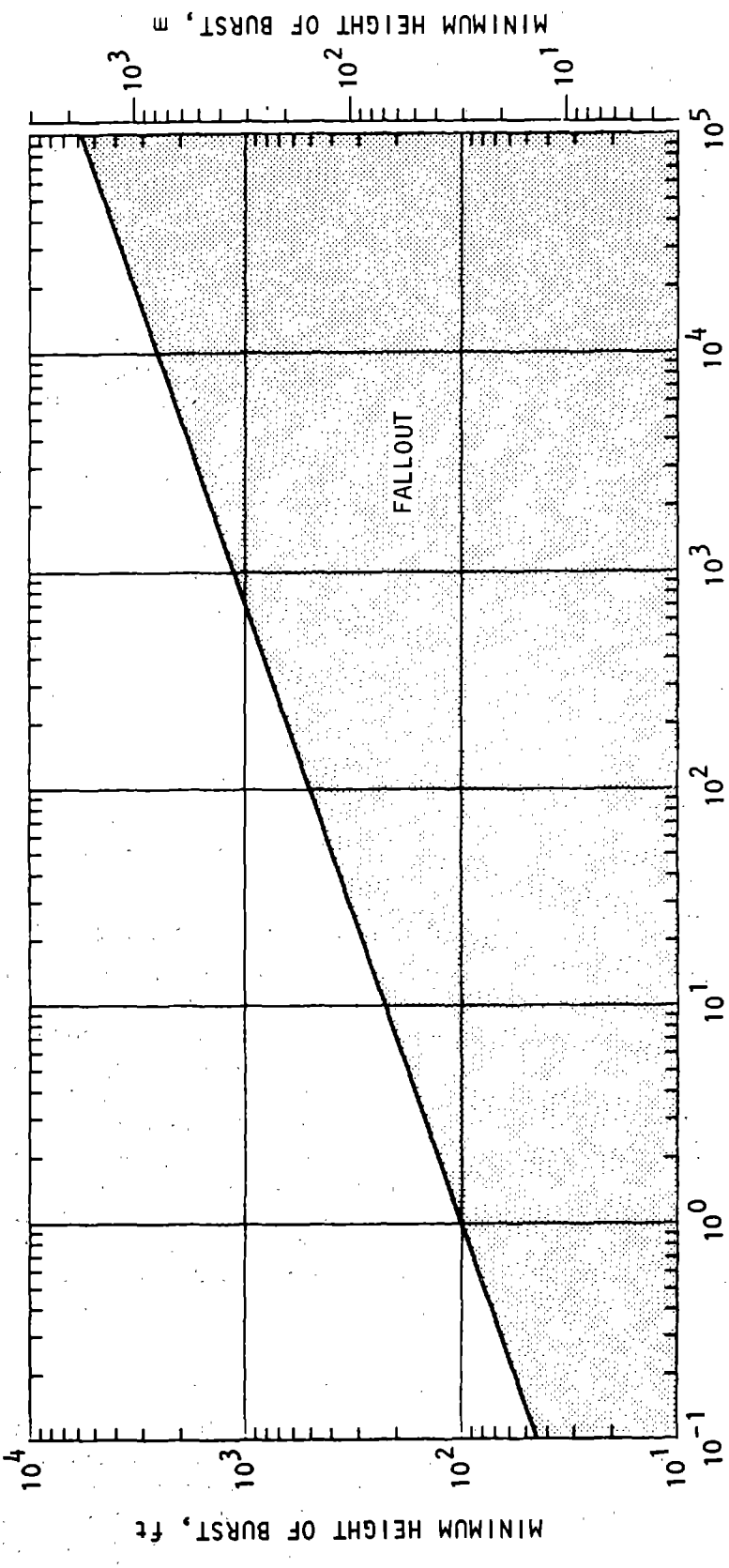

Figure 15-15. Minimum Height of Burst Below Which Fallout Occurs as a Function of Yield (DNA, 1972)

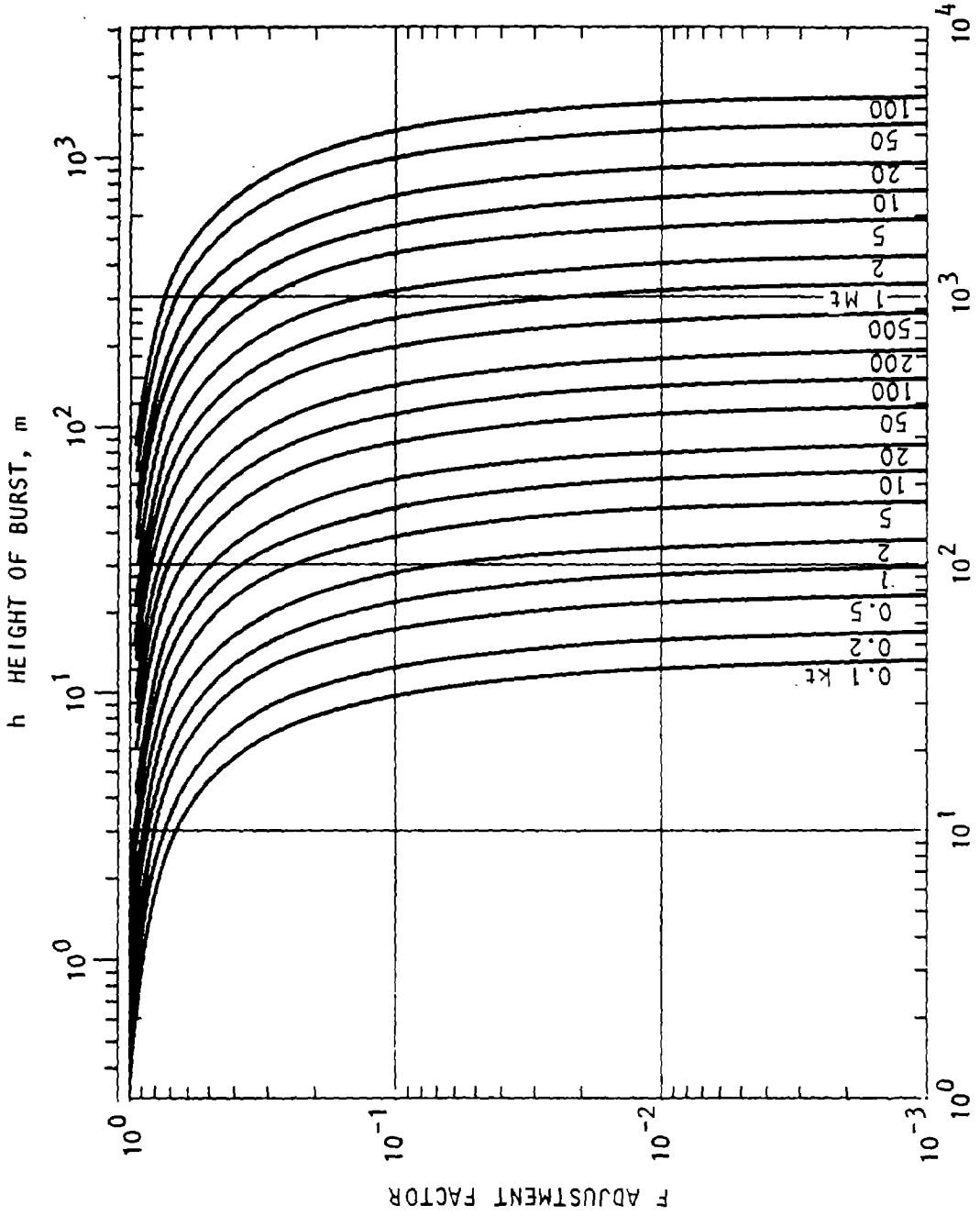

Figure 15-16. Height of Burst Adjustment Factors for Various Yields (DNA, 1972)

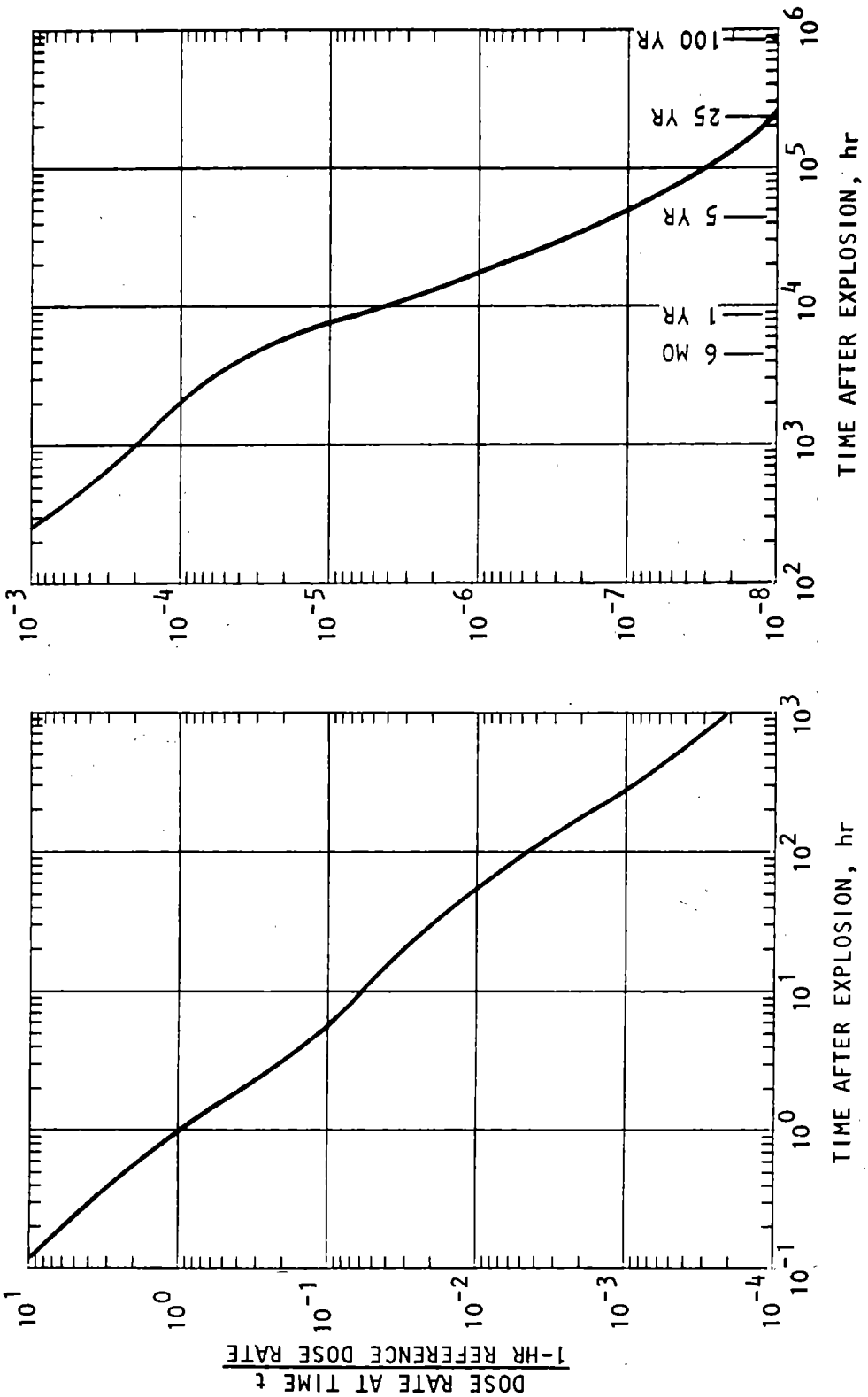

Figure 15-17. Fission Product Decay Factors Normalized to Unity at 1 Hour After Detonation (DNA, 1972)

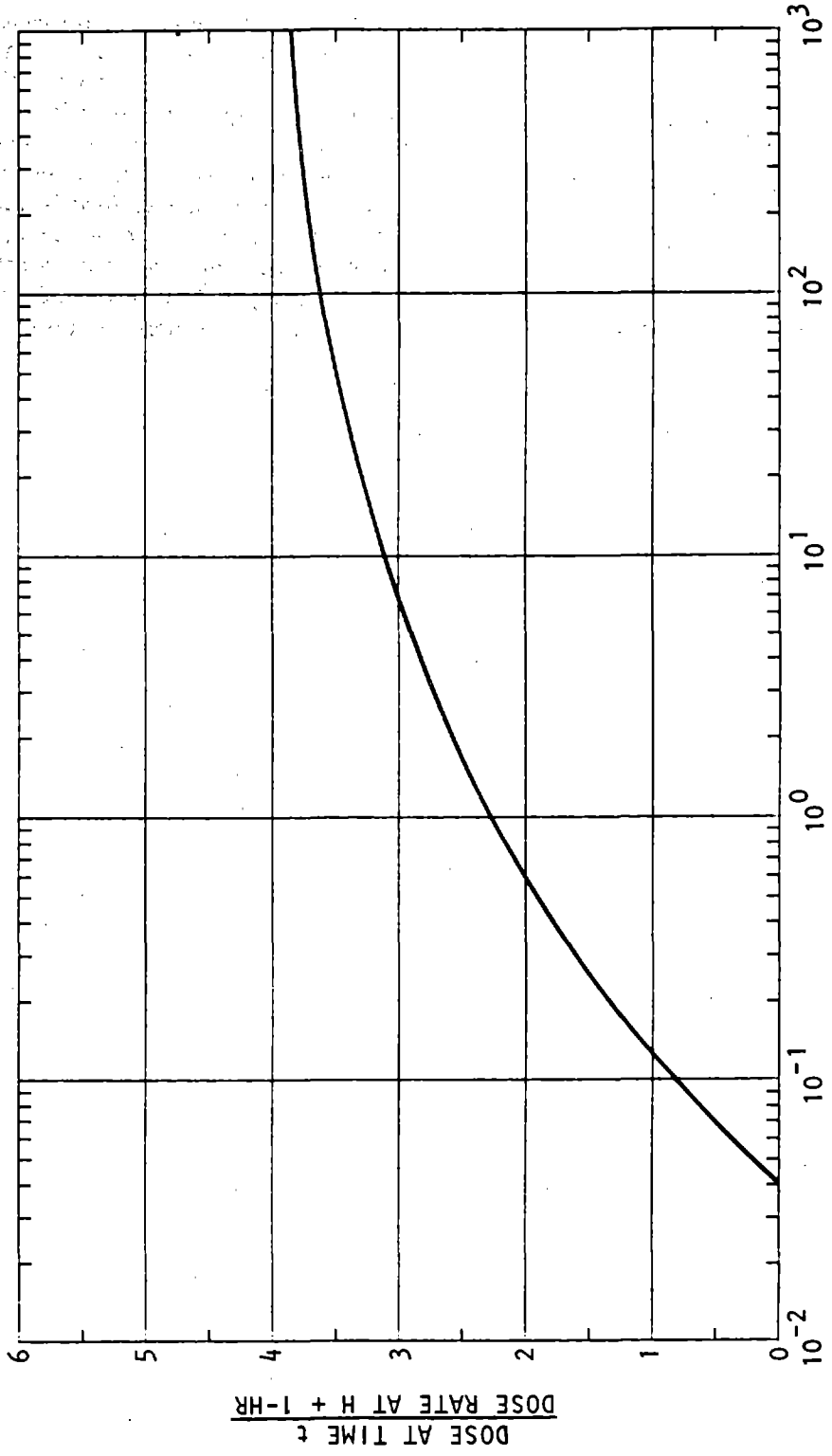

Figure 15-18. Normalized Dose Accumulated in a Fallout Contaminated Area from H + 1 Hour to H + 1000 Days (DNA, 1972)

b. The effect of yield and HOB uncertainties on producing the dose rate uncertainty can be computed from

$$\Omega_{D'}^2 = \Omega_F^2 + \frac{1}{\left(\log \frac{Z}{W^n} - \gamma\right)^4} \left\{\left[\beta n + B\left(\log \frac{Z}{W^n} - \gamma\right)^2\right]\Omega_W^2 + \beta^2\Omega_Z^2\right\} \quad (15\text{–}1)$$

where

$$B = \begin{cases} 1.824, & W \leq 9.2\ R^{2.96}\ \text{kt} \\ 0.824, & W > 9.2\ R^{2.96}\ \text{kt} \end{cases}$$

$$B = \begin{cases} 0.273, & Z/W^{0.35} \geq 337\ \text{ft/kt}^{0.35} \\ 0 & Z/W^{0.35} < 337\ \text{ft/kt}^{0.35} \end{cases}$$

$\gamma = 2.11$

$n = 0.35$

Ω_Z and Ω_W are the uncertainties of HOB and yield, respectively; and Ω_F is associated with the uncertainty in the wind. It is suggested that radiation contours similar to that shown in figure 15–1 be constructed for wind vectors corresponding to the mean value of the winds aloft data and for the means plus their corresponding standard deviations. From these data two radiation dose rates can be determined—one for the mean wind condition (call it $\bar{D}$), and another for the mean plus the standard deviation wind condition (say D_σ). Therefore, compute

$$\Omega_F = \frac{D_\sigma - \bar{D}}{\bar{D}} \quad (15\text{–}2)$$

APPENDIX A
GLOSSARY

Airblast: The overpressure signal following the shock wave driven through the air by an explosion.

Airblast-induced Ground Shock: Ground response caused by passage of the airblast over the ground surface.

Alpha Particle: A helium atom stripped of its two electrons; a helium nucleus.

Azimuthal Magnetic Field: A magnetic field whose field lines are circles in planes parallel to the ground surface.

Beta Particle: A free electron.

Burst: Explosive release of energy, explosion.

Burst Configuration: Description of the location of the explosive center of growth relative to the ground plane, and to the target or observation point.

Burst Elevation: Height of burst; distance from the ground surface up to the explosive CG.

Compton Current: The current resulting from the collision of gamma rays with air molecules and the outward displacement of electrons detached by the collisions.

Continuous Coverage Region: The area where sufficient ejecta is deposited to provide complete coverage of the ground surface.

Crater:

Apparent Crater: The open hole left after a cratering explosion, smaller than the true crater due to partial filling by fallback.

True Crater: The excavation or hole defining the limit of dissociation (separation) of the natural site material.

Crater-induced Ground Shock: Late time stress and particle motion signals attributed to crater formation.

Cratering Efficiency: The ratio of crater volume to weapon yield for cratering explosions.

Debris: Ejecta deposited on the ground surface; wreckage from damaged structures or vegetation.

Decay: Decrease in amplitude; also, radioactive decay, the natural fission process which leads eventually to the formation of stable (nonradioactive) substances.

Delivery Accuracy: The CEP of a weapon system or delivery system.

Deposition Region: The source region for EMP; the region where the primary gamma ray interactions with the atmosphere occur.

Depth of Burst (DOB): The distance from the ground surface down to the explosive center of gravity; the depth of burial.

Direct-induced Ground Shock: Ground response resulting from the coupling of energy in the ground in the vicinity of the crater.

Dynamic Pressure: One-half the product of the density and square of the particle velocity of air behind the shock front.

Ejecta: Material thrown out of the region surrounding ground zero during crater formation.

Ejecta Dust Cloud: The portion of ejecta particles forming a dust cloud subject to prevailing wind forces.

Electromagnetic Pulse (EMP): The "radio flash" on broad band electric and associated magnetic fields resulting from nuclear explosions.

Engulfment Radius: The maximum radius of the fireball.

Enhanced Weapon:	A weapon designed to enhance some aspect of bomb performance, e.g., the neutron bomb or an earth penetrating reentry vehicle/warhead, which respectively enhance neutron radiation at the expense of blast and ground shock and ground shock at the expense of airblast and radiation.
Equivalent Ejecta Thickness:	An ejecta depth based on uniform azimuthal distribution which ignores the normally observed ray pattern and azimuthal variation.
Equivalent Yield:	The yield of a weapon detonated under different conditions that would produce the same effect at the point of observation.
Fallback:	Material lofted by the cratering process which does not escape but drops back into the crater.
Fallout:	Radioactive bomb case debris and dust which settles out of the dust cloud.
Fireball:	The high temperature, high pressure expanding plasma core produced by a nuclear explosion.
Fission:	The splitting of unstable heavy element atoms accompanied by the release of energy.
Fluence Spectrum:	A spectrum relating radiation intensity (fluence) to energy level.
Free Field:	Locations in the air or ground unaffected by the presence of man-made structures.
Fuel Density:	A measure of the availability of fuel for evaluating firestorm potential, i.e., weight of fuel per unit ground surface area.
Fusion:	The combination of light nuclei into heavier nuclei accompanied by the release of energy; the basis of thermonuclear (hydrogen) bombs.
Gamma Rays:	Radiation similar to visible light or x-rays but with very short wavelengths; hard x-rays.
Ground Shock:	The ground stress and ground motion resulting from direct energy deposition and/or airblast loading from an explosion.
Ground-Surface Dust Cloud:	The portion of the low-lying dust cloud comprising dust that originates from the ground surface (outside the crater).
Ground Zero (GZ):	The point on the ground surface directly above or below the burst point.
Height of Burst (HOB):	The elevation of the explosion's center of gravity above the ground surface.
"High Yield" Weapon:	A general class of nuclear weapons that release a major portion of their energy as radiation; high yield to mass ratio devices.
Hydrodynamic:	Fluid like; pertaining to the expansion of the hot plasma core during the early phases of a nuclear explosion.
Impedance:	The product of material density, ϱ, and a characteristic wave speed, c.
Impulse:	The integral of the overpressure, usually for the positive phase duration.
Laydown Pattern:	An attack strategy utilizing the delivery of a number of weapons for subsequent simultaneous detonation. Delivery may be in an array to attack point, line, or areal targets.
Load:	The integral of the product of the dust concentration and the air-intake-volume rate over a lapsed time.

Low-lying Dust Cloud: The dust cloud that remains in contact with the ground surface.

"Low Yield" Weapons: A general class of weapons which release a major portion of their energy as kinetic energy of bomb case debris; low yield to mass ratio devices.

Mach Reflection Region: The ground surface region below a low-altitude burst where reflected shock waves overtake and merge with the incident shock waves to form a Mach stem.

Mach Stem: The nearly vertical shock front formed by the merging of reflected and incident shock waves in the Mach reflection region.

Million Electron Volts (MeV): Temperature or energy unit for high energy particles.

Multiple Burst Attack:

Laydown Pattern: An attack using simultaneous detonation of an array of previously delivered weapons.

Sequential Attack: Repeated attack of a target, especially when cratering is a primary kill mechanism, or can be used to dig out a buried target; also known as Nail Driving attack.

"Nail Driving:" A sequential multiple-burst attack designed to dig out and kill a buried target.

Neutrons: A particle of neutral electrical charge found in most atomic nuclei; atomic weight ≈ 1.

Neutron-induced Gamma Activity: Residual radioactivity induced in soil by neutron bombardment during a nuclear explosion.

Nuclear Radiation: The alpha, beta, and gamma radiation resulting from a nuclear explosion. Commonly divided into intitial or prompt radiation ($0 < t < 1$ min) and residual radiation ($t > 1$ min).

Nuclear Weapons: Weapons whose explosive energy is the result of fission or fusion processes. Includes both atomic (fission) and thermonuclear (fission/fusion) weapons.

Outrunning: The arrival of ground signals propagated through underlying higher velocity layers at the ground surface before the arrival of the airblast shock front.

Overpressure: The airblast pressure (in excess of the ambient pressure) resulting from an explosion.

Pattern Bursts: Multiple burst attacks utilizing simultaneous detonation of an array of weapons.

Plastic Zone: The zone of soil/rock surrounding a crater in which significant plastic deformation has occurred.

Polar Electric Field: An electric field normal to the earth's surface; a part of the EMP signal associated with an azimuthal magnetic field.

Positive Phase (duration): The length of time the airblast signal shows a positive overpressure.

Precipitation Scavenging: Removal of radioactive dust from the dust cloud of a nuclear explosion by rain; rainout.

Precursor (shock): A shock wave running ahead of the normal shock front, caused by radiative heating of thermally nonideal surfaces.

Rad: A unit of absorbed radiation dose equivalent to 100 ergs of radiation per gram of absorbing material or tissue.

Radial Electric Field: An electric field directed radially from the center (of a nuclear explosion).

Radiant Exposure: The amount of thermal radiation received per unit area (cal/cm^2).

Radiated Pulse:	That portion of the EMP disturbance radiated by the induced electric currents.
Radiation Dose:	Total quantity of ionizing (nuclear) radiation.
Rainout:	Removal of radioactive dust from a nuclear dust cloud by precipitation; precipitation scavenging; rain-induced fallout.
Reflectance:	Ratio of the radiant energy reaching a surface facing the fireball to that which would reach the same surface in the absence of clouds, the ground, and other reflective surfaces.
Regular Reflection Region:	The region on the ground surface below a low altitude burst where the reflected wave does not overtake and merge with the incident shock; the region within a circle of radius equal to the height of burst, centered at ground zero.
Rupture Zone:	A region surrounding the true crater in which cracking and crushing occur. It, in turn, is surrounded by the plastic zone.
Secondary Gamma Radiation:	Gamma radiation produced by neutron interaction with materials outside the nuclear weapon.
Sequential Detonation:	An attack strategy in which a target is repeatedly attacked, such as the "nail driving" attack to dig out and kill a buried target.
Shake:	10^{-8} second
Shock Wave:	The air-blast wave propagated by an explosion, characterized by discontinuous rise to peak pressure.
Slant Range:	Spherical range from the explosive center of gravity to the point of interest.
Spontaneous Ignition:	Ignition as the result of radiant exposure to the thermal pulse from a nuclear explosion.
Superseismic:	Ground signals moving faster than the airblast shock front.
Temperature Inversion:	Layer of air in which the temperature increases with height.
Thermal Efficiency:	Ratio of the thermal energy radiated by the fireball to the total energy release or yield of the weapon.
Thermal Radiation:	Radiation from the fireball in the ultra-violet, visible, infrared spectral bands.
Thermally Ideal Surfaces:	Perfectly reflective, nonabsorbing surface, e.g., water, ice.
Thermally Nonideal Surfaces:	Absorbtive, nonreflective surface.
Transition Height:	The minimum burst elevation for which dust pickup and fallout do not occur.
Transmittance:	Ratio of the radiant energy reaching a surface facing the fireball to that which would reach the surface through a perfectly transparent atmosphere.
Triple Point:	The point at which the Mach stem and incident reflected shocks intersect.
Waveform:	The time-dependent amplitude history of the signal.
Weapon Design:	Weapon construction factors influencing the performance of a nuclear weapon; *cf.* enhanced weapon.
X-ray:	A gamma-like radiation not associated with nuclear explosions.
Yield:	Explosive energy released by a nuclear explosion, commonly expressed in terms of the weight of an energy equivalent TNT charge.

APPENDIX B
BIBLIOGRAPHY

Abramowitz, M., editor. *Handbook of Mathematical Functions with Formulas, Graphs, and Mathematical Tables* (U). Washington, DC: National Bureau of Standards, 1972.

Air Force Weapons Lab (AFWL). *Electromagnetic Pulse Environment Handbook* (U), AFWL-EMP-Phenomenology 1-1. Kirtland AFB, NM: AFWL, Jan 1972 (AD 519 380L) (Secret RD).

Allison, J.M. *Investigation of Dust Lofting Mechanisms* (U), DNA-2842F. Redondo Beach, CA: TRW, Oct 1971 (AD 521 641L) (Secret RD).

Ang, A.H-S. and Cornell, C.A. "Reliability Bases of Structural Safety and Design (U)," *Proc. ASCE Struct. Div.* 100:ST9 Sep 1974.

Amer. Soc. of Civil Eng. (ASCE). *Structural Analysis and Design of Nuclear Plant Facilities* (draft). New York; ASCE, 1976.

Army Eng. Waterways Exp. Station (AEWES). *True Crater and Permanent Displacement Measurements for Simulated Low-Yield Nuclear Explosions, Phase 2*, DNA-PR-0012. Vicksburg, MS: AEWES, Feb 1976.

Army Eng. Waterways Exp. Station (AEWES). *True Crater and Permanent Displacement Measurements for Simulated Low-Yield Nuclear Explosions, Project ESSEX 1, Phase 3*, DNA-PR-0028. Vicksburg, MS: AEWES, Feb 1977.

Brode, H.L. *A Review of Nuclear Explosion Phenomena Pertinent to Protective Construction* (U), R-425-PR. Santa Monica, CA; Rand Corp., May 1964 (AD 601 139).

Brode, and Lewis, J.G., *Implications of Recent Air-Blast Studies to Damage of Hardened Structures* (U), Marine del Rey, CA: R&D Assoc., Oct 1975.

Cooper, H.F., Jr. *Empirical Studies of Ground Shock and Strong Motions in Rock* (U), DNA-3245F, Santa Monica, CA: R&D Assoc., Oct 1973 (RDA-TR-3601-002).

Cooper, H.F., Jr. *On Crater-Induced Ground Motions for Near-Surface Explosions* (U), AFWL-TR-71-72. Kirtland AFB, NM: AFWL, Nov 1971 (SECRET RD).

Crawford, T.V. "Diffusion and Deposition of the Schooner Clouds," in *Symp. on Engineering with Nuclear Explosives, Las Vegas, NV, Jan 14-16, 1970*, Vol. 1, pp. 381-399. Washington, DC: U.S. Atomic Energy Commission, May 1970.

Crawford, R.E.; Higgins, C.L.; Bultman, E.H. *The Air Force Manual for Design and Analysis of Hardened Structures, Final*, AFWL-TR-74-102. Albuquerque, NM: Civil Nuc. Systems Corp., Oct 1974 (AD B004 152L).

Defense Nuclear Agency (DNA). *Capabilities of Nuclear Weapons* (U), DNA-EM-1, Pt. 1. Washington, DC: DNA Jul 1972 (AD 526 125) (Secret RD).

General Electric-TEMPO. *DNA EMP (Electromagnetic Pulse) Handbook: Resources* (U), DNA-2114H-4. Santa Barbara, CA: GE-TEMPO Nov 1972 (AD 522 310) (Confidential).

_____. *Nuclear Weapons Blast Phenomena* (U), 5 vols with supplements, DASA-1200. Santa Barbara, CA: GE-TEMPO, 1972 (AD 516 107, AD 513 590L, AD 511 266L, AD 527 669).

_____. *Nuclear Weapons Effects Computer Code Directory* (U), DNA-3540F. Santa Barbara, CA: GE-TEMPO, Oct 1974 (AD C005 880) (Confidential).

Effects of Nuclear Weapons, DA Pamphlet 50-3, 1977 Washington, DC: DA, 1977.

Higgins, C.J. *An Analysis of Outrunning Ground Motions* (U), AFWL-TR-74-220. Albuquerque, NM: Civil Nuc. Systems Corp. May 1975.

Kerr, J.W. *Nuclear Weapons Effects in a Forest Environment-Thermal and Fire* (U), TR-2-70. Santa Barbara: GE-TEMPO, Jul 1971.

Murrell, D.W. *Earth Motion and Stress Measurements, Project LH 302, Operation DIAL PACK* (U), WES-TR-H-74-3. Vicksburg, MS: Army Eng. Waterways Exp. Station, Apr 1974.

Murrell, D.W. and Carleton, H.D. *Operation MINE SHAFT, Ground Shock from Underground and Surface Explosion in Rock* (U), WES-MS-2159 and -2160. Vicksburg, MS: Army Eng. Waterways Exp. Station Apr 1973.

Perrett, W.R. and Bass, R.C. *Free-Field Ground Motion Induced by Underground Explosions* (U), SAND-74-0252. Albuquerque, NM: Sandia Labs. Feb 1975.

Post, R.L., Jr. *Ejecta Distributions from Near-Surface Nuclear and HE Bursts* (U), AFWL-TR-74-51. Kirtland AFB, NM: Air Force Weapons Lab., Dec 1974 (AD 919 941L).

Powers, J.T. *Precursor Sweep-Up Dust Cloud Model and Thermal Layer Model Development*, DNA-3876F. McLean VA: Science Applications, Dec 1975 (AD B015 409L).

Rooke, A.D., Jr.: Carnes, B.L.; and Davis, L.K. *Cratering by Explosion, a Compendium and an Analysis* (U), TR N-74-1. Vicksburg, MS: WES, Jan 1974.

Rooke, A.D. and Meyer, J.W. *An Assessment of the State-of-the Art for Vulnerability and Hardness Analysis of Ballistic Missile Defense Facilities* (U), TR-N-72-12, Chapt. 4: Ejecta. Vicksburg, MS: Army Eng. Waterways Exp. Station, Dec 1972 (AD 915 372L).

Sauer, F.M. *Nuclear Geoplosics*: Pt. 4, *Empirical Analysis of Ground Motion and Cratering*, DASA-1285-4. Menlo Park, CA: Stanford Res. Inst. May 1964 (AD 443 593).

Science Applications, Inc. (SAI). *Status of Neutron and Gamma Output from Nuclear Weapons* (U), DASA-2567. La Jolla, CA: SAI, May 1971.

Seebaugh, W.R. *Studies of the Nuclear Crater Ejecta Environment*, DNA-3640F. McLean, VA: Science Applications, Inc., Jun 1975 (AD B006 841L).

Swatosh, J.J., Jr. *Nuclear Weapons Effects: Dust and Air Temperature Environment*. Chicago, IL: IIT Res, Inst., Feb 1971 (AD 729 426).

Tewes, H.A. "Results of the Schooner Excavation Experiment," in *Symp. on Engineering with Nuclear Explosives, Las Vegas, NV, Jan 14-16, 1970, Vol. 1, pp 306-333. Washington, DC: U.S. Atomic Energy Comm., May 1970.*

Young, G.A. *The Physics of the Base Surge*, NOLTR-64-103. White Oak, MD: Naval Ordnance Lab., Jun 1965 (AD 618 733).

By Order of the Secretary of the Army:

JOHN A. WICKHAM, JR.
General, United States Army
Chief of Staff

Official:

ROBERT M. JOYCE
Major General, United States Army
The Adjutant General

Distribution:

To be distributed in accordance with DA Form 12-34B requirements for TM 5-800 Series: Engineering and Design for Real Property Facilities.

RECOMMENDED CHANGES TO EQUIPMENT TECHNICAL PUBLICATIONS

THEN. . JOT DOWN THE DOPE ABOUT IT ON THIS FORM. CAREFULLY TEAR IT OUT. FOLD IT AND DROP IT IN THE MAIL'

SOMETHING WRONG WITH THIS PUBLICATION?

FROM: (PRINT YOUR UNIT'S COMPLETE ADDRESS)
Your mailing address

DATE SENT
Date you tilled out form.

PUBLICATION NUMBER	PUBLICATION DATE	PUBLICATION TITLE
TM 9-XXXX-XXX-XX	Date ot TM	Title ot TM

BE EXACT . PIN-POINT WHERE IT IS

PAGE NO	PARA-GRAPH	FIGURE NO	TABLE NO
400		183	
512		191	

IN THIS SPACE TELL WHAT IS WRONG AND WHAT SHOULD BE DONE ABOUT IT:

Change illustration Reason Tube end shown a sembled on wrong side ot lever cam.

Figure 191, item 3 has the wrong NSN. Supply rejects orders for this item. The NSN shown here is not listed in the AMDF or the MCRL.

Please give us the correct NSN and P/N.

SAMPLE

PRINTED NAME. GRADE OR TITLE. AND TELEPHONE NUMBER
John Smith, S. SGT. 6/4/XXX

SIGN HERE
John Smith

DA FORM 1 JUL 79 2028-2

PREVIOUS EDITIONS ARE OBSOLETE.

P.S.—IF YOUR OUTFIT WANTS TO KNOW ABOUT YOUR RECOMMENDATION MAKE A CARBON COPY OF THIS AND GIVE IT TO YOUR HEADQUARTERS

REVERSE OF DA FORM 2028-2

FILL IN YOUR UNIT'S ADDRESS

FOLD BACK

DEPARTMENT OF THE ARMY

OFFICIAL BUSINESS
PENALTY FOR PRIVATE USE $300

POSTAGE AND FEES PAID
DEPARTMENT OF THE ARMY
DOD 314

U.S. MAIL

Commander
US Army Corps of Engineers
ATTN: DAEN-ECE-T
Washington, DC 20314

TEAR ALONG PERFORATED LINE

SAMPLE

RECOMMENDED CHANGES TO EQUIPMENT TECHNICAL PUBLICATIONS

SOMETHING WRONG WITH THIS PUBLICATION?

FROM: (PRINT YOUR UNIT'S COMPLETE ADDRESS)

DATE SENT

PUBLICATION NUMBER	PUBLICATION DATE	PUBLICATION TITLE
TM 5-858-2	6 July 1984	Weapon Effects

BE EXACT. . .PIN-POINT WHERE IT IS

PAGE NO	PARAGRAPH	FIGURE NO	TABLE NO

IN THIS SPACE TELL WHAT IS WRONG AND WHAT SHOULD BE DONE ABOUT IT:

PRINTED NAME, GRADE OR TITLE, AND TELEPHONE NUMBER

SIGN HERE

DA FORM 1 JUL 79 2028-2

PREVIOUS EDITIONS ARE OBSOLETE.

P.S.--IF YOUR OUTFIT WANTS TO KNOW ABOUT YOUR RECOMMENDATION MAKE A CARBON COPY OF THIS AND GIVE IT TO YOUR HEADQUARTERS.

REVERSE OF DA FORM 2028-2

FILL IN YOUR UNIT'S ADDRESS

FOLD BACK

DEPARTMENT OF THE ARMY

OFFICIAL BUSINESS
PENALTY FOR PRIVATE USE $300

POSTAGE AND FEES PAID
DEPARTMENT OF THE ARMY
DOD 314

U.S. MAIL

Commander
US Army Corps of Engineers
ATTN: DAEN-ECE-T
Washington, DC 20314

TEAR ALONG PERFORATED LINE

RECOMMENDED CHANGES TO EQUIPMENT TECHNICAL PUBLICATIONS

THEN. . JOT DOWN THE DOPE ABOUT IT ON THIS FORM, CAREFULLY TEAR IT OUT, FOLD IT AND DROP IT IN THE MAIL!

SOMETHING WRONG WITH THIS PUBLICATION?

FROM: (PRINT YOUR UNIT'S COMPLETE ADDRESS)

DATE SENT

PUBLICATION NUMBER	PUBLICATION DATE	PUBLICATION TITLE
TM 5-858-2	6 July 1984	Weapon Ettects

BE EXACT . .PIN-POINT WHERE IT IS

PAGE NO	PARA-GRAPH	FIGURE NO	TABLE NO

IN THIS SPACE TELL WHAT IS WRONG AND WHAT SHOULD BE DONE ABOUT IT:

PRINTED NAME, GRADE OR TITLE, AND TELEPHONE NUMBER

SIGN HERE:

DA FORM 1 JUL 79 2028-2

PREVIOUS EDITIONS ARE OBSOLETE.

P.S.--IF YOUR OUTFIT WANTS TO KNOW ABOUT YOUR RECOMMENDATION MAKE A CARBON COPY OF THIS AND GIVE IT TO YOUR HEADQUARTERS.

FILL IN YOUR UNIT'S ADDRESS

FOLD BACK

DEPARTMENT OF THE ARMY

OFFICIAL BUSINESS
PENALTY FOR PRIVATE USE $300

POSTAGE AND FEES PAID
DEPARTMENT OF THE ARMY
DOD 314

U.S. MAIL

TEAR ALONG PERFORATED LINE

Commander
US Army Corps of Engineers
ATTN: DAEN-ECE-T
Washington, DC 20314

RECOMMENDED CHANGES TO EQUIPMENT TECHNICAL PUBLICATIONS

SOMETHING WRONG WITH THIS PUBLICATION?

FROM: (PRINT YOUR UNIT'S COMPLETE ADDRESS)

DATE SENT

PUBLICATION NUMBER	PUBLICATION DATE	PUBLICATION TITLE
TM 5-858-2	6 July 1984	Weapon Effects

BE EXACT. . PIN-POINT WHERE IT IS

PAGE NO	PARA-GRAPH	FIGURE NO	TABLE NO

IN THIS SPACE TELL WHAT IS WRONG AND WHAT SHOULD BE DONE ABOUT IT:

PRINTED NAME, GRADE OR TITLE, AND TELEPHONE NUMBER

SIGN HERE

DA FORM 1 JUL 79 2028-2

PREVIOUS EDITIONS ARE OBSOLETE.

P.S.--IF YOUR OUTFIT WANTS TO KNOW ABOUT YOUR RECOMMENDATION MAKE A CARBON COPY OF THIS AND GIVE IT TO YOUR HEADQUARTERS

REVERSE OF DA FORM 2028-2

FILL IN YOUR UNIT'S ADDRESS

FOLD BACK

DEPARTMENT OF THE ARMY

OFFICIAL BUSINESS
PENALTY FOR PRIVATE USE $300

POSTAGE AND FEES PAID
DEPARTMENT OF THE ARMY
DOD 314

U.S. MAIL

Commander
US Army Corps of Engineers
ATTN: DAEN-ECE-T
Washington, DC 20314

TEAR ALONG PERFORATED LINE